Liaison interfaciale et inhibition de la corrosion par les inhibiteurs organiques 2-mercaptobenzothiazole et 2-mercaptobenzimidazole sur le cuivre

Vishant Garg

PSL UNIVERSITÉ PARIS

THÈSE DE DOCTORAT

DE L'UNIVERSITÉ PSL

Préparée à l'École Nationale Supérieure de Chimie de Paris

Interfacial bonding and corrosion inhibition mechanisms of 2-mercaptobenzothiazole and 2-mercaptobenzimidazole organic inhibitors on copper

Soutenue par

Vishant Garg

Le 22 Avril 2024

École doctorale n°388

Chimie Physique et Chimie Analytique de Paris Centre

Spécialité

Chimie Physique

Composition du jury :

Christine BLANC Professeur, Toulouse INP - ENSIACET, France	*Présidente du jury*
J.M.C. MOL Professeur, Technische Universiteit Delft, The Netherlands	*Rapporteur*
Ingrid MILOSEV Professeur, Jožef Stefan Institute, Slovenia	*Rapporteure*
Anne-Sophie MAMEDE Maître de conférences, Université de Lille, France	*Examinatrice*
Vincent MAURICE Directeur de recherche, CNRS, Chimie ParisTech - PSL Université, France	*Co-directeur de thèse*
Philippe MARCUS Directeur de recherche, CNRS, Chimie ParisTech - PSL Université, France	*Directeur de thèse*

Chimie Paris ParisTech | PSL

Acknowledgements

The pursuit of knowledge by unravelling the mysteries of science is a quest that involves many people. For this endeavour to succeed, we need people to work together so that we can achieve something great, to improve our lives, our society, and our earth. Similarly, this thesis is the result of the hard work of numerous people to whom I am forever indebted. The contribution of some is from their love and support, while others have contributed to the work directly. Nevertheless, I am truly grateful to every single one of you, without whom this project would not have been fruitful.

First and foremost, I would like to thank Dr. Philippe Marcus, my thesis director, for giving me the wonderful opportunity to work in his laboratory and for fulfilling my lifelong dream of living in Paris. He has always been open to my ideas and has helped me immensly to grow as a researcher. It has been an absolute honour to work under his guidance and to learn from one of the leading scientists in the field of corrosion science. Thank you for your supervision, for your profound knowledge and insights, and for the confidence in me and my work the past three years.

Next is a man of few words, but words which are worth their weight in gold. To Dr. Vincent Maurice, co-supervisor of my thesis. Thank you for your everlasting guidance, for your support, for believing in me, and expecting the most out of me. Thank you for answering all my stupid questions and for showing me the way when I was lost. For your prompt feedback and constructive comments for the analysis of the results and the materialisation of the articles. One memory that particularly stands out is the nine hundred and fifty something odd corrections for the first draft of our first article. Despite that, he always reassured me in

times of self-doubt and helped me move past it. Although it was initially intimidating and overwhelming to work under his supervision, it has been an experience like no other.

I would like to extend my deepest and heartfelt gratitude to Dr. Frédéric Wiame, co-supervisor of my thesis, and the finest teacher I have ever had. His guidance has been exceptional and has allowed me to flourish and learn new things every day. Thank you for being patient with me as I embarked on the road to study surface science. For dropping everything you were doing and taking out the time for me whenever I knocked on your door. For explaining things to me multiple times so that I would understand a concept and for reassuring me when I found things too difficult, even though I always ended up with more questions after discussing with you. Thank you for all the life and career advice and for all the conversations we had. For holding my hand when all hope was lost and for boosting my self-confidence everytime we got a review for our articles. For making me realise that we need to stop and celebrate our achievements by taking me out to lunches after each article was published. Thank you for all the Belgian chocolates, for being our Saint Nicolas, and for so much more.

A special thanks to Dr. Sandrine Zanna for helping me with planning, conducting, and analysis of the XPS experiments. Despite your busy schedule, you always managed to make time for me, for work or just for some conversation. Thank you for the all the encouragement and for the wonderful conversations we had throughout my time here in the lab. I would like to thank Dr. Antoine Seyeux for his help with the ToF-SIMS experiments, the data analysis, and especially for teaching me this technique with the utmost patience. I would also like to thank Dr. Jolanta Światowska, representative of the doctoral school ED 388 from PSL and team member of PCS, for helping me navigate the complexities of the doctoral school administrative processes. In addition, her constant support and concern for me always made me feel fostered.

I would like to thank the entire PCS team, including my fellow PhD's and Postdoc's, for their constant support and enjoyable presence. Special thanks to Ben, Zhiheng, Angele (Xueying), Yaqing, Guanhua, Ismail, Alex (Xin), Asma, and Maxime. I really enjoyed my time in this lab with all of you. Thank you for the lunches, for the Friday drinks, and for all the great conversations we have had these last few years. To the fresh faces in the lab - Julien, Thomas, Sudharshan, Minli, Mathilde, Yuchen, and Yuxin, I hope that we will share a wonderful time ahead. Lastly, I would like to extend my heartfelt gratitude to Aurélie. This list would be incomplete without her. An amazing soul who came into our lives one day, enlightened it with her wondrous spirit and cheerful presence, and forever changed my perspective on life. Thank you for all you have done for me, for the coffees, the desserts, and most importantly for your company.

This research in corrosion science would not have been possible without my alma mater – Delft University of Technology, where I obtained my masters' degree. It was there that I was introduced to the corrosion field by Dr. J.M.C. (Arjan) Mol and Dr. Yaiza Gonzalez Garcia. Thank you for the inspiring lectures and for all the invigorating discussions we had. I would also like to thank Yaiza for taking me up as a student for my master thesis project, where I began my journey of corrosion science research. I learned a lot during that period and am ever grateful to you.

A big shout out to Dr. Emmanouela Michailidou, my daily supervisor for the master thesis. She has been an inspiration in my journey throughout and always been an immense support. She was the one to teach me everything about electrochemistry including how to make a 0.1 M NaCl solution. Her work ethic, immense knowledge, and excellent laboratory skills, both in terms of conducting experiments and cleanliness in the lab, made me aspire to conduct myself in a similar way. Thank you Emina.

On that note, I would also like to thank the other institutions that I have studied in and have moulded me into the person that I am today. Thank you to St. Paul's School Darjeeling, SRM University, and HAN University of Applied Sciences and to all the teachers and professors who have been with me every step of this arduous journey.

Moving on, I would like to thank all my friends who have been there for me. Through thick and thin, through happiness and sadness, and through all the difficult times we faced together – Vishrut, Arsel, Yannick, Achin, Anirudh, Arjun, Rupak, and Akshay. Thank you all for putting up with me and for all the moments we shared together, the concerts, the F1 races, the trips, and especially the hangout sessions. I have cherished each moment with you all and am ever grateful that I found my family in you all. Special thanks to Meru, who helped me for everything in Paris, from finding a house, to all administrative matters, for all the French translations, and most importantly for being an awesome friend. I am glad that we were able to meet again after our bachelors' and rekindle our friendship. There are other numerous friends who have been a very important part of my life and I want to thank all of them too. I may not have named you individually and I do apologise for that, but your affection remains close to my heart.

Next is someone who is very special to me and is one of the most important people in my life, my best friend Iris. A kind and compassionate being with a heart of gold and a smile that can brighten the darkest of days, who has always been by my side and never lost faith in me, even when I lost faith in myself. Thank you for always supporting me and believing in me. From all the small things such as reminding me to take my vitamins and sending me new music, to all the big things like lending an ear whenever I needed to talk to someone

and hyping up my achievements. Thank you for being the best friend anyone could ever ask for in their life. I must also thank Petri for always making me smile with a constant supply of memes every single day. Kiitos!!

It goes without saying that none of this would have been possible without the love and support of my wonderful family. Thank you to Mummy and Papa for everything. For believing in me and encouraging me to chase my dreams. Thank you for always being there for me, even if you are ten thousand kilometres away. Thank you to Monu Didi and Tonu Didi for your love and especially for spoiling me as the youngest in the family. I am lucky to have two amazing sisters who care so much about me and always look out for me. To my nephew Divyam, his confidence in me always made me feel that I was doing something relevant and worthwhile. To Naaniji, my beloved grandmother, thank you for your love and support. Your presence in my life always makes me feel blessed. A special shout out to Aditya bhaiya for his perpetual support of my career and his faith in me. I love you all and couldn't have done it without your presence in my life. Lastly, I am forever grateful to the one, the creator, the higher power of the universe. It is with your blessings that I have been able to achieve everything in my life. Thank you. What comes next shall be marvellous!!!

This project has received funding from the European Research Council (ERC) under the European Union's Horizon 2020 research and innovation program (ERC Advanced Grant number 741123, Corrosion Initiation Mechanisms at the Nanometric and Atomic Scales - CIMNAS). The ToF-SIMS equipment has been partially funded by Région Ile-de-France.

Contents

Introduction **1**

Thesis Overview 2

1 State of the art **5**

1.1 Corrosion 5

1.1.1 Principles of corrosion 6

1.1.2 Types of corrosion 8

1.1.3 Relation between pH and potential: Pourbaix diagrams 13

1.1.4 Protection against corrosion 15

1.2 Copper 18

1.2.1 Passivation of copper 19

1.2.2 Corrosion of copper 23

1.2.3 Effect of chloride ions 24

1.3 Inhibitors 26

1.3.1 Mechanisms of inhibitor action 26

1.3.2 Types of inhibitors 27

1.3.3 Inhibitors for copper 29

1.3.4 2-mercaptobenzothiazole (2-MBT) 30

1.3.5 2-mercaptobenzimidazole (2-MBI) 32

2 Experimental apparatus and methodology **35**

2.1 Sample preparation 35

2.2 Surface Preparation . . . 35
2.2.1 Mechanical Polishing . . . 36
2.2.2 Electrochemical polishing . . . 37
2.3 Cleaning the apparatus . . . 39
2.4 Electrochemistry . . . 40
2.4.1 Preparation of electrolytes . . . 40
2.4.2 Classical cell . . . 41
2.4.3 Micro-cell . . . 43
2.4.4 Electrochemical experiments . . . 43
2.5 X-ray Photoelectron Spectroscopy . . . 47
2.5.1 Basic Principles and Instrumentation . . . 47
2.5.2 Experimental Parameters . . . 51
2.5.3 Treatment of data . . . 52
2.5.4 Thickness estimation . . . 55
2.6 Time-of-Flight Secondary Ion Mass Spectrometry . . . 60
2.6.1 Basic Principles and Instrumentation . . . 61
2.6.2 Experimental parameters . . . 62
2.6.3 Treatment of data . . . 64
2.6.4 Selection of Ion profiles . . . 64

3 Surface state of copper 67
3.1 Experimental . . . 68
3.2 Oxide-free copper . . . 68
3.3 Mechanically polished copper . . . 71
3.4 Electrochemically polished copper . . . 74
3.5 Conclusion . . . 78

4 Enhanced corrosion inhibition of copper in acidic environment by cathodic control of interface formation with 2-mercaptobenzothiazole 79
4.1 Experimental . . . 80
4.2 Cathodic pre-treatment of the surfaces . . . 80
4.3 Anodic dissolution of copper and its inhibition by 2-MBT . . . 82
4.4 ToF-SIMS depth profiling of the inhibiting interface . . . 85
4.5 Interfacial bonding and thickness estimation by XPS analysis . . . 88
4.6 Conclusion . . . 98

5 Adsorption of 2-mercaptobenzothiazole organic inhibitor and its effects on copper anodic oxidation in alkaline environment 99

5.1 Experimental 100
5.2 2-MBT effects on native oxide film reduction and anodic surface oxidation. . 100
5.3 Surface analysis of 2-MBT-covered oxidized interface. 105
5.4 Interface structure and composition. 113
5.5 Effects of pH on the interface. 115
5.6 Conclusion 117

6 Inhibition of the initial stages of corrosion by 2-mercaptobenzothiazole adsorption and the effects of interfacial oxides on copper in neutral chloride conditions 119
6.1 Experimental 120
6.2 Formation of the 2-MBT organic barrier layer 120
6.3 Inhibition of oxidation and corrosion initiation 133
6.4 Influence of environment on the adsorption of 2-MBT 138
6.5 Conclusion 141

7 Interfacial bonding and corrosion inhibition of 2-mercaptobenzimidazole organic films formed on copper surfaces under electrochemical control in acidic chloride solution 143
7.1 Experimental 144
7.2 Reduction of native oxides by cathodic pre-treatment of the interface 144
7.3 Surface analysis after adsorption of 2-MBI 146
7.4 Corrosion inhibition by 2-MBI organic films 158
7.5 Effects of anodic polarisation on the 2-MBI layer 162
7.6 Conclusion 172

Conclusions and perspectives 173

A Résumé étendu de thèse 179

List of References 217

Introduction

The natural degradation of metals, i.e. corrosion, is a perilous phenomenon that results in the failure of metal structures. It also causes issues associated with safety, damage to the environment, economical, and even loss of life. Several large-scale accidents such as the collapse of the Berlin congress hall in 1980 (Germany), the Bhopal gas leak incident in 1984 (India), the explosion of a gas pipeline in New Mexico (USA) in 2000, the Refugio oil spill in 2015 (USA), and more recently the collapse of the Morandi bridge in Italy (2018) occurred due to issues related to corrosion. These incidents have proven that the impacts of corrosion can be severe and need to be taken seriously. Therefore, it is imperative to study the science behind it so that methods and techniques can be developed to better protect metals and metal structures from failure.

Copper has been used by mankind since as early as 8000 BC due to its wide-ranging properties of malleability, ductility, and electrical and thermal conductivity among others. In prehistoric ages, it was used for coins, sculptures, tools, jewelry, bells, and vessels. In more recent times, copper is used for electrical wires, plumbing, construction, and industrial machinery, along with jewelry, coins, and sculptures like in the prehistoric days. The conditions for the use of copper are not always optimal; pipelines are usually buried underground or in the sea, electrical components and electronics deal with high temperatures, industrial machineries usually operate at high acidity conditions, and sculptures and construction parts must deal with moisture along with the pollutants in the air.

Although copper naturally forms a passive oxide film on its surface, it does not guarantee protection to the metal. In acidic conditions or in the presence of aggressive ions, copper

undergoes corrosion attack. Due to the widespread use of copper in critical applications, it is necessary to protect it from corrosion to prevent catastrophic incidents. This role falls to inhibitors, one of the corrosion protection methods. These are chemical compounds that "inhibit" the reactions occurring on a metal surface, thus reducing the rate of corrosion or even blocking it entirely.

2-mercaptobenzothiazole (2-MBT) and 2-mercaptobenzimidazole (2-MBI) are sulphur based organic compounds that are used as corrosion inhibitors for metals such as steels, copper, copper alloys, zinc, and aluminium alloys. Despite their wide scale acceptance and use as inhibitors, the detailed mechanisms by which the molecules interact with copper surfaces and subsequently their protective mechanisms in real-world conditions remain ambiguous. Moreover, the role of native surface oxides of copper on the interfacial bonding mechanisms and corrosion inhibition properties has been overlooked for the most part. The present work aims to clarify these issues along with determining the role of pH on the adsorption of the inhibitor molecules, the effect of electrochemical cathodic control of the surface on adsorption mechanisms, the influence of different active sites in the molecules, and lastly the stability of the organic films on anodic polarization. This was achieved by using an integrated approach of electrochemical methods and surface science analytical techniques such as X-ray photoelectron spectroscopy (XPS) and time-of-flight secondary ion mass spectrometry (ToF-SIMS).

Thesis Overview

The first chapter deliberates on the state of the art and provides a detailed literature review on the topic. It starts by recounting the principles of corrosion along with other key aspects of corrosion. It also details the passivation and corrosion of copper in various media and factors that may influence these phenomena. An introduction to inhibitors is given along with the mechanisms of inhibitor action so as to provide the reader with a background on the topic. Finally, the two sulphur based organic inhibitors, 2-MBT and 2-MBI, are reviewed in detail with a special focus on the bonding mechanisms and their role on corrosion inhibition.

Chapter two presents the experimental procedures, the instrumentation, and the techniques that have been used for this study. The procedure for sample preparation along with the set-up for the electrochemical experiments are described. The basic principles of XPS and ToF-SIMS are recalled followed by a detailed description of the experimental parameters used to characterize the surfaces and the subsequent data treatment of the analysis.

The third chapter characterizes the various copper surfaces - oxide free surface, mechanically polished surface, and electro-chemically polished surface. This is done in order to define the references (binding energies and full width at half maximums) of the copper sample for the

purpose of XPS analysis. Additionally, the effect of electro-polishing the copper sample is realized thus demonstrating its need prior to any experimental work.

In the fourth chapter, the corrosion inhibition offered by 2-MBT to copper surfaces in an acidic chloride media is investigated. Two differing surfaces are produced by cathodic pre-treatment of the copper surfaces either in the presence of or absence of the inhibitor. The surfaces are characterized by XPS and ToF-SIMS after adsorption of the inhibitor molecule followed by corrosion tests (cyclic voltammetry) to determine the efficacy of the pre-treatment methods for 2-MBT adsorption and consequently corrosion inhibition. A model is used to quantify the oxide layer and organic layer thickness which aids in the comparison of the two pre-treatment methods. Lastly, the anodically polarized samples were studied by surface analyses techniques to evaluate the changes in the organic layer and the formation of corrosion products, if any.

Chapter 5 discusses the adsorption of 2-MBT on copper in a 0.1 M NaOH solution along with its effects on anodic oxidation of the surfaces. Although a similar experimental approach is used for the analysis of the subject with surface analysis by XPS and ToF-SIMS and electrochemical tests by cyclic voltammetry, the objective of this chapter differs greatly. Here, the effect of 2-MBT on oxide film growth is investigated by first reducing the native oxide film and subsequently adsorbing the 2-MBT inhibitor on the surface in absence of chloride ions. Next, anodic oxidation tests were performed, in the Cu(I) potential range, to determine the effect of 2-MBT on the surface. The surface is characterized at the reduced state and the anodic state to examine the changes on anodic polarization, especially the effect of trapped oxide islands. Finally, a comparison is made on the adsorption of the molecule in an acidic and an alkaline environment based on both adsorption mechanisms and quantification of the thin films formed.

The sixth chapter evaluates the inhibition of the initial stages of corrosion of copper in a 0.5 M NaCl solution by 2-MBT. Additionally, the effects of interfacial oxides on the formation of the barrier layer have been scrutinized. Using an analogous approach to the previous two chapters, the formation of the organic barrier layer by initially cathodically pre-treating the surface followed by exposure to the inhibitor is studied by surface analysis. Next, cyclic voltammetry tests are performed to determine the inhibition of oxide growth as well as corrosion initiation by 2-MBT. Since this chapter concludes the work on 2-MBT adsorption in various media, a comprehensive passage describes the role of pH on the adsorption of 2-MBT on copper.

In chapter 7, the corrosion inhibition of copper by 2-MBI organic films in an acidic chloride medium is studied. The methodology used for this chapter is similar to that of chapter 4 to enable a fair comparison between the two inhibitors. Cathodic pre-treatment is used to

reduce the native oxides and the surfaces are then exposed to the inhibitor. The 2-MBI organic films formed on copper are characterized by XPS and ToF-SIMS. Corrosion tests are carried out to determine the inhibition offered by the organic films which are formed under different conditions. The evolution of the 2-MBI organic films upon polarization are evaluated by surface analysis techniques. Lastly, a model is presented to illustrate the structure of the formed organic films on the two copper surfaces and their evolution upon anodic polarization.

The major findings of the work have been presented in the conclusion. It is shown that despite numerous prior works on this topic, several major advances have been made in understanding the bonding mechanisms of 2-MBT and 2-MBI organic inhibitors on copper in various media, and ultimately the enhanced corrosion protection of copper by the two sulphur-containing organic inhibitors.

CHAPTER 1

State of the art

1.1 Corrosion

Corrosion is the process of degradation of materials due to exposure to the environment. It is a phenomenon experienced by most metals, except for noble metals such as gold and platinum. Corrosion causes a loss of strength of the material and can even alter the visage of the material. It results in a slow failure/destruction of the metals thus causing extensive damage, which has been estimated to be approximately 3.4% of the world's gross domestic product (GDP) [1]. Corrosion affects many fields and applications such as buildings, bridges, vehicles, airplanes, drinking water systems, oil and gas pipelines, railroads, and every other application where a metal is used. Figure 1.1 shows two artefacts from the Louvre Museum in Paris, one made from bronze while the other is made from gold, originating from Greece from the same time period (750 - 650 B.C.). While the bronze artefact shows scaling on its surface, the gold artefact does not exhibit any signs of degradation and maintains its lustre even after more than 2600 years.

The impacts of corrosion can be direct and indirect. Direct impacts refer to the damage caused by the failure, costs for the replacement of the material and/or the structure, as well as corrosion prevention costs [2]. Indirect impacts of corrosion, on the other hand, refers to things such as plant downtime, loss of product, safety issues, and most importantly the environmental effects caused by them [2]. In some cases, the indirect impacts of corrosion

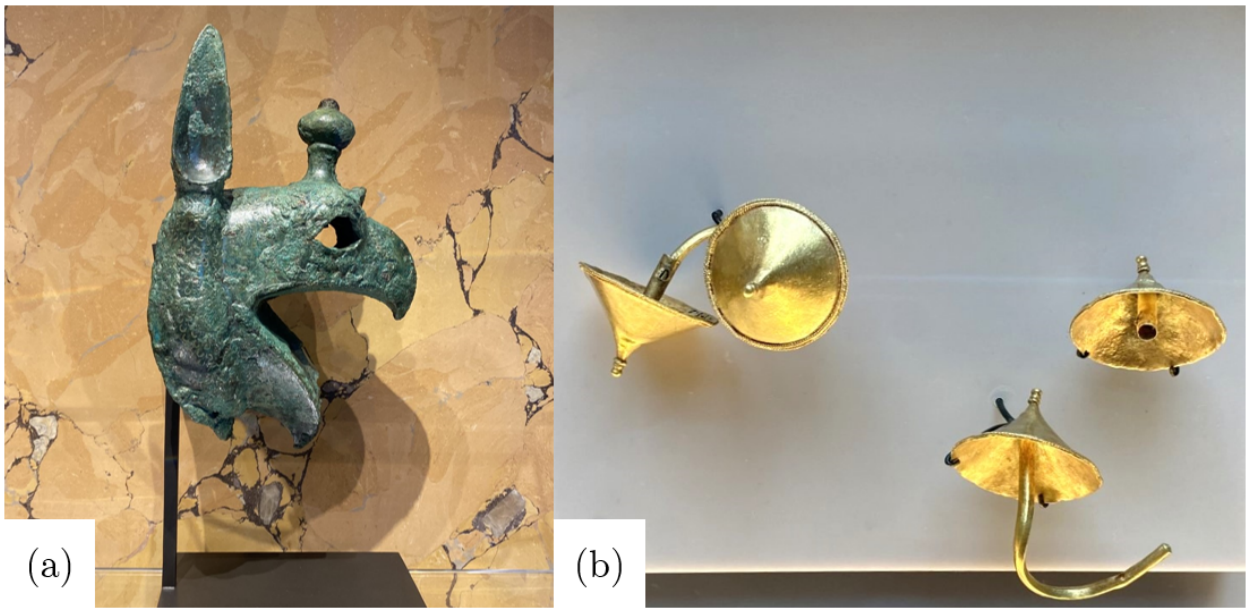

Figure 1.1: (a) A monumental griffin head made of bronze around the year 650 B.C. (Greece) that shows scaling due to corrosion attack on the ornament. (b) Clothing fasteners made of gold from the time period of 750 - 725 B.C. (Greece) showing no visible degradation of the material. Both images were taken by the author in the Louvre Museum, Paris.

may be much more severe and may far outweigh the direct impacts caused by it.

The Eiffel tower, which was completed in 1889, still stands today as one of the most iconic structures ever built by mankind. Since the entire structure is built by iron, it needs to be repainted every 7 years to protect the tower from corrosion. However, despite regular maintenance and periodic painting of the tower, corrosion of the iron structure can be observed in numerous parts of the tower, as seen in Figure 1.2.

Therefore, it is imperative to study this issue and prevent the degradation of metals as much as possible. This is done by using coatings, inhibitors, surface treatments to cover the metal surface, or in some cases, using other metals which are more prone to corrosion as sacrificial protection, or by adding alloying elements to the metal to form a protective oxide layer, or even by simply optimal design of structures which can prevent corrosion.

1.1.1 Principles of corrosion

The corrosion of a metal is an electrochemical process, which means that a flow of electrons occurs along with a chemical reaction during the process. Therefore, during electrochemical corrosion, two half-cell reactions occur at the same time but in different regions of the metal. If an electron is lost during the process, the reaction is known as an oxidation reaction, while

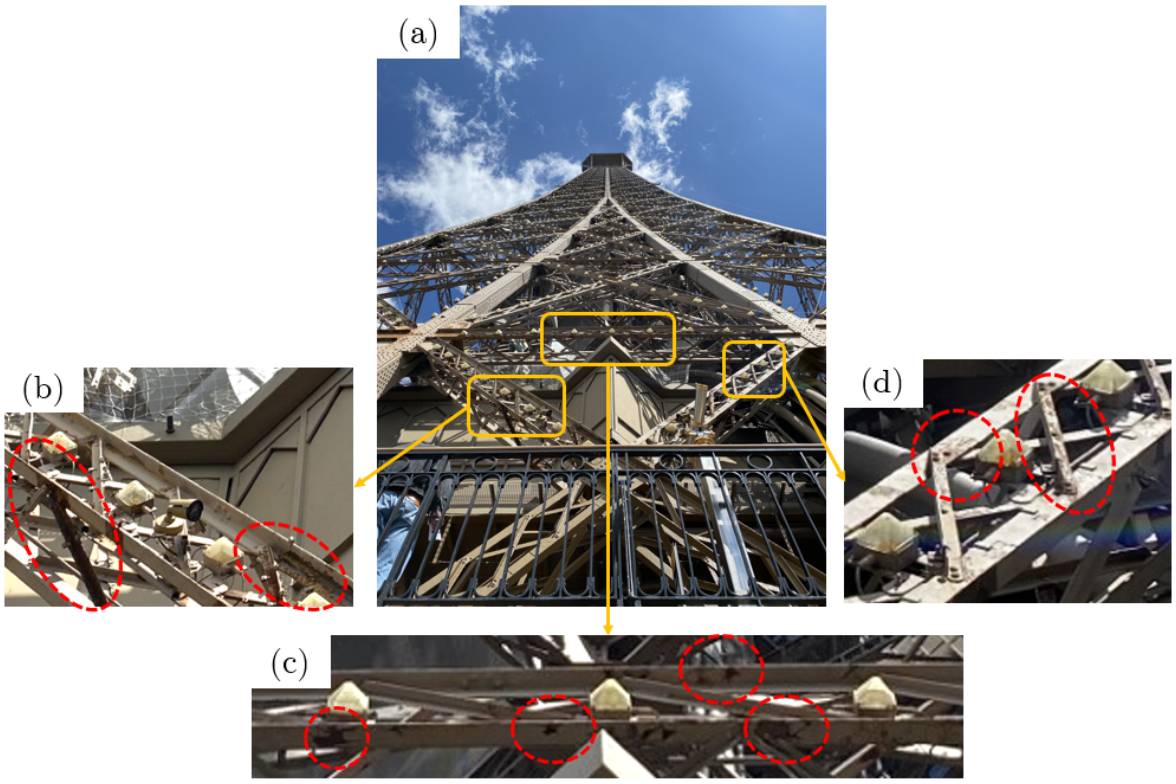

Figure 1.2: (a) The resounding 135-year-old Eiffel tower located in Paris, France. (b-d) Sections of the tower where corrosion of the iron structure is visible to the human eye. The images were taken by the author.

the gain of an electron is called a reduction reaction. The regions where the half-cell reaction occur are called anode for the oxidation reaction and cathode where the reduction reaction occurs. Figure 1.3 shows a schematic of the corrosion process with the anode and cathode regions along with the reactions occurring at each region.

The dissolution of metal, which causes the release of electrons, is an anodic process. This reaction is where the metal undergoes corrosion, and it is given as follows:

$$\mathrm{M} \longrightarrow \mathrm{M}^{\mathrm{n}+} + \mathrm{n}\mathrm{e}^{-}$$

Meanwhile, the reduction reaction depends on both the electrolyte and the environmental conditions in which the reaction is taking place. For example, in an acidic environment where the oxygen concentration is low within the electrolyte, the reaction is given as follows:

$$2\,\mathrm{H}^{+} + 2\,\mathrm{e}^{-} \longrightarrow \mathrm{H}_2$$

The above reaction is called the hydrogen evolution reaction, and it occurs due to the high concentration of H^{+} ions in the acidic environment combining with the electrons released during the dissolution of the metal.

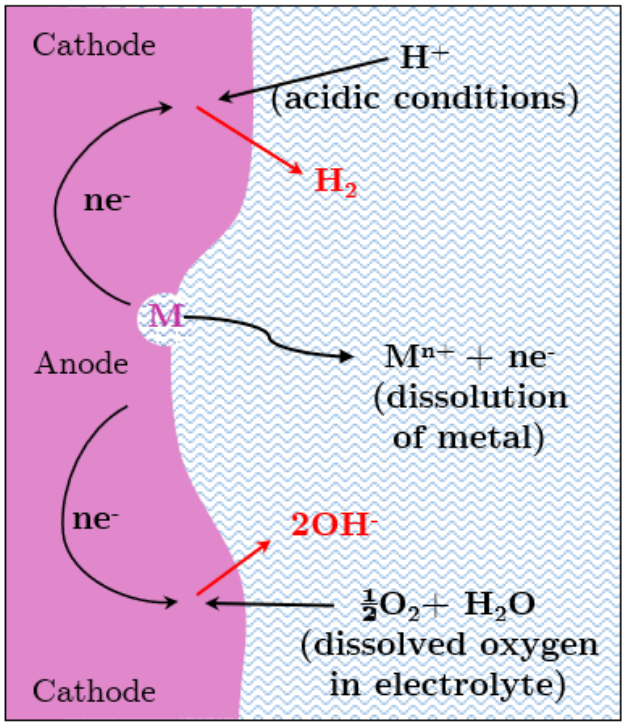

Figure 1.3: Schematic showing the process of corrosion with the anodic and cathodic reactions occurring for a metal M in an aqueous electrolyte.

On the other hand, in an aqueous electrolyte of neutral or basic pH with dissolved oxygen, the reduction reaction that occurs is called the reduction of dissolved oxygen to hydroxyl ions, and is given as follows:

$$\tfrac{1}{2}\,O_2 + H_2O + 2\,e^- \longrightarrow 2\,OH^-$$

1.1.2 Types of corrosion

Corrosion can be classified into two main categories: dry corrosion and wet corrosion. Dry corrosion occurs when the material chemically reacts with gasses in a dry environment. This process is especially expedited by high temperatures. Wet corrosion, also referred to as aqueous corrosion, occurs through electron transfer in the presence of liquids and is typically at room temperature. Wet corrosion needs 3 elements to occur - the metal, water, and a corrodent, such as oxygen, acids, agressive ions (such as Cl^- ions), CO_2, H_2S, or bacteria. The absence of even one of these three elements prevents corrosion from occurring.

Corrosion can occur in different forms in a material depending on the type of metal and the environmental it is exposed to. The most common type of corrosion in metals is general corrosion, also known as uniform corrosion. In general corrosion, the attack is uniformly distributed over the surface of the metal. Figure 1.4 illustrates the general corrosion attack

on a metal surface. Despite the wide coverage of general corrosion, it is not regarded as the most serious form of corrosion since it is relatively easy to predict based on the metal/alloy and the environmental conditions that cause it to corrode.

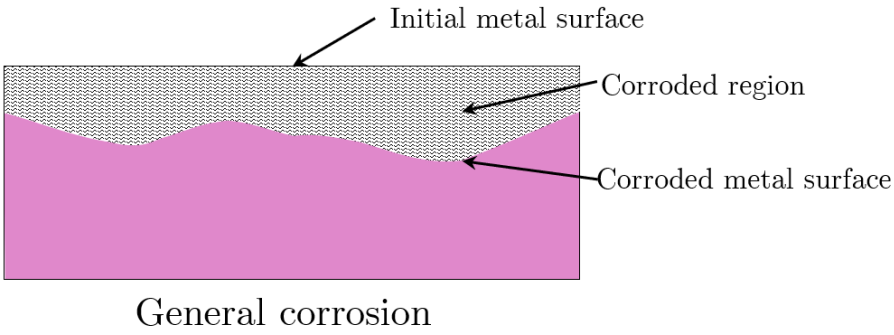

Figure 1.4: Schematic showing general corrosion attack on a metal surface.

Localised corrosion, on the other hand, is considered more serious in regard to the failure of a metal. It refers to the sudden and severe attack of the metal confined to a small surface area, while the remaining area undergoes attack at a much slower rate. The types of localised corrosion are pitting corrosion, intergranular corrosion, crevice corrosion, filiform corrosion, and microbial corrosion. These types of attack are shown in the illustrations given in Figure 1.5 and a few examples of the various types of corrosion observed by the author are shown in Figure 1.6.

- Pitting corrosion is a form of highly localised corrosion resulting in deep penetrations and cavities only in a few locations on the material. It is considered to be much more dangerous than uniform corrosion since it is more difficult to detect, predict, and protect against. Pitting is usually caused by aggressive ions such as Cl^-, Br^-, I^-, $SO_3{}^{2-}$, $NO_3{}^-$ ions which penetrate the self-formed oxide layer, which otherwise protects the metal surface, and then locally attacks the metal substrate [3–5].
- Intergranular corrosion is the selective attack of grain boundaries or closely adjacent regions without appreciable attack on the grains themselves. This form of corrosion is usually associated with chemical segregation effects or specific phases precipitated on the grain boundaries. Therefore, intergranular corrosion is mostly prevalent in alloys.
- Crevice corrosion occurs in confined spaces to which the access of the working fluid from the environment is limited thus creating a stagnant solution in that region. This type of attack tends to occur in crevices formed under gaskets, washers, fasteners, lap joints, and other similar geometries.
- Filiform corrosion is an attack that occurs on painted or coated surfaces. It results

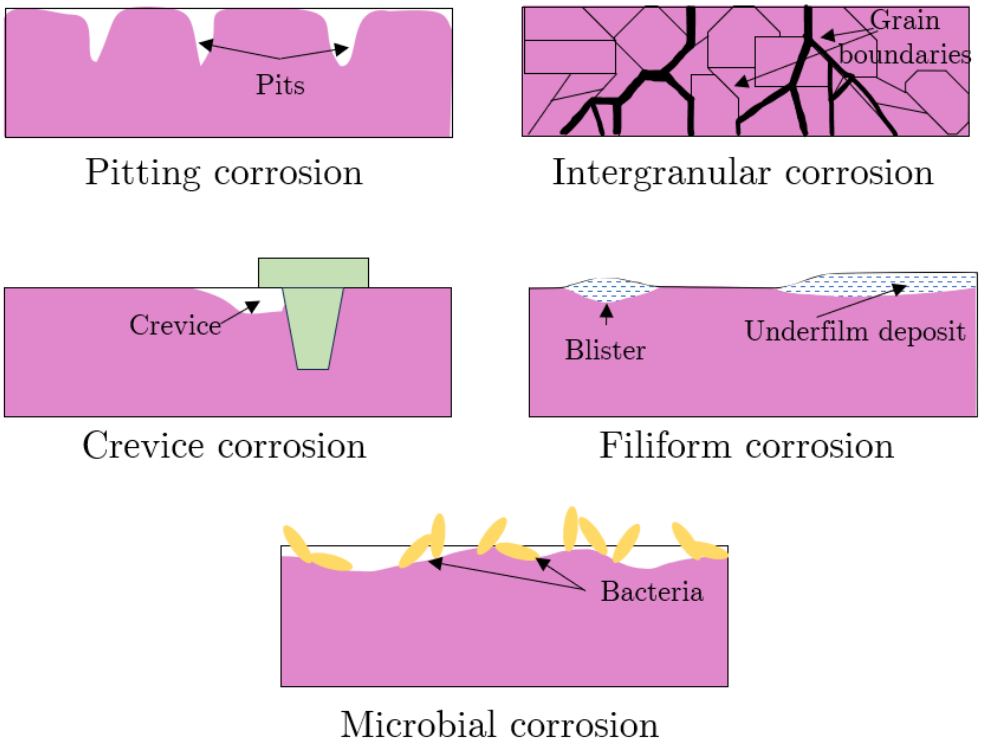

Figure 1.5: Illustration of the various forms of localised corrosion attack that can occur on a metal.

in threadlike superficial under-film corrosion originating from coating defects on the surface.

- Microbial corrosion, also known as microbiologically influenced corrosion (MIC), is a type of attack caused by micro-organisms such as fungi, algae, or bacteria. The microbes present in the environment, attach to the host metal and grow in biofilms [6, 7]. These can affect the cathodic and/or anodic reactions, thus altering the electrochemistry at the biofilm/metal interface and accelerating the corrosion process.

The environmental factors of a material, such as exposure to certain elements, can also be a cause of its degradation resulting in a brittle fracture of the material. This type of attack is referred to as environmentally induced/assisted cracking. The different types of environmentally induced cracking are stress corrosion cracking, corrosion fatigue, and hydrogen-induced cracking. These are shown in the illustrations in Figure 1.7.

- Stress corrosion cracking occurs due to a combined effect of the corrosive environment and the tensile stresses, which can originate from inside or from outside the metal. The resulting cracks grow very fast eventually leading to failure. The landing gears of aircrafts are often affected by this type of degradation.

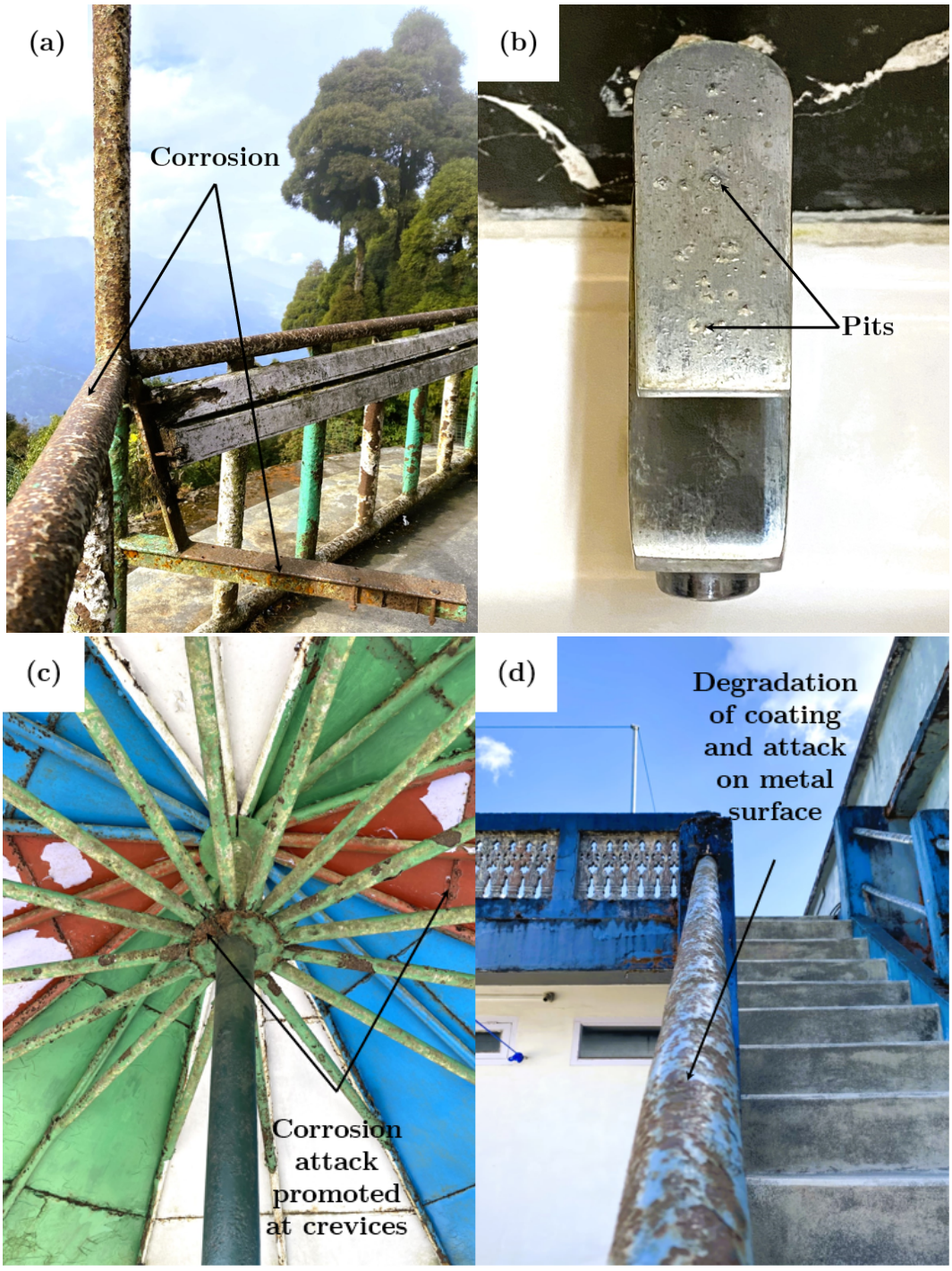

Figure 1.6: The different types of corrosion attack observed by the author: (a) general corrosion on the structure of a gazebo and its bench frame that has been exposed to the environment for a very long period of time. (b) pits formed on a stainless-steel tap due to high quantity of impurities in the water, (c) corrosion attack promoted on the joints (crevices) of an outdoor tent structure, and (d) attack on the surface of a metal pipe after degrardation of the applied coating.

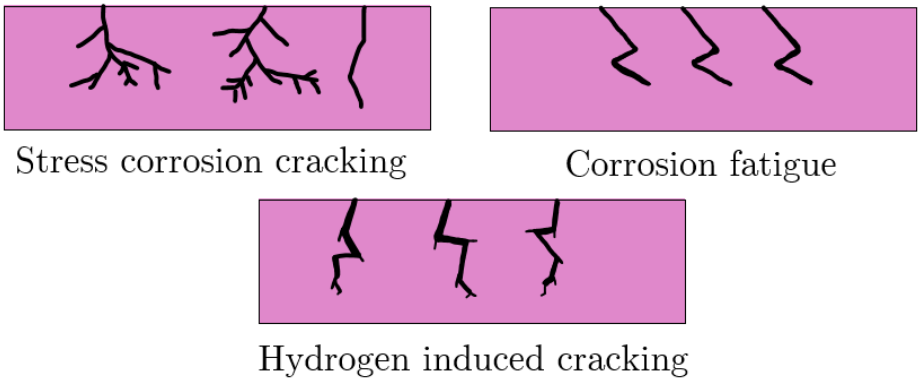

Figure 1.7: Illustration showing the various forms of environmentally induced cracking that can occur on a metal.

- Corrosion fatigue is the result of cyclic stresses on a material in a corrosive environment. It usually occurs in structures that are prone to vibrations such as aircraft wings, bridges, and offshore platforms.
- Hydrogen induced cracking or hydrogen embrittlement is caused by the permeation of hydrogen within a metal, reducing the ductility and load-bearing capacity of the metal, thus causing cracking and failure of the metal at stresses below the yield stress.

Lastly, we have a type of corrosion that falls in neither category mentioned above. However, this type of corrosion is rather serious and affects almost every application where two different metals or even alloys of the same metal are in electrical contact with each other. This type of corrosion is called galvanic corrosion. It is an accelerated corrosion process that occurs due to an electrical contact of the metal with a more noble metal in a corrosive environment. For example, if aluminium is in contact with copper, aluminium being less noble will corrode while copper will be protected in the corrosive environment. A schematic showing galvanic corrosion is given in Figure 1.8.

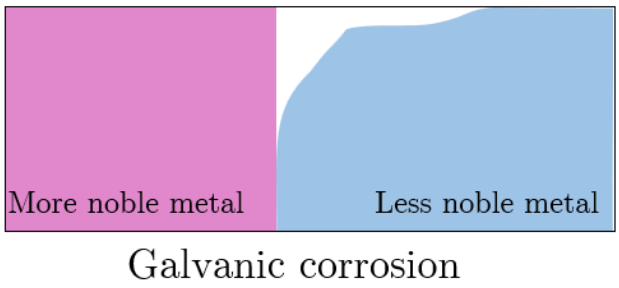

Figure 1.8: Schematic showing the attack on a less noble metal due its galvanic effect with a more noble metal.

Galvanic corrosion plagues every structure where metals are in contact, even in cases of

minimal contact. Welds between metals or even in the same metal experience galvanic attack due to the change in metal properties on welding. A screw or a bolt passing through another metal is also grounds for galvanic attack, if the metal/alloy used for the screw is different from the metal. Therefore, galvanic corrosion can have drastic consequences if it is not considered while designing and building the metal-based component.

Figure 1.9 shows a galvanic couple of a copper pipe and a stainless-steel tap. Due to the higher corrosion resistance of stainless steel, copper acts as the anode and undergoes galvanic attack. Additionally, the attack is more pronounced on the hot water tap side due to the effect of heat on the corrosion reactions occurring on the system.

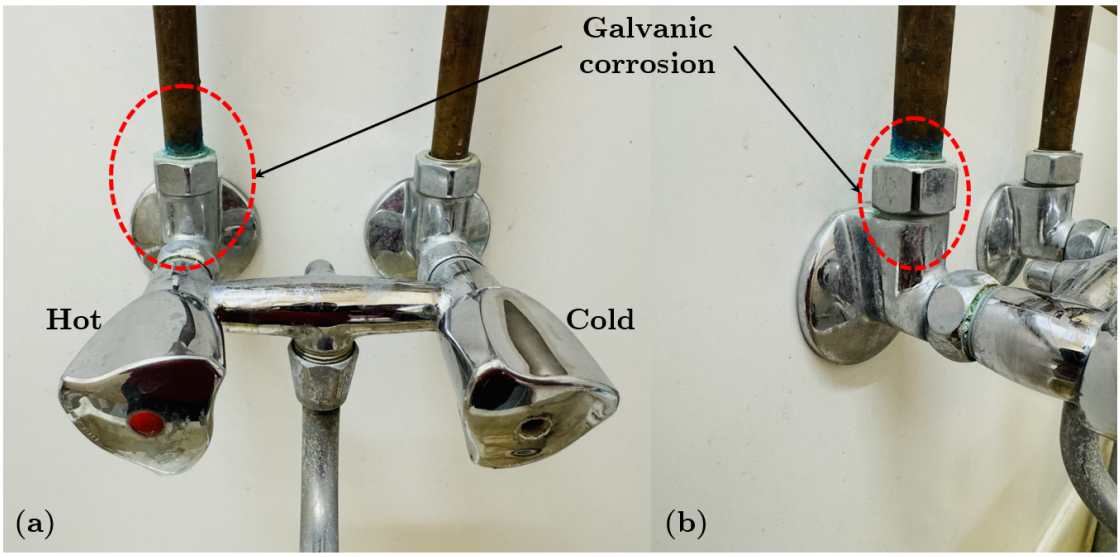

Figure 1.9: Galvanic attack at the interface between a copper pipe and a stainless-steel tap. Copper undergoes attack as it is less resistant to corrosion than stainless steel. (a) Front-view of the entire tap showing both the hot and cold water pipes, and (b) Side-view showing the hot water pipe.

1.1.3 Relation between pH and potential: Pourbaix diagrams

The corrosion of metals depends on both the pH of the environment and the potential applied to the metal. Therefore, a relation between the two factors gives us an equilibrium plot which defines the regions of corrosion, immunity, and passivity of a metal. These E-pH plots for metals are referred to as "Pourbaix diagrams," first constructed by Marcel Pourbaix in 1945 [8]. The Pourbaix diagrams also indicate regions where certain species of the metal are thermodynamically stable. A general Pourbaix diagram of a metal (M) is shown in Figure 1.10, with the regions of immunity, passivity, and corrosion marked.

Before we go into the details of the Pourbaix diagram, it is necessary to understand the

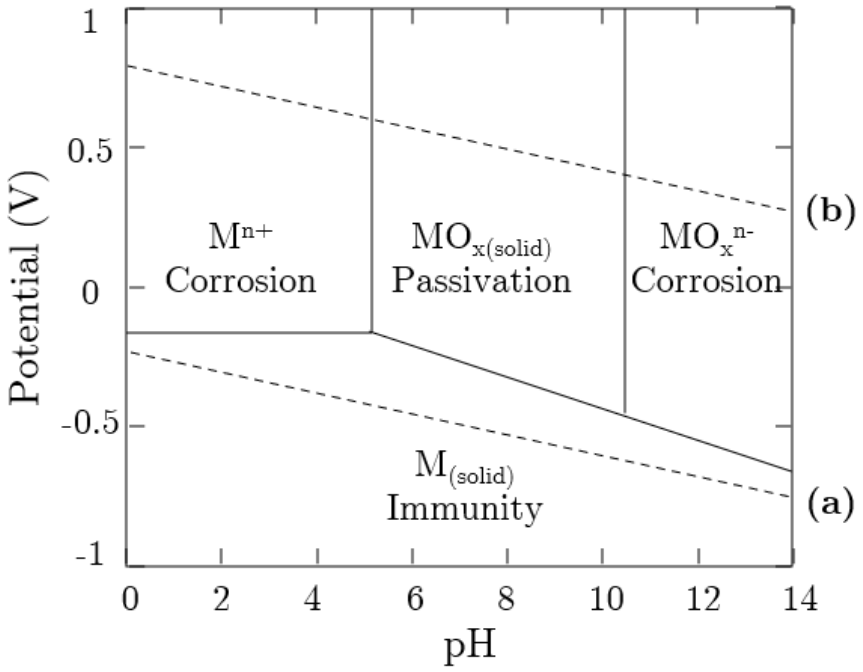

Figure 1.10: The Pourbaix diagram constructed for the system of a metal M and water at a fixed temperature.

states of the metal that are shown in the diagram. We have already discussed about the corrosion of a metal in detail above. Here, we exemplify what the immunity and passivity of a metal entail. The immunity of a metal is defined as the state in which the metal is thermodynamically stable in a particular environment and therefore corrosion does not occur spontaneously. For example, gold and platinum exhibit immunity in atmospheric conditions and do not undergo corrosion spontaneously.

Passivity is referred to as the reduction in chemical/electrochemical activity of a metal due to the reaction of the metal with its environment, thus forming a protective film on the metal surface. The protective film formed on most metals is usually metal oxides or metal hydroxides such as Cu_2O on copper and Al_2O_3 or $Al(OH)_3$ on aluminium. These act as a physical barrier against the corrodent thus restricting its access to the metal surface.

The regions of corrosion, passivity, and immunity of metal M as a function of pH and potential are shown in Figure 1.10. Below the potential of -0.7 V, this metal exists in its metallic state at all pH conditions and therefore exhibits immunity from corrosive attack. In acidic conditions, from pH 0 to 5, the immunity of the metal is extended up to a potential of -0.2 V, above which the metal undergoes corrosion attack to form M^{n+} ions. In neutral and near neutral conditions, i.e. between the pH of 5 and 10, the metal exhibits passivation. This occurs due to the oxidation of its surface resulting in the formation of a protective oxide layer

MO_X. Finally, above the pH of 10, in highly basic conditions, the metal again undergoes corrosion.

The region between the two dashed lines in the Pourbaix diagram indicates the stability region of liquid water. The top line corresponds to the anodic evolution of oxygen while the bottom dashed line corresponds to the hydrogen evolution reaction [8, 9]. When the potential applied is below the line (a) at a certain pH value, the cathodic evolution of hydrogen gas (H_2) occurs. Above line (a), H_2 gas is not stable, instead its oxidized species H^+ ions is stable in acidic conditions and OH^- ions is stable in basic conditions. These reactions are given as follows:

In acidic solutions:

$$2\,H^+ + 2\,e^- \longrightarrow H_2$$

In basic solutions:

$$2\,H_2O + 2\,e^- \longrightarrow H_2 + 2\,OH^-$$

When the potential applied is higher than the line (b), water molecules are oxidised to obtain oxygen gas.

$$2\,H_2O \longrightarrow O_2 + 4\,H^+ + 4\,e^-$$

The reactions discussed above are derived from the Pourbaix diagram of water [8], thus giving us the stability of water and its ions under various conditions.

1.1.4 Protection against corrosion

The consequences of corrosion demand that the metals used for various applications need to be protected from corrosion. In each field, whether it is aviation, construction, automobiles, medical implants, energy production, or electrical devices, there needs to be a control against corrosion. However, in each application, the type of protection varies due to the feasibility of the protection method used.

1. Proper selection of metal - The first and most important type of protection against corrosion that can be considered is the proper selection of the metal or alloy. An appropriate selection of metal/alloy for a particular application can avoid major corrosion issues. The selected metal/alloy may not even require further protection if the metal fits the application. One major area where this protection method is applicable is the appropriate selection of screws and bolts based on the metal it will be attached to. Ideally, the screw or the bolt should be of the same metal/alloy as the structure so as to avoid the formation of a galvanic couple. However, this is not feasible since the

metal may not have the required physical properties to function as a screw or bolt. Therefore, one needs to consider the activity or the nobility of the metal in question and use a screw/bolt with similar activity.

2. Efficient design of structures - Another method of corrosion control is an efficient design of the metal structures. This method too can avoid numerous issues in terms of corrosion. This method includes avoiding crevices, making smooth bends instead of sharp corners, adequate ventilation and drainage of regions that may accumulate moisture or water, heat treatment of welded regions, and avoiding or minimizing contact between two different metals.

3. Cathodic protection - Cathodic protection is a method of corrosion protection in which the metal to be used is forced to behave as a cathode. This is executed by two different methods. The first method is called impressed current method where a direct current is applied to the metal in the opposite direction of the corrosion current to counter its effects [10]. The second method is the use of a protective anode which is connected to the metal to be protected [11]. This method uses the principle of galvanic corrosion by taking a protective anode with a higher activity. This anode then undergoes corrosion while connected to the metal to be protected, thus sacrificing itself. An example of the sacrificial anode method is the use of zinc or magnesium for protection of iron and its alloys [12, 13]. Both these methods are widely used for protection of pipelines that are buried in the soil and for the protection of ship hulls from seawater.

4. Modifying the environment - Just as proper selection of metals and better design of structures can help control corrosion, modifying the environment conditions can also curtail corrosion on metals. This is achieved by eliminating dissolved oxygen from the electrolyte, reducing moisture in the environment, or by reducing the acidity of the environment. However, these methods have limited applications and cannot be used everywhere. For example, an oil pipeline that is at the bottom of the ocean is exposed to moisture, oxygen, and even acidity, all of which cannot be modified at that scale.

5. Surface treatments - Surface treatments such as chemical treatments, passivation, anodizing, are effective methods for corrosion protection of metals. They alter the state of the surface mostly by forming films that are non-porous, thus restricting the exposure of the surface to the environment. The anodizing of aluminium is a widely used method for the protection of aluminium and its alloys.

6. Protective coatings - The use of protective coatings for corrosion protection has found its way into numerous applications such as pipelines for oil, automobiles, aerospace structures, and even for protection of bridges and other metallic structures. They can

be metallic, organic, polymer, and even ceramic based coatings. Coatings function as inert barriers at certain temperatures, pressure, and environments, which prevents the contact of the metal to the environment. Coatings can be multi-layered, each serving a different purpose such as protection, adhesion, and aesthetic, or they can also serve the same purpose of protection but with redundancy for increased protection.

7. Inhibitors - Lastly, inhibitors can also be used for protection of metals against corrosion. They are chemical compounds that are introduced in minute quantities to supress the corrosion reactions from occuring on the metal. This is discussed further in detail in the following section.

1.2 Copper

Copper, derived from the latin term "Cyprium aes," which means a metal from Cyprus, is a transition metal with an atomic number of 29 and a molecular weight of 63.546 g/mol [14]. The structure of copper is that of a face centred cubic (FCC) crystal structure. It is the 25th most abundant element in the earth and is one of the few metals which is also found in its metallic form, along with various copper ores. The colour of copper metal is described as a reddish golden, or alternatively as a pinkish orange, lustrous colour. Due to its high melting point of 1083°C [14], copper is an excellent conductor of heat and electricity. Additionally, it is a soft metal with high ductility and malleability.

The properties of copper allow it to be used extensively for numerous applications. Some of its uses are as follows:

- Electrical wires and components,
- Pipes for drinking water and sewage systems,
- Roofing of buildings,
- Industrial machinery such as heat exchangers,
- Pipeline components for oil and gas transport,
- Cannisters for nuclear waste storage and burial,
- Jewellery and coins.

One of the most well-known examples of copper used for building a structure is the Statue of Liberty in New York, USA, which was inaugurated in 1886. Although the 46 metres copper statue was initially a hue of brown, it turned green over the years due to the formation of patina on its surface from its interaction with oxygen, moisture, and carbon dioxide from the atmosphere, completing its transformation by 1920. Figure 1.11 shows a bronze replica of the Statue of Liberty located at the Île aux Cygnes in Paris.

For further use of copper, especially in cases where higher strength is required, it is alloyed with other metals to obtain superior properties. Copper has numerous alloys, as many as 400 different types. However, the most commonly used copper alloys are brass (alloyed with zinc), bronze (alloyed with tin or aluminium), and cupronickel (alloyed with nickel). Copper is also alloyed with silver and gold for jewellery applications due to their increased hardness, malleability, melting point, and finally a more elegant hue. A few examples of the use of copper alloys are given in Figure 1.12.

Figure 1.11: The Statue of Liberty is one of the best examples of the use of copper metal. The green film on the copper structure is due to its interaction with water, carbon dioxide, and air, resulting in the formation of patina. The image given above is a bronze replica of the Statue of Liberty located at the Île aux Cygnes, Paris.

1.2.1 Passivation of copper

The passivation of copper occurs by the formation of oxide and hydroxide films on its surface, depending on the potential and the pH [15, 16]. To understand this better, we consider the Pourbaix diagram of copper metal in a water system at 25°C [8, 17], given in Figure 1.13. From the Pourbaix diagram, we observe that copper undergoes corrosion below pH 5 in acidic conditions and also above pH 13 in highly alkaline conditions. On the other hand, when the potential is less than -0.2 V, copper is in its immune or metallic state in all pH conditions.

Copper experiences passivity in the pH range between 5 and 13, with the formation of Cu_2O (Cu(I)) oxide layer initially. Cu_2O, also known as cuprous oxide, is a red coloured solid compound that forms naturally on copper surfaces exposed to air. At higher potentials, copper is further oxidized to its Cu(II) state, resulting in the formation of CuO oxide layer,

Figure 1.12: Alloys of copper used for various applications: (a) A brass utensil from India used for cooking, (b) a bronze fibule (fastener) from the time period of 750 - 700 B.C. (Greece), and (c) a gold-silver-copper alloy reliquary triptych from the year 1254 A.D. (Abbaye de Floreffe, Belgium). Images (b) and (c) were taken at the Louvre Museum, Paris.

which is a black solid. These oxide layers are known to protect the copper metal surface from corrosion attack since they physically hinder the access of the corrosive ions to the metal surface, therefore not allowing the electrolyte to directly interact with the metal. The oxidation of copper metal to its oxides in air is given by the following equations [18]:

$$4\,Cu + O_2 \longrightarrow 2\,Cu_2O$$

$$2\,Cu_2O + O_2 \longrightarrow 4\,CuO$$

When the oxidation of copper metal occurs in the presence of water, Cu(I) oxide or Cu_2O is formed by the following reaction [16, 19]:

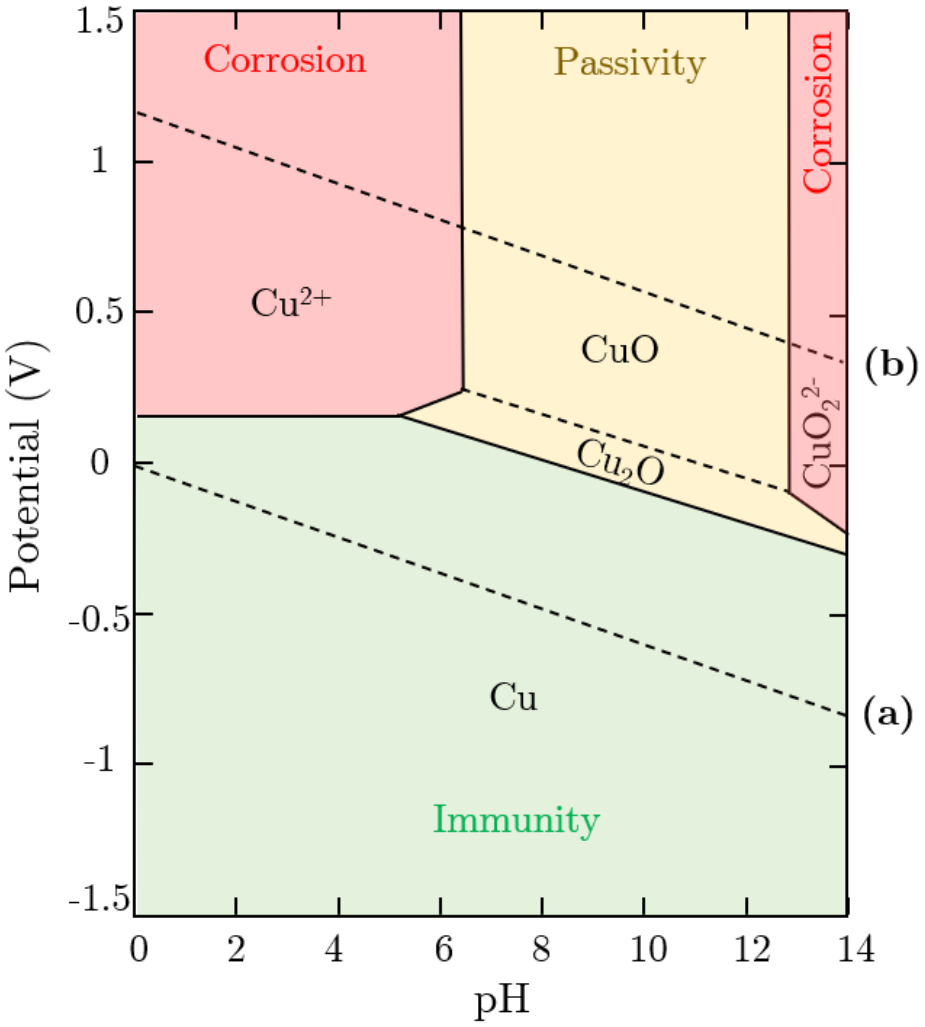

Figure 1.13: The Pourbaix diagram of a copper-water system at 25°C. The figure is recreated from the Atlas of Electrochemical Equilibria in Aqueous Solutions by Marcel Pourbaix [8].

$$2\,Cu + H_2O \longrightarrow Cu_2O + 2\,H^+ + 2\,e^-$$

The oxidation of copper has been studied in detail by numerous authors [20–28]. Among others, Wiame et al. discussed the initial stages of copper oxidation when copper is exposed to gaseous oxygen at low pressure [27], while Pinnel et al. studied the effect of temperature and air quality on the growth of copper oxide [28]. Several studies were also performed on the formation of the oxide layers by anodic polarization of the surface in alkaline solutions such as NaOH, KOH, and borate buffer solutions [20–26]. In alkaline environment, it has been evidenced that copper first oxidizes to form a Cu_2O layer of approximately 1 nm in thickness above the copper metal surface upon anodic polarization. This is followed at higher potential by the formation of a $Cu(OH)_2$ (copper(II) hydroxide) and CuO mixed second layer of 2 - 4 nm thickness on top of the Cu_2O oxide layer [22, 25, 26]. An illustration showing the

structure of the oxide layers in an alkaline environment are given in Figure 1.14.

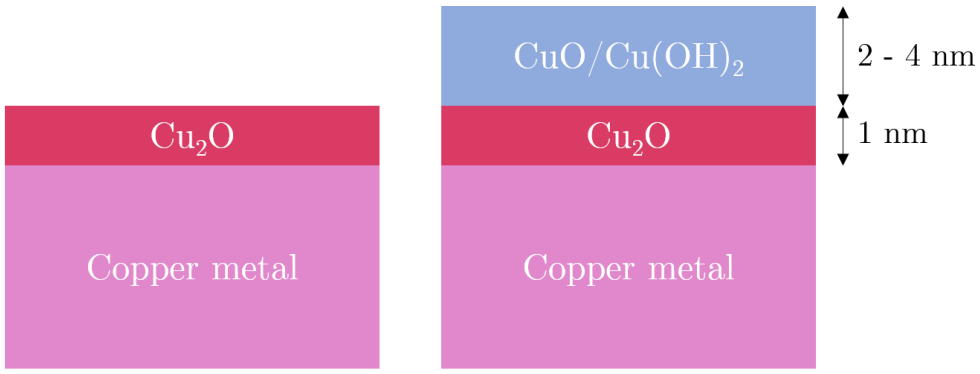

Figure 1.14: Schematic showing the structure of the copper oxide films on the copper metal surface in alkaline conditions. The illustrations are recreated from the work of Kunze et al. [25]

The oxidation of copper in a weak alkaline environment has been theorized by two methods. The first method [29] hypothesizes that copper is first oxidized to form copper(I) hydroxide which is adsorbed on the surface. This is then further oxidized to form copper(I) oxide, i.e. Cu_2O.

$$Cu + H_2O \longrightarrow Cu(OH)_{ads} + H^+ + e^-$$

$$2\,Cu(OH)_{ads} \longrightarrow Cu_2O + H_2O$$

Alternatively, the second method suggests the direct oxidation of copper to form Cu_2O, similar to the oxidation of copper in water [22, 30].

$$2\,Cu + H_2O \longrightarrow Cu_2O + 2\,H^+ + 2\,e^-$$

Once the copper(I) oxide or Cu_2O is formed, further oxidation results in the formation of both $Cu(OH)_2$ and CuO. This is given by the following reactions [22, 30]:

$$Cu_2O + 3\,H_2O \longrightarrow 2\,Cu(OH)_2 + H_2$$

$$Cu_2O + H_2O \longrightarrow 2\,CuO + 2\,H^+ + 2\,e^-$$

In highly alkaline solutions, i.e. when the concentration of OH^- ions is higher, the oxidation of copper follows a slightly different mechanism [20, 21, 23, 31]. First, the adsorption of OH^- ions occurs by the following reaction:

$$Cu + OH^- \longrightarrow Cu\text{–}OH_{ads} + e^-$$

Next, the oxidation of copper to copper(I) oxide takes place along with the conversion of the adsorbed hydroxides to copper(I) oxide. These are given by the following reactions:

$$2\,\mathrm{Cu{-}OH_{ads}} \longleftrightarrow \mathrm{Cu_2O} + \mathrm{H_2O}$$

$$2\,\mathrm{Cu} + 2\,\mathrm{OH^-} \longrightarrow \mathrm{Cu_2O} + \mathrm{H_2O} + 2\,\mathrm{e^-}$$

Cu_2O is then further oxidized to CuO and $Cu(OH)_2$ by the following reactions:

$$\mathrm{Cu_2O} + 2\,\mathrm{OH^-} + \mathrm{H_2O} \longrightarrow 2\,\mathrm{Cu(OH)_2} + 2\,\mathrm{e^-}$$

$$\mathrm{Cu_2O} + 2\,\mathrm{OH^-} \longrightarrow 2\,\mathrm{CuO} + \mathrm{H_2O} + 2\,\mathrm{e^-}$$

Additionally, if the entire Cu_2O is already oxidized while the high potential is applied, CuO is formed by a direct reaction from Cu, which is given as follows [20]:

$$\mathrm{Cu} + 2\,\mathrm{OH^-} \longrightarrow \mathrm{CuO} + \mathrm{H_2O} + 2\,\mathrm{e^-}$$

1.2.2 Corrosion of copper

Copper, like most metals, is susceptible to corrosion attack in certain environments despite its high nobility among other metals. The types of corrosion attack that have been reported for copper are mainly general corrosion, intergranular attack, and pitting corrosion. If the conditions are met, copper can also undergo crevice corrosion and galvanic corrosion. Despite the use of copper as an antimicrobial agent, it is also susceptible to microbiologically induced corrosion with the sulphate-reducing bacteria considered as the most corrosive micro-organism for copper [6].

Although copper is somewhat protected in neutral and alkaline environments due to the formation of a passive oxide film that covers and protects the surface [20, 21, 30, 32], it is highly vulnerable to attack in acidic environments where this oxide film readily dissolves thus leaving the metal substrate exposed to corrosive agents [15, 33–36]. As seen from the Pourbaix diagram in Figure 1.13, in acidic conditions where the pH is less than 5, copper undergoes corrosion. This has been attributed to the instability of the copper oxide layers in this pH range, which usually protects the metallic substrate by acting as a physical barrier between the environment and the metal. The dissolution of the copper oxide in an acidic environment is given by the reaction below:

$$\mathrm{Cu_2O} + 2\,\mathrm{H^+} \longrightarrow 2\,\mathrm{Cu^+} + \mathrm{H_2O}$$

The exposed metal substrate then undergoes attack by the following reaction [37]:

$$2\,\mathrm{Cu} + 4\,\mathrm{H^+} + \mathrm{O_2} \longrightarrow 2\,\mathrm{Cu^{2+}} + 2\,\mathrm{H_2O}$$

1.2.3 Effect of chloride ions

In environments where the pH is higher than 5, i.e. in neutral and alkaline conditions, it is expected that the oxide layers are stable and prevent corrosion. However, this is not always the case. Aggressive species such as chlorides and nitrates in high concentrations can still penetrate these oxide layers to interact with the metallic substrate [33, 34, 38], causing passivity breakdown and the initiation of localized corrosion [39–42].

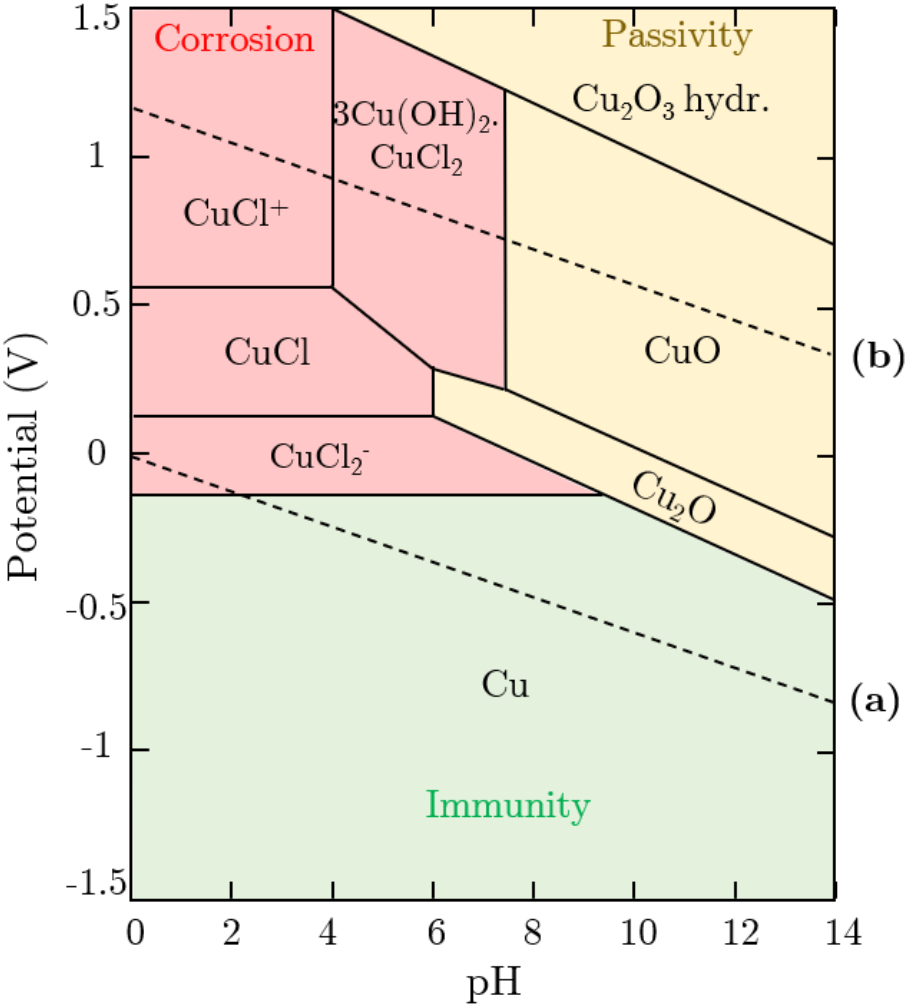

Figure 1.15: Pourbaix diagram of a copper-chlorine-water system at 25°C with a chloride concentration of 1 mol/kg. The Pourbaix diagram is recreated from the work of F. King [18].

The Pourbaix diagram for the Cu-Cl-H_2O system at 25°C for a chlorine concentration of 1 mol/kg [18] is given in Figure 1.15. The regions of corrosion in the acidic domain for this system has increased compared to that of the Cu-H_2O system seen in Figure 1.13. Additionally, the formation of copper chloride species begins at a potential of -0.2 V, initiating corrosion attack on the metal. This is at a lower potential compared to the system without chlorides,

where corrosion initiates at 0.2 V.

Chloride ions also compete with water molecules for adsorption on the metal surface, thus poisoning or even blocking the formation of the passive oxide film that otherwise provides protection to the substrate in pH conditions where copper oxides are stable (pH > 5) [37, 39]. On passivated copper surfaces, chloride ions can adsorb and penetrate the surface oxide film, causing passivity breakdown followed by initiation of localised corrosion (pitting) with the formation of copper chlorides [3, 34, 43, 44]. The breakdown of the passive oxide film has been widely discussed and it has been proposed to occur locally at weak sites of the protective layer including grain boundaries and defective sites in the oxide film [5, 16, 39, 45–47].

The electro-dissolution of copper in chloride containing acidic solutions has been hypothesized by three different mechanisms [33–36, 48, 49]. Although the end result for all three reactions is the formation of cuprous chloride, it is the process which is still unclear to this date. The first hypothesis considers the direct formation of $CuCl_2^-$ from the metal when it interacts with chloride ions [48, 49]. The second one hypothesizes that the copper metal is first converted to Cu^+ ions, after which it interacts with chloride ions to form $CuCl_2^-$ [34].

1st hypothesis:

$$Cu + 2\,Cl^- \longrightarrow CuCl_2^- + e^-$$

2nd hypothesis:

$$Cu \longrightarrow Cu^+ + e^-$$

$$Cu^+ + 2\,Cl^- \longrightarrow CuCl_2^-$$

Lastly, in the third hypothesis, copper interacts with chloride ions to initially form a cuprous chloride species which is adsorbed on the copper surface. This is followed by the formation of a soluble $CuCl_2^-$ film [29, 33, 35, 36, 50].

3rd hypothesis:

$$Cu + Cl^- \longrightarrow CuCl_{ads} + e^-$$

$$CuCl_{ads} + Cl^- \longrightarrow CuCl_2^-$$

In neutral and alkaline conditions, $CuCl_2^-$ may further undergo hydrolysis to form copper(I) oxide [34, 51, 52], as shown by the reaction below. However, the formation of $CuCl_2^-$ by the electro-dissolution of copper remains the same as in acidic media.

$$2\,CuCl_2^- + 2\,OH^- \longrightarrow Cu_2O + H_2O + 4\,Cl^-$$

1.3 Inhibitors

One technique for corrosion control is the application of inhibitors, which are chemical compounds that suppress reactions from occurring on a metal surface by forming an isolating barrier on the surface, thus inhibiting corrosion of the metal [37, 53–55]. An illustration showing the inhibitor barrier layer formed on a metal surface is given in Figure 1.16. These compounds are added in very small quantities either to the environment, such as in the electrolyte or within the coatings, or directly to the metal surface, which can in turn reduce the rate of corrosion or block it entirely.

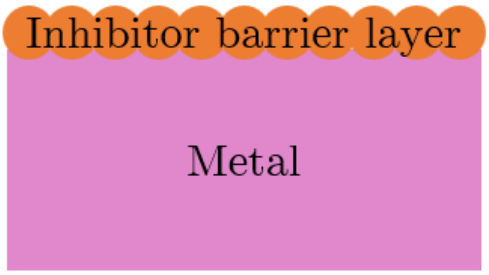

Figure 1.16: Schematic of an inhibitor deposited on a metal surface forming a barrier layer.

The application of inhibitors for corrosion control and prevention is widespread. It is used in pipelines for oil and gas, for aeronautic applications, in cooling systems, and other industrial applications. For a particular inhibitor to be viable for its use on a metal, it needs to fulfill certain requirements. The main criteria for inhibitor selection are as follows:

- The inhibitor should be commonly available,
- It should be cost effective,
- It should be effective for the metal and its application,
- It should have no/limited toxicity,
- It should not have any adverse effects on the environment,
- It must not deteriorate the properties of the material - chemical, physical, or mechanical.

1.3.1 Mechanisms of inhibitor action

Corrosion inhibitors interact with the metal surface by one of three mechanisms to protect the surface [56, 57]. These mechanisms are as follows:

Oxide film formation - In this mechanism of corrosion protection, the inhibitors use the dissolved oxygen in the electrolyte as an oxidant, thus promoting the formation of a condensed

and non-porous oxide film on the metal surface. This results in the blocking of the metal ionization process, thereby slowing down the corrosion of the metal. This mechanism of inhibitor action has a high efficiency in corrosion protection and is therefore widely used.

Precipitation film formation - By this mechanism, the inhibitor molecules either react with other inhibitor molecules or with metal ions that have been released from prior corrosion of the metal. The resulting compound precipitates on the surface as a film and can block the anodic regions, the cathodic regions, or the entire surface of the metal, thus resulting in suppression of chemical reactions that may occur on the metal surface.

Adsorption film formation - Some inhibitors adsorb on the metal surface to form a barrier layer between the corrosive species and the metal surface. This can occur by physisorption of the molecule or by chemisorption of the molecule. Physisorption uses physical attractive forces between the molecule and the metal surface such as hydrogen bonds, Van der Waals forces, or polar forces to attract the molecules to the surface thereby forming an adsorption film. On the other hand, chemisorption occurs due to the sharing of electrons between the metal surface and the polar part of the inhibitor molecule. This results in a stronger and more stable chemical bond between the molecule and the metal surface. However, this also changes the charge state and the interfacial properties of the metal surface and is thereby an irreversible process.

1.3.2 Types of inhibitors

Inhibitors can be classified based on two principal factors: the chemical nature of the inhibitor molecule, or the effect of the inhibitor molecule on the electrochemical reactions occurring. Based on its chemical nature, corrosion inhibitors can be divided into two types - organic inhibitors and inorganic inhibitors.

Organic inhibitors - As the name suggests, these inhibitors are chemical compounds that are mainly carbon based. They have been widely accepted due to their compatibility with numerous metals, effectiveness in a wide range of temperatures, good solubility in water and solvents, low toxicity, and low costs. These inhibitors usually have at least one active site or a heteroatom that is capable of either exchanging electrons with the metal and/or interacting with the metal surface to form bonds [57]. Nitrogen, oxygen, phosphorous, and sulphur are some of the heteroatoms which act as active sites when they are present in the inhibitor molecule. The structure of the organic inhibitors defines the efficiency of their protective capabilities. Organic inhibitors are known to protect the metal surface by adsorbing and forming a protective film on the surface. The concentration of the inhibitor plays an important role on the efficiency of the inhibitor with the corrosion rate decreasing as the concentration

of the inhibitor added is higher [57]. Organic inhibitors include groups of amines, phosphates, azoles, amino acids, carboxyls, and so on [37, 55, 57].

Inorganic Inhibitors - These inhibitors are usually mineral molecules and protect the surface by either passivating the surface by promoting oxide layer formation, or by precipitating on the surface [56, 57]. Either method restricts the access of the corrodents to the metal surface by forming a barrier between the corrodents and the metallic surface. These inhibitors are used for applications where organic inhibitors are not reliable such as at high temperatures and for long periods of time. Inorganic inhibitors include compounds with groups of chromates, phosphates, molybdates, calcium salts, zinc salts, lithium salts, cerium salts and so on [55, 58–60]. However, the use of inorganic molecules as inhibitors has decreased drastically in the last few years due to new legislation which forbids the use of highly toxic compounds as inhibitors. One such example is the hexavalent (VI) chromium compounds, which although is an excellent corrosion inhibitor, is highly toxic to humans and to the environment [61].

Corrosion inhibitors can be classified into three types based on their effect on the electrochemical reactions. These are anodic inhibitors, cathodic inhibitors, and mixed inhibitors.

Anodic inhibitors - These inhibitors suppress the anodic reactions that occur during the corrosion process, namely the dissolution of metal. They reduce the rate of anodic oxidation reaction by forming a protective oxide film on the surface of the metal. This blocks the active sites on the metal, which usually act as anodes during the corrosion process, and increases the corrosion potential to higher values [60]. Therefore, anodic inhibitors are also referred to as passivating inhibitors [57]. Although the anodic inhibitors seem perfect in theory, a scratch in the protective film and an insufficient concentration of the inhibitor results in a severe corrosion attack of the exposed area. Therefore, anodic inhibitors are often used with great caution.

Cathodic inhibitors - These inhibitors slow down the cathodic reactions occurring on a metal during the corrosion process by poisoning the hydrogen reduction reaction or by scavenging the oxygen present in the system [60]. Alternatively, cathodic inhibitors may precipitate selectively on cathodic sites thus limiting the diffusion of the reducing species to the metal surface [57]. Therefore, the corrosion potential is reduced by these types of inhibitors.

Mixed inhibitors - They are inhibitors which suppress both the anodic and cathodic reactions. They usually form films on the metal surface that block both anodic and cathodic sites, thus reducing or even blocking corrosion on a metal surface.

1.3.3 Inhibitors for copper

Numerous studies have been carried out to determine effective inhibitors of all types for the protection of copper. Inorganic inhibitors such as chromates, molybdates, and tetraborates have been used previously to reduce the rate of copper corrosion [37]. However, these compounds present challenges such as higher toxicity for chromates and low efficiency of corrosion protection for molybdates and tetraborates. Therefore, alternative inhibitors which satisfy these conditions were studied.

Green corrosion inhibitors and natural corrosion inhibitors such as caffeine and cannabis have also been experimented to restrict the corrosion rate of copper while considering the impacts of corrosion inhibitors on the environment [55, 62, 63]. However, these molecules are still in their infancy for corrosion inhibition and need to be studied further, despite exhibiting promising results.

Organic inhibitors such as amines, azole derivatives, amino acids, and Schiff bases have been established as some of the most important corrosion inhibitors for copper [64]. As discussed earlier, they have been widely accepted due to their common availability, compatibility with numerous metals, and lower toxicity. Benzotriazole (BTA) is one of the most common organic inhibitors for copper and has been studied by several researchers [31, 53, 65–70]. It is classified as an anodic-type inhibitor, although it has also shown to inhibit cathodic oxygen reduction [65]. It interacts with Cu(I) ions resulting in the formation of a Cu(I)-BTA complex which aids in the protection of the copper surface [53, 55, 65]. This is made possible due to the presence of three nitrogen atoms in the molecule ($C_6H_5N_3$) which act as heteroatoms and are active sites for bonding with the metal ions.

2-Mercaptobenzoxazole (MBO), another organic inhibitor with a sulphur, nitrogen, and oxygen atom attached to a benzene ring (C_7H_5NOS), has also been established as an efficient corrosion inhibitor for copper [69, 71, 72]. It acts as a mixed inhibitor, inhibiting both anodic and cathodic reactions that may occur on a metal surface, thus reducing the corrosion rate.

Other organic inhibitors that have been investigated for copper protection include imidazole, triazole, tetrazole, benzothiazole, dodecanethiol, dibenzylsulphoxide, 2-mercaptobenzimidazole, and 2-mercaptobenzothiazole [31, 54, 55, 70, 73–76]. In this work, the corrosion inhibition offered by sulphur-based organic molecules such as 2-mercaptobenzothiazole and 2-mercaptobenzimidazole has been investigated.

1.3.4 2-mercaptobenzothiazole (2-MBT)

2-Mercaptobenzothiazole (2-MBT), with the chemical formula $C_7H_5NS_2$, is an organic compound used primarily for the vulcanisation of rubber. However, it has also found its way into the world of corrosion as a corrosion inhibitor for numerous metals and their alloys. 2-MBT consists of a benzene ring (C_6H_4) which is bonded to 1 S and 1 N endocyclic atoms, forming another cycle with an additional C atom. The C atom in the second ring is further bonded to an exocyclic S atom. Depending on the environmental conditions, 2-MBT exists in its thiol, thione, or thiolate form [77–79]. The different conformers of the 2-MBT molecule are shown in Figure 1.17.

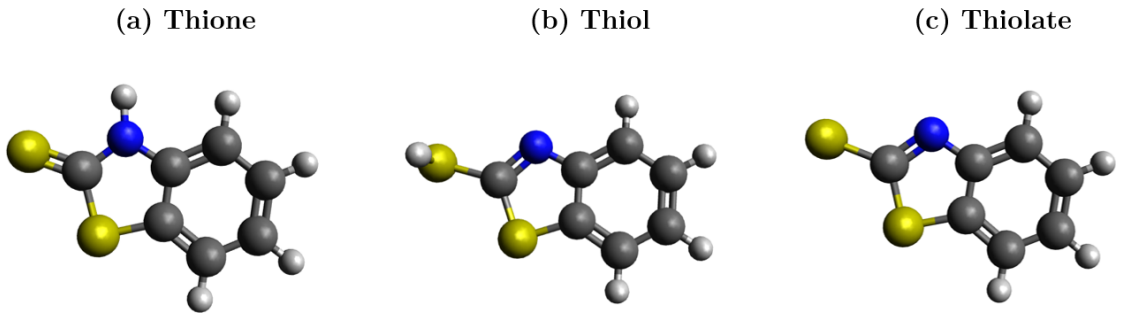

Figure 1.17: Models illustrating the various conformers of the 2-MBT molecule ($C_7H_5NS_2$) (a) thione form, (b) thiol form, and (c) thiolate form. The yellow atoms represent the sulphur, the blue atoms represent the nitrogen, the grey atoms represent the carbon, and the white atoms represent the hydrogen atoms in the molecule.

The thione form of the 2-MBT molecule is said to be more stable over the thiol form in both solid and vapour phase [77]. In aqueous environments, the dominant conformer depends on both the type of solvent and the pH of the environment. In acidic environments, the thione form is the dominant conformer of the molecule, whereas the thiolate form (ionized thiol conformer) is the dominant one in alkaline environments [78, 80]. In environments where the pH is between 4 and 9, both the thione and thiolate forms of 2-MBT co-exist [80], since the pKa of 2-MBT is 6.9 [81].

Depending on the conformer of the molecule, the last H atom is bonded to either the endocyclic nitrogen or the exocyclic sulphur atom in the molecule [82, 83]. The S and N heteroatoms with high electron density are active sites that can coordinatively bond with metal atoms, enabling the molecule to strongly adsorb and to form a dense and protective film on the surface of the metal [83–89].

Bonding mechanisms of 2-MBT with copper

There have been several experimental works addressing the bonding mechanisms of 2-MBT with copper surfaces, including the role of the sulphur and nitrogen atoms. Some authors concluded that the interaction between the molecule and the metal surface occurs via both sulphur atoms of the molecule [84], while others reported that it was only via the exocyclic sulphur atom [87]. Additionally, the involvement of the nitrogen atom along with the exocyclic sulphur has also been proposed [83, 89].

Controlling the metallic or oxidized state of the surface is a prerequisite to a better understanding of the bonding mechanisms of the molecule. In the work of Wu et al. [84–86], the interface was prepared and controlled under ultra-high vacuum followed by the deposition of 2-MBT from the vapour phase in ultra-low-pressure conditions. It was shown that 2-MBT adsorbs on oxide-free metallic copper surfaces as well as on oxidized copper surfaces by its two sulphur atoms along with some free sulphur atoms dissociated from the molecule. Moreover, increasing the exposure to the molecule resulted in the build-up of multilayers of the organic film, which was in agreement with work on Density functional theory (DFT) modelling on metallic copper [90].

Density functional theory (DFT) modelling has shown that, depending on the thione or thiolate conformer of the molecule, the bonding of the 2-MBT molecule differs with the metallic or oxidized copper surface. In the thione form, there would be two modes of adsorption for 2-MBT, both in an upright configuration via its S atoms covalently bonded to metallic Cu or via its exocyclic S atom bonded to oxidized Cu. It also suggests that besides the sulphur bonding, there can be a hydrogen bonding between the NH group of the molecule and the surface oxygen atoms [88, 91, 92]. However, the possibility of N(H) bonding has eluded experimental work for the most part. In the thiolate form, the N and exocyclic S atoms would covalently bond to the surface also in an upright configuration [90, 91]. Therefore, it is well-established from modelling studies that 2-MBT can strongly bonds to copper and form a protective barrier layer on the surface [90, 91, 93].

The formation of metal-organic complexes due to an interaction between the 2-MBT molecules and copper (metal/oxides) has also been suggested [79, 80, 87, 94], though only a few authors have been able to validate the formation of these Cu(I)-2-MBT complexes experimentally [79, 80, 87].

The adsorption mechanisms of the 2-MBT molecule from an aqueous solution can also be altered by other factors such as the presence of residual native oxides, the nature of the electrolyte and its pH, the inhibitor concentration, and the presence of impurities or aggressive species.

2-MBT against corrosion

2-mercaptobenzothiazole (2-MBT) is a well-known inhibitor that has been shown to efficiently protect metals such as copper, aluminium alloys, and stainless steels from corrosive attack [67, 95, 96]. It is used due to its dexterity as a mixed-type inhibitor, restricting both anodic and cathodic reactions that may occur on the metal surface [67, 97]. It has been shown to protect copper from corrosion in varying degrees depending on the environment and its pH, the surface state of the metal substrate, and the concentration of the inhibitor [53, 70, 79, 80, 87–89, 95].

In acidic environment, it has been demonstrated that 2-MBT reduces the rate of anodic dissolution of copper metal [70, 95]. However, since not stable at low pH, the passive oxide film cannot play a significant role in protecting the surface and the 2-MBT layer must form directly on the metallic substrate to protect it.

In neutral chloride environment, the 2-MBT layer has been shown to inhibit the growth of copper oxide as well as the corrosion of the metallic substrate [88, 89]. However, these works were carried out on copper surfaces covered by an air-formed oxide and therefore the extent of protection offered by the 2-MBT layer to the chloride ions is not ascertained.

The effect of 2-MBT layers on copper in an alkaline environment mostly focused on the local passivation at emergent grain boundaries [98]. Therefore, the corrosion protection of copper in alkaline environment by 2-MBT has not been established yet.

1.3.5 2-mercaptobenzimidazole (2-MBI)

2-mercaptobenzimidazole (2-MBI), $C_7H_6N_2S$, is often used as an organic corrosion inhibitor to protect metals such as copper, copper alloys, zinc, stainless steels, and aluminium alloys [66, 72, 75, 76, 99–105]. The 2-MBI molecule consists of a benzene ring (C_6H_4) bonded to two nitrogen atoms, which forms another cycle with a carbon atom attached between them, as shown in Figure 1.18. This carbon atom is also bonded to an exocyclic sulphur atom, the bonding of which depends on the environment thus dictating the dominant conformer of the molecule [106].

In the work of Ansar et al. [107], it was determined that 2-MBI exists predominantly in the thione form in the solid state and in polar solvents. On the other hand, in strongly basic solution, 2-MBI ionizes to its thiolate conformer. The changes in the dominant conformer occur due to the pKa of the molecule, which is 10.4 [107, 108], thus determining the stability of the molecule according to the pH of the environment and the other species present in that environment. The various conformers of the 2-MBI molecule are depicted in Figure 1.18.

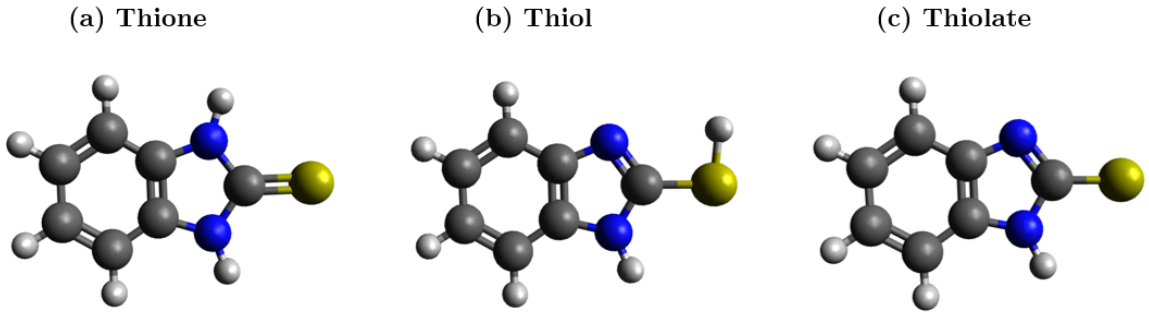

Figure 1.18: Models illustrating the various conformers of the 2-MBI molecule ($C_7H_6N_2S$): (a) thione form, (b) thiol form, and (c) thiolate form. The yellow atoms represent the sulphur, the blue atoms represent the nitrogen, the grey atoms represent the carbon, and the white atoms represent the hydrogen atoms in the molecule.

Bonding mechanisms of 2-MBI with copper

Several researchers have investigated the adsorption of 2-MBI organic molecule and its various aspects for its use as a corrosion inhibitor, both experimentally and theoretically [31, 99, 100, 109–111]. The adsorption of 2-MBI from the vapour phase on clean, 2-D oxide, and 3-D oxide-covered copper surfaces was investigated in the works of Wu et al. [99, 100]. It was found that 2-MBI adsorbed on metallic copper surfaces by its sulphur and both nitrogen atoms with the molecule lying flat on copper. On oxidized surfaces, the bonding occurred via the sulphur atom and only one nitrogen atom with a tilted geometry on the surface. These bonding mechanisms between the 2-MBI molecule and copper were also suggested by Density Functional Theory (DFT) calculations in the work of Chiter et al. [110, 111], thus exhibiting good agreement between theoretical and experimental work. Additionally, these findings also corroborated the results of Finsgar et al. [109], who found that 2-MBI bonds to the oxidized copper by its S and N atoms, thus resulting in a tilted position on the surface.

The formation of the Cu(I)-MBI complex film has been proposed by a few authors [79, 108, 112]. Chadwick and Hashemi [79] observed that the Cu(I)-MBI complexes were formed mainly due to the dissolution of copper oxides in acidic environment which provided a steady supply of Cu^+ ions for the complexes. On prolonged exposure to the acidic solution, the thickness of the complex films increased due to additional Cu^+ ions generated by the anodic dissolution of the copper metal, thus relating the thickness of the complex film to the pH of the solution. On the other hand, Xue et al. [112] reported that the complex films formed between Cu and 2-MBI are different depending on the oxidation state of copper. When 2-MBI reacted with copper oxides, the result was the formation of Cu(I)-2-MBI complex film with the C=S bond intact in the 2-MBI molecule, whereas when the molecule interacted with metallic copper,

the complex film formed was mainly $Cu^{+}MBI^{-}$ or $Cu_2{}^{+}MBI^{2-}$ with the C=S bond being split in the 2-MBI molecule.

Despite these numerous works, there remains some ambiguity on the formation and protective capabilities of the organic 2-MBI film formed on metallic copper and oxidized copper surfaces, especially in the presence of aggressive species such as chloride ions which can compete with the inhibitor molecules to interact with the metal.

2-MBI against corrosion

2-MBI has been proven as an effective corrosion inhibitor for copper, mostly due to the presence of S and N heteroatoms which, as active sites, allow the molecule to bond and form a dense and protective film on the metal surface [69, 101, 102].

Finsgar et al. demonstrated that 2-MBI acts as a mixed inhibitor and is indeed effective against corrosion in a 3% NaCl solution [102]. They also showed that 2-MBI exhibited an effectiveness of 87.5% on corrosion inhibition based on a 180-day immersion test in the chloride solution. Meanwhile, Sharma et al. [101], studied the inhibition of intergranular corrosion by 2-MBI on copper using in-situ electrochemical scanning tunnelling microscopy. They established that 2-MBI protects copper, although imperfectly, from corrosion, and also suggested the formation of Cu(I)-MBI reaction products that may be the reason for protection against dissolution in an acidic environment.

The complex films reported by Xue et al. [112] were suggested to be protective against corrosion. However, the complex film formed by an interaction with metallic copper was reported to be less defective and therefore more protective than the complex film formed by the interaction between 2-MBI and oxidized copper.

CHAPTER 2

Experimental apparatus and methodology

2.1 Sample preparation

Polycrystalline samples obtained from high-purity cast electrolytic tough pitch copper (ETP-Cu) were used for experimental analysis, as in previous work [95, 98, 101, 113–115]. These samples were prepared at the University of Ghent, Department of Materials, Textiles, and Chemical Engineering in the group of Prof. K. Verbeken, by performing 2-6 cycles of cryogenic rolling after immersion in liquid nitrogen followed by annealing of the samples for 1 minute at 200°C [116, 117]. The purity of these samples has been verified by ToF-SIMS in previous work [116], showing that the quantities of sulphur and oxygen are well below the detection limit, indicating minimal contamination of the samples. This will also be verified later on in our work.

2.2 Surface Preparation

Surface preparation of the samples is a necessary step before performing any experiment involving surface reactions. In electrochemistry, a clean and mirror-finished surface is necessary to ensure that the electrochemical reactions occurring are not influenced by additional external factors. For example, contamination of the surface could lead to galvanic effects between the contaminants and the metal surface during polarisation tests, and it could also prevent

the adsorption of the inhibitors on the surface. Defects on the surface, such as scratches and pits, may result in preferential attack on these sites due to the difference in surface energy between the ideal surface and the defect region. This can result in the change of pH locally thus accelerating the effects of the electrochemical measurements. In surface analysis techniques too, a clean and flat surface is desired for a better analysis. A contaminated surface will result in various anomalies in XPS measurements such as the attenuation of signals by the contamination layer, increased full widths at half maximum (FWHM), and shifted binding energies. A flat surface aids in the acquisition of a better signal to noise ratio for the XPS spectra. In ToF-SIMS spectrometry, a clean surface is imperative as well, since it is a highly sensitive technique that can detect contaminations at very low concentrations (around parts per million (ppm)). The depth profiles obtained from ToF-SIMS are highly dependent on the surface roughness due to the position of the analysis and the sputtering guns at 45° angle to the surface. Sharper profiles in the in-depth analysis are obtained for smoother surfaces. Therefore, to avoid these issues and obtain reliable data from the experiments, surface preparation is performed by two steps, namely mechanical polishing and electrochemical polishing.

2.2.1 Mechanical Polishing

The surfaces to be studied were mechanically ground using silicon carbide abrasive papers from 600 grit up to 4000 grit to achieve a flat surface, by removing any major surface scratches and corrosion products that may be present on the surface. The samples were abundantly rinsed with ethanol and ultra-pure water (Millipore, resistivity > 18.2 MΩ.cm) after each step of grinding.

To achieve a mirror finish surface, the samples were then mechanically polished using diamond pastes of particle size 6 µm, 3 µm, 1 µm, and finally 0.25 µm on their corresponding polishing discs. The polishing was performed using a Struers LaboPol-4 polishing machine equipped with LaboForce-1, as seen in Figure 2.1. The applied load on each sample was 10 kN. The use of the LaboForce-1 supplement allows the polishing to be performed automatically which ensures that all the samples are evenly polished. Meanwhile, the load applied assures us that the samples are laying completely flat on the polishing disc, assuming the load is evenly distributed, which then prevents the formation of a gradient on the surface during this process. An alcohol-based lubricant (2-propanol) was used to spread the diamond paste on the polishing disc effectively. Each polishing step was performed for a longer time-period than the previous step, ranging from 10 minutes for the 6 µm polishing step, to 25 minutes for the 0.25 µm polishing step. This ensures that all the scratches formed by the preceding step are completely removed by the succeeding step, which is verified by observing the sample

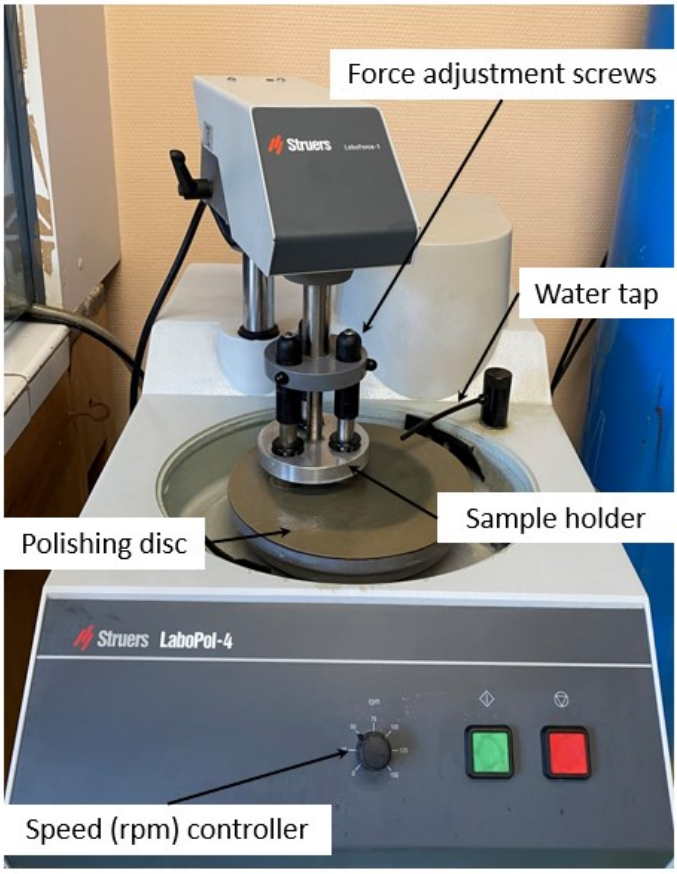

Figure 2.1: The Struers LaboPol-4 polishing machine equipped with the LaboForce-1 attachment for the polishing of the copper samples.

under an optical microscope after each polishing step.

The samples were rinsed with ethanol and ultra-pure water thoroughly before progressing to the next stage to remove the diamond particles from the previous step. After the last step of mechanical polishing, the samples were ultrasonically cleaned for 5 minutes in successive baths of acetone, ethanol, and ultra-pure water.

2.2.2 Electrochemical polishing

The electrochemical polishing of copper was first proposed by Jacquet in 1936 [118]. The author observed that when an aqueous solution of orthophosphoric acid is used to anodically etch a copper surface, it turns bright and smooth as though it had been polished. Over the years, several researchers have investigated this process to understand the mechanisms of electrochemical polishing [119–122] and to determine the formation of various copper-phosphate compounds from this process [123, 124]. Meanwhile, the work of Gabe [125] focused on optimizing the process in terms of concentration of the acid, the potential to be

applied, the optimal time necessary, the effect of temperature, and so on. The findings of these works establish that electrochemical polishing of copper results in a smoother, cleaner, and relatively oxide free surface (the oxide film grows back in air after the process).

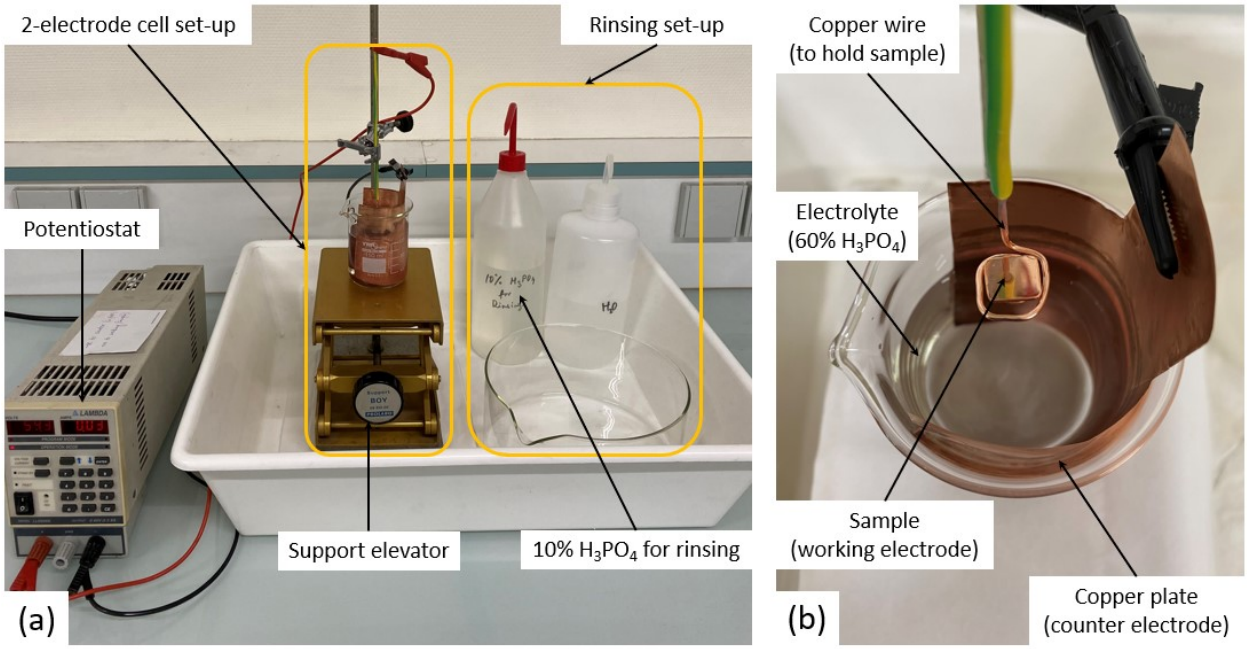

Figure 2.2: The electrochemical polishing set-up used for the copper samples showing (a) the 2-electrode set-up connected to the potentiostat and the rinsing set-up used after electrochemical polishing, and (b) the copper sample placed on the working electrode along with the counter electrode in the cell.

Therefore, we perform electrochemical polishing on the copper samples to remove the cold-work layer leftover from mechanical polishing, and to remove any contaminations that may persist on the surface [126]. It was performed using a two-electrode setup with the copper sample as the working electrode and a copper plate as a counter electrode in a bath of 60% orthophosphoric acid (H_3PO_4) solution [125], as shown in Figure 2.2.

Before electrochemically polishing the sample, the copper wire which is used to hold the sample was cleaned by electrochemically polishing it for 15 seconds at 3 V. Next, the sample was placed on the clean copper wire and a constant voltage of 1.4 V was applied to the system. The sample was slowly immersed into the orthophosphoric acid solution. Once the sample was immersed, the electrochemical polishing process initiates thus dissolving the top layer and removing the contaminations from the surface. This process was carried out for 4 minutes after which the sample is slowly lifted out of the solution. Finally, the sample was rinsed with a 10% solution of H_3PO_4, followed by ultra-pure water, and then dried using nitrogen.

2.3 Cleaning the apparatus

The apparatus used for the experiments, including the electrochemical cells, the O-rings, and the glassware, were cleaned prior to the experiments to prevent any contamination. They were first rinsed with a solution of sulphuric acid (H_2SO_4) and 30% hydrogen peroxide (H_2O_2), mixed in the ratio 2:1, at room temperature. This step removes most contaminants including residue from various metallic species due to the aggressive nature of the cleaning solution. They were then rinsed with ultra-pure water. The Kel-F cells were then boiled in concentrated nitric acid (HNO_3) for 5 minutes to remove any additional contaminants, organic or metallic, that may accumulate on the pseudo-reference electrode, after which they were rinsed again with ultra-pure water. This step was exclusive only to the Kel-F electrochemical cells and was not performed for the O-rings, since the nitric acid would dissolve the O-rings.

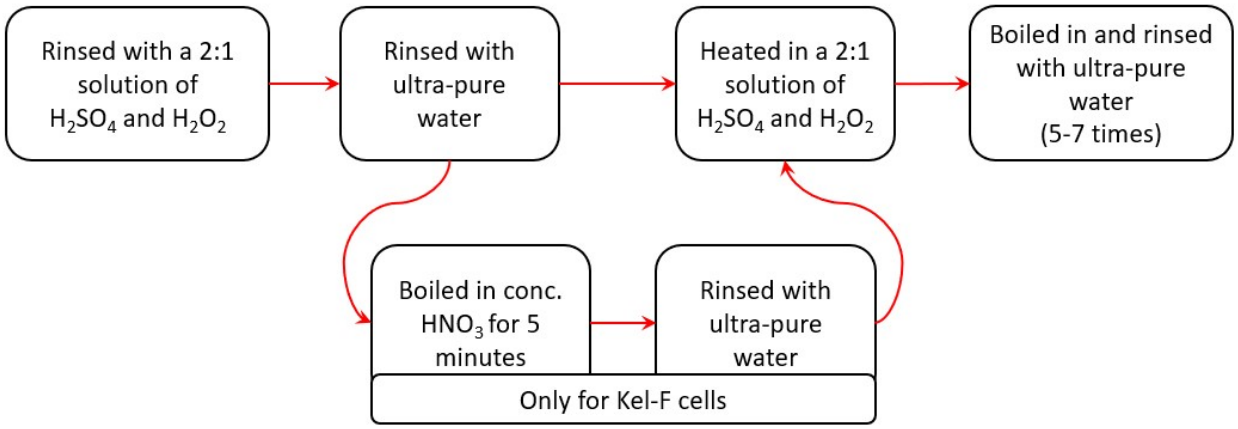

Figure 2.3: A flow chart showing the cleaning process used for the removal of contaminations from the apparatus, which were to be used for electrochemical measurements.

Next, the apparatus was heated with the 2:1 mixture of H_2SO_4 and H_2O_2 until the disappearance of the bubbles, indicative of the depletion of H_2O_2, to eliminate the remaining contaminants. Finally, several cycles of boiling and rinsing in ultra-pure water (minimum 5) were performed to remove any traces of the acid from the earlier stages of cleaning. A flow chart showing the procedure is given in Figure 2.3. This method of cleaning has been proven to be very effective since we observe minimal contaminations on our surfaces from both XPS and ToF-SIMS measurements, which was a prerequisite for this study.

2.4 Electrochemistry

2.4.1 Preparation of electrolytes

The electrolytes used for the experiments are given in Table 2.1, according to the environment along with the measured pH at room temperature. Each environment consists of an electrolyte without the presence of an inhibitor which was used as the reference electrolyte, and an electrolyte with the inhibitor, 2-MBT or 2-MBI, present.

Table 2.1: The concentration of the base electrolyte along with the concentration of the inhibitor used for the electrochemical experiments with their measured pH values.

Environment	Inhibitor concentration	Measured pH at 25°C (± 0.1)
0.1 M NaOH	-	13.5
	1 mM 2-MBT	13.6
	1 mM 2-MBI	13.6
10 mM HCl	-	2.3
	0.1 mM 2-MBT	2.6
	1 mM 2-MBI	2.4
0.5 M NaCl	-	5.3
	0.1 mM 2-MBT	5.2

The NaOH inhibitor solutions were prepared by adding the desired quantity of the inhibitor powder in the solution and mixing well by stirring with a glass rod for 2 minutes. Meanwhile, the preparation of the inhibitor solutions for the HCl and NaCl environments were rather elaborate. This was due to the low solubility of the inhibitor(s) especially in lower pH environments [127, 128]. This was also the reason why a lower concentration of 2-MBT was used for the acidic and near neutral solutions.

To prepare the HCl and NaCl inhibitor solutions, the desired quantity of the inhibitor was measured and added to the reference solution in a conical flask. The flask was topped off with ultra-pure water to fill it to its maximum level. A magnetic stirrer bar, previously cleaned, was inserted in the flask to aid in stirring. The conical flask was then placed on a heater with a magnetic stirring function and was set to 70°C heating and constant stirring at 1200 rpm, inside a fume hood. The flask was covered with a perforated lid, especially constructed for this set-up, to allow evaporation of the excess water while preventing contamination. Meanwhile,

the monitoring of temperature was carried out by inserting the thermostat rod in a separate water-filled beaker which was placed on the same heating pad. This set-up, shown in Figure 2.4, allowed us to avoid any contamination that may be present on the thermostat rod. This solution was heated for 7 - 10 days till the inhibitor powder was completely dissolved. After evaporation of the excess water, and the solution was transferred to a volumetric flask for experimental use. All chemicals used were of analytical grade and were provided by Sigma Aldrich and VWR chemicals.

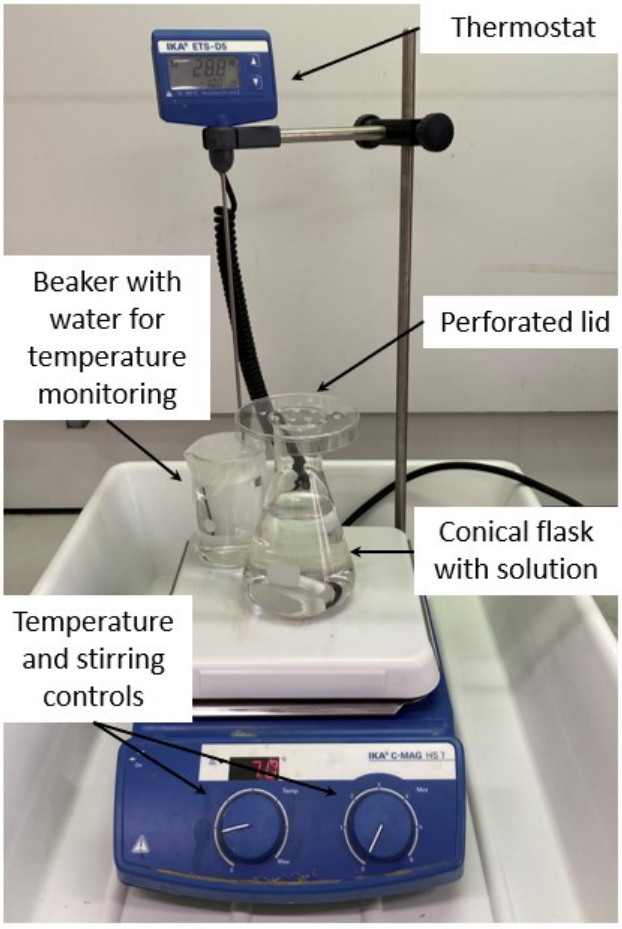

Figure 2.4: The set-up used for the preparation of electrolytes in acidic and neutral media where the inhibitor molecules have a very low solubility.

2.4.2 Classical cell

A classical electrochemical cell using a three-electrode setup was used for electrochemical measurements. This set-up is shown in Figure 2.5. The sample was used as the working electrode enclosed in a Teflon tube sample holder, a platinum mesh as the counter electrode, and a saturated calomel electrode (SCE) as the reference (+0.2415 V vs SHE). An electrolytic salt bridge was used between the reference electrode and the cell to avoid contamination of

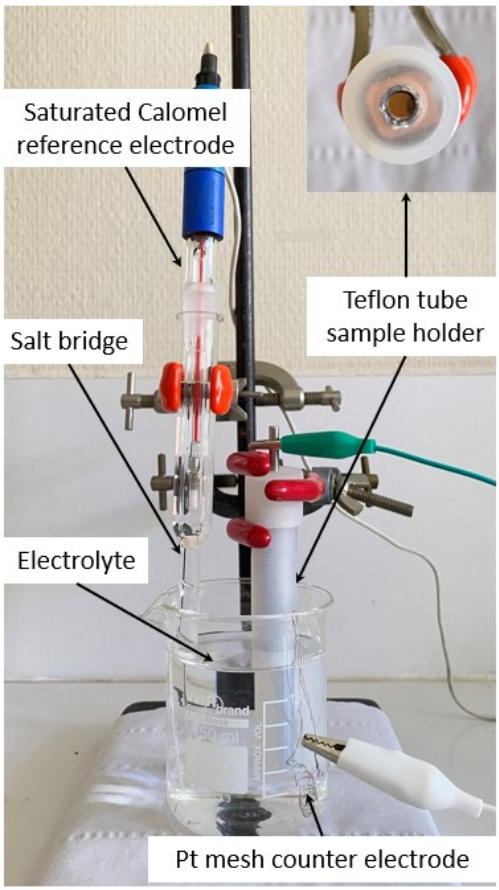

Figure 2.5: The classical 3-electrode cell used for the electrochemical experiments using a saturated calomel electrode (SCE) for the reference, a platinum mesh for the counter electrode, and the copper sample as the working electrode (shown in top-right inset).

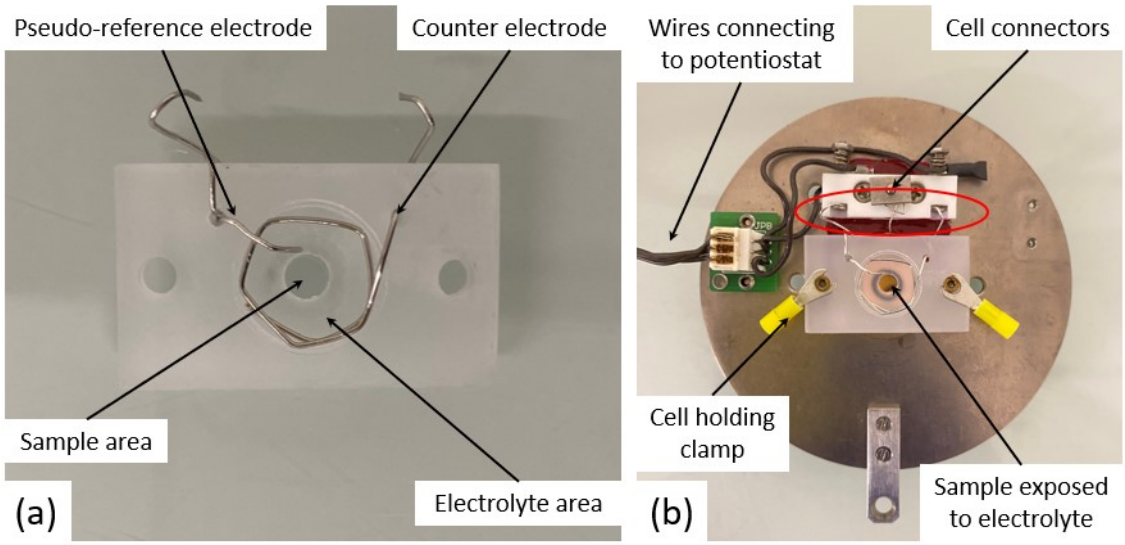

Figure 2.6: (a) The Kel-F micro-cells used for the electrochemical experiments with the platinum counter and pseudo reference electrodes. (b) The assembled micro-cell set-up with the sample, the cell, and the connections leading to the potentiostat.

either component. An O-ring was used between the sample holder and the sample to ensure no leakage of the electrolyte and to delimit an area of 0.16 cm^2 for experimental analysis. The classical cell contained an electrolytic volume of 150 ml. The experiments were performed using a Biologic SP 200 potentiostat and EC-lab collection software.

2.4.3 Micro-cell

The Kel-F, or polychlorotrifluoroethylene (PCTFE), cells used for the electrochemical experiments are shown in Figure 2.6a. These cells were used mainly to keep consistency between previous works carried out using the same apparatus [24, 25, 95, 98, 101, 113–117, 129]. It has a three-electrode set-up with the sample as a working electrode, a platinum counter electrode, and a platinum pseudo-reference electrode. The cell has a volume of approximately 350 - 400 µl for the electrolyte. An O-ring was used between the cell and the sample to ensure no leakage of the electrolyte and to delimit an area of 0.16 cm^2 for experimental analysis. The assembled micro-cell with the copper sample and the electrical connections are shown in Figure 2.6b. The experiments were performed using a PicoStat bi-potentiostat and Picoscan software from Agilent Technologies.

Prior to each experiment, the cells were cleaned by the methodology described earlier, and the pseudo-reference electrode was calibrated by performing the experiment in a classical electrochemical cell. The shift in potential determined for the pseudo reference electrode was +0.75 V vs SHE (+0.51 Vs SCE) for experiments performed with HCl, and +0.32 V vs SHE (+0.08 vs SCE) for the experiments performed with NaOH, as seen below in Figure 2.7 where the CVs obtained in the classical cell and Kel-F cells are plotted and their respective shifts calculated.

2.4.4 Electrochemical experiments

Cathodic pre-treatment

Cathodic pre-treatment was performed prior to the experiments in order to reduce the surface native oxide film. This was done either in the presence or absence of the inhibitor in the solution. After immersion of the samples at the open circuit potential (OCP), the potential was swept cathodically, with a scan rate of 20 mV/s, to the onset of hydrogen evolution and then swept back up to the potential where the measured current was approximately 0 ± 2 µA. The potentials for the onset of hydrogen evolution and the point of zero current depends on the electrolyte used and its pH. These values are specified later in the individual chapters. The cathodic pre-treatment cycle was repeated 2 more times to ensure maximum reduction of the surface native oxides.

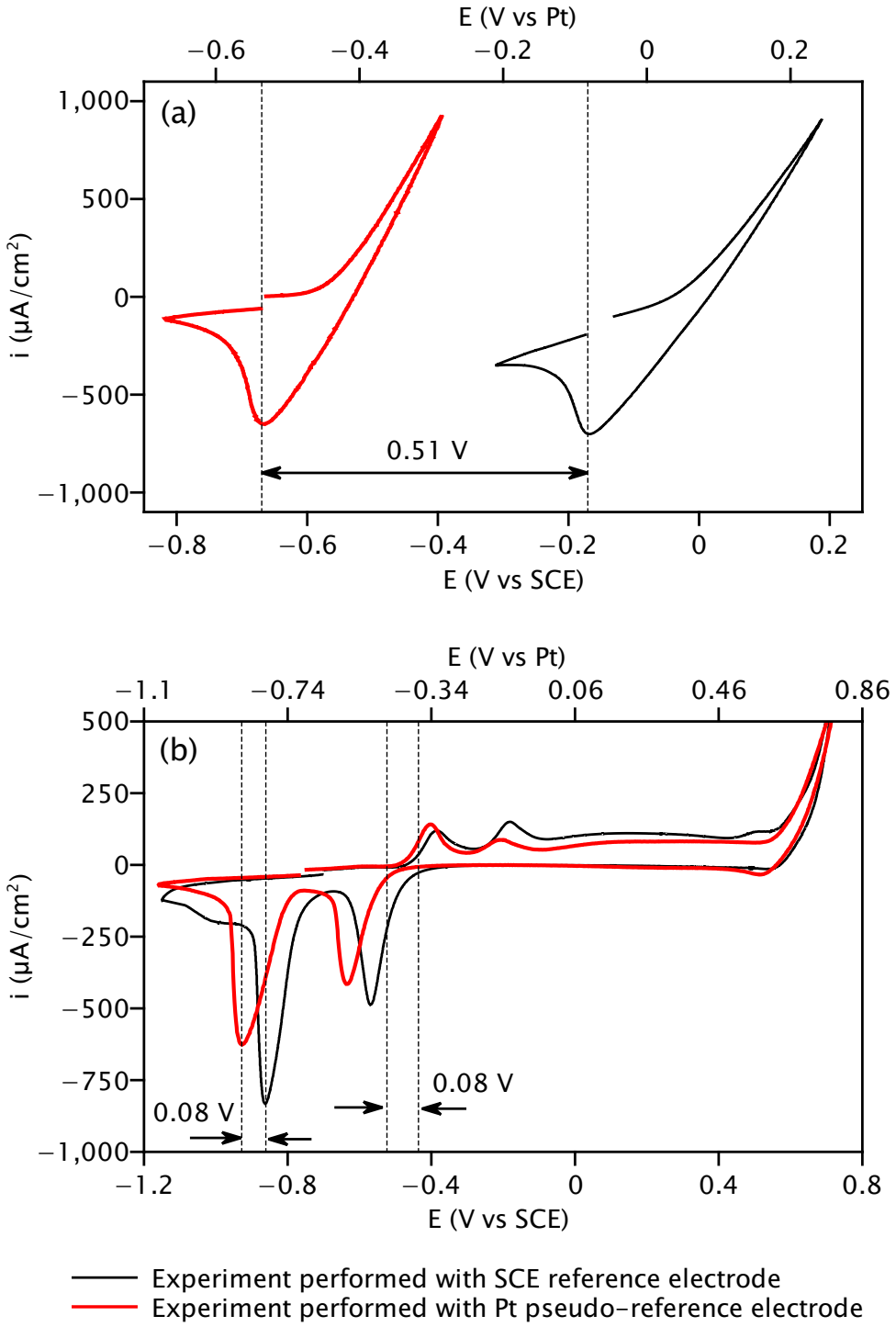

Figure 2.7: The cyclic voltammograms obtained for copper in (a) 10 mM HCl and (b) 0.1 M NaOH, using the classical cell with the saturated calomel electrode (SCE) in black and the Kel-F micro cell with the pseudo reference electrode (Pt) in red. The shifts are determined by taking the cathodic peaks into account and calculating the difference in potential between the two experiments.

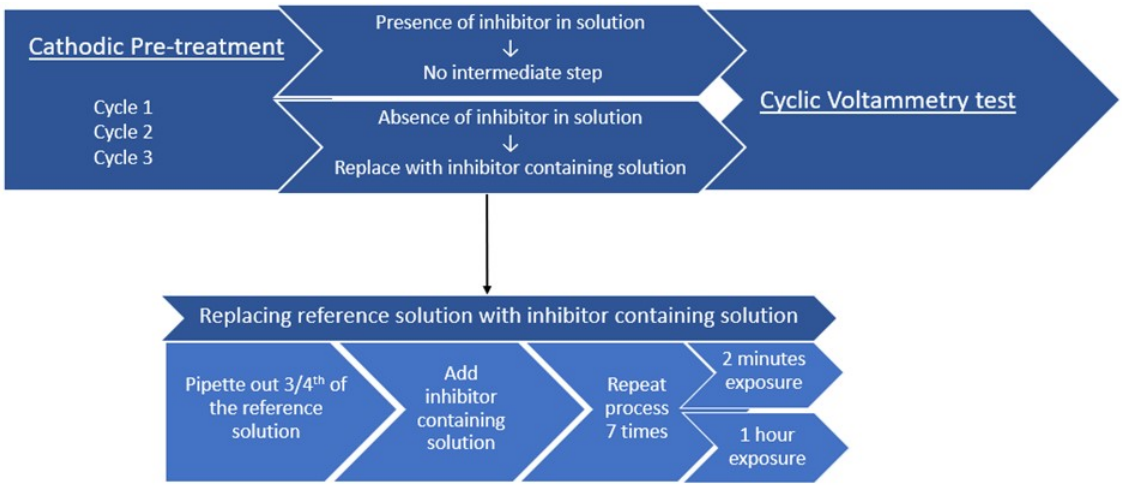

Figure 2.8: Schematic showing the cathodic pre-treatment process conducted in both the reference solution without inhibitor and the inhibitor containing solution. For the cathodic pre-treatment process in the reference solution without the inhibitor, the method of replacing the solution is also detailed here.

For the substrates pre-treated in presence of the inhibitor in the solution, the cyclic voltammetry tests were carried out right after cathodic pre-treatment of the substrate. For the substrates pre-treated in absence of the inhibitor in the solution, the reference solution was replaced with an inhibitor containing solution after the 3rd cathodic pre-treatment cycle. A pipette was used to remove 3/4th of the solution in the cell (approx. 250 - 300 µl in the micro-cell, 100 - 125 ml in the classical cell), and subsequently an equal amount of the inhibitor containing solution was introduced while the substrate and the electrodes of the cell remained immersed and connected. This process was repeated 7 times to ensure that the replaced solution in the cell had the appropriate concentration of the inhibitor. Following this, the substrates were exposed in the solution for either 2 minutes or 1 hour, at a fixed potential, as defined later, before initiating the cyclic voltammetry tests. A schematic of the process from cathodic pre-treatment to cyclic voltammetry tests is given in Figure 2.8.

Cyclic Voltammetry

After cathodic pre-treatment of the surfaces and adsorption of the organic inhibitors, cyclic voltammetry tests were carried out to determine the corrosion/oxidation inhibition behaviour of the copper surfaces in various conditions. These tests were performed by sweeping the potential from the point of zero current, to the anodic peak, corresponding to the initiation of corrosion for the HCl and NaCl experiments and oxidation of Cu(I) range for the NaOH experiments, followed by reverse sweeping to the onset of hydrogen evolution, and then back to the starting potential. The experiments were performed with a scan rate of 20 mV/s.

Each experiment was repeated 3 times each to ensure reproducibility of the results.

Analysis of electrochemical data

To determine the anodic and cathodic charge densities from the cyclic voltammetry curves obtained, the corresponding current density was integrated with respect to the time-period of each step. The sum of the values resulted in the charge densities of the anodic and cathodic branches of the curve.

Faraday's law [130] was applied to estimate the equivalent thicknesses of (a) the reduced oxides (from the pre-treatment cycles), (b) the reacting copper metal (cyclic voltammetry tests of all environments), and (c) the oxide grown during polarisation (NaOH and NaCl experiments), using the charge densities determined by the method given above. The formula is given as:

$$\delta = \frac{qV_m}{zF} \tag{2.1}$$

where, δ is the thickness estimated (m), q is the charge density (anodic or cathodic) determined from the experiments (C/m^2), V_m the molar volume of the reacting material (m^3/mol), z the number of electrons exchanged, and F the Faraday's constant (96485.33 C/mol). The Faraday's constant represents the amount of charge carried by one mole of electrons and is given by the elementary charge (e = 1.6023 x 10^{-19} C) times the number of electrons in 1 mol, i.e. the Avogadro's number (6.023 x 10^{23}). The values of molar volume and number of electrons exchanged with respect to the state of copper ions are given in Table 2.2.

Table 2.2: The values of molar volume (V_m) and the number of electrons exchanged (z) used for the estimation of equivalent thickness of the concerning species using Faraday's law.

	Molar Volume (V_m)	Number of electrons exchanged (z)
Cu	7.1 cm^3/mol	1
Cu(I) / Cu_2O	23.9 cm^3/mol	2
Cu(II) / CuO	12.4 cm^3/mol	1
Cu(II) / $Cu(OH)_2$	29 cm^3/mol	1

2.5 X-ray Photoelectron Spectroscopy

X-ray photoelectron spectroscopy (XPS) is a highly surface sensitive spectroscopic technique which is both qualitative and quantitative. It allows us to obtain information such as the chemical environment of the surface atoms, the elemental composition of the surface layers of a material, and the structure of the surface. As a surface science technique, XPS is a component of the ultra-high vacuum (UHV) system. UHV prevents environmental contamination of the substrate surface, and it also ensures that the electrons ejected from the surface reach the detector.

XPS is based on the principles of photoelectric effect, a phenomenon discovered by Heinrich Hertz in 1883 [131]. The photoelectric effect shows that when a material is provided energy due to irradiation from electromagnetic radiation, electrons can be ejected from the material. In 1905, Albert Einstein suggested a quantum theoretical explanation of the photoelectric effect, postulating that light consists of tiny packets of energy which are quantifiable, known as photons, which when absorbed by the solid, emits photoelectrons carrying information of the solid from which they are emitted [132]. Numerous progressions were made both in theory and experimentally in the following years, paving the way for the development of XPS. However, the major breakthrough was made in the mid 1950's in Uppsala by Kai Siegbahn, who recorded the first high resolution XPS spectra ever. It was not until 1967 when Siegbahn published a comprehensive book with the explanation of the technique that he called electron spectroscopy for chemical analysis (ESCA) [133]. For his contribution to the development of high-resolution electron spectroscopy, Siegbahn was awarded the Nobel prize in Physiscs in 1981.

2.5.1 Basic Principles and Instrumentation

The photoelectric effect is the emission of electrons when electromagnetic radiation (light, X-rays, ultraviolet rays) hits a material, as shown in Figure 2.9. The electrons emitted from the material due to this effect are referred to as photoelectrons.

In X-ray photoelectron spectroscopy, an X-ray source is used to produce photons of a certain energy, which are directed towards the sample surface. This in turn causes excitation within the sample and can cause emission of a photoelectron with a kinetic energy of E_k, as shown in Figure 2.10. These photoelectrons are detected, and their kinetic energy is measured to determine the chemical environment of the atom they were ejected from. This is possible through the binding energy of the electron E_b, which is characteristic of the emitting atom. If we know the kinetic energy E_k, the photon energy hv, and the work-function ϕ, the binding energy of the emitted electron can be calculated using the equation given below.

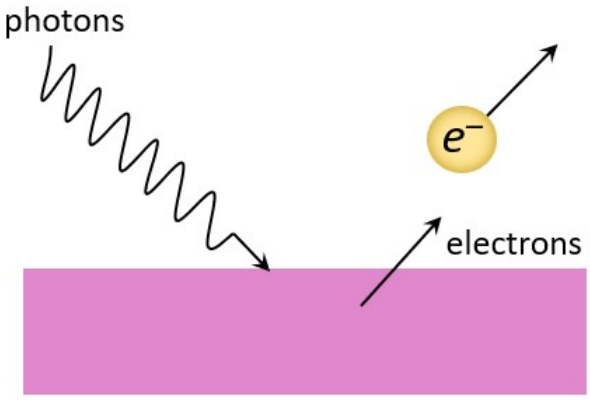

Figure 2.9: Schematic diagram showing the principle of the photoelectric effect.

$$E_b = hv - E_k - \phi \tag{2.2}$$

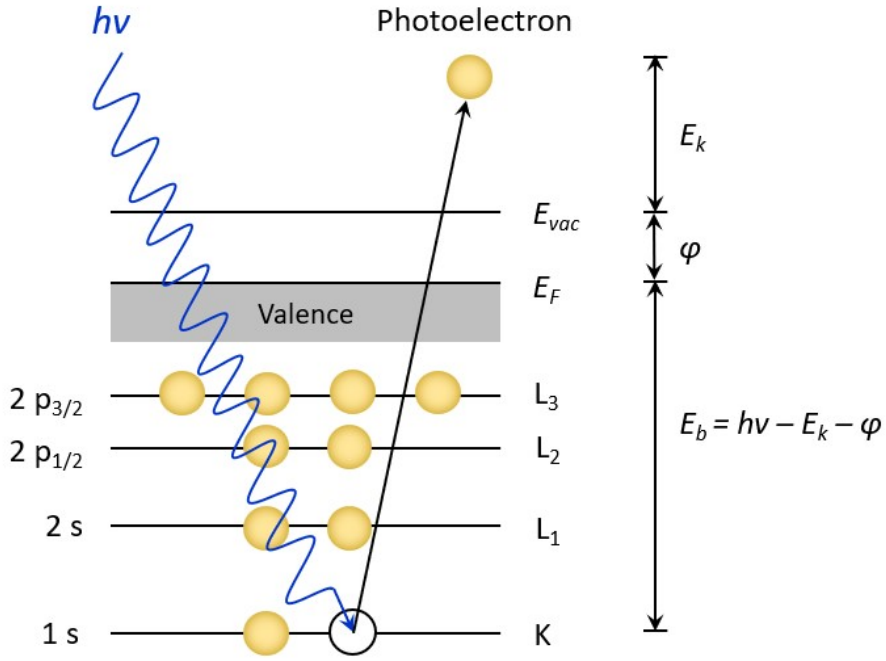

Figure 2.10: Schematic showing the process of photoemission of a core level electron from a material.

When a core electron is emitted from the material as a photoelectron, it results in a vacancy hole in the core level from which the electron is emitted. This can lead to the fall of an electron from a higher energy level to the vacancy hole, causing the release of energy, which may be transferred to another electron. This electron, due to its increased energy, is then ejected as an Auger electron and this process is referred to as Auger emission. Figure 2.11

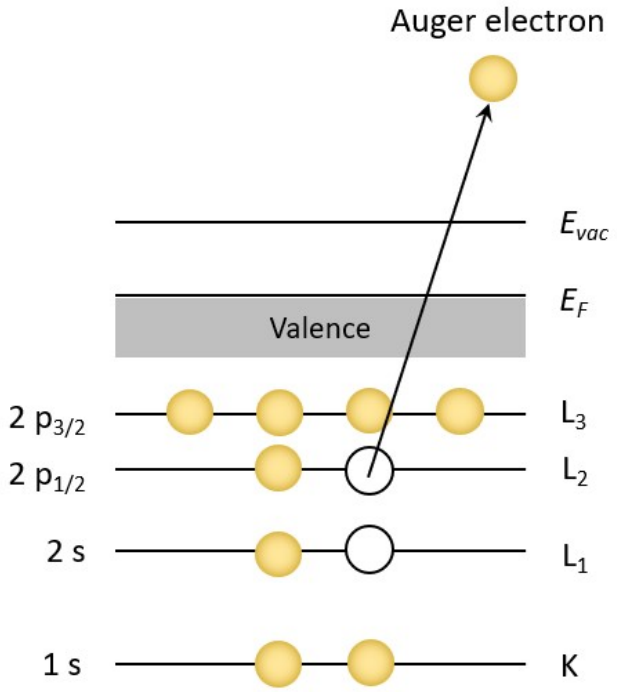

Figure 2.11: Schematic showing the emission process of a KL_1L_2 Auger electron.

shows a schematic of the emission of a KL_1L_2 Auger electron.

The inelastic mean free path, λ, is the average distance an electron can travel in a material without undergoing a change in its kinetic energy. The value of λ is usually very small (less than 3 nm) for electrons with a kinetic energy more than 10 eV, as shown in Figure 2.12. It also depends on the material that the photoelectron is being emitted from. Approximately 95% of the detected photoelectrons in XPS comes from a depth of 5 λ from the surface (approximately 10 nm), showing the surface sensitivity of the XPS technique.

Figure 2.13 shows a schematic of the XPS instrument and its main components. An X-ray source is used to produce photons of a certain energy, which depends on the type of source used. The most common types of sources used are Mg Kα or Al Kα sources with a radiation energy (hv) of 1253.6 eV and 1486.6 eV, respectively [134]. We used a monochromatized Al Kα X-ray source for an improved resolution of the spectra.

An electron energy analyser measures the kinetic energy of the ejected electrons from the surface. We use a 180° hemispherical analyser in our system, a deflection analyser that operates like a band-pass filter, which opens a window for only a small energy band around a given energy. The multichannel electron detector (6 channeltrons) receives the electrons arriving from the surface, through the hemispherical analyser, and is responsible for the counting of electrons thus continuously recording the spectra over time.

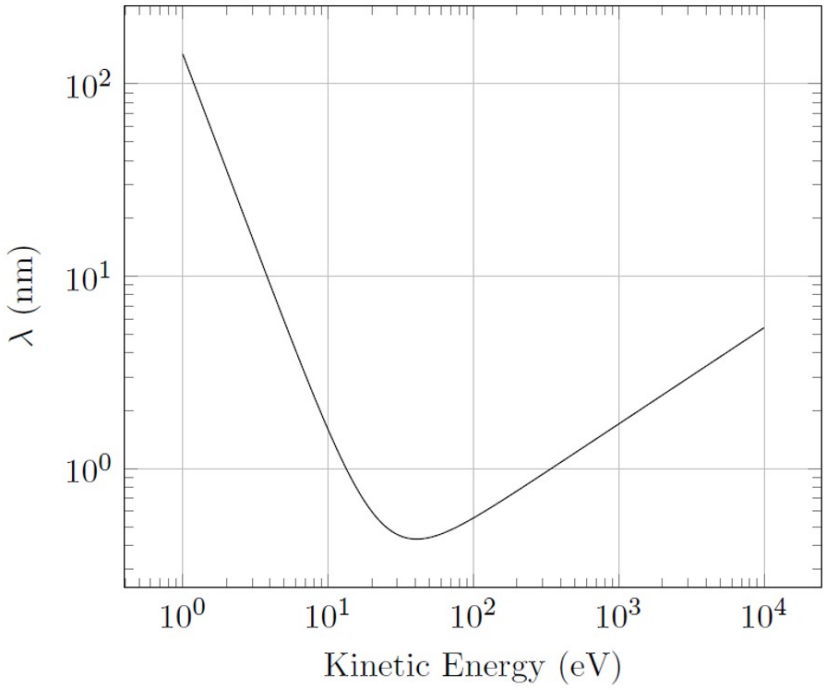

Figure 2.12: Variation in the inelastic mean free path as a function of the kinetic energy.

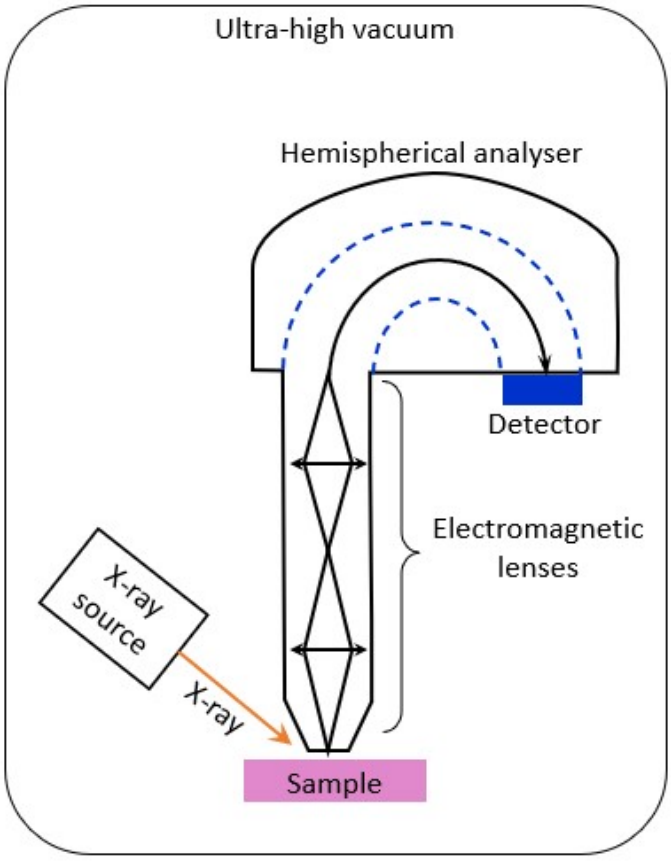

Figure 2.13: Schematic diagram showing the main components of the XPS instrument.

2.5.2 Experimental Parameters

XPS analysis was performed with a Thermo Electron Escalab 250 Xi spectrometer, shown in Figure 2.14, of base pressure less than 10^{-10} mbar. An X-ray spot size of 900 μm in diameter was used. XPS survey spectra were recorded between −10 and 1350 eV at a pass energy of 50 eV and a step size of 1 eV. High-resolution spectra of the C 1s, N 1s, O 1s, Na 1s, S 2p, Cl 2p, Cu 2p core levels, Cu LMM Auger transition, and the Fermi level were recorded with a pass energy of 20 eV at a step size of 0.1 eV. The spectra were recorded at 90° take-off angle of the collected photoelectrons.

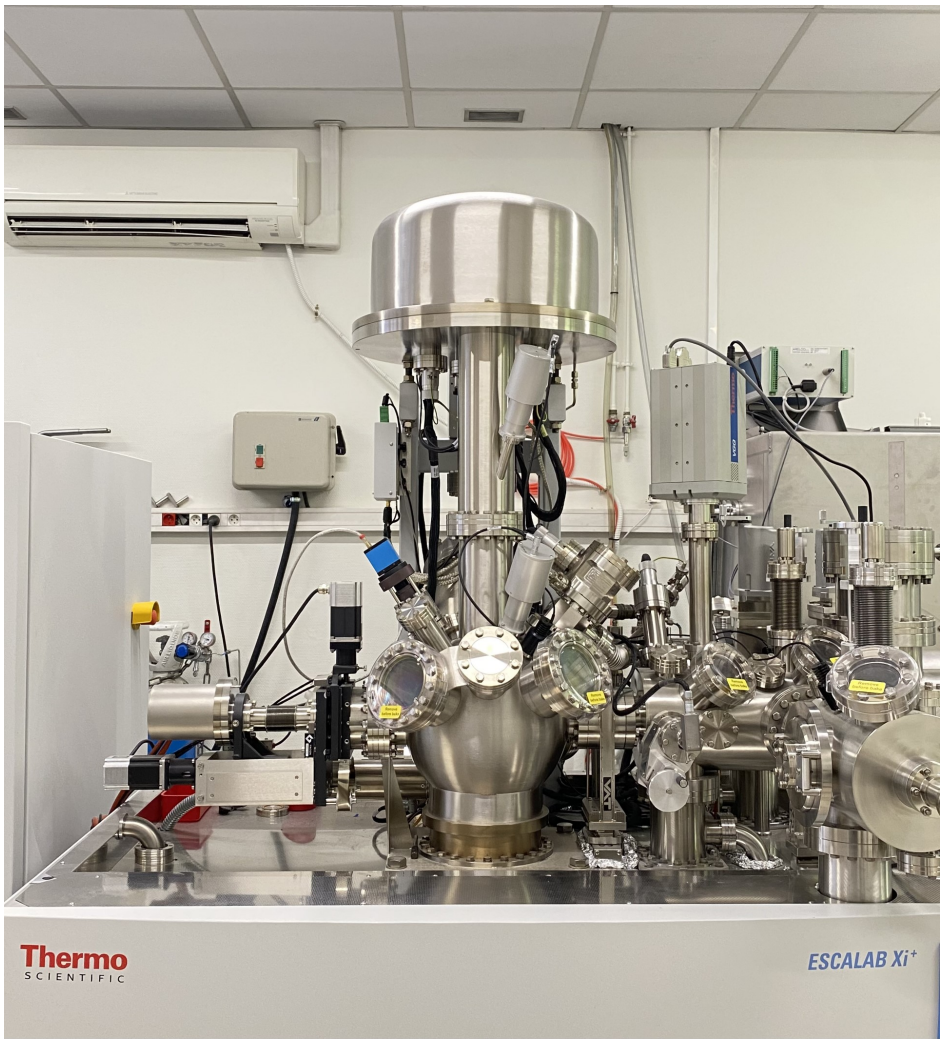

Figure 2.14: The Thermo Electron Escalab 250 Xi XPS spectrometer used for this study.

2.5.3 Treatment of data

Referencing of the Binding Energies using Fermi level

One of the first steps for the treatment of XPS data is the referencing of the binding energies. Although an overlooked step, it is essential to perform a correct referencing of the BE, since it is through the BE that we identify the chemical state of the ejected photoelectrons from the surface. The use of adventitious carbon (AdC) is widespread for the calibration of the BE scale. However, a major drawback to this method relates to the uncertainty of the true nature of the adventitious carbon and the appropriate reference values, which have a wide range from 284.6 to 285.2 eV for the C1s electrons [135]. Additionally, in the past few years this range used for the AdC has increased further in literature, from 284 eV to 285.6 eV, as reported by Greczynski et al. [135].

Since we used a conductive material to be analysed, the energy reference of the detected atoms that is used is the Fermi level of the sample, a known energy of a reference peak that can be used for calibration. This is possible because for a conductive material, the connection of the sample with the analyser causes the Fermi level of both the sample and the analyser to be equal due to electron transfer through the electrical connection [134]. Therefore, the Fermi level is defined as the natural "0 eV" on the BE scale, and any shift in the Fermi level is applied to the entire spectra, thus referencing the binding energies correctly.

To perform the referencing of the BE from Fermi level, the Fermi level is recorded during an XPS measurement, and the data is plotted as shown in Figure 2.15. The plotted data can then be fit using the Fermi-Dirac distribution. Using this fit, we can determine the correction or shift that must be applied so that we obtain the Fermi level at exactly 0 eV. We can also obtain the fermi level position from the maximum of the derivative of the curve. This is shown in Figure 2.15 where the Fermi level of a clean copper sample was recorded and fit and the derivative of the slope was also calculated. Once this was performed, we observed that the Fermi level was at -0.15 eV, which thus requires a shift of 0.15 eV to the positive side for BE correction. Therefore, all the spectra of this measurement were shifted by 0.15 eV for proper binding energy referencing.

Curve fitting

Curve fitting, also known as peak fitting, is the process used to extract information from the spectral data for numerous techniques [136]. The objective of curve fitting high-resolution core level XPS spectra with a set of component peaks is to separate the photoemission signal originating from distinct elemental or chemical states. The position of a component peak provides evidence for assigning it to an elemental or chemical environment. The FWHM (full

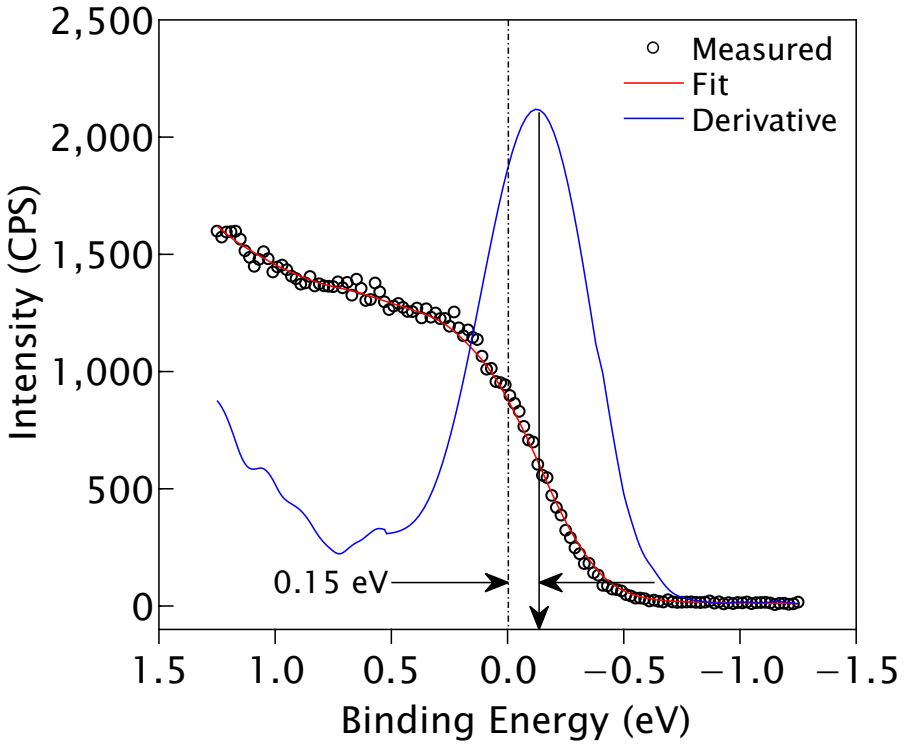

Figure 2.15: The Fermi level correction used to reference the binding energy for the XPS spectra of a clean copper sample.

width at half maximum) and peak line shapes are indicators of the chemical and physical environment of the atom. Quantitative information about the concentration of the chemical states identified is inferred by measuring the relative area of each component peak. There are two main aspects to the curve fitting process: the background adjustment and the decomposition of the component peaks.

The background intensity represents electrons which were initially photoemitted but lose their energy on the way to the surface [136]. This background energy tends to increase at lower kinetic energies of the spectra due to accumulation of all the photoelectrons of higher kinetic energies that have lost some energy. The intensity of a measured peak from an XPS spectra sits on a background intensity which needs to be considered for quantitative analysis. To take into account this background, one of the following three models is generally used: linear background,"Shirley background", or "Tougaard background" [137].

A linear background uses a straight line drawn from above the peak to a point below the peak, which makes it very convenient. However, this simple method does not take into account the numerous processes associated with the background formation and is therefore riddled with large errors. In XPS, the background at a lower kinetic energy is usually higher than that at a higher kinetic energy, as mentioned earlier. The Shirley background takes this fact in to

account and makes a basic assumption that the number of inelastically scattered electrons contributing to the background increase is directly proportional to the total photoelectron flux [135]. Therefore, in this case, the background intensity at the BE is proportional to the total peak area in the energy range defined by the BE and the end point on the low BE side of the peak [135].

The Tougaard background considers the initial energy distribution function and the inelastic scattering of electrons, and thus relies on a quantitative description of the physical processes that lead to the background [137]. This results in a reliable background and eventually a more precise peak component intensity. However, it requires a large energy range for a reasonable fit, and it also depends on in-depth elemental distributions of the substrate [134]. Due to these complications, the Tougaard background is less frequently used, as long as the Shirley method provides a reasonable accuracy.

We have used an iterative Shirley type background for all the spectra considered in our measurements. For both the linear and Shirley type of background subtraction, the choice of start and end points of BE strongly influence the intensity of the peak measured. Therefore, it is imperative to select an appropriate BE range which considers the entire component peak (not too close to the peak) and does not include other stray components (not too far from the peak). This is done by considering numerous start and end points and evaluating the increase or decrease in intensity due to a change in the BE selection. Once the change in intensity is within a desired error margin, which is less than 3% in our case, the binding energies selected as start and end points are kept consistent for all the curve fittings of an element.

The next step of the curve fitting process is the decomposition of the peaks. This is the process that gives us the intensities of the components relating to the various chemical states of the electrons ejected from the surface of the sample. Decomposition is a very intricate process which needs to be performed with the utmost care and understanding of the fitting process. A poor set of initial guesses can cause the fitting algorithm to direct the fit into a local minimum that is not representative of the sample physics and chemistry. This means that the curve fitting process can give a mathematically good fit even if the component peaks in the final fit are not chemically or physically reasonable [136]. Therefore, for decomposition of the spectra, constraints such as binding energy ranges, FWHM, line shapes, and intensity ratio of spin-orbit doublets were applied to ensure proper fitting of the curves. The details corresponding to the decomposition of the spectra are provided later along with the results. The curve fitting of the core-level spectra was performed with the Thermo Fischer scientific software Avantage, while the Cu LMM Auger spectra were decomposed using the CasaXPS software.

2.5.4 Thickness estimation

The data from the XPS results, mainly the intensities of components obtained from decomposition of peak components, can be used to estimate the thickness of thin films on the surface of the material. This is possible by using the equation used for calculating the intensity $\mathrm{d}I$ of a photoelectron peak from an element, within a layer of thickness $\mathrm{d}z$, found at a depth of z, and is given by:

$$\mathrm{d}I = kFSN\sigma T \exp \frac{-z}{\lambda \sin \theta} \mathrm{d}z \tag{2.3}$$

where k is a constant depending on the experimental parameters, F ($\mathrm{m}^{-2}\mathrm{s}^{-1}$) the photon flux, S (m^2) the analysed area, N (m^{-3}) the density of emitting atoms, σ (m^2) the photoionisation cross section, T the analyser transmission function, λ (m) the inelastic mean free path, and θ the emission angle of photoelectrons (take-off angle).

To estimate the thickness of the thin-films, oxide film and 2-MBT film in this case on copper metal, we must first construct a model representative of the qualitative results obtained. Several models were considered for this procedure, the first being a model where the two layers are continuous, homogeneous, and the 2-MBT layer is entirely above the oxide layer. However, as will be seen later, this was discarded due to irrefutable proof of direct 2-MBT bonding to metallic copper. Therefore, the oxide layer could not be continuous and the 2-MBT layer could not be homogeneous in distribution. The second notable model considered was a model where the above factors were taken into account, and the 2-MBT film had a uniform thickness on the entire surface. However, this was rejected as well due to inconsistencies in the results obtained when comparing the difference between that of the photoelectron intensities of the oxygen and copper spectra and the Cu LMM auger spectra. Therefore, we considered a model where we take into account the non-continuous oxide layer (islands of oxide), and a 2-MBT layer which forms on both the oxide layer and the metallic substrate, as shown in Figure 2.16.

For the validity of this model, certain assumptions need to be considered to allow us to estimate both the thickness and coverage of the films. These assumptions along with their need for consideration are listed below.

- The Cu substrate is assumed to have infinite thickness, which means thickness greater than the escape depth of the analysed photoelectrons, i.e. greater than 5 λ (99% of the electrons).
- The thickness of the oxide islands is assumed to be uniform since we cannot estimate

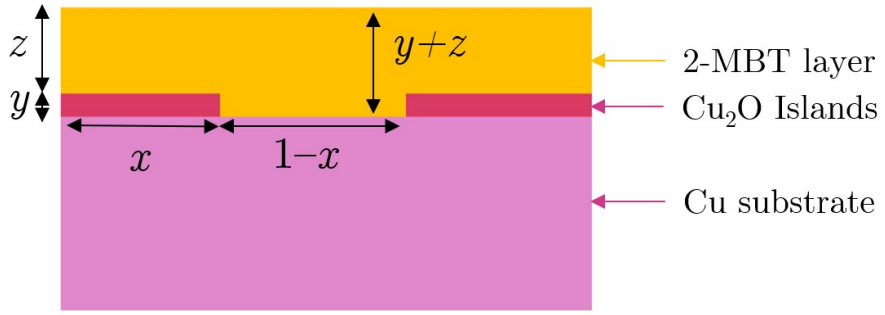

Figure 2.16: Illustration of the bi-layer model of the interface along with the dimensions of the thin films, where x is the total coverage of the oxide islands, y the thickness of the oxide islands, z the thickness of the 2-MBT layer on top of the oxide islands, $1-x$ the coverage of sulphur bonded directly to the metallic copper substrate , and $y+z$ the thickness of the 2-MBT layer above the metallic substrate non-covered by oxide.

the thickness of each oxide island individually.

- The surface of the 2-MBT layer is assumed to be conformal with that of the underlying metallic substrate, i.e. the thickness of the 2-MBT layer above the metallic substrate is considered to be the sum of the thickness of the oxide islands and the thickness of the 2-MBT layer above the oxide islands. Although this may not be the exact case for the differently pre-treated substrates on which the inhibitor is adsorbed, we have found that this assumption results in values which are more consistent than if we consider a model where the 2-MBT layer thickness is uniform throughout (same thickness of 2-MBT on the metallic substrate and on the oxide islands).

- The intensity of the entire Cu $2p_{3/2}$ peak is used as representative of copper metal, thus ignoring the contributions of copper oxide in this peak. This is only valid if the quantity of the oxides is very low, i.e. below 1 nm of equivalent thickness, so that the effect it has on the results is within the uncertainty range.

- For the 2-MBT molecules directly sulphur-bonded to metallic copper, we assume that the molecules are bonded in an upright position and therefore the thickness of the layer is taken as 0.8 nm (height of 2-MBT molecule). This assumption considers previous works where it was observed that the 2-MBT molecule adsorbs mostly in an upright position [84, 85]. Although in various cases the molecule can adsorb by 2 of its hetero-atoms (sulphur/sulphur or sulphur/nitrogen), the change it would have on the thickness is only 0.1 nm for every layer of 2-MBT, which is within the margin of error.

- The surface contamination layer on top of the substrate is ignored for quantitative analysis. This is done because (i) we cannot distinguish between the carbon originating

from contamination and the carbon that originates from the 2-MBT molecule, and (ii) the attenuation due to this contamination layer would affect all the subsequent layers underneath it. Therefore, we ignore the effect of the contamination layer on the bi-layer model.

In order to estimate the values of the thickness and coverage of the layers mentioned above, the photoelectron intensities of Cu 2p, N 1s, S 2p (S3 component relating to S bonded to metallic Cu), and O 1s (O3 component related to copper oxide (Cu_2O)) were input in the system of equations (Eq. 2.4, 2.5, and 2.6) expressing the attenuation of the photoelectron intensity for the constructed model, as shown in Figure 2.16, which are expressed as follows:

$$\frac{I_{S3}}{I_{O3}} = \frac{\sigma_S T_S N_S^{MBT} \lambda_S^{MBT} (1-x) \left[1 - \exp\left(\frac{-0.8}{\lambda_S^{MBT}}\right)\right] \exp\left(\frac{-(y+z)}{\lambda_S^{MBT}}\right)}{\sigma_O T_O N_O^{Cu_2O} \lambda_O^{Cu_2O} x \left[1 - \exp\left(\frac{-y}{\lambda_O^{Cu_2O}}\right)\right] \exp\left(\frac{-z}{\lambda_O^{MBT}}\right)} \tag{2.4}$$

$$\frac{I_{O3}}{I_{Cu}} = \frac{\sigma_O T_O N_O^{Cu_2O} \lambda_O^{Cu_2O} x \left[1 - \exp\left(\frac{-y}{\lambda_O^{Cu_2O}}\right)\right] \exp\left(\frac{-z}{\lambda_O^{MBT}}\right)}{\sigma_{Cu} T_{Cu} \begin{pmatrix} N_{Cu}^{Cu} \lambda_{Cu}^{Cu}\, x \exp\left(\frac{-y}{\lambda_{Cu}^{Cu_2O}}\right) \exp\left(\frac{-z}{\lambda_{Cu}^{MBT}}\right) \\ + (1-x) \exp\left(\frac{-(y+z)}{\lambda_{Cu}^{MBT}}\right) \\ + N_{Cu}^{Cu_2O} \lambda_{Cu}^{Cu_2O}\, x \left[1 - \exp\left(\frac{-y}{\lambda_{Cu}^{Cu_2O}}\right)\right] \exp\left(\frac{-z}{\lambda_{Cu}^{MBT}}\right) \end{pmatrix}} \tag{2.5}$$

$$\frac{I_N}{I_{O3}} = \frac{\sigma_N T_N N_N^{MBT} \lambda_N^{MBT}\, x \left[1 - \exp\left(\frac{-z}{\lambda_N^{MBT}}\right)\right] + (1-x) \left[1 - \exp\left(\frac{-(y+z)}{\lambda_N^{MBT}}\right)\right]}{\sigma_O T_O N_O^{Cu_2O} \lambda_O^{Cu_2O} x \left[1 - \exp\left(\frac{-y}{\lambda_O^{Cu_2O}}\right)\right] \exp\left(\frac{-z}{\lambda_O^{MBT}}\right)} \tag{2.6}$$

where, x is the total surface coverage of oxide islands, y the thickness of oxide islands, z the thickness of 2-MBT layer above the oxide islands, $y + z$ the thickness of 2-MBT layer above the metallic Cu, I the intensity of the photoelectrons, λ the inelastic mean free path, T the transmission function of the analyser, σ the photoionization cross section, and N the density of emitting atoms.

Using an iterative process and solving the equations numerically, Equation 2.4 is used to determine the surface coverage of the residual oxide islands (x) using the intensities of the S3 component (sulphur bonded to metallic Cu) and O3 component (oxygen from metal oxide (Cu_2O)). Equation 2.5 enables us to extract the thickness of the oxide islands (y) from the intensities of the O3 component intensity and Cu 2p peak. Lastly, Equation 2.6 gives us the thickness of the 2-MBT organic layer above the oxide islands (z) using the intensities of the N 1s peak and O3 component.

The uncertainties on the thickness and coverage values were estimated by the general formula

Table 2.3: Values for the inelastic mean free path (λ), the transmission function of the analyser (T), the photoionization cross section (σ), and the density of emitting atoms (N) used for the estimation of thickness and coverage of the thin films on copper.

λ (Inelastic mean free path) (nm)	$\lambda^{\mathrm{Cu}}_{\mathrm{Cu\ 2p}}$	1.01
	$\lambda^{\mathrm{Cu_2O}}_{\mathrm{Cu\ 2p}}$	1.23
	$\lambda^{\mathrm{MBT}}_{\mathrm{Cu\ 2p}}$	1.64
	$\lambda^{\mathrm{MBT}}_{\mathrm{S\ 2p}}$	3.26
	$\lambda^{\mathrm{MBT}}_{\mathrm{N\ 1s}}$	2.78
	$\lambda^{\mathrm{MBT}}_{\mathrm{C\ 1s}}$	3.01
	$\lambda^{\mathrm{MBT}}_{\mathrm{O\ 1s}}$	2.50
	$\lambda^{\mathrm{Cu_2O}}_{\mathrm{O\ 1s}}$	1.80
T (Transmission function)	$T_{\mathrm{S\ 2p}}$	2931
	$T_{\mathrm{N\ 1s}}$	3233
	$T_{\mathrm{Cu\ 2p}}$	4264
	$T_{\mathrm{O\ 1s}}$	3429
σ (Photoionization cross section) (normalised to C 1s cross section)	$\sigma_{\mathrm{C\ 1s}}$	1.00
	$\sigma_{\mathrm{S\ 2p}}$	1.68
	$\sigma_{\mathrm{N\ 1s}}$	1.80
	$\sigma_{\mathrm{O\ 1s}}$	2.93
	$\sigma_{\mathrm{Cu\ 2p_{3/2}}}$	16.73
N (Density of emitted atoms) ($\mathrm{mol/cm^3}$)	$N^{\mathrm{Cu}}_{\mathrm{Cu}}$	0.141
	$N^{\mathrm{Cu_2O}}_{\mathrm{Cu}}$	0.084
	$N^{\mathrm{MBT}}_{\mathrm{S}}$	0.017
	$N^{\mathrm{MBT}}_{\mathrm{N}}$	0.009
	$N^{\mathrm{Cu_2O}}_{\mathrm{O}}$	0.042

for the propagation of uncertainty, Equation 2.7, where the uncertainty of each parameter was considered as a function of the variable to be determined.

$$\sigma(Y) = \sqrt{\sum_{i=1}^{n} \left(\frac{\partial Y}{\partial X_i}\right)^2 \sigma^2(X_i)} \tag{2.7}$$

Table 2.3 compiles the values of λ, T, σ, and N used for these equations. The values of the photoionization cross-section σ at 1486.6 eV photon energy were taken from the Scofield database [138], those of the transmission function of the analyser T were given by Thermo Fisher, and the values of the inelastic mean free path λ were determined using the Tanuma Powell Penn (TPP) - 2M formula [139].

2.6 Time-of-Flight Secondary Ion Mass Spectrometry

Time-of-Flight Secondary Ion Mass Spectrometry (ToF-SIMS) is an ultra-sensitive surface analysis technique used to perform elemental, isotopic, and molecular analysis of surfaces. The technique involves bombarding the surface with ions which cause a collision cascade with the subsequent emission of species (electrons, neutral particles, and ions) from the surface (around 1 nm in depth), as shown in Figure 2.17. Among all the ejected species, only the ionized surface atoms or atom clusters are detected by a Time-of-Flight analyser.

The first ion sputtering observations were performed by J. J. Thompson in 1910 [140]. However, only after key developments in the vacuum pump technology in the 1940's were the first SIMS instruments developed and constructed. Although many projects worked on the development of SIMS instruments independently between 1940's - 1960's, it was Alfred Benninghoven at the University of Münster, Germany, who was accredited with the development of ToF-SIMS. This was due to his method of static SIMS, where he introduced a very low primary ion current density that allowed for the analysis of the first few surface layers of the solid [141].

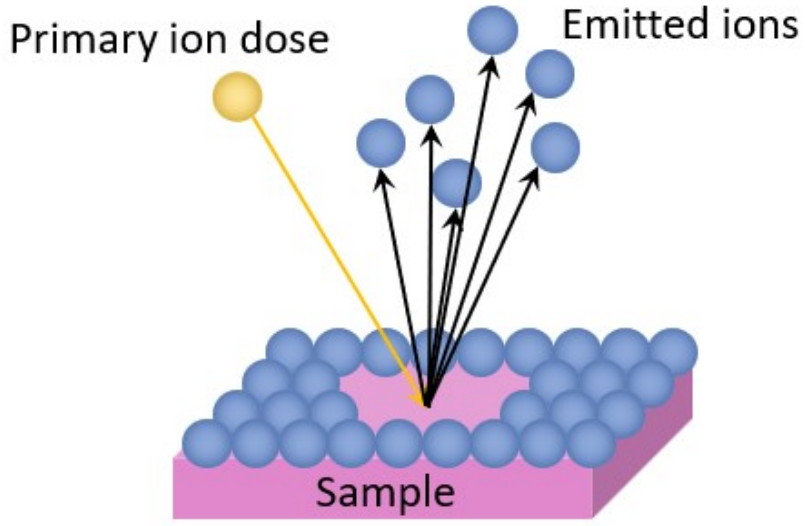

Figure 2.17: Schematic diagram showing the working principle of ToF-SIMS.

ToF-SIMS measurements are performed in ultra-high vacuum (UHV), which protects the surface from contamination and limits the interaction (recombination) between the produced secondary ions and the environment. Contrary to dynamic SIMS spectrometry, ToF-SIMS is known as a static measurement, meaning that the total primary ion dose remains lower than 10^{12} /cm^2 (the atomic or molecular surface density is in the order of 10^{15} /cm^2), assuring

that a nearly non-perturbed surface is probed by the primary ions. Thus, the analysis is restricted to the first few surface layers of the solid [141]. Due to a large variation in ionization probabilities among different materials, ToF-SIMS is mostly considered to be a qualitative technique. Nevertheless, quantitative measurements can be obtained by comparing the results with standard substrate of similar matrices.

2.6.1 Basic Principles and Instrumentation

The main components of the spectrometer, as shown in Figure 2.18, are:

- A primary ion gun (usually a liquid metal ion gun (LMIG)),
- A sputtering ion gun,
- The ToF-SIMS analyser, composed of the ion flying tube and the secondary ion detector.

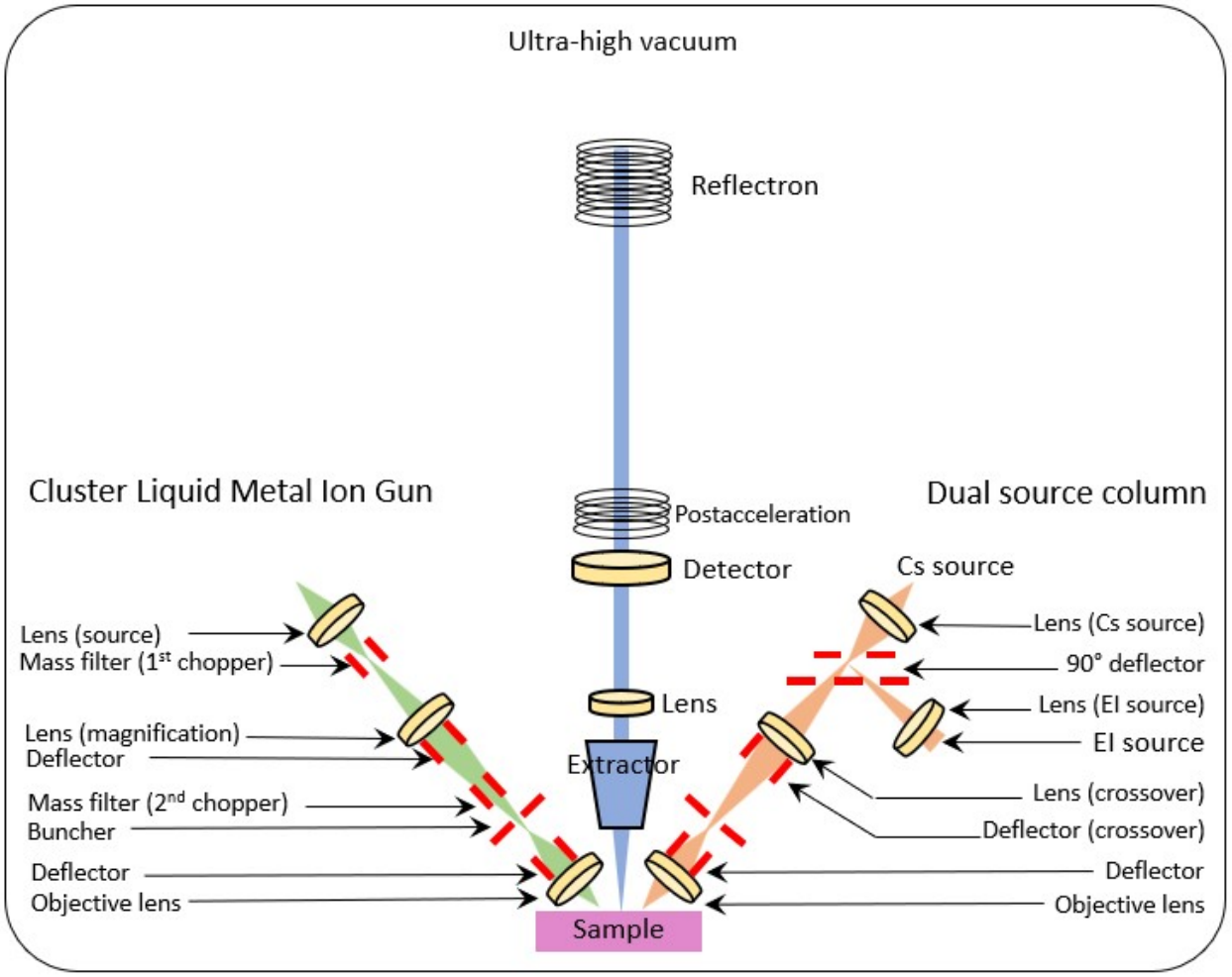

Figure 2.18: Schematic showing the main components of the ToF-SIMS 5 spectrometer.

For a ToF-SIMS analysis, initially the sample is bombarded with few keV kinetic energy

pulsed primary beam of charged monoatomic (Bi^+, Ga^+, or Au^+) or cluster ($Bi_3{}^+$, $Bi_3{}^2+$, $Ar_n{}^+$) ions from a liquid metal ion gun (LMIG), which is focused on the substrate by a series of lenses, deflectors, and a buncher in the optics column. The emitted ions, produced by the collision of the primary ions with the substrate, are then accelerated in the spectrometer by an electric potential difference (U) to a common kinetic energy and enter the Time-of-Flight analyser. This analyser sorts the ions by their mass/charge ratio, which is determined by the time they need to travel from the entrance of the analyser to the detector. For a given charge, lighter ions travel faster through the analyser, since the time of flight (ToF) is directly proportional to the square root of the mass/charge ratio. This relation is given below in Equation 2.8.

$$t = \frac{L}{v} = L\sqrt{\frac{m}{2qU}} \tag{2.8}$$

where, t is the time needed to travel through the flying ion tube to the analyser, L is the length of the flying ion tube, v is the velocity of the secondary ions, q is the charge of the secondary ions, U is the electric potential difference used to accelerate the produced secondary ions, and m is the mass of the secondary ions. This in turn allows for identification of the ions by measuring the time taken for the secondary ions to arrive at the analyser. To achieve a higher mass resolution, a combination of a reflectron (ion mirror) and a linear drift path is installed, which then extends the flight path and thus increases the differences between the flight times of each ion thereby increasing the mass resolution.

To perform in-depth analysis of the sample (depth profiling), two ion beams operate alternatively in the dual beam mode. A sputtering ion gun (usually O^+, Cs^+, $Ar_n{}^+$ cluster ions) is used to sputter a crater on the surface in a controlled manner, while after each sputtering step, the bottom of the crater is analysed by the primary ion beam. By this method, mass spectra are recorded at each step thus obtaining a detailed in-depth elemental profile by plotting the intensity of a characteristic secondary ion as a function of the sputtering time.

2.6.2 Experimental parameters

The in-depth elemental analysis of this work was performed using a ToF-SIMS 5 spectrometer (IonTof - Münster Germany), shown in Figure 2.19, operating at a base pressure of 5 x 10^{-9} mbar. High current (HC) bunched mode was used for performing analysis using Bi^+ primary ions of 25 keV energy at a target current of 1.2 pA over an area of 100 x 100 μm^2. Depth profiles were obtained by interlacing analysis in static SIMS conditions with sputtering using a Cs^+ ion gun of 0.5 keV delivering a 20 nA target current over a 500 x 500 μm^2 area. The

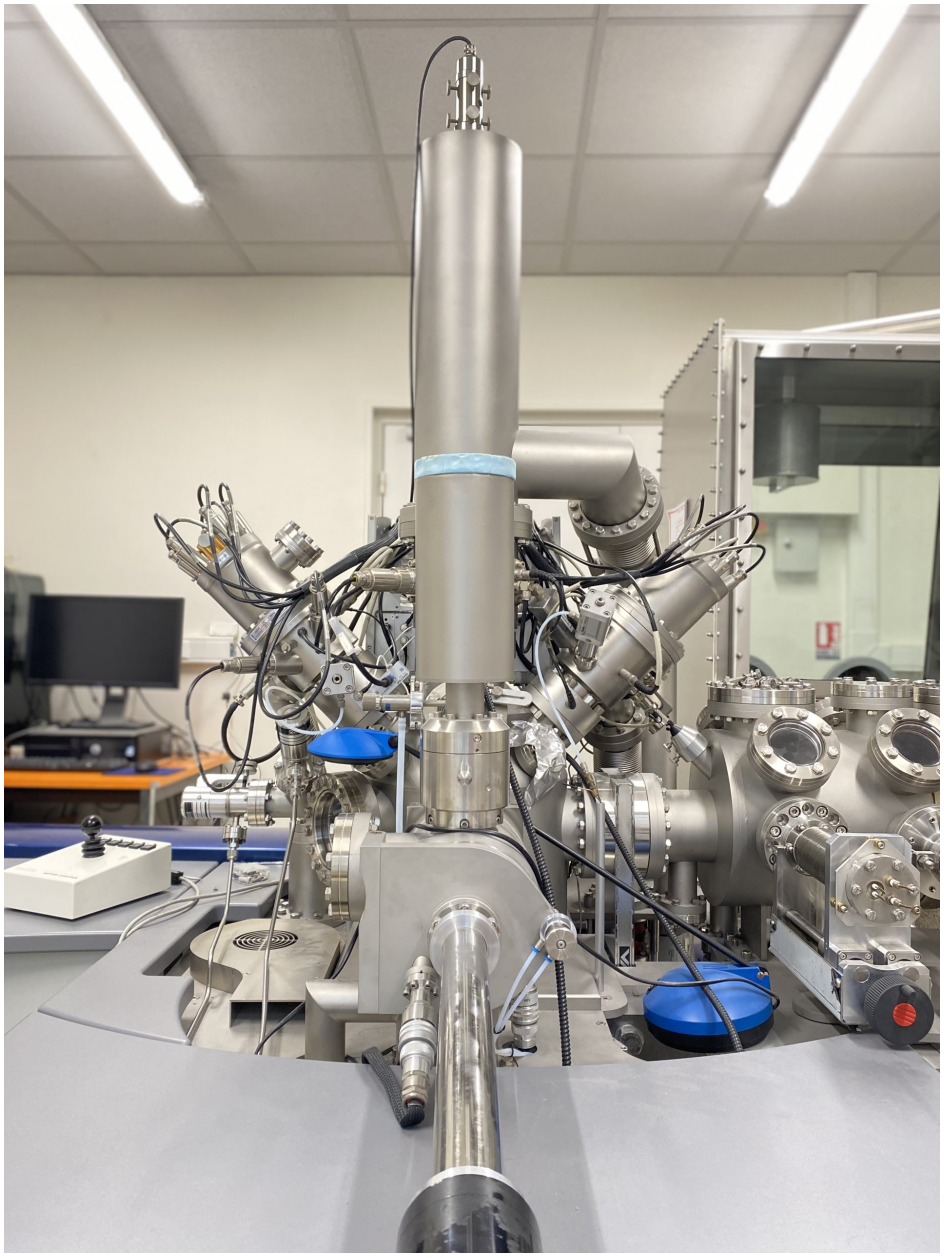

Figure 2.19: The ToF-SIMS 5 spectrometer by IonTof used for this study.

combined use of Bi^+ primary ions and Cs^+ sputtering ions enable us to analyse both the organic and inorganic surface layers. Both ion beams were at an incidence of 45° with respect to the sample surface and well-aligned to ensure analysis at the centre of the sputtered crater. Negative secondary ions were recorded because of their higher sensitivity to fragments coming from the oxide matrices. Three measurements were recorded from different regions on each sample to ensure reproducibility. SurfaceLab software v6.5 was used for data acquisition and post processing analysis.

2.6.3 Treatment of data

Prior to the construction of the depth profiles, the data must be well calibrated. This was performed using the signals of the C^- (12.0035 amu), N^- (14.0161 amu), S^- (31.9743 amu), Cu^- (62.9335 amu), Cs^- (132.9064 amu), Bi^- (208.9852 amu), and other ions with a distinct signature along a wide range of mass interval to ensure proper calibration. Next, the selection of the characteristic signals was carried out meticulously to reconstruct the depth profiles. Signals which were either saturated or too weak could not be considered since they would not give any beneficial information for analysis. Additionally, care was taken to ensure that there was no overlapping of peaks from several elemental peaks due to their similarity in mass.

2.6.4 Selection of Ion profiles

The ions selected for the depth profiles were Cu^- characteristic of the metal substrate, O^- of the overall oxygen, CuO^- and Cu_2O^- representative of the metal oxide, and $^{37}Cl^-$ as the chlorine adsorbed on the surface. On substrates exposed to 2-MBT organic inhibitor, the $C_7H_4NS_2^-$, C_2N^-, C_2S^-, and $^{34}S^-$ ions were selected as they are characteristic of the 2-MBT molecule, its molecular fragments of nitrogen and of sulphur, and the overall sulphur, respectively. Lastly, the $CuC_7H_4NS_2^-$ ions were selected as characteristic of the Cu-2-MBT interaction, both as bonding between the molecule and the metallic/oxidized substrate and as possible metal-organic complexes.

On substrates exposed to the 2-MBI organic inhibitor, the $C_7H_4N_2S^-$ ion profile was selected as characteristic of the 2-MBI molecule. The CuS^- and CuN_2^- ion profiles were selected as representative of Cu interaction with the 2-MBI molecule fragments of sulphur and nitrogen. The $CuC_6H_4NS^-$ ion profile was considered as representative of an interaction between copper and the 2-MBI molecule, including the contribution arising from metal-organic complexes formed. The selected ions for both 2-MBT and 2-MBI adsorbed copper samples along with their mass (amu) and represented species are detailed in Table 2.4.

Table 2.4: Characteristic secondary ions selected for in-depth elemental analysis by ToF-SIMS

	Characteristic Ion	Mass (amu)	Represented Species
All samples	Cu^-	62.9335	Copper metal
	O^-	15.9976	Overall Oxygen
	CuO^-	78.9244	Copper oxide
	Cu_2O^-	141.8563	Copper oxide
	$^{37}Cl^-$	36.9707	Overall Chlorine
2-MBT adsorbed copper samples	$^{34}S^-$	33.9685	Overall Sulphur
	C_2N^-	38.0063	Nitrogen fragment of 2-MBT
	C_2S^-	55.9762	Sulphur fragment of 2-MBT
	$C_7H_4NS_2^-$	165.9895	2-MBT molecule
	$CuC_7H_4NS_2^-$	228.8619	Copper-2-MBT interaction
2-MBI adsorbed copper samples	CuN_2^-	90.9325	Copper-Nitrogen interaction
	CuS^-	94.9039	Copper-Sulphur interaction
	$C_7H_4N_2S^-$	149.0219	2-MBI molecule
	$CuC_6H_4NS^-$	184.9208	Copper-2-MBI interaction

CHAPTER 3

Surface state of copper

Surface analysis techniques such as XPS and ToF-SIMS are highly sensitive techniques, as discussed in the previous chapter. Factors such as surface contamination and roughness of the surface can modify the results drastically thus making the analysis process unnecessarily difficult. Therefore, it is imperative to first study the reference surfaces used for our experiments. This allows us to correctly interpret any changes occurring on the surface during the experiments compared to the initial surface state used.

In this chapter, we study the surface state of an oxide-free copper surface prepared in UHV conditions, a mechanically polished copper surface, and an electrochemically polished copper surface using XPS. The copper surface prepared in UHV was studied to obtain reference binding energies, FWHM, and line shapes of the spectra obtained for an oxide free surface. The mechanically polished copper sample was analysed to investigate the effects of polishing and the presence of any possible contaminants. Finally, the electrochemically polished copper surface was studied to determine the changes occurring during the electrochemical polishing process, namely the presence and quantity of contaminations that persist and the nature of the oxide layer that forms on the surface after electrochemical polishing.

3.1 Experimental

The copper samples were prepared by first mechanically polishing them down to 0.25 μm using diamond pastes and an alcohol-based lubricant, as described earlier in Chapter 2. The electrochemical polishing process used has also been detailed earlier in Chapter 2.

To obtain an oxide-free copper surface, the sample was first prepared by mechanically polishing it down to 0.25 μm, followed by rinising with acetone, ethanol, and ultra-pure water, after which it was introduced to the ultra-high vacuum system of base pressure 10^{-11} mbar. Several cycles of ion sputtering and annealing the surface were performed in the UHV system to prepare the surface. Argon ions of 0.5 keV energy with a pressure of 10^{-6} mbar and filament current of 10 mbar was used for sputtering the surface for a time-period of 120 seconds. The sample was then annealed by progressively heating up to 600°C and keeping the temperature constant for 2 hours under UHV conditions to reconstruct and recrystallise the surface. This cycle of sputtering and annealing was repeated 10 times to obtain an oxide-free surface with minimal contaminations.

3.2 Oxide-free copper

The XPS survey spectra of the oxide-free copper surface is given below in Figure 3.1 with the intensity plotted vs binding energy. The binding energies have been referred to the Fermi level of the sample. We observe that all the peaks observed in the survey spectra, other than the valence band, correspond to the orbital shells of copper and its Auger peaks. This indicates that the sputtering process has been effective in removing the topmost surface layers of the substrate, which include the oxide layer and the contamination layer.

The Cu 2p, O 1s, C 1s, N 1s, S 2p, and Cu LMM Auger spectra of the oxide-free copper substrate are given in Figure 3.2. The Cu 2p spectrum shows two peaks at 932.8 eV and 952.7 eV corresponding to the $2p_{3/2}$ and $2p_{1/2}$ contributions of the spin-orbit doublet, respectively. Using a Shirley background, the Cu $2p_{3/2}$ peak was decomposed, thus obtaining a FWHM of 0.9 eV. Since the other possible chemical states have similar binding energies to that of the Cu metal component, as shown in Table 3.1, we first analyse the other spectra before making comments on the oxide presence and quantity.

The O 1s spectrum shows that the presence of oxygen on the substrate is negligible with the absence of any discernible peak in the spectrum. This confirms that the BE of Cu $2p_{3/2}$ for metallic copper is indeed 932.8 eV with a FWHM of 0.9 eV. The N 1s and S 2p spectra do not exhibit any peak at all. They indicate that the quantities of these elements in the substrate are negligible, confirming that this is indeed a high-purity copper sample.

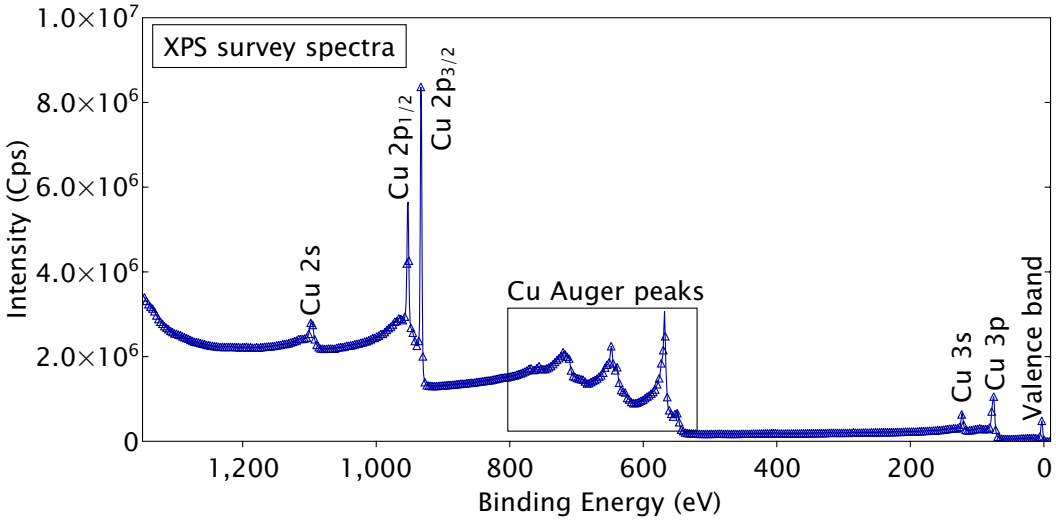

Figure 3.1: XPS survey spectra of an oxide-free copper surface prepared under UHV conditions.

The C1s spectrum shows the presence of some carbon species still remaining after ion sputtering. These species on the surface are most likely from contamination of the surface. Since we are not interested in the exact nature of these species, we do not decompose this C 1s spectrum. However, the quantity of these contaminants is of concern to us, therefore we added a Shirley type background to determine its intensity and subsequently its C/Cu ratio which was calculated to be 0.010 ± 0.001. This reveals that the total carbon present on the copper sample is only 1%.

Lastly, the Cu LMM Auger spectrum, which exhibits the line-shape of the Cu(0) ion profile, is presented. As we have already seen from the O 1s spectrum, there are no oxides remaining on the surface. Therefore, this spectrum is used as reference for the Cu(0) profile for the following analyses of the Cu LMM Auger spectra.

Table 3.1: Binding energies of various surface states of copper for the Cu $2p_{3/2}$ spin orbit, obtained from literature [142–144].

Copper species	Binding Energy (eV)
Cu metal	932.7 ± 0.1
Cu_2O	932.6 ± 0.1
CuS	932.5 ± 0.1
Cu_2S	932.9 ± 0.1
CuCl	932.4 ± 0.1
CuO	933.6 ± 0.1

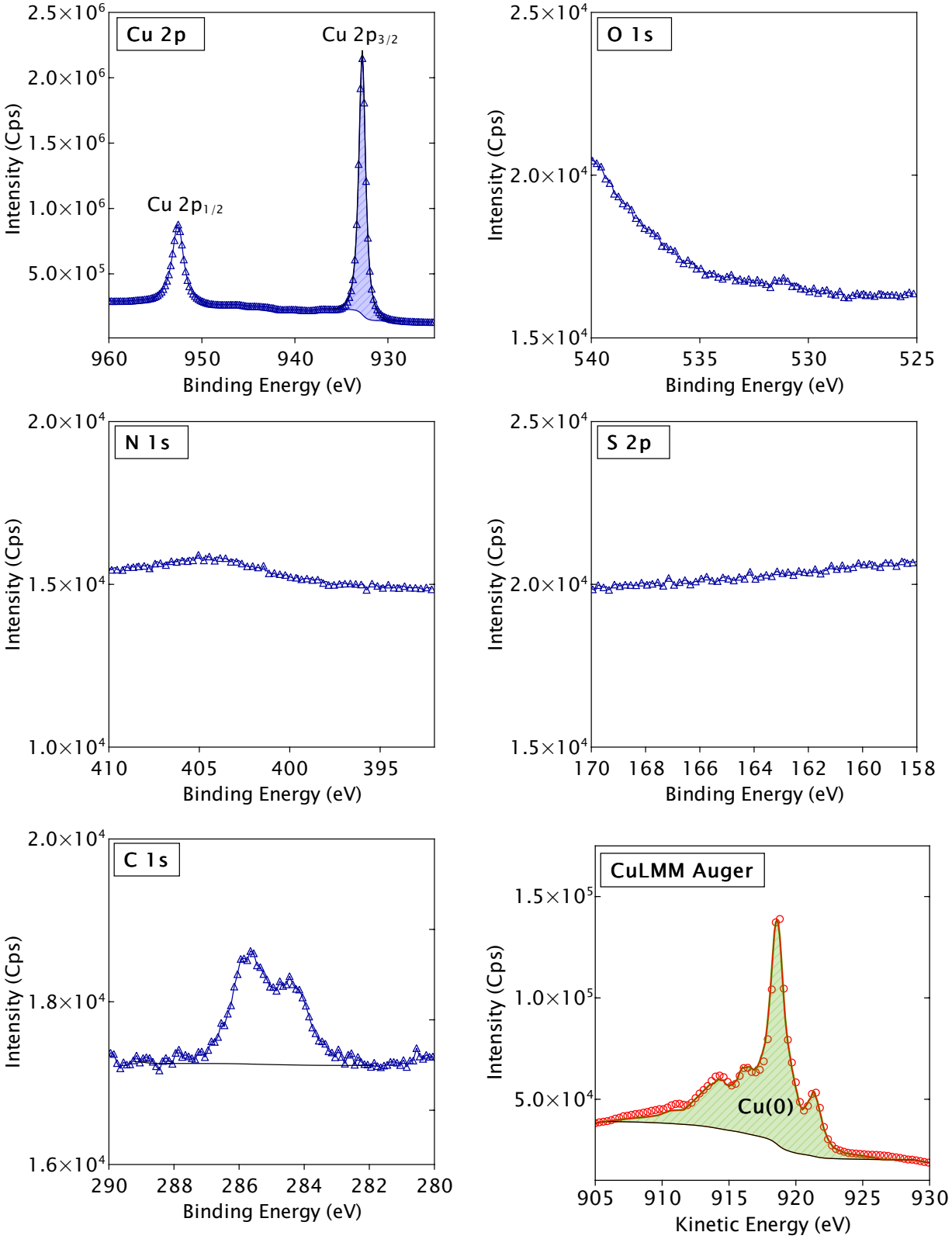

Figure 3.2: XPS Cu 2p, O 1s, C 1s, N 1s, S 2p core levels, and Cu LMM Auger spectra of an oxide-free copper surface prepared under UHV conditions.

3.3 Mechanically polished copper

The survey spectra of a polished sample of copper is given in Figure 3.3. Compared to the survey spectra of the oxide-free copper surface, seen above in Figure 3.1, we observe a couple of additional peaks, namely O 1s, C 1s, and their Auger peaks. Since these samples are prepared under normal atmospheric conditions, the presence of these components is warranted. The O 1s component is likely due to the oxide films on the surface and from contamination from air, while the C 1s component arises from contamination on the surface. This is even though the samples were cleaned rigorously in ultrasonic baths of acetone, ethanol, and ultra-pure water successively after the mechanical polishing process. The N 1s and S 2p components, also representative of contaminants found in the air, are not seen here either due to their complete absence or their low intensity. To evaluate the surface state after mechanical polishing better, high-resolution core level spectra of Cu 2p, O 1s, C 1s, N 1s, S 2p, and Cu LMM Auger spectra were recorded. These spectra are shown in Figure 3.4.

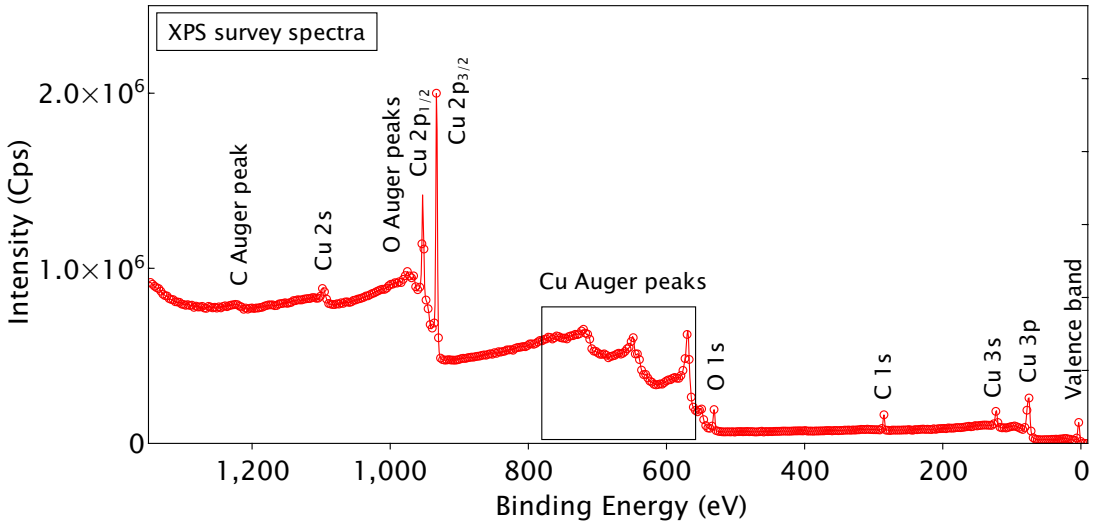

Figure 3.3: XPS survey spectra of a mechanically polished copper surface down to 0.25 µm using diamond paste solution.

The Cu 2p spectra for the polished copper sample is quite like that observed for the oxide-free copper sample. A single component (Cu1) is observed for the $2p_{3/2}$ at 932.8 eV which cannot be decomposed further due to overlapping of elements, as mentioned earlier. However, this Cu1 peak has an increased FWHM by 0.1 eV, compared to that of the oxide-free copper surface. Additionally, we observe a weak satellite at approximately 947 eV. These features in the Cu 2p spectrum are highly representative of copper oxide (CuO) films on the surface [145].

The O 1s spectrum exhibits a large peak here, unlike the previous case where no peak was

observed. The metal oxide components generally occur between the binding energies of 529 – 531 eV [83, 86, 142–144, 146]. The shoulders at higher binding energies, 531.5 and 532.6 eV, correspond to hydroxides and water/contamination adsorbed on the surface, respectively [83, 143, 144, 146]. Since this is not the surface state we use for the experiments, we are not interested in the species found here and therefore we do not decompose the spectra. However, a Shirley type background was added to allow us to determine the intensity and the atomic ratio of the components, which will later allow us to compare the results from the electrochemically polished copper sample. The O/Cu atomic ratio for the mechanically polished copper sample was determined to be 0.31 ± 0.13.

The C 1s spectrum also shows a considerably large peak here, with the C/Cu atomic ratio determined to be 0.38 ± 0.01. This shows that samples prepared in air can have significant quantities of contamination which may interfere with the experiments and the analysis of the results later. The N 1s and S 2p spectra exhibit small peaks here. Since these peaks were not observed on the oxide-free copper sample, we know that they originate from contamination species on the surface. The N/Cu atomic ratio determined was 0.006 ± 0.001, whereas the S/Cu atomic ratio was 0.015 ± 0.001, both substantially lower than the C/Cu ratio. This indicates that the contamination on the surface by nitrogen and sulphur is comparatively lower.

Regardless, the XPS spectra obtained for the polished copper sample shows that despite maintaining high standards of cleanliness during the mechanical polishing process and the rigorous ultrasonic cleaning of the sample, there is still a large amount of contamination on the surface. Given that we work with organic molecules consisting of carbon, nitrogen, and sulphur, the three elements which are often associated with contaminants, any work performed on a mechanically polished sample will lead to errors in the analysis of the XPS results. Therefore, it is crucial to either remove the contaminants completely or reduce them significantly so that when we perform surface analysis of the samples, we do not obtain higher intensities, increased FWHMs, and shifted binding energies.

The Cu LMM Auger spectrum of the mechanically polished sample shows three contributions, which are associated to Cu(0), Cu(I), and Cu(II). The Cu(II)/Cu(0) ratio obtained was 0.11 ± 0.01 whereas the Cu(I)/Cu(0) ratio was 0.69 ± 0.03 , indicating that we have a much larger quantity of Cu_2O compared to CuO. The presence of these two contributions would also explain the increased FWHM and the satellite peak observed in the Cu 2p spectrum discussed earlier.

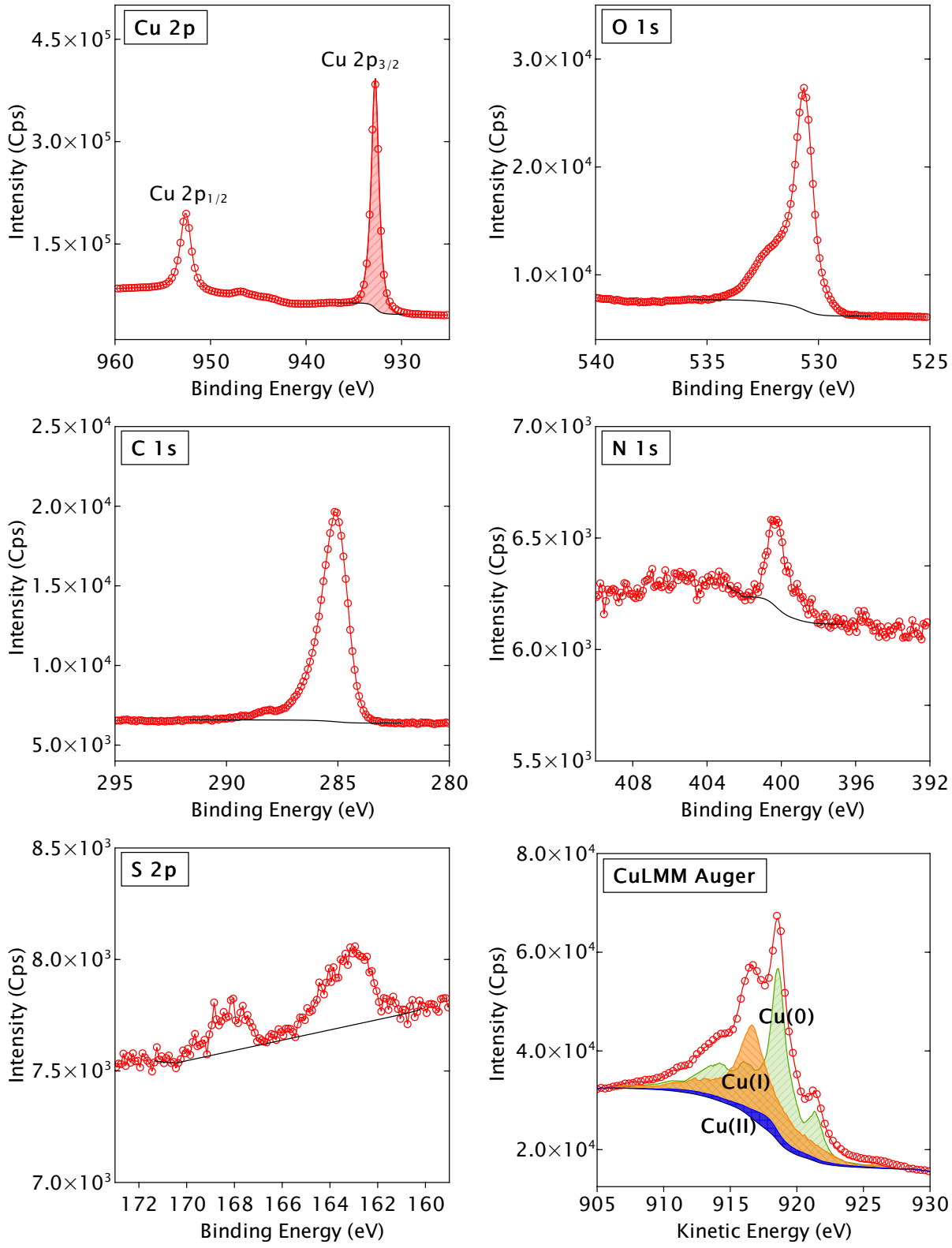

Figure 3.4: XPS Cu 2p, O 1s, C 1s, N 1s, S 2p core levels, and Cu LMM Auger spectra of mechanically polished copper surface down to 0.25 µm using diamond paste solution.

3.4 Electrochemically polished copper

The XPS survey spectra of copper after electrochemical polishing using a 60% H_3PO_4 solution is given in Figure 3.5. We observe that there is a reduction in the C 1s intensity measured for this sample compared to a mechanically polished sample (Figure 3.3). However, we have the presence of an additional element, phosphorous, in the survey spectra. To investigate these changes further, we study the core level spectra of the elements given in Figure 3.6.

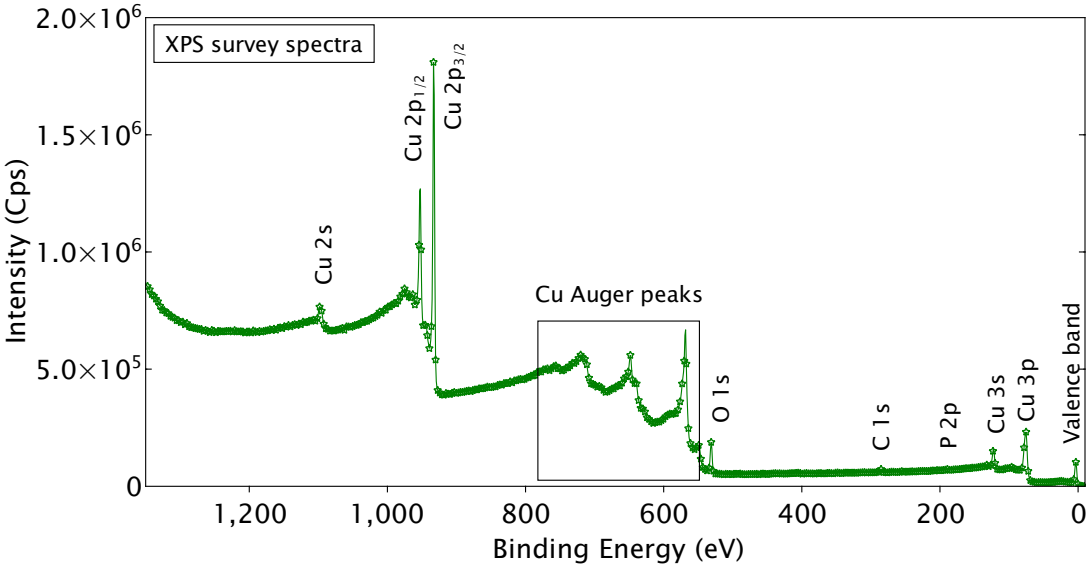

Figure 3.5: XPS survey spectra of an electrochemically polished copper surface using a using a 60% H_3PO_4 solution.

The Cu 2p scan exhibits two components, Cu 1 and Cu 2, for the Cu $2p_{3/2}$ spin orbit. The Cu 1 component at 932.8 eV corresponds to Cu(0) and Cu(I), as mentioned earlier, with an FWHM of 1 eV. The second component, Cu 2, at 935.5 eV with an FWHM of 1.5 eV, has not been seen earlier on the oxide-free sample or the mechanically polished sample. It is also not representative of CuO since its BE is expected to be at 933.6 eV, as mentioned earlier in Table 3.1, which is lower than the current species by 1.9 eV. We also observe a satellite peak/shake-up feature at approximately 945 eV, which is again at a different BE than that observed for CuO. In the work of Biesinger [147], where they analysed the XPS spectra of various copper compounds and species, they observed a similar satellite peak at 945 eV for the copper-phosphate compound $Cu_3(PO_4)_2$. Therefore, this satellite peak could be an indication of the formation of copper-phosphate films on the surface.

The P 2p spectrum is decomposed by its spin orbit doublet 3/2 and 1/2 with a split of 0.84 eV [144]. It exhibits one component for the $2p_{3/2}$ orbit at 132.6 eV, which corresponds to PO_3 (phosphonates) and PO_4 (phosphate) groups [144, 148]. The P/Cu atomic ratio on the

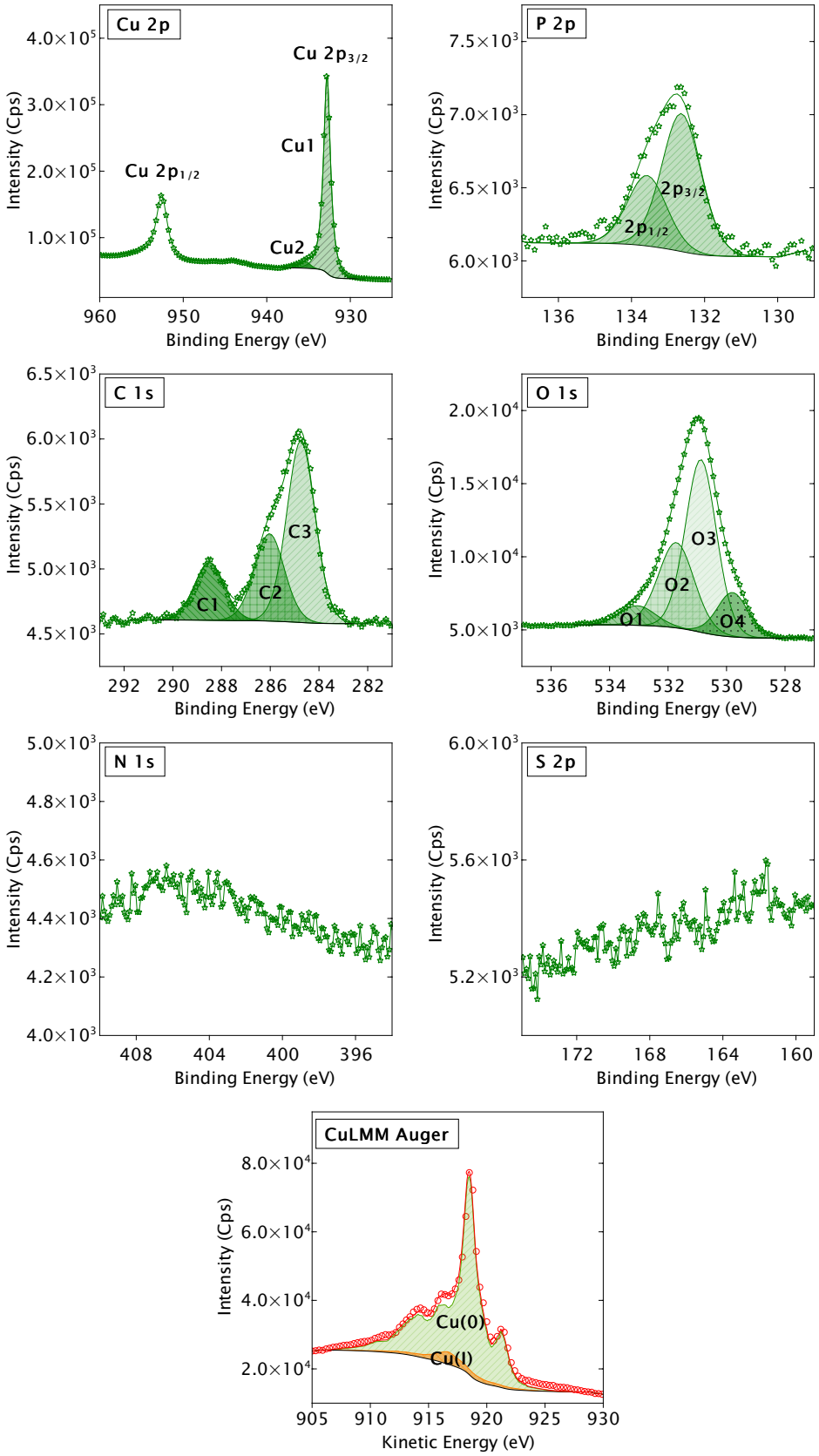

Figure 3.6: XPS Cu 2p, P 2p, O 1s, C 1s, N 1s, S 2p core levels, and Cu LMM Auger spectra of an electrochemically polished copper surface using a 60% H_3PO_4 solution.

electrochemically polished sample was determined to be 0.031 ± 0.001.

The C 1s spectra exhibits 3 components: C1 at 288.5 eV (FWHM 1.5 eV), C2 at 286.0 eV (FWHM 1.5 eV), and C3 at 284.8 eV (FWHM 1.4 eV). The C1 component corresponds to carbonates, C2 to alcohols, C-N, and C-S bonds, and C3 to C-C and C-H bonds [144]. These 3 components arise from contamination on the surface generally due to contaminants in the environment (air, water). The C/Cu ratio from this sample was determined to be 0.065 ± 0.002, with an 18% contribution from the C1 component, 28% from the C2 component, and 54% from the C3 component. On comparing the C/Cu ratio of the mechanically polished and electrochemically polished samples, we observe that the amount of carbon on the electropolished sample is significantly lower. Therefore, there is a definite effect of the electrochemical polishing step in reducing/removing contamination that persist from the mechanical polishing step.

For the O 1s scan we observe 4 components: O1 at 533.1 eV, O2 at 531.7 eV, O3 at 530.9 eV, O4 at 529.8 eV. These components are assigned to adsorbed water for O1, hydroxides for O2, phosphates and/or carbonates for O3, and metal oxides for O4 [83, 86, 142–144, 146]. The O/Cu atomic ratio for the electrochemically polished sample is 0.26 ± 0.01. However, a closer look reveals that the O3 component itself contributes to approximately 60% of this value. If we subtract the contribution of carbonates from the O3 peak by using the atomic ratio of the C1 peak from the C 1s spectrum with respect to Cu, we have a remainder of 0.138 for the O3/Cu atomic ratio. This value is almost 4 times that of the P/Cu ratio, thus confirming that we do have the presence of phosphates (PO_4) on the surface. Additionally, if we consider the ratio of the Cu2 component from the Cu 2p spectrum with respect to Cu(total), we observe that the order of magnitude is rather similar, thus suggesting that the Cu2 peak is most likely a component originating from the interaction between copper and phosphates. In the work of Rokosz et al. [149], they observed similar peaks for the Cu $2p_{3/2}$, although formed under different conditions. They proposed that the peaks at higher binding energies, between 934 and 938 eV, correspond to copper-phosphate compounds formed.

The presence of this phosphate film has been suggested earlier by Hoar and Farthing in 1952 [119] and by Gabe in 1972 [125]. They also suggested that the phosphate films formed on the surface are passive, however these phosphate films are easily dissolved or washed away. This could be why others such as Fang [124] did not observe any such film on the copper surface after electropolishing. In our work, we have found that phosphate films are present on the surface after electro-polishing, but not after the susequent immersion of the copper samples in other electrolytes during the experiments, as shown in the following chapters. This suggests that although in our experiments the phosphate film is not "easily" washed away, it eventually dissolves and is washed away during the electrochemical experiments,

thus limiting its interference on our experiments.

In the work of Aksu in 2009 [123], several copper-orthophosphate species were proposed based on the thermodynamic stability of these species as a function of concentration and pH. They suggested that the formation of anodic films due to electropolishing, such as $Cu_3(PO_4)_2$ or $Cu_3(PO_4)_2.3H_2O$, is unlikely due to the pH range and the need for immense concentrations of both copper and orthophosphate in the aqueous solution. However, they did suggest that this compound is predominantly formed at pH values greater than 4.5. Therefore, it is possible that the formation of the copper-phosphate films on the electrochemically polished copper samples occurs during the rinsing step after the electrochemical polishing process, where we rinse the sample with a 10% solution of H_3PO_4 followed by ultrapure water which would increase the pH and thus make the conditions more favourable to form the copper-phosphate films.

The N 1s and S 2p spectrum show negligible intensities, if any at all considering the signal to noise ratio. This is like that of the oxide-free copper surface, seen earlier in Figure 3.2. This confirms that the electrochemical polishing of copper does play a crucial role in the preparation of the sample surface, mainly in removing the excess contaminants that persist on the surface after mechanical polishing.

The Cu LMM Auger spectrum for the electrochemically polished sample exhibits the Cu(0) and Cu(I) components. We can see that Cu(I) has a very low intensity here, also reflected by the ratio between Cu(I) and Cu(0) which is 0.09 ± 0.01, much lower than that of the mechanically polished sample. This indicates that the oxide film on the surface is very thin, possibly on the order of a monolayer thickness, despite the sample being exposed to air during transfer to the UHV chamber for XPS analysis. This is therefore most likely an effect of the presence of the phosphate film on the surface which does not allow the growth of the oxide film on the copper substrate.

We do not however observe Cu(II) in the Cu LMM Auger spectrum, despite observing the Cu2 component in the Cu 2p spectrum and the satellite peak at 945 eV. This is most likely due to a different Auger structure of the copper-phosphate films compared to that of the CuO films, which is therefore not represented in the Cu LMM Auger spectrum.

3.5 Conclusion

The surface state of oxide-free, mechanically polished, and electrochemically polished copper has been studied by XPS analysis. It was shown that the oxide-free copper sample prepared under UHV is free from contaminants such as oxygen, sulphur, and nitrogen. The binding energy and FWHM of the oxide-free copper were also recorded for an accurate reference of metallic copper.

Although mechanical polishing of the sample is necessary to obtain an even surface that is free of scratches, we observed that there was a significant quantity of contaminants found on the surface. We also observed an increased FWHM of the Cu 2p peak due to the presence of copper oxides on the surface, formed in the presence of air. The oxide film formed on the surface after mechanical polishing was predominantly Cu_2O, although a small quantity of CuO was also observed. It was established that the surface state of copper after mechanical polishing is not as clean as one would expect, despite ultrasonically cleaning the copper sample in acetone, ethanol, and ultra-pure water after the polishing process.

The electrochemically polished copper sample exhibited much less contaminants on the surface compared to the mechanically polished sample, with negligible quantities of sulphur and nitrogen and a reduced quantity of carbon observed. However, the presence of a copper-phosphate species was observed on the surface, formed either during the electrochemical polishing process or the rinsing process after the electrochemical polishing. This copper-phosphate film was key in limiting the growth of the oxide film on the copper surface after electrochemical polishing and dissolves/washes away during the electrochemical experiments conducted after electrochemical polishing. It was concluded that electrochemical polishing of copper results in a cleaner surface state of the copper sample and is preferred as the starting point of our experiments over the mechanically polished surface state of copper.

CHAPTER 4

Enhanced corrosion inhibition of copper in acidic environment by cathodic control of interface formation with 2-mercaptobenzothiazole

This chapter is based on the work published in Electrochimica Acta by V. Garg, S. B. Sharma, S. Zanna, A. Seyeux, F. Wiame, V. Maurice, and P. Marcus, entitled "Enhanced corrosion inhibition of copper in acidic environment by cathodic control of interface formation with 2-mercaptobenzothiazole." [150]

In this chapter, the adsorption and corrosion inhibition of 2-MBT on copper were studied in a hydrochloric acidic medium in which copper does not passivate. The formation of the inhibitive layer was controlled by applying different cathodic pre-treatment methods. Cyclic voltammetry (CV) was applied to determine the protection offered by the 2-MBT organic inhibitor layer against the anodic dissolution of copper. Surface analysis by X-ray photoelectron spectroscopy (XPS) and time of flight – secondary ion mass spectrometry (ToF-SIMS) was used to investigate the bonding mechanisms of the 2-MBT molecule to the copper surface, including the role of the native oxides in the formation of the organic inhibitor layer, the effect of increased exposure time to the inhibitor, and the stability of the organic inhibitor layer upon anodic polarisation.

4.1 Experimental

The samples were prepared as described earlier in Chapter 2. The electrochemical experiments were performed using the Kel-F cells. The Pt pseudo-reference was calibrated before each experiment (+0.75 V vs SHE). The electrolytes were a 10 mM HCl aqueous acid solution of pH 2.3 as the reference solution without the inhibitor and a 10 mM HCl + 0.1 mM 2-MBT aqueous solution of pH 2.6 as the solution with inhibitor.

Cathodic pre-treatment was performed prior to the experiments in order to reduce the air-formed native oxides (Cu_2O). After immersion at the open circuit potential (OCP), the potential was swept cathodically to the onset of hydrogen evolution (down to −0.05 V vs SHE) and then swept back up to the value of +0.10 V vs SHE with a scan rate of 20 mV/s. This was repeated two times. The anodic dissolution tests were performed by sweeping the potential until the anodic apex of +0.37 V vs SHE, followed by reverse sweeping to −0.05 V vs SHE, and then back to the start point at +0.10 V vs SHE with a scan rate of 20 mV/s. To ensure reproducibility, the electrochemical experiments were repeated three times.

Surface analysis was performed after cathodic pre-treatment, i.e., in the as-obtained cathodically reduced metallic state of the interface (reduced state), and after sweeping the potential to the anodic apex, i.e., in the anodically polarized state (anodic state). Once the electrochemical tests were performed, the cell was disconnected and the samples were rinsed with ultra-pure water, dried using nitrogen, and immediately transferred to the UHV chambers for analysis with XPS and ToF-SIMS. The details of XPS and ToF-SIMS measurements have been described in the experimental chapter.

4.2 Cathodic pre-treatment of the surfaces

The cathodic pre-treatment curves obtained in the absence and presence of 2-MBT in the 10 mM HCl aqueous solution are presented in Figure 4.1, with the current density obtained in $\mu A/cm^2$ as the potential is swept cathodically and back. The corresponding cathodic charge from each of these curves was calculated by integrating the current density with respect to time and are presented in Table 4.1 along with the equivalent thickness of reduced oxides, δ. The latter was calculated using Faraday's law, given earlier in the experimental chapter Equation 2.1.

It is observed that for both cases, the first cycle of the cathodic pre-treatment reduces a significant amount of Cu_2O, i.e., more than 2 nm in equivalent thickness. For the pre-treatment in the absence of 2-MBT, the amount of copper oxide reduced in the second cycle is much lower, and nearly negligible in the third cycle reaching an equivalent thickness markedly

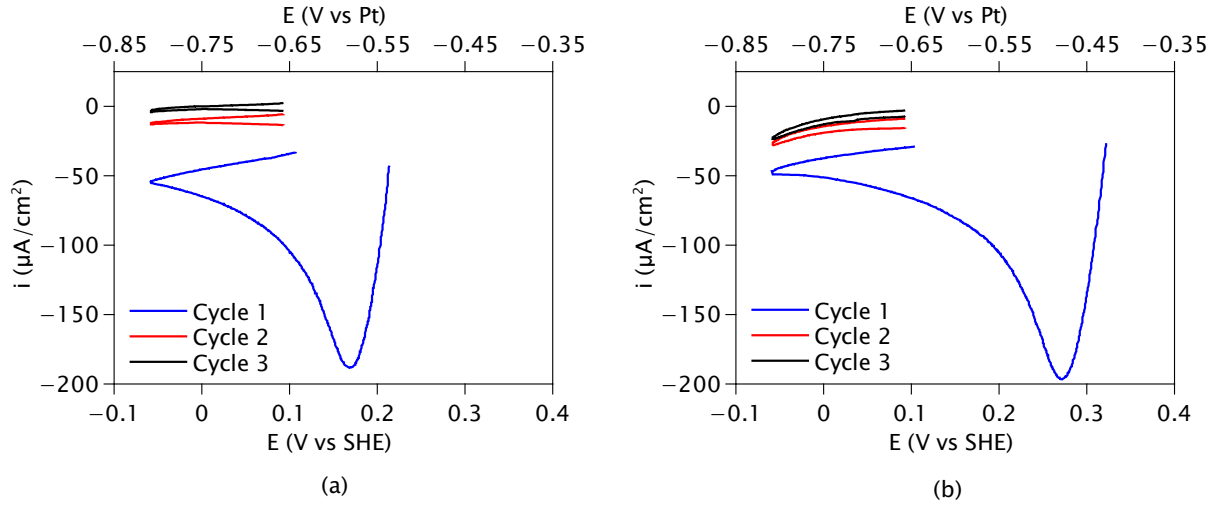

Figure 4.1: Cyclic voltammograms showing the three cathodic pre-treatment curves of copper obtained with a scan rate of 20 mV/s in (a) 10 mM HCl solution (without inhibitor), and (b) 10 mM HCl + 0.1 mM 2-MBT solution (with inhibitor).

less than that of a monolayer of Cu_2O (0.208 nm from the bulk structure). This suggests that all native copper oxide initially present has been reduced, which is supported by the current density value of 0 $\mu A/cm^2$ measured at the end of the third cycle. In these experimental conditions, dissolution of the native oxide is initiated immediately upon immersion in the 10 mM HCl solution, before the first cycle, due to the instability of copper oxide in the low pH of the solution. Therefore, it is likely that the total equivalent thickness of the native oxide is larger than that measured by cathodic pre-treatment. Thus, after the third cycle, a fully metallic state of the copper surface seems achieved in these pre-treatment conditions, although the presence of remaining traces of copper oxide, most likely formed during transfer of the samples in air, is indicated by surface analysis as shown further on.

The same cannot be said for the cathodic pre-treatment in the presence of the inhibitor. In this case, the total equivalent thickness of Cu_2O reduced in all three cycles is larger, which we assign to less oxide being dissolved upon immersion at OCP in the 2-MBT-containing HCl solution, due to the inhibitive effect 2-MBT molecules adsorbed on the native oxide-covered surface. The third cycle still reduces approximately a monolayer thickness of the native oxides. Additionally, the current density value at the end of the third cycle is slightly negative, which suggests that there were still oxides being reduced at this stage. This lower efficiency of the cathodic pre-treatment in reducing the native oxide within the three cycles is assigned to 2-MBT forming an inhibitor film covering the native oxide surface and poisoning the electrochemical reduction reaction. As a result, oxide islands, protected by the 2-MBT layer, could remain on the metallic substrate. Copper atoms, possibly unreduced, could also be

Table 4.1: Cathodic charge density (q) and equivalent thickness (δ) of copper oxide reduced during the three cathodic pre-treatment cycles of copper in 10 mM HCl solution (without inhibitor), and in 10 mM HCl + 0.1 mM 2-MBT solution (with inhibitor).

	Pre-treatment in HCl		Pre-treatment in HCl + 2-MBT	
	Charge density q ($\mu C/cm^2$)	Reduced Cu_2O δ (nm)	Charge density q ($\mu C/cm^2$)	Reduced Cu_2O δ (nm)
Cycle 1	1697 ± 38	2.10 ± 0.04	1907 ± 78	2.36 ± 0.10
Cycle 2	165 ± 9	0.20 ± 0.01	295 ± 29	0.37 ± 0.04
Cycle 3	32 ± 5	0.04 ± 0.01	185 ± 11	0.23 ± 0.01

trapped in the organic layer and form complexes with the 2-MBT molecules, as suggested by previous works reporting the possibility of forming Cu-MBT metal-organic complexes although in different conditions [79, 80, 94, 151].

4.3 Anodic dissolution of copper and its inhibition by 2-MBT

Figure 4.2 shows the cyclic voltammograms of anodic dissolution performed for 4 different conditions: (i) in 10 mM HCl without inhibitor, (ii) in 10 mM HCl + 0.1 mM 2-MBT after cathodic pre-treatment in presence of the inhibitor, and (iii) and (iv) also in 10 mM HCl + 0.1 mM 2-MBT but after cathodic pre-treatment in the absence of the inhibitor; (iii) was obtained immediately (2 min) after replacing the 2-MBT-free solution by the 2-MBT-containing solution while (iv) was obtained after 1 hour of exposure to the inhibitor solution.

For the inhibitor-free reference solution, a very high anodic current density is measured, continuously increasing from approximately +0.15 V vs SHE and indicating the dissolution of copper. $CuCl^-$ or $CuCl_2$ form on the surface of the metal due to the adsorption of chloride ions in these conditions, and the Cu(I) ions dissolve as $CuCl_2^-$, as reported previously [33, 35].

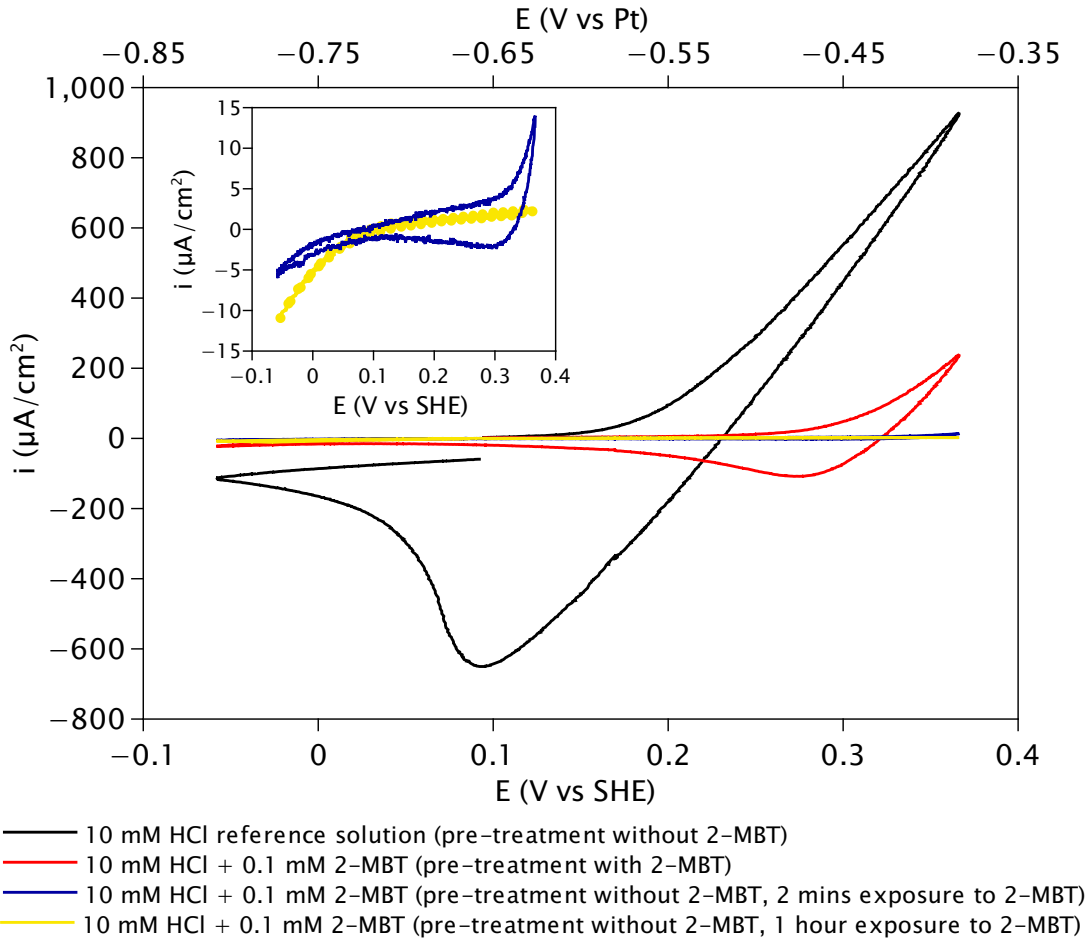

Figure 4.2: Cyclic voltammograms of copper showing anodic dissolution in the absence or presence of 2-MBT in different pre-treatment conditions (scan rate of 20 mV/s). The inset shows the enlarged cyclic voltammograms of the two experiments performed after pre-treatment without 2-MBT.

The cathodic sweep exhibits a peak at approximately +0.10V vs SHE, indicating re-deposition of the dissolved copper.

For the CV performed in 10 mM HCl + 0.1 mM 2-MBT after pre-treatment in the presence of 2-MBT, we observe an anodic shift in the initiation of dissolution to about +0.25 V vs SHE, and a lower rise of the anodic current density. This indicates protection of the copper metal surface against anodic dissolution by the organic film of 2-MBT molecules formed at the surface, as previously observed and discussed [95].

The CVs performed after pre-treatment in absence of 2-MBT, enlarged in the inset of Figure 4.2, show even better protection performance for the inhibitor on copper in acidic chloride

Table 4.2: Anodic and cathodic charge densities determined from the anodic dissolution tests along with the equivalent thickness of copper metal reacting and irreversibly dissolved during the test and calculated using Faraday's law (Equation 2.1).

	Electrolyte used for CV, Pre-treatment condition	Anodic charge q_a ($\mu C/cm^2$)	Cathodic charge q_c ($\mu C/cm^2$)	Cu reacting (nm)	Cu dissolved (nm)
a	10 mM HCl ref, Pre-treatment w/o 2-MBT.	7032 ± 13	4503 ± 55	5.17 ± 0.01	1.86 ± 0.03
b	10 mM HCl + 0.1 mM 2-MBT, Pre-treatment with 2-MBT.	733 ± 24	704 ± 31	0.54 ± 0.02	0.02 ± 0.01
c	10 mM HCl + 0.1 mM 2-MBT, Pre-treatment w/o 2-MBT, 2 mins exposure to 2-MBT.	52 ± 7	28 ± 2	0.04 ± 0.01	0.02 ± 0.01
d	10 mM HCl + 0.1 mM 2-MBT, Pre-treatment w/o 2-MBT, 1 hr exposure to 2-MBT.	38 ± 1	28 ± 4	0.03 ± 0.01	0.01 ± 0.01

conditions. The two CVs exhibit much flatter curves as well as larger anodic shifts compared both to the reference solution (10 mM HCl) and the CV performed after pre-treatment in presence of inhibitor (10 mM HCl + 0.1 mM 2-MBT). This indicates that the absence of inhibitor during cathodic pre-treatment results in the formation of a less defective and consequently more protective organic barrier layer. The even flatter curve of the CV obtained after 1 hour exposure to 2-MBT before anodic polarization indicates optimization of the barrier properties with increased exposure time. Figure 4.3 shows that the barrier properties are already optimized after 15 minutes of exposure to 2-MBT after cathodic pre-treatment in the inhibitor-free solution.

The anodic and cathodic charges for each curve were calculated by integrating the anodic and cathodic current densities, respectively, with respect to time, and the equivalent thicknesses of Cu metal reacting and dissolved during the cycle were determined using (Equation 2.1). Results are compiled in Table 4.2. The amount (equivalent thickness) of Cu irreversibly dissolved was deduced from the difference between anodic and cathodic charge densities (q_a–q_c). For each experiment with 2-MBT, the anodic charge and therefore the equivalent thickness of reacting copper decrease markedly, by a factor of 10 between the test in reference solution and the test performed after pre-treatment with inhibitor, by another factor of 14

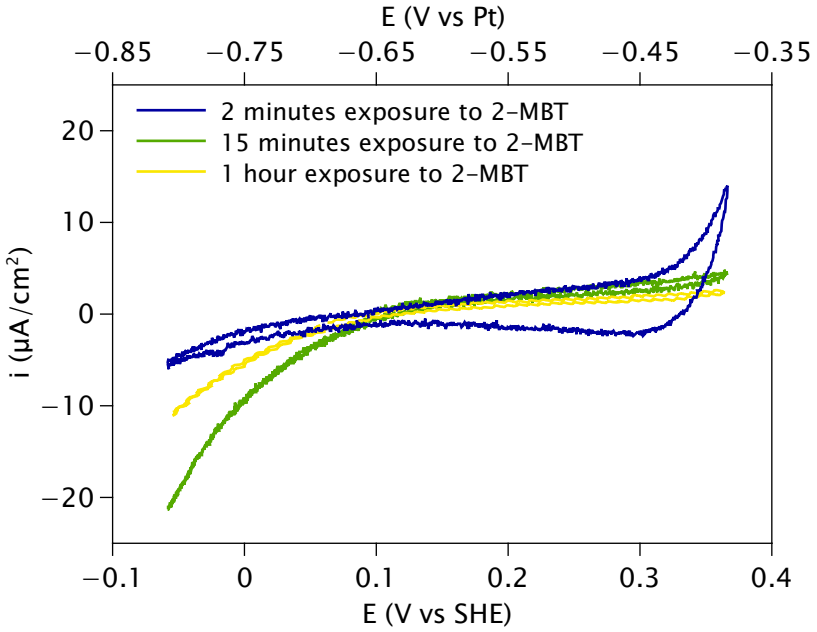

Figure 4.3: Cyclic voltammograms of copper showing anodic dissolution in the presence of 2-MBT after different exposure times to 2-MBT prior to anodic polarization (scan rate of 20 mV/s).

after pre-treatment without inhibitor, and finally by an additional factor of 1.4 after pre-treatment without inhibitor followed by 1 hour exposure to the inhibitor. This evidences that controlling the conditions of formation of the inhibiting barrier layer by electrochemical means and minimizing the presence of native oxides does play an important role in the mitigation of the dissolution of copper and is instrumental for optimizing the barrier properties of the interfacial organic film.

4.4 ToF-SIMS depth profiling of the inhibiting interface

Surface analysis by ToF-SIMS and XPS was applied to the inhibiting interfaces formed in the 2-MBT-containing HCl solution after cathodic pre-treatment in presence or absence of the inhibitor. In the latter case of pre-treatment in absence of 2-MBT, the interface was optimized by 1 hour exposure to 2-MBT after performing the cathodic pre-treatment in the inhibitor-free solution. Hereafter, we discuss the ToF-SIMS depth profiling data shown in Figure 4.4 for the inhibiting interfaces obtained in the cathodically reduced metallic state.

The ToF-SIMS depth profiles in Figure 4.4 display the intensity of the selected secondary ions plotted in logarithmic scale vs the sputtering time, the latter being related to the depth from the initial topmost surface. The selected ions were $C_7H_4NS_2^-$, C_2N^-, C_2S^-, and $^{34}S^-$ ions, characteristic of the 2-MBT molecule, its fragments of nitrogen, its fragments of sulphur, and

the overall sulphur, respectively. Additionally, Cu^-, O^-, Cu_2O^-, $^{37}Cl^-$ ions were selected as they are characteristic of the metallic substrate, the oxides, and the chloride adsorbed on the surface. The positions of each interface or layer was defined by the maximum intensity of the corresponding ions with an uncertainty of 5%.

Cu^- being more characteristic of metallic Cu, was used to define the position where the metallic Cu substrate is reached. It corresponds to 7 and 10 seconds of sputtering time after pre-treatment with and without 2-MBT, respectively. On both depth profiles, the organic layer, characterized by the $C_7H_4NS_2^-$, C_2N^- and C_2S^- ions, covers the metallic substrate, which confirms that 2-MBT is adsorbed on the metallic substrate. However, it can be noticed that the intensity of the $C_7H_4NS_2^-$ ions is maximum at the topmost surface, whereas those of the C_2N^- and C_2S^- ions are maximum in the inner part of the organic layer. This indicates, that 2-MBT forms multilayers with an inner chemisorbed layer (yellow regions on the profiles) and an outer physisorbed multilayer (pink regions on the profiles), as observed previously for adsorption of the molecule from the gas phase [83–86] and in neutral aqueous solution [88]. The position of the C_2S^- intensity maximum is closer to the substrate than that of the C_2N^- intensity maximum, which indicates that 2-MBT bonds to the surface via the two S atoms, in agreement with the work of Vernack et al. [88].

Interestingly, the Cu_2O^- signal exhibits a maximum intensity slightly before reaching the metallic Cu region (Cu^-). This indicates that, although the reduction pre-treatment was applied, Cu oxide islands (marked in blue on the profiles) remain locally on the surface, in agreement with the electrochemical analysis above. The $^{34}S^-$ secondary ions, characteristic of sulphur atoms from the intact and/or dissociated molecules, peak at a larger depth than the C_2S^- ions, characteristic of the intact molecule, and concomitantly with the Cu_2O^- ions, indicating that sulphur atoms are also bonded to the metal surface. Since the C_2S^- ions curve remains behind the C_2N^- curve, there is no indication of the nitrogen atoms bonding to copper.

Looking at the Cl^- signal, one observes that it exhibits its maximum intensity in the outer region (marked in pink), assigned to the physisorbed MBT layer. However, the intensity of Cl^- signal decreases strongly in the inner chemisorbed MBT layer (marked in yellow). This is consistent with the chemisorbed MBT layer drastically reducing the interaction of chloride ions with the copper substrate by acting as a physical barrier between them.

The differences in the depth profiles of both experiments relate to the thickness of the interface. A thicker 2-MBT organic layer is observed in the case of pre-treatment without 2-MBT followed by 1 hour exposure to the inhibitor (Figure 4.4b) than in the case of pre-treatment with 2-MBT (Figure 4.4a), which would enhance the efficiency of the protection against

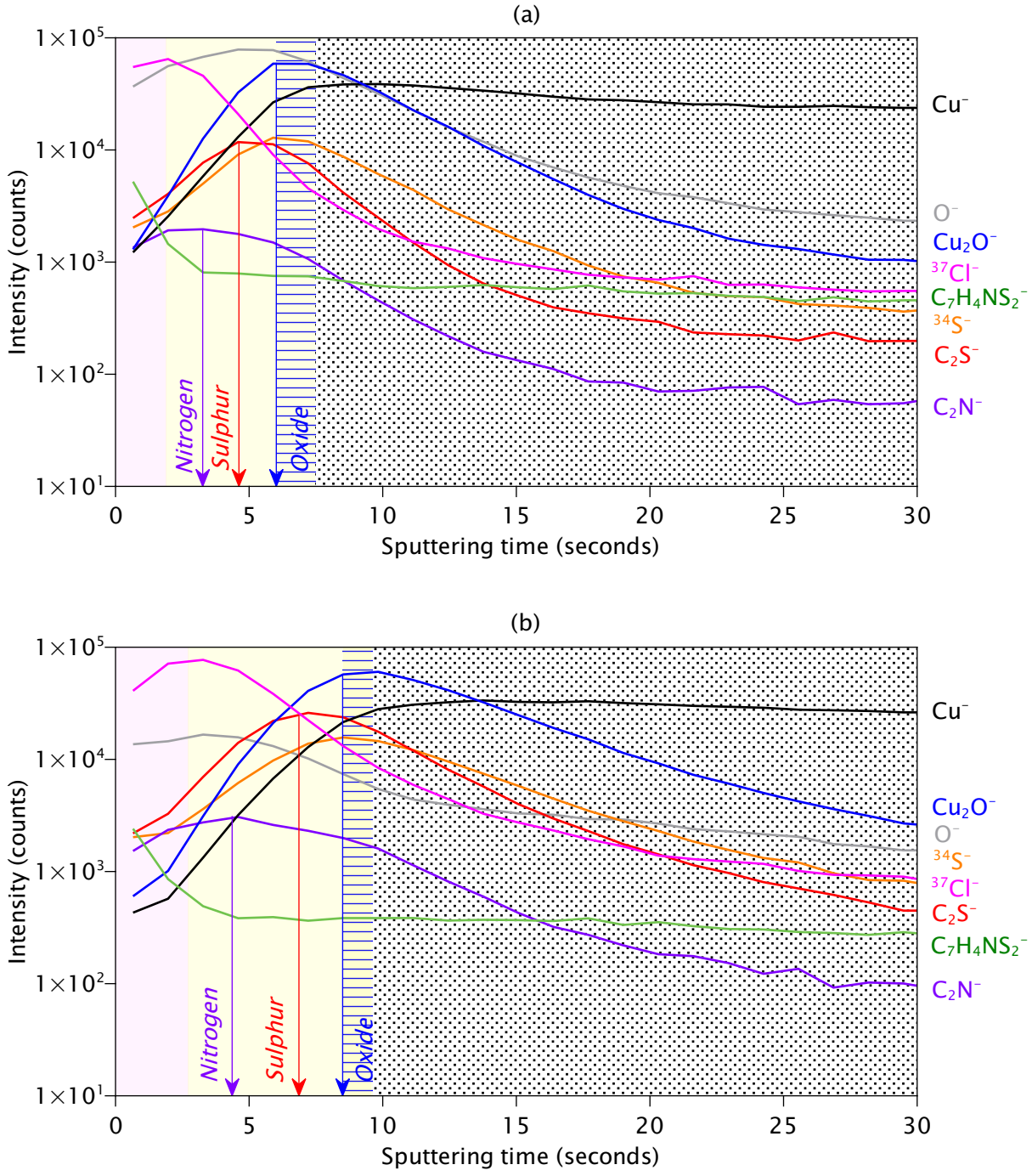

Figure 4.4: ToF-SIMS depth profiles of the inhibiting interface obtained in reduced state (a) after cathodic pre-treatment with 2-MBT, and (b) after cathodic pre-treatment without 2-MBT followed by 1 hour of exposure to the inhibitor.

dissolution as revealed by the anodic polarization tests.

4.5 Interfacial bonding and thickness estimation by XPS analysis

Figure 4.5 shows the XPS Cu 2p, Cl 2p, S 2p, C 1s, N 1s and O 1s core level spectra obtained in this work, in this case after exposure to the solution of 10 mM HCl + 0.1 mM 2-MBT in reduced state, after pre-treatment in the presence of 2-MBT. A summary of the elemental components observed in this work with their binding energies (BE), full widths at half maximum (FWHM), and assignments is given in Table 4.3. The assignment of the components from the 2-MBT molecule are depicted in Figure 4.6.

The copper Cu 2p spectrum showed the $2p_{3/2}$ – $2p_{1/2}$ spin-orbit doublet at 932.8 – 952.6 eV BE. The $2p_{3/2}$ component can correspond to three states that are too close to be resolved: the Cu(0) metallic state at 932.6 eV, the Cu(I) oxidized state at 932.7 eV, and Cu−2S at 932.9 eV [142, 143]. Cu(II) oxide is not observed in this spectrum; it would appear at 933.5 eV along with satellite peaks, which are characteristic of the Cu(II) oxide [142, 143]. Analysis of the Cu composition using the Cu LMM Auger spectrum is discussed below.

The Cl 2p spectrum was decomposed in $2p_{1/2}$ – $2p_{3/2}$ spin-orbit doublets with a branching ratio of 0.5 and splitting of 1.60 eV. The Cl $2p_{3/2}$ (Cl1) component at 198.3 eV corresponds to chlorine adsorbed on the surface [74, 144]. Another Cl $2p_{3/2}$ component (Cl2), at a binding energy of 199.0 eV and corresponding to CuCl [144], was only observed after anodic polarization in the 2-MBT-free HCl reference solution, as shown in Figure 4.7. This is consistent with the inhibition properties of 2-MBT blocking the access of chloride ions to the copper substrate surface and thus preventing the formation of CuCl surface species.

$2p_{1/2}$ – $2p_{3/2}$ spin-orbit doublets, with a branching ratio of 0.5 and splitting of 1.18 eV, were also considered for peak fitting the S 2p spectrum. Three components/chemical states, labelled S1, S2, and S3, were observed in agreement with previous work [84]. The S1 component at 164.2 eV corresponds to the endocyclic sulphur from the 2-MBT molecule not bonded to metallic copper. The S2 component at 162.8 eV corresponds to the exocyclic sulphur from the molecule, also not bonded to metallic copper. These two components can also correspond to the S atoms of the molecules bonded to copper oxides and/or forming multilayers physically adsorbed on the surface [70, 84, 86, 88]. The S3 component at 161.9 eV is sulphur bonded directly to metallic copper, which was also observed when exposing a clean metallic Cu surface to H_2S [142]. This component can originate from either of the two sulphur atoms, endocyclic or exocyclic, from the intact molecules bonded to metallic copper. It can also be

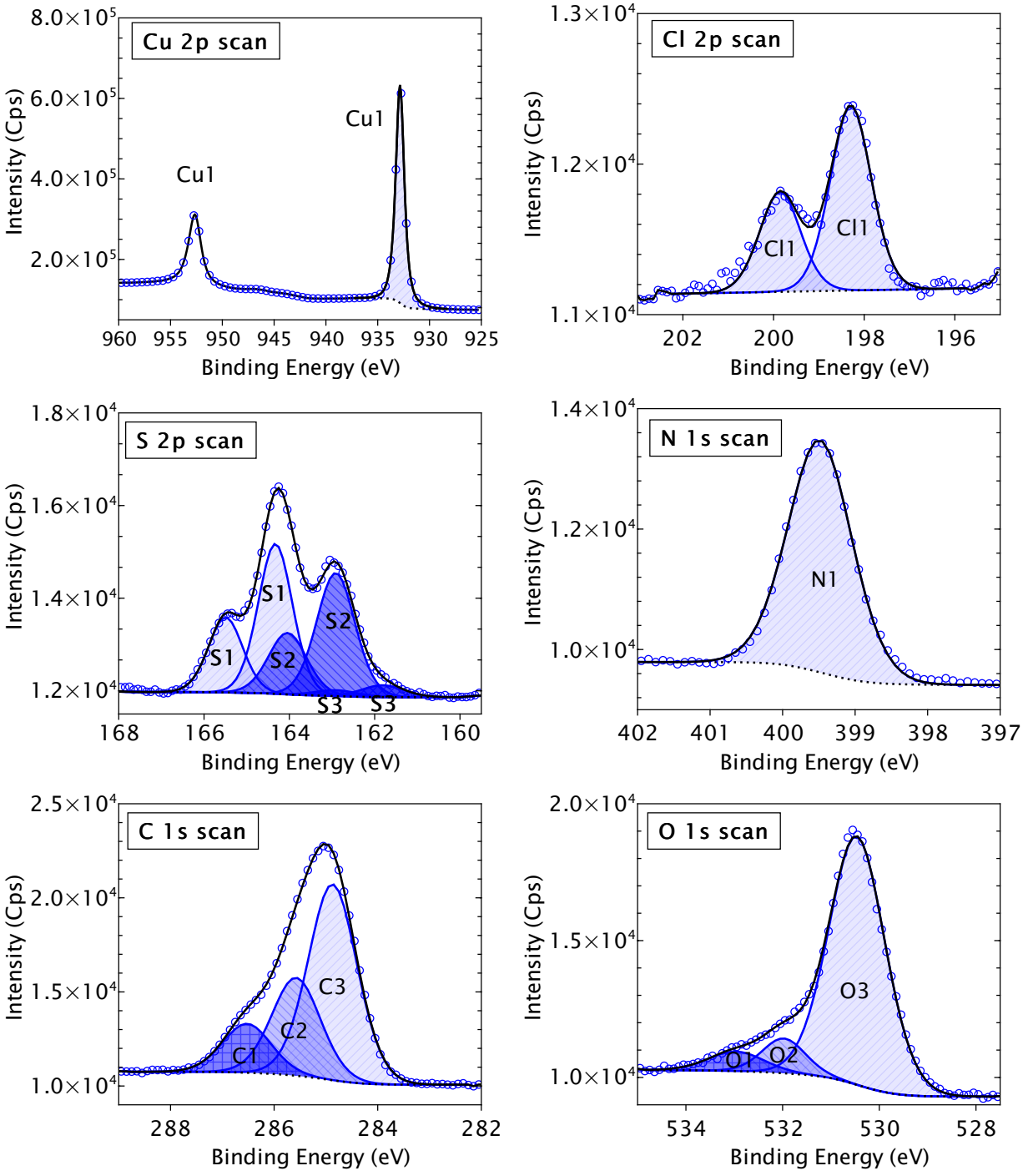

Figure 4.5: XPS Cu 2p, Cl 2p, S 2p, N 1s, C 1s, and O 1s core level spectra after exposure to the solution of 10 mM HCl + 0.1 mM 2-MBT in reduced state, after pre-treatment in the presence of 2-MBT.

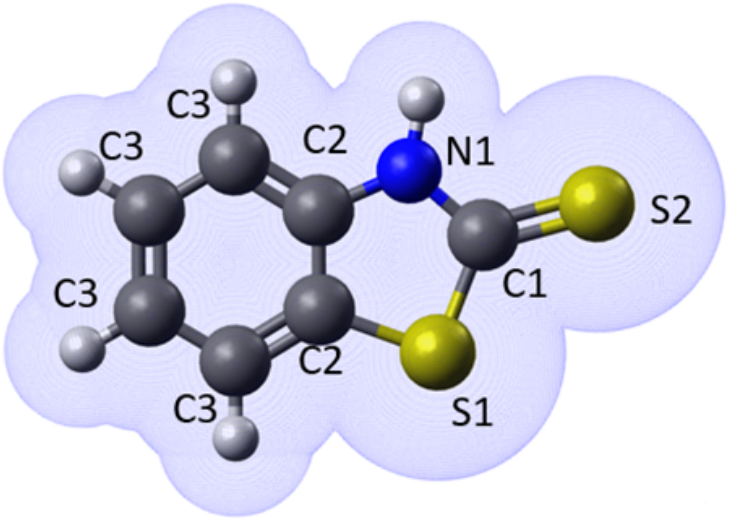

Figure 4.6: 2-MBT chemical structure (thione form) and the assigned chemical states of the components obtained from their respective binding energies during XPS analysis.

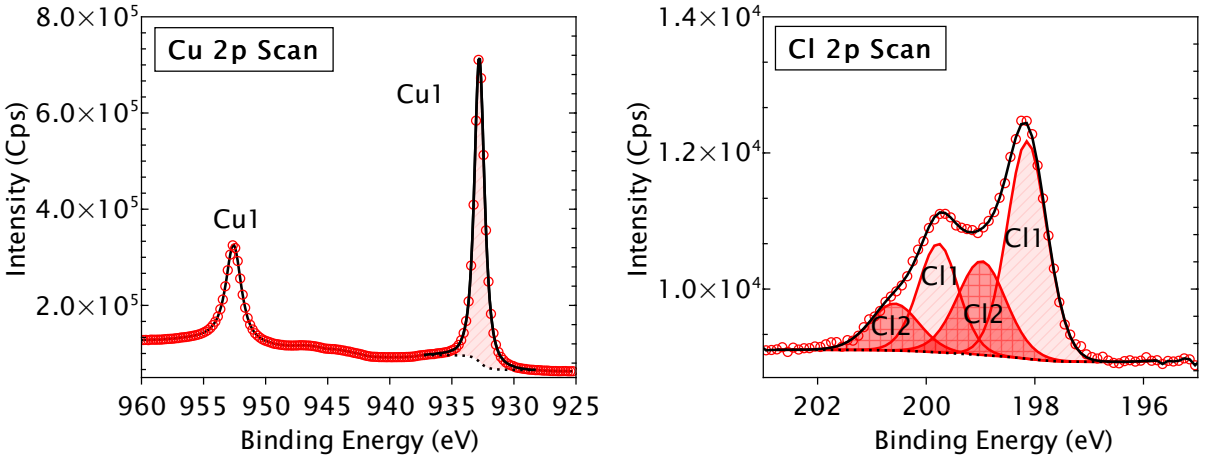

Figure 4.7: XPS Cu 2p and Cl 2p core level spectra after exposure to the solution of 10 mM HCl in anodic state, after pre-treatment in the absence of 2-MBT.

Table 4.3: Elemental core levels and Auger transition components observed in XPS analysis from this work with their Binding Energies (BE) / Kinetic Energies (KE), Full Width at Half Maximum (FWHM) and their assigned chemical states. Uncertainty ranges are derived from the uncertainty of the curve fitting procedure.

Peak component		BE (± 0.1 eV)	FWHM (± 0.2 eV)	Assignment
Cu $2p_{3/2}$		932.8	1.0	Cu $2p_{3/2}$
		932.6		Cu(0) metal [142, 143]
		932.7		Cu(I) oxide [142, 143]
		932.9		Cu(I) sulphide [142, 143]
N 1s		399.4	1.1	N not bonded to metallic Cu
S $2p_{3/2}$	S1	164.2	1.0	Endocyclic S not bonded to metallic Cu (2-MBT)
	S2	162.8	1.0	Exocyclic S not bonded to metallic Cu (2-MBT)
	S3	161.9	1.0	S bonded to metallic Cu
C 1s	C1	286.4	1.1	C=S, residual contamination
	C2	285.5	1.1	C-N, C-S
	C3	284.8	1.1	C-C, C-H
O 1s	O1	532.9	1.6	H_2O adsorbed
	O2	531.4	1.4	OH
	O3	530.2	1.4	O from metal oxide (Cu_2O)
Cl $2p_{3/2}$	Cl1	198.3	1.1	Adsorbed chloride
	Cl2	199.0	0.9	Copper chloride (CuCl)
Cu LMM	Cu (0)	918.4 (KE)		Cu metal
	Cu (I)	916.6 (KE)		Cu oxide

free sulphur atoms that have dissociated from the molecule and then bonded to metallic Cu [83, 84, 86].

The N 1s spectrum was fitted with one peak component observed at 399.4 eV and originating from the nitrogen atoms of the molecules that are not bonded to copper [70, 84]. From previous work, we know that the N bonded to Cu is expected at 399.8 eV [84]. The slight shift observed in the BE (+0.3 eV) compared to other in situ XPS studies is most likely due to the influence of the exposure to air during transfer to XPS [83, 89].

The carbon C 1s spectrum was decomposed into three peaks/chemical states. The C1 component at 286.4 eV corresponds to C=S bonds in the molecule, the C2 component at 285.5 eV to C–N and C–S bonds, and the C3 component at 284.8 eV to C–C and C–H

bonds in the benzene ring [70, 84]. Since the carbon atoms in these chemical states are in the ratio 1:2:4 in the 2-MBT molecule, the experimental observation of this intensity ratio is indicative of the adsorption of most of the 2-MBT molecules in the intact form, like in previous experiments of adsorption from the gas phase [84].

The oxygen O 1s spectrum was decomposed into three components: O1 at 532.9 eV corresponding to oxygen adsorbed on the surface from water and/or from exposure to air, O2 at 531.4 eV from hydroxides formed on the surface, and O3 at 530.2 eV from the oxygen atoms of the copper oxide matrix, Cu_2O in this case [83, 86, 142, 143]. From the XPS survey spectra (not shown), it was also determined that there was essentially no presence of residual phosphorous from the electrochemical polishing process indicating no interference of this procedure on the experiments.

Table 4.4: Normalized intensities (NI) (±3 %) and relative intensities (RI) of the elemental core level components and Auger transition highlighting the changes between the two pre-treatment methods and their respective reduced and anodic states.

Peak component		Pre-treatment with 2-MBT				Pre-treatment without 2-MBT			
		Reduced state		Anodic state		Reduced state		Anodic state	
		NI (a.u.)	RI (%)	NI (a.u.)	RI (%)	NI (a.u.)	RI (%)	NI (a.u.)	RI (%)
N 1s		0.27	100	0.26	100	0.44	100	0.39	100
	S1	0.31	50	0.30	49	0.50	49	0.46	48
S $2p_{3/2}$	S2	0.29	45	0.27	45	0.46	45	0.39	41
	S3	0.03	5	0.04	6	0.06	6	0.11	11
	C1	0.34	14	0.44	14	0.51	14	0.48	14
C 1s	C2	0.68	29	0.88	29	1.03	29	0.96	29
	C3	1.35	57	1.76	57	2.06	57	1.92	57
	O1	0.04	5	0.14	15	0.15	44	0.08	13
O 1s	O2	0.13	15	0.32	33	0.07	20	0.21	35
	O3	0.70	80	0.50	52	0.12	36	0.32	52
Cu LMM	Cu(0)	12.39	84	12.20	89	10.27	95	10.56	89
	Cu(I)	1.93	16	1.19	11	0.40	5	1.09	11

Table 4.4 compiles the normalized intensities (±3%) and the relative intensities of the elemental components according to the electrochemical conditions of formation and treatment of the interface. It is observed that the relative intensities of the C 1s components always remain in the molecular ratio mentioned above. The N 1s component also remains unchanged owing to the presence of only one chemical state, i.e. N not bonded to Cu. However, we do

observe a change in the relative intensities of the O 1s, Cu LMM, and S 2p components. The O3 component assigned to metal oxide (Cu_2O) has a similar trend to the Cu(I) component from the Cu LMM spectrum discussed next. The changes observed in the relative intensities of the S 2p components are discussed subsequently.

Since the Cu(I) oxide component is indistinguishable from the Cu(0) metal component in the Cu 2p spectrum, we also recorded and decomposed the Cu LMM Auger spectrum in order to discriminate the contributions of copper oxide and copper metal. The Cu LMM Auger spectrum obtained in different interfacial conditions are shown in Figure 4.8. They were decomposed by peak fitting using the line-shapes of Cu(0) and Cu(I) obtained from reference spectra measured on metallic Cu and oxidized samples in the same analytical conditions, as done by others [86, 142, 146].

We can observe in Figure 4.8(a) that, although the intensity of Cu(I) is quite weak compared to that of Cu(0), it is markedly higher than that in Figure 4.8(c) where the cathodic pre-treatment was done in absence of the inhibitor. This agrees with the electrochemical analysis from which we deduced more efficient reduction of the native oxides by cathodic pre-treatment in absence of the inhibitor. In Figure 4.8(b), we observe a decrease in the Cu(I) intensity after anodic polarization (anodic state) compared to that measured after cathodic pre-treatment (reduced state) in Figure 4.8(a). This is indicative of dissolution of the oxide remnants during polarization followed by additional adsorption of 2-MBT molecules, as observed by the slight increase in relative intensity of the S3 component (S bonded to metallic Cu) in Table 4.4. In Figure 4.8(c), the almost negligible Cu(I) intensity is consistent with the lower intensity O3 component in the O 1s spectrum (Table 4.4). It cannot be fully excluded that these oxide traces result from re-oxidation of the surface during air transfer due to the imperfections in the organic barrier film formed by 2-MBT after electrochemical preparation. After anodic polarization (Figure 4.8(d)), we observe an increase in the Cu(I) intensity. It is proposed that during polarization, defects are formed on the organic barrier layer. These unprotected regions would re-oxidize during air transfer after the experiment.

Using the intensities of the Cu 2p, O 1s, N 1s, S 2p spectra, we performed quantitative analysis by applying a bi-layer model of attenuation of the photoelectron intensity in order to estimate the thickness of the organic inhibitor layer and the coverage and thickness of the residual oxide islands present at the interface. A schematic of the bi-layer model used is shown in Figure 2.16 in Chapter 2. This model, taking oxide islands into consideration, as deduced from the ToF-SIMS and XPS measurements indicating the presence of islands of oxides and sulphur bonding to metallic Cu, allows us to further discuss the effects of the electrochemically controlled conditions of formation of the interface on its inhibition properties. Although this model results in high uncertainties for the extracted values, the

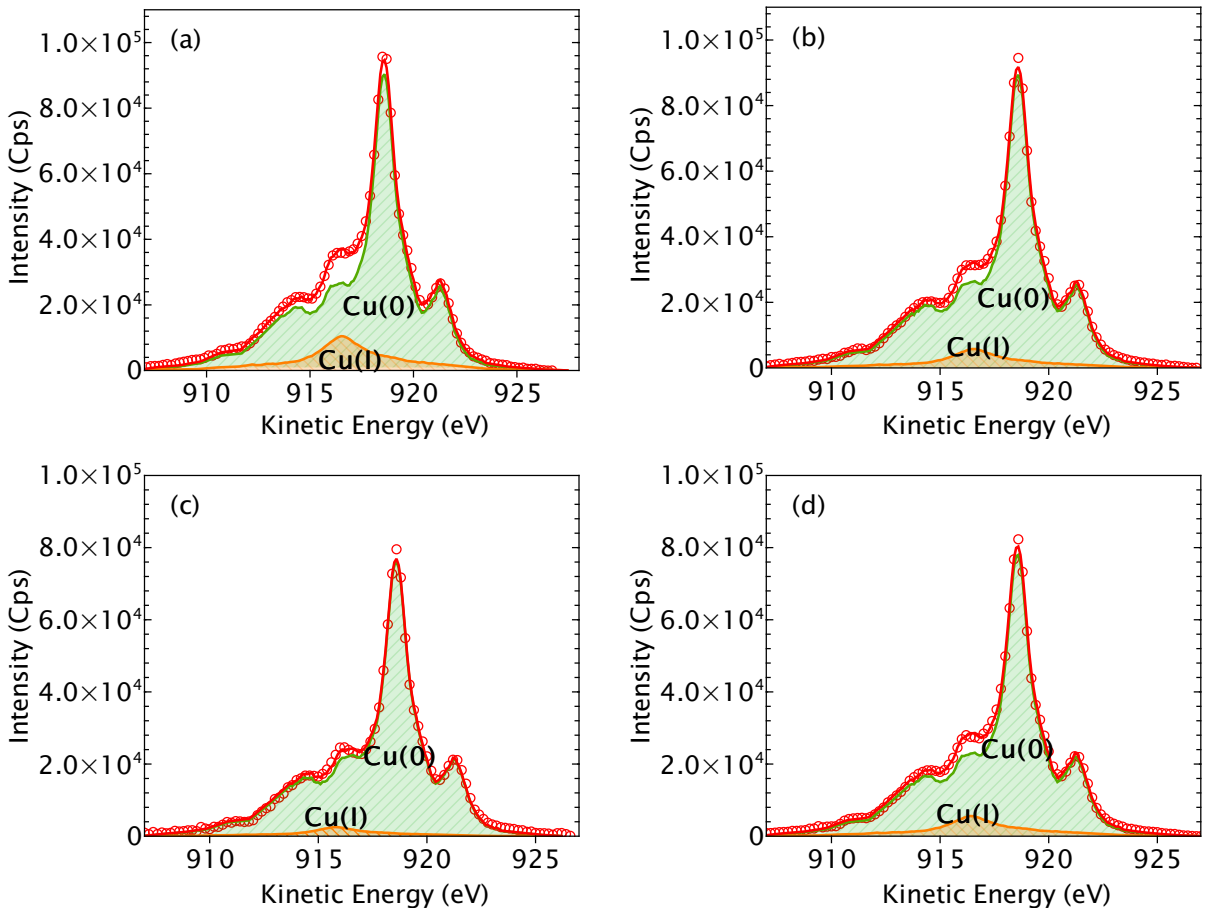

Figure 4.8: Cu LMM Auger spectra obtained for experiments done in 10 mM HCl + 0.1 mM 2-MBT at (a) reduced state, pre-treatment with MBT, (b) anodic state, pre-treatment with MBT, (c) reduced state, pre-treatment w/o MBT, 1 h MBT exposure, (d) anodic state, pre-treatment w/o MBT, 1 h MBT exposure.

results are comparable between the experiments, and in conjunction with the intensities (normalized and relative intensities) of the components reported in Table 4.4. For the sake of easier comparison, the equivalent thickness of the oxide and 2-MBT layers were calculated by weighting the thickness with the coverage of each layer. Table 4.5 compiles the obtained values. A graphical display of the results is presented schematically in Figure 4.9.

It is observed that whatever the pre-treatment conditions, with 2-MBT or without 2-MBT (and subsequent 1 hour exposure to 2-MBT), the coverage of oxide islands is high, and their thickness relatively low (less than 0.5 nm), the latter even reaching 0.14 nm in the reduced state of the interface after pre-treatment without 2-MBT which is less than a monolayer (0.208 nm). In these optimized conditions of formation of the interface (Figure 4.9 c–d), the equivalent thickness of the remaining oxide is 0.11 nm, also lower than that of a monolayer, suggesting that the actual coverage of remaining oxide islands is overestimated with our model,

Table 4.5: Coverage and thickness values of the copper oxide islands and 2-MBT organic inhibitor layer determined from quantitative analysis of the XPS results using the bi-layer model. The uncertainty on the coverage was estimated to be ± 10%, and the uncertainty on the thicknesses were estimated to be ± 0.2 nm.

	Conditions of interface formation	Coverage of Cu_2O islands (%)	Thickness of Cu_2O islands (nm)	Equivalent thickness of Cu_2O (nm)	Thickness of 2-MBT layer above oxides (nm)	Thickness of 2-MBT layer above metallic Cu (nm)	Equivalent thickness of 2-MBT layer (nm)
a	Pre-treatment with MBT, reduced state	90	0.47	0.42	0.97	1.44	1.02
b	Pre-treatment with MBT, anodic state	87	0.36	0.31	0.98	1.34	1.03
c	Pre-treatment w/o MBT, 1 h MBT exposure, reduced state	78	0.14	0.11	2.19	2.33	2.22
d	Pre-treatment w/o MBT, 1h MBT exposure, anodic state	62	0.38	0.24	1.94	2.32	2.08

possibly due to inhomogeneous thickness of the oxide islands. This significant decrease in the amount of oxide remaining at the interface agrees with the electrochemical data presented above and with the variation of the Cu LMM Auger line-shape measured by XPS in Figure 4.8 c–d. It supports our explanation that, when present during pre-treatment, the 2-MBT molecules, pre-adsorbed on the oxide surface, poison the electrochemical reduction reaction which results in significantly more oxide trapped at the interface.

The oxide traces observed after pre-treatment without 2-MBT in the solution could result from incomplete efficiency of the applied conditions despite the absence of remaining oxide indicated by the electrochemical data. As stated above, re-oxidation of the 2MBT-protected surface during air-transfer for surface analysis cannot be fully excluded. Additionally, Table 4.5 (Figure 4.9) also shows that the 2-MBT layer is significantly thicker in the case of pre-treatment without the inhibitor with subsequent 1 hour exposure to 2-MBT. This indicates that lower quantities, including lower coverage, of remaining interfacial oxide on the surface, possibly along with the increased exposure time to the inhibitor molecule, enhance the deposition of multilayers of the organic molecule on the surface, resulting in thicker and better protective barrier layers.

After anodic polarization of the interface with more remaining oxide, i.e., cathodically pre-

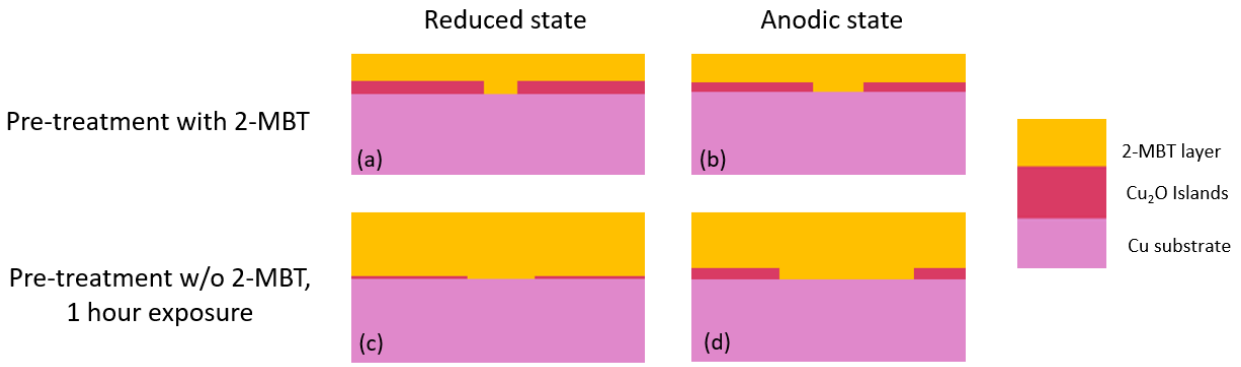

Figure 4.9: Schematic showing the differences in coverage and thickness of the oxide islands and thickness of the 2-MBT layer as determined from XPS surface analysis for (a) reduced state, pre-treatment with MBT, (b) anodic state, pre-treatment with MBT, (c) reduced state, pre-treatment w/o MBT, 1 h MBT exposure, (d) anodic state, pre-treatment w/o MBT, 1 h MBT exposure.

treated with 2-MBT (Figure 4.9 a–b), it is observed that the oxide islands thickness slightly decreases whereas their coverage remains nearly unchanged. It is proposed that, due to the formation of defects in the 2-MBT barrier layer upon anodic polarization, the acidic electrolyte (pH = 2.6) may penetrate the barrier layer, access the oxide surface, and thus at least partially dissolve the interfacial oxide layer. This alteration of the barrier properties of the 2-MBT layer is reflected by a slight decrease in thickness of the interfacial oxide (Table 4.5). In the experiment where the interface is cathodically pre-treated in the absence of 2-MBT (Figure 4.9 c–d), the quantities of the remaining oxides are extremely low to begin with. After anodic polarization, defects are formed in the 2-MBT layer but there is little to no oxide beneath to dissolve. Once the sample is removed from the cell and transferred in air for analysis, the defective areas formed in the 2-MBT barrier layer do not protect the surface from re-oxidation, and thus thicker islands of oxides are locally formed, as observed from the values estimated in Table 4.5 and visualised in Figure 4.9).

In previous work on 2-MBT deposited from the gas phase, it has been shown that sulphur could dissociate from the molecule and bond with metallic copper in the form of free atomic sulphur detected as part of the S3 component in the XPS S 2p core level spectrum [84]. In order to determine if this is also the case in the present experiments, atomic ratios between sulphur and nitrogen were calculated. In the 2-MBT molecule, the stoichiometric ratio between these elements is 2:1. However, from quantitative analysis of the XPS data, we determine that we always have an excess of sulphur, as shown in Figure 4.10, confirming that, in our case, we also have free sulphur atoms that are bonded to the metal. Therefore, the S3 component in the S 2p spectrum corresponds to both the molecule bonded to metallic

copper via its S atoms as well as to free sulphur atoms bonded to the metallic copper surface. We also observe in Figure 4.10a that there is a trend to an increase in sulphur in the anodic state compared to the cathodically reduced state in either case of pre-treatment. Hence, it is suggested that during anodic polarization some of the 2-MBT molecules tend to dissociate resulting in free sulphur atoms bonded to the metallic copper surface. This alteration appears consistent with formation defects of the protective 2-MBT layer, compromising its barrier properties.

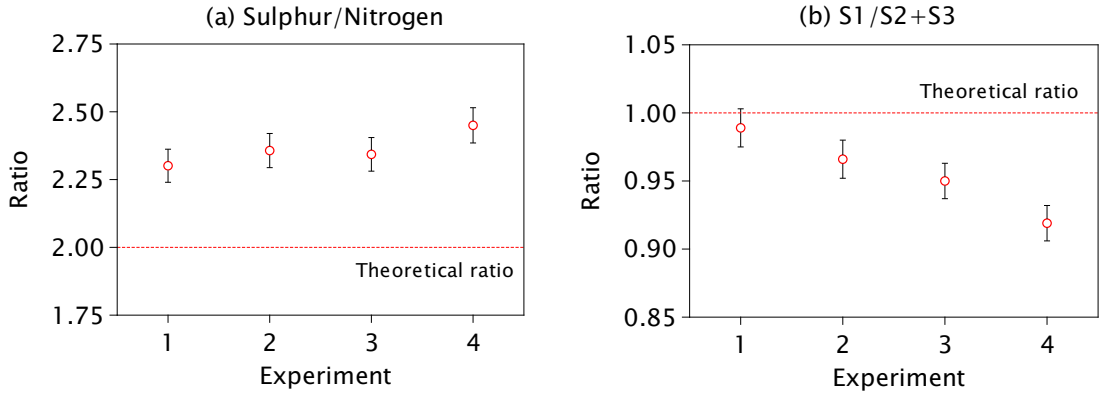

Figure 4.10: Atomic ratios of (a) S : N, and (b) S1 : S2+S3, determined from the component intensities of the XPS S 2p and N 1s spectra. (Exp. 1) Pre-treatment with MBT, reduced state, (Exp. 2) Pre-treatment with MBT, anodic state, (Exp. 3) Pre-treatment w/o MBT, 1 h MBT exposure, reduced state, (Exp. 4) Pre-treatment w/o MBT, 1 h MBT exposure, anodic state.

The origin of the S3 component was determined by analysing the atomic ratio between the S1, S2 and S3 components (Figure 4.10b). It was determined that the ratio between S1 and the combination of S2 and S3 components result in a value close to 1, which is the proper ratio between the endocyclic S1 and exocyclic S2 sulphur. Therefore, it is suggested that the S3 component mainly comes from S2, the exocyclic sulphur from the 2-MBT molecule. We observe in Figure 4.10b that after anodic polarization in either pre-treatment condition of the interface, there is a slight decrease in this ratio, indicating that the quantity of S1 has decreased. This suggests that during anodic polarization, this is the endocyclic sulphur (S1 component) in some of the 2-MBT molecules that tends to dissociate to give free sulphur bonded to metallic copper (along with dissociated S2 exocyclic sulphur) in the defective regions of the barrier layer. This is also observed in Table 4.4 by the relative intensities of the sulphur components where we also observe a decrease in the S1 and S2 components but an increase in the S3 component after anodic polarisation for both the experiments. This results in an increased coverage in the bonding between the 2-MBT molecule/sulphur atoms and the metallic copper substrate after anodic polarisation, as seen in Table 4.5, Figure 4.9.

4.6 Conclusion

The formation of the 2-MBT inhibiting interface by electrochemical cathodic control and how it enhances the corrosion resistance of copper in an acidic environment was investigated by applying electrochemistry and advanced surface analysis. The barrier properties of the 2-MBT organic protective layer are highly influenced by the cathodic pre-treatment protocol applied to reduce the native oxide initially present on the copper surface. Advanced elimination of the native oxide, as confirmed by ToF-SIMS and XPS, promotes the formation of a thicker, and likely less defective, inhibitor multilayer, more protective in the anodic dissolution regime of copper. Enhanced inhibition is obtained when the cathodic pre-treatment is performed in the inhibitor-free solution prior to time optimization of 2-MBT adsorption under cathodic control of the interface. When performed in an inhibitor-containing solution, the cathodic pre-treatment is less effective in fully reducing the native oxide, owing to mitigation of the reduction reaction by pre-adsorption of 2-MBT on the oxidized surface.

In an acidic environment, the 2-MBT molecules (thione conformer) bond to both metallic copper and residual copper oxide islands via their sulphur atoms. No signature of bonding via the nitrogen atom was found from XPS, in agreement with ToF-SIMS. An excess of sulphur was observed from XPS (S3 component from S 2p spectrum), indicating partial dissociation of the molecules to release atomic sulphur, mostly originating from the exocyclic S atoms and bonded to metallic copper exposed in between the residual oxide islands. Upon anodic polarisation, a trend of further dissociation of the inhibitor molecule was observed, which was reflected by increased coverage of sulphur bonded to metallic copper, now mostly originating from the endocyclic S atoms. This anodic alteration of the protective 2-MBT layer would induce the formation of defects, thus compromising the barrier properties, as suggested by the ex-situ in-air reactivity of the interface.

CHAPTER 5

Adsorption of 2-mercaptobenzothiazole organic inhibitor and its effects on copper anodic oxidation in alkaline environment

This chapter is based on the work published in Journal of The Electrochemical Society by V. Garg, S. Zanna, A. Seyeux, F. Wiame, V. Maurice, and P. Marcus, entitled "Adsorption of 2-mercaptobenzothiazole organic inhibitor and its effects on copper anodic oxidation in alkaline environment." [152]

The aim of this chapter is to clarify the role of 2-MBT on the anodic oxidation of copper by adsorption of the molecule on a well-controlled metallic surface of copper in a strong alkaline medium (0.1 M NaOH solution), without the presence of chlorides. Cyclic voltammetry (CV) tests were performed to determine how the oxide growth is altered by the 2-MBT organic inhibitor layers pre-adsorbed in different pre-treatment conditions. Anodic oxidation is studied in the Cu(I) potential range, which allows us to evaluate the effects of 2-MBT on the oxide layer that forms directly on the bare metallic substrate. The absence of chlorides eliminates their interference in the understanding of the oxidation process in a 2-MBT-containing alkaline solution. Surface analysis was performed to investigate the bonding mechanisms of the 2-MBT molecule to the copper surface, the role of surface native oxides in the formation of the interface with the inhibitor, the effect of increased exposure time to the inhibitor, and the formation of metal-organic complexes.

5.1 Experimental

The samples were prepared as described earlier in Chapter 2. The electrochemical experiments were performed using the Kel-F cells. The Pt pseudo-reference was calibrated before each experiment (+0.32 V vs SHE). The electrolytes used for the experiment were a reference 0.1 M NaOH aqueous alkaline solution of pH 13.5 without the inhibitor, and a 0.1 M NaOH + 1 mM 2-MBT aqueous solution of pH 13.6 as the solution with inhibitor.

Cathodic pre-treatment was performed prior to the experiments in order to reduce the surface native oxide film in (a) the absence of 2-MBT, or in (b) the presence of 2-MBT in the solution. After immersion at the open circuit potential (OCP), the potential was swept cathodically, with a scan rate of 20 mV/s, to the onset of hydrogen gas evolution (−0.90 V vs SHE) and then swept back up to the value of −0.45 V vs SHE. This was repeated 2 more times. The anodic oxidation tests were performed by sweeping the potential from −0.45 up to +0.10 V vs SHE, followed by reverse sweeping to −0.90 V vs SHE, and then back to −0.45 V vs SHE with a scan rate of 20 mV/s. The electrochemical experiments were repeated 3 times each to ensure reproducibility.

Surface analysis was performed in the cathodically reduced state of the interface (reduced state at −0.45 V vs SHE), and in the anodically polarized state (anodic state at +0.10 V vs SHE). The experimental conditions performed to achieve the reduced state and anodic state are summarized in Figure 2.8 in Chapter 2. Once the desired electrochemical state was achieved, the cell was disconnected, the samples rinsed with ultra-pure water, dried using nitrogen, and transferred within less than 2 minutes for analysis by XPS and ToF-SIMS.

5.2 2-MBT effects on native oxide film reduction and anodic surface oxidation.

Three cycles of cathodic pre-treatment were applied by cyclic voltammetry in order to reduce the native oxide film formed on the copper substrate following surface preparation. The three pre-treatment CVs obtained in the 0.1 M NaOH reference solution are shown in Figure 5.1a, and those obtained in a 0.1 M NaOH + 1 mM 2-MBT solution in Figure 5.1b, with the current density measured as the potential is swept cathodically and back.

For the experiment in the NaOH reference solution (Figure 5.1a), a very high negative current with a peak at −0.57 V vs SHE is observed in the first cathodic pre-treatment cycle, corresponding to a large quantity of native Cu_2O being reduced. The measured cathodic charge density was 2311 ± 192 $\mu C/cm^2$ and the corresponding equivalent thickness of the

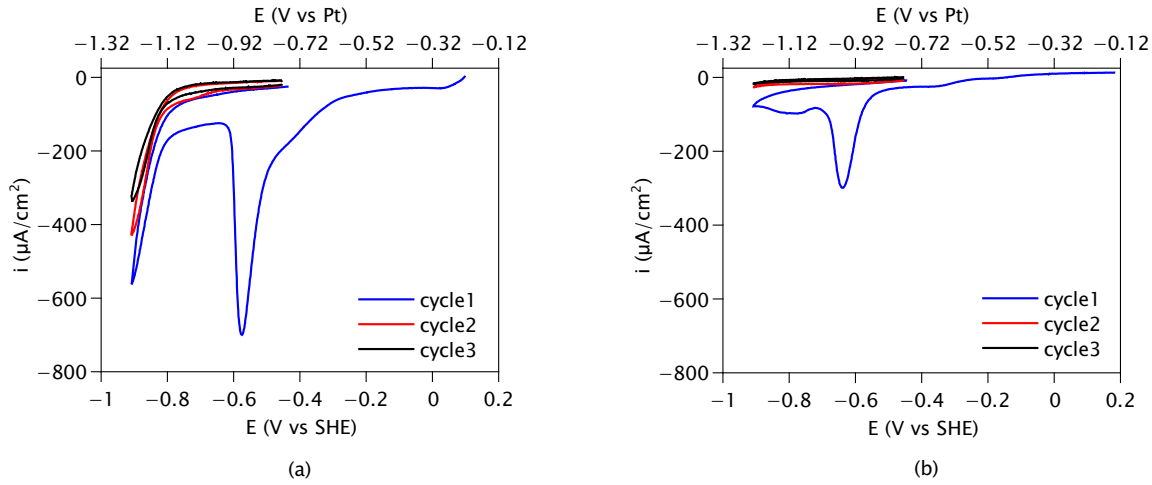

Figure 5.1: Cathodic pre-treatment CVs for copper in (a) 0.1 M NaOH reference solution (no inhibitor), and (b) 0.1 M NaOH + 1 mM 2-MBT solution (with inhibitor). Scan rate is 20 mV/s.

reduced native oxide film was 2.9 ± 0.2 nm, estimated using Faraday's law [130], where the molar volume (V_m) of Cu_2O is 23.9 cm^3/mol and the number of electrons exchanged (z) per Cu_2O molecule is 2. The next two cycles of cathodic pre-treatment show negligible cathodic charge densities with no distinct cathodic reduction peak in the potential range where the reduction of the native oxide is expected, suggesting that most of the native oxide film initially formed on the copper surface has been reduced during the first cathodic pre-treatment cycle. Noteworthy is that prior to the first cycle, when the sample is exposed to the 0.1 M NaOH solution at OCP, oxidation of the surface occurs due to the high pH of the solution. This could contribute to a large fraction of the initial oxides measured by electro-reduction.

For the cathodic pre-treatment with 2-MBT present in the NaOH solution (Figure 5.1b), we observe that the cathodic current of the first pre-treatment cycle, forming a peak shifted at −0.62 V vs SHE, is much lower than in the absence of the inhibitor. The cathodic charge density was measured to be 937 ± 124 μC/cm^2 and the equivalent thickness of reduced Cu_2O was 1.2 ± 0.2 nm, a decrease by a factor of 2.5 compared to the oxide reduced in absence of 2-MBT. It is suggested that the 2-MBT molecules are adsorbed on the oxide film surface already at OCP, forming an organic layer that hinders the reduction reactions [98]. This hindering effect is supported by the lower cathodic current measured in the presence of 2-MBT in the potential range (from OCP to about −0.3 V vs SHE) preceding the reduction of Cu_2O, as well as by the negative shift of the Cu_2O reduction peak. Alternatively, it is possible that upon exposure to the 2-MBT + NaOH solution, the oxide film growth is restricted at OCP conditions due to the interaction of 2-MBT with the surface. Therefore, the lower cathodic current measured could be due to the electro-reduction of the thinner

film present in this case. We also observe that the evolution of hydrogen gas does not occur by this pre-treatment method at the potential −0.8 V vs SHE, unlike that observed for the pre-treatment in absence of the inhibitor. This again indicates the hindering effect of 2-MBT on the cathodic reactions within this potential range and is consistent with 2-MBT behaving as a mixed inhibitor (anodic and cathodic) [97].

The next two cycles of cathodic pre-treatment performed in presence of the inhibitor show negligible measured cathodic current densities, indicating that either the oxides are completely reduced or that the reduction of the oxide film is blocked due to the presence of 2-MBT on the surface. Consequently, much more Cu(I) oxide subsists at the interface after pre-treatment in the presence than in the absence of 2-MBT in the NaOH solution, as confirmed by surface analysis discussed hereafter.

The CVs for anodic oxidation performed after varying the pre-treatment conditions of the interface are shown in Figure 5.2 (a–d). Figure 5.2a corresponds to the test done in the 0.1 M NaOH reference solution. The other three CVs correspond to the tests performed in presence of 1 mM 2-MBT in the 0.1 M NaOH solution, performed after cathodic pre-treatment in the absence of 2-MBT followed by 2 minutes (Figure 5.2b) and 1 hour (Figure 5.2c) of exposure to the inhibitor solution at −0.45 V vs SHE, and after cathodic pre-treatment in the presence of 2-MBT (Figure 5.2d). The conditions of the interface formation are similar to those studied in Chapter 4 on copper in acidic conditions. The charge densities (anodic and cathodic) for each experiment were determined by integrating the current densities with respect to time, and the equivalent thickness of oxide grown during polarization was determined from the cathodic charge density, assuming that (a) the entire anodic charge corresponds only to oxide grown during the experiment and (b) that all the oxides formed during the anodic branch of the CV are reduced during the cathodic branch of the CV. The results are presented in Table 5.1 along with the standard error of the measurements.

It is observed that for the solution with no inhibitor, Figure 5.2a, oxidation initiates at around −0.40 V vs SHE, with the Cu(I) anodic peak measured at approximately -0.05 V vs SHE. This rise in current density corresponds to the formation of Cu_2O oxide, as observed by others [20, 22–24, 98]. The initial small feature at approximately -0.30 V vs SHE, prior to the oxidation of the surface, has been associated to the adsorption of OH^- ions [23, 24], possibly forming the soluble $Cu(OH)_2^-$ species [20]. Polarization beyond the potential of 0.05 V vs SHE leads to further oxidation in the Cu(II) range to form $Cu(OH)_2$ and CuO, as observed by additional experiments and in other works [20–26, 153]. During the cathodic sweep, a single peak is obtained at −0.36 V vs SHE which indicates the conversion of Cu_2O oxide back to Cu(0) metallic copper. After the potential reaches −0.8 V vs SHE, a sharp increase in the negative current density is observed which corresponds to H_2 evolution [154].

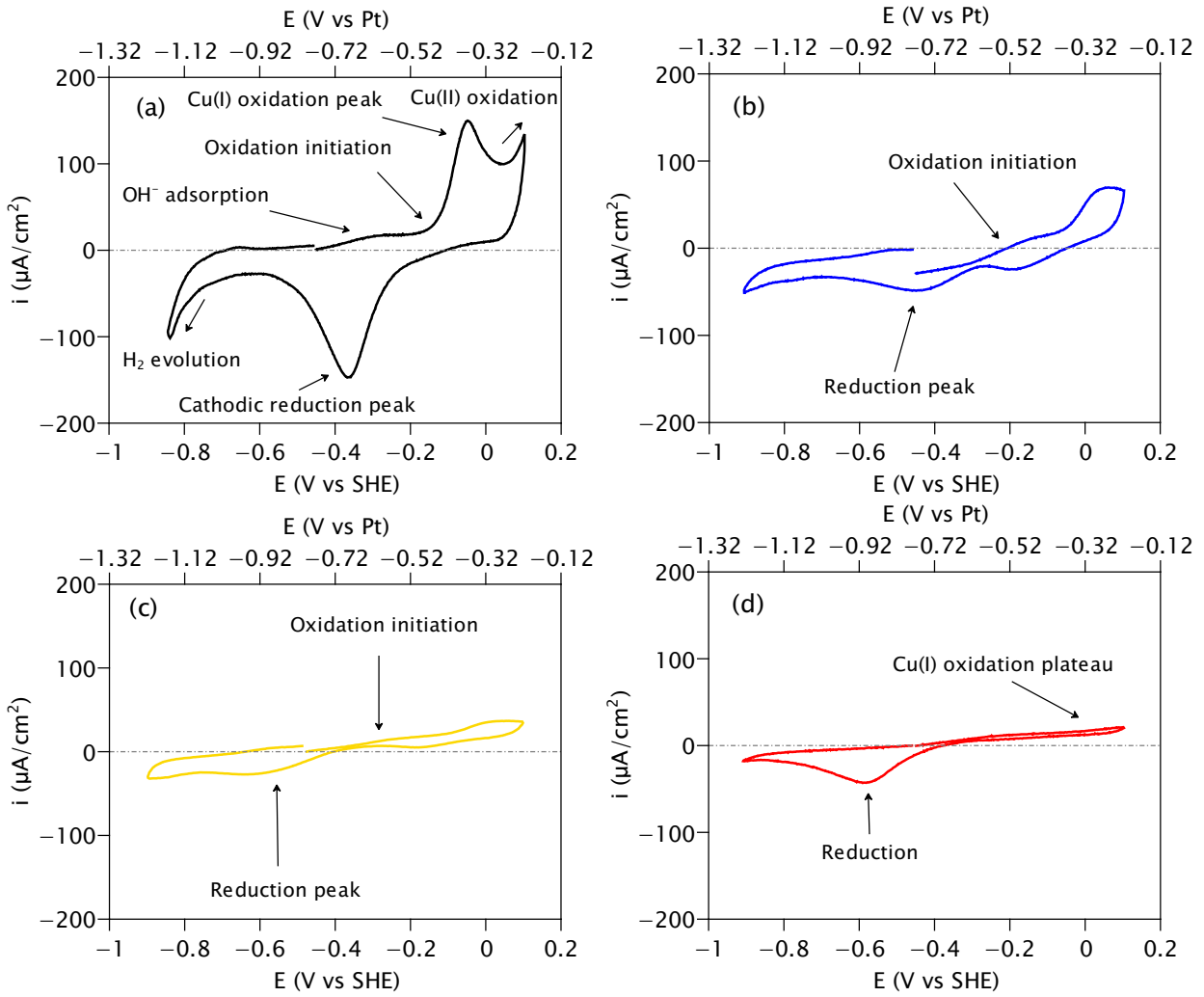

Figure 5.2: Anodic oxidation CVs for copper in (a) 0.1 M NaOH reference solution following pre-treatment without 2-MBT, and in 0.1 M NaOH + 1 mM 2-MBT solution following (b) pre-treatment without 2-MBT and 2 minutes exposure to 2-MBT, (c) pre-treatment without 2-MBT and 1 hour exposure to 2-MBT, and (d) pre-treatment with 2-MBT. Scan rate is 20 mV/s.

The CV performed after pre-treatment without 2-MBT following 2 minutes of exposure to the inhibitor (Figure 5.2b) exhibits a lower current density in the Cu(I) oxidation range compared to the reference solution CV (Figure 5.2a). The increase in the current density starts at a potential of −0.31 V vs SHE, and the oxidation peak is shifted positively to approximately 0.05 V vs SHE. It is proposed that, in the absence of residual native oxides, an organic film of 2-MBT molecules is formed on the metallic substrate surface exposed to the 2-MBT-containing solution at −0.45 V vs SHE. However, the exposure time of 2 minutes is too short to complete the formation of an organic barrier film efficiently blocking surface oxidation during subsequent anodic polarization. The organic layer formed in these

Table 5.1: Anodic and cathodic charge densities determined from the anodic oxidation tests along with the equivalent thickness of oxide film grown during the anodic oxidation test and determined from the cathodic charge density.

	Electrolyte used for CV, Pre-treatment condition	Anodic charge ($\mu C/cm^2$)	Cathodic charge ($\mu C/cm^2$)	Equivalent thickness of oxide film grown (nm)
a	0.1 M NaOH ref Pre-treatment w/o 2-MBT	1409 ± 10	1252 ± 5	1.55 ± 0.01
b	0.1 M NaOH + 1mM 2-MBT, Pre-treatment w/o 2-MBT, 2 mins exposure to 2-MBT	937 ± 51	779 ± 7	0.96 ± 0.01
c	0.1 M NaOH + 1mM 2-MBT, Pre-treatment w/o 2-MBT , 1 hour exposure to 2-MBT	799 ± 28	356 ± 6	0.44 ± 0.01
d	0.1 M NaOH + 1mM 2-MBT, Pre-treatment with 2-MBT	537 ± 1	514 ± 1	0.64 ± 0.01

conditions is likely locally defective, or would break down locally upon polarization, thus allowing for the growth of anodic oxide. The barrier effect is supported by the positive shift of the oxidation peak still observed in the Cu(I) range and by the lower thickness of oxide film grown compared to the reference solution CV (by a factor of approximately 1.5), as seen in Table 5.1.

Like for the experiment reported in Figure 5.2b, performing the Cu(I) oxidation test in the 2-MBT-containing solution after cathodic pre-treatment in absence of 2-MBT followed by 1 hour of exposure to the inhibitor (Figure 5.2c) results in anodic Cu(I) oxidation starting at around -0.31 V and peaking at approximately 0.05 V vs SHE. However, in this case, the current density increase is slightly reduced, indicating higher hindrance to oxide growth. This suggests that the increase in exposure time to 2-MBT allows for the completion of a less defective organic barrier layer, possibly more resistant to breakdown, and thus more effective in blocking anodic activity.

For the test performed in the 2-MBT-containing solution and after cathodic pre-treatment in the presence of 2-MBT (Figure 5.2d), a much lower anodic activity is observed, without any peak of Cu(I) oxidation. The low rise of anodic current indicates that even though

it is significantly reduced, oxidation still occurs on the surface leading to the formation of copper oxides, as attested by the cathodic reduction peak measured at -0.58 V vs SHE on the subsequent reverse scan. The significant reduction in the anodic charge density is by a factor of approximately 2.6 compared to the reference solution CV (Figure 5.2a), and by a factor of 1.5 compared to the CV performed after pre-treatment in absence of 2-MBT followed by 1 hour exposure to 2-MBT (Figure 5.2c), as seen in Table 5.1. This inhibition of the anodic activity agrees with previous work on the effect of 2-MBT on copper passivation [98]. This is assigned to the barrier layer of organic molecules and metal-organic complexes formed by 2-MBT on the residual interfacial layer of native oxide which stabilizes the interface by impinging anodic oxide growth in the Cu(I) potential range [31, 80].

5.3 Surface analysis of 2-MBT-covered oxidized interface.

The ToF-SIMS elemental depth profiles of the interfaces obtained after cathodic pre-treatment in the absence of 2-MBT in the solution followed by 1 hour of exposure to 2-MBT, and after cathodic pre-treatment in the presence of 2-MBT in the solution, are presented in Figure 5.3 (a, b). They display the intensity of the selected secondary ions in logarithmic scale vs the sputtering time, which relates to the depth from the top surface.

Like in Chapter 4 and in recent works [88], the Cu^- and Cu_2O^- ions were selected as characteristic of the metal substrate and metal oxide, respectively, and the $C_7H_4NS_2^-$, C_2N^-, C_2S^-, and $^{34}S^-$ ions as representative of the 2-MBT molecule and its molecular fragments of nitrogen and sulphur, and overall sulphur, respectively. Lastly, the $CuC_7H_4NS_2^-$ ions were selected as characteristic of the Cu-2-MBT interaction, both as bonding on the metallic/oxidized substrate and possible metal-organic complexes. The positions of each layer was defined by the maximum intensity of the corresponding ions with an uncertainty of 5%.

For the depth profile obtained at the reduced state after pre-treatment in the absence of 2-MBT followed by 1 hour exposure to 2-MBT (Figure 5.3a), the interface with the metallic copper substrate is observed at 20 seconds of sputtering time, based on the position at which the Cu^- ions profile reaches its maximum intensity. The maximum intensity of the Cu_2O^- ions profile is seen at 18 seconds of sputtering time, confirming that some copper oxide remains from the native oxide film, although very thin, on the metallic substrate. Similar to the previous chapter (4), we observe that the intensity of $C_7H_4NS_2^-$ ions is maximum at the topmost surface, followed by the C_2N^- ions and the C_2S^- ions, respectively. This is consistent with 2-MBT forming multilayers, as seen by deposition of 2-MBT in vapour phase

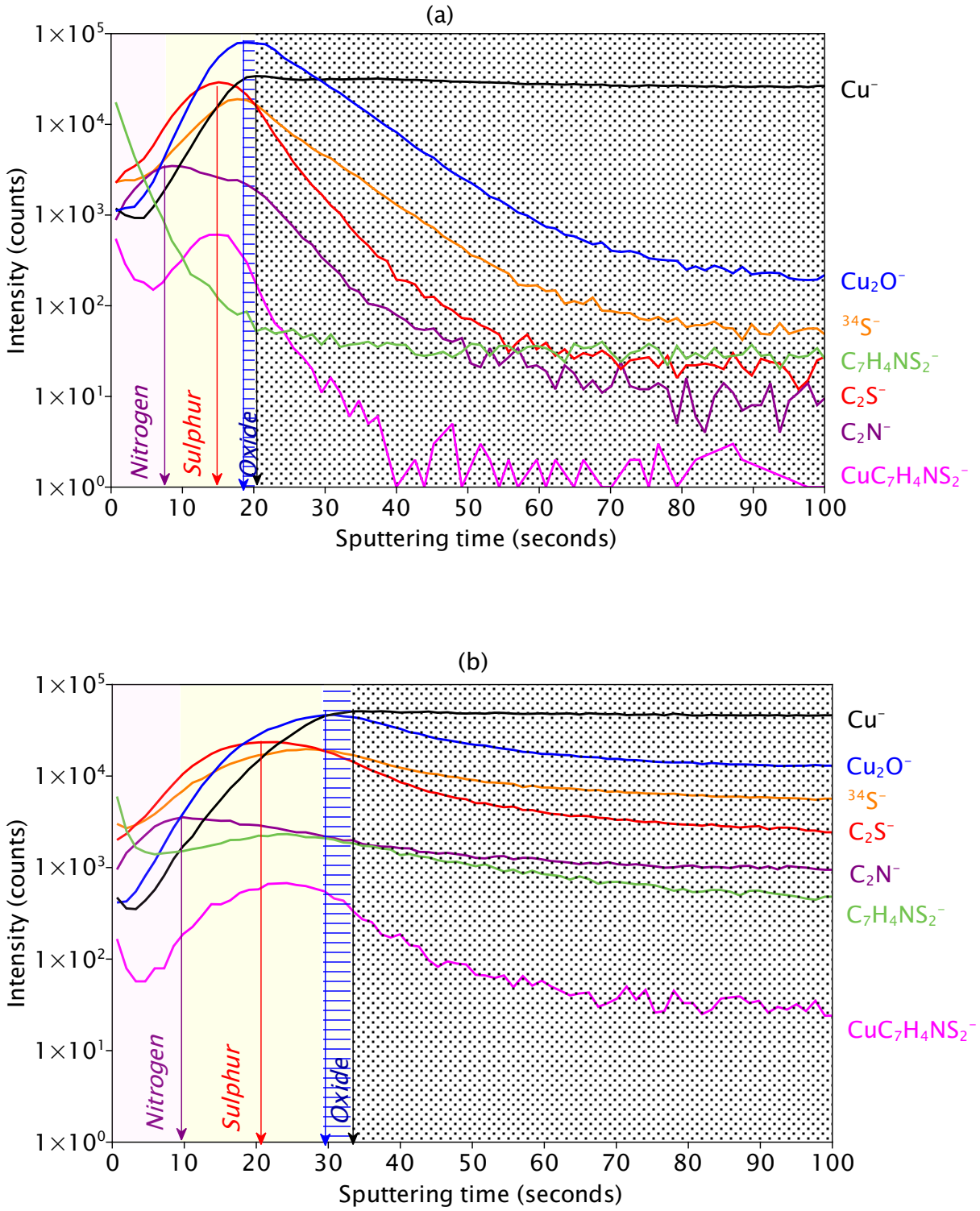

Figure 5.3: ToF-SIMS depth profiles of the inhibiting interfaces obtained in reduced state after (a) cathodic pre-treatment in the absence of 2-MBT followed by 1 hour of exposure to 2-MBT and, (b) cathodic pre-treatment in the presence of 2-MBT.

[83, 84, 86] as well as in neutral aqueous solution [88], with the innermost layer chemically bonded to the partial oxide-covered surface via the sulphur atoms of the molecule and the outer layers physisorbed on the surface. The maxima of the $^{34}S^-$ ions is deeper than that of the C_2S^- ions and much closer to the metallic substrate suggesting that there are regions where sulphur (both from the molecule and free dissociated sulphur) is directly bonded to metallic copper in the non-oxide-covered regions of the surface. This is attested by the fact that the maximum of the Cu_2O^- profile occurs nearly at the same depth as that of the $^{34}S^-$ ions, indicating that instead of a complete layer, the oxides are present as islands which are distributed on the surface, which thus enables the sulphur to bond directly to the metal.

The $CuC_7H_4NS_2^-$ ion profile, of which the maximum intensity is observed between the C_2S^- and $^{34}S^-$ ion profiles, indicates that the 2-MBT molecules of the inner layer bond to both metallic and oxidised Cu. The higher intensity of the $CuC_7H_4NS_2^-$ ions observed at the topmost surface also indicates bonding between the molecules and Cu in the outermost layers of the multilayer organic film, most likely forming Cu-2-MBT metal-organic complexes. This is also evidenced in the Cu^- ion profile, where a slightly higher intensity for the initial 4 seconds of sputtering time is observed, in agreement with the profile of $CuC_7H_4NS_2^-$ ions, indicating an interaction between the Cu ions and the 2-MBT molecule. Although observed in different conditions, the formation of metal-organic complexes can be inferred from the observation of Cu-2-MBT complexes reported previously [31, 80, 94, 151].

In reduced state obtained after pre-treatment in the presence of 2-MBT (Figure 5.3b), the interface with the Cu metal region is at 34 seconds of sputtering time, indicating that the covering oxide and organic layers are markedly thicker in this case. Regarding the interfacial oxide, its presence is supported by the maximum intensity of the Cu_2O^- ion profile measured at 29 seconds, which is at a longer sputtering time from the maximum of the Cu^- ions (characteristic of the metallic Cu) than in the previous case. This demonstrates that the remaining copper oxide film or islands are much thicker here. Regarding the organic multilayer, it is also thicker than in the previous case according to the larger width of the corresponding region, as indicated by the $CuC_7H_4NS_2^-$ and the $C_7H_4NS_2^-$ profiles. The sequence of the intensity maxima of the depth profiles indicates that it is similarly structured with the inner layer primarily interacting with the partial oxide-covered surface via the S atoms of the molecules and the physically adsorbed outer layers as multilayers and/or bonded to Cu to form metal-organic complexes, as mentioned above. However, for the $C_7H_4NS_2^-$ profile, a small increase in intensity is observed in the inner 2-MBT chemisorbed layer, unlike the previous case, which is most likely representative of the Cu-2-MBT complexes that could be present in this region. Although the $CuC_7H_4NS_2^-$ ion profile exhibits this increase as well in the inner layer, it cannot be completely resolved since the $CuC_7H_4NS_2^-$ ion profile is

characteristic of both the bonding on the metallic/oxidized substrate and the metal-organic complexes. Lastly, a slower decay of the intensities is observed here for all secondary ions in the substrate region compared to the previous case (pre-treatment in absence of 2-MBT, 1 hour exposure to 2-MBT), suggesting roughening of the interface for this sample.

The Cu LMM Auger spectra obtained in reduced and anodic states after pre-treatment in the absence or presence of the inhibitor are shown in Figure 5.4. They were decomposed in order to determine the contributions of the Cu(0) and Cu(I) components, corresponding to copper metal and copper oxide respectively, and thus to evaluate the effects of the pre-treatment methods on the presence of interfacial oxides. The decomposition was done by least square fitting, using as components the 2 line-shapes measured, in same analytical conditions, on metallic copper and on oxidized copper reference (Cu_2O thick film) samples, like previously done [86, 142, 146]. Figure 5.4 (a, b) shows the contributions of the Cu(0) and Cu(I) components obtained after pre-treatment in the absence of 2-MBT followed by 1 hour exposure to 2-MBT at the reduced state and anodic state.

It is observed that the intensity of the Cu(I) component is very low here, with the Cu(I)/Cu(0) intensity ratios 0.07 $\pm$ 0.01 and 0.05 $\pm$ 0.01 for the reduced state and the anodic state, respectively. This low intensity of the component corresponding to Cu(I) oxide indicates that the pre-treatment method is effective in both reducing the native oxides and allowing for the inhibitor molecules to form a dense and protective barrier layer. As seen from the CV tests in Figure 5.2c, this barrier layer impedes the formation of Cu(I) oxide in large quantities upon anodic polarization. It also prevents re-oxidation of the sample during transfer through air that would occur in the defective regions of the barrier layer, like observed for 2-MBT layers deposited from the gas phase and imperfectly protecting against re-oxidation [84]. In fact, we observe a minimal decrease, if at all considering the margin of error, for the Cu(I)/Cu(0) intensity ratio in the anodic state of the interface, whereas the CV data shows an increase in current density upon polarization indicating oxidation of the surface (Figure 5.2c). A possible explanation is that, in the reduced state, a fraction of the defective areas of the thin 2-MBT barrier layer are re-oxidized in air which then leads to a slightly higher intensity of the Cu(I) component, whereas after anodic polarization these defective sites may be covered by the inhibitor, which would protect them from re-oxidation. This will also be discussed in detail later.

On the samples pre-treated in the presence of the inhibitor molecule, Figure 5.4 (c, d), it is observed that despite the reduction of the native oxides by cathodic pre-treatment, a large quantity of Cu(I) ions subsists at the interface resulting in much thicker oxide islands than in the previous case, supporting our hypothesis that the presence of 2-MBT during pre-treatment hinders the reduction of the native oxide film present on the surface. In Figure

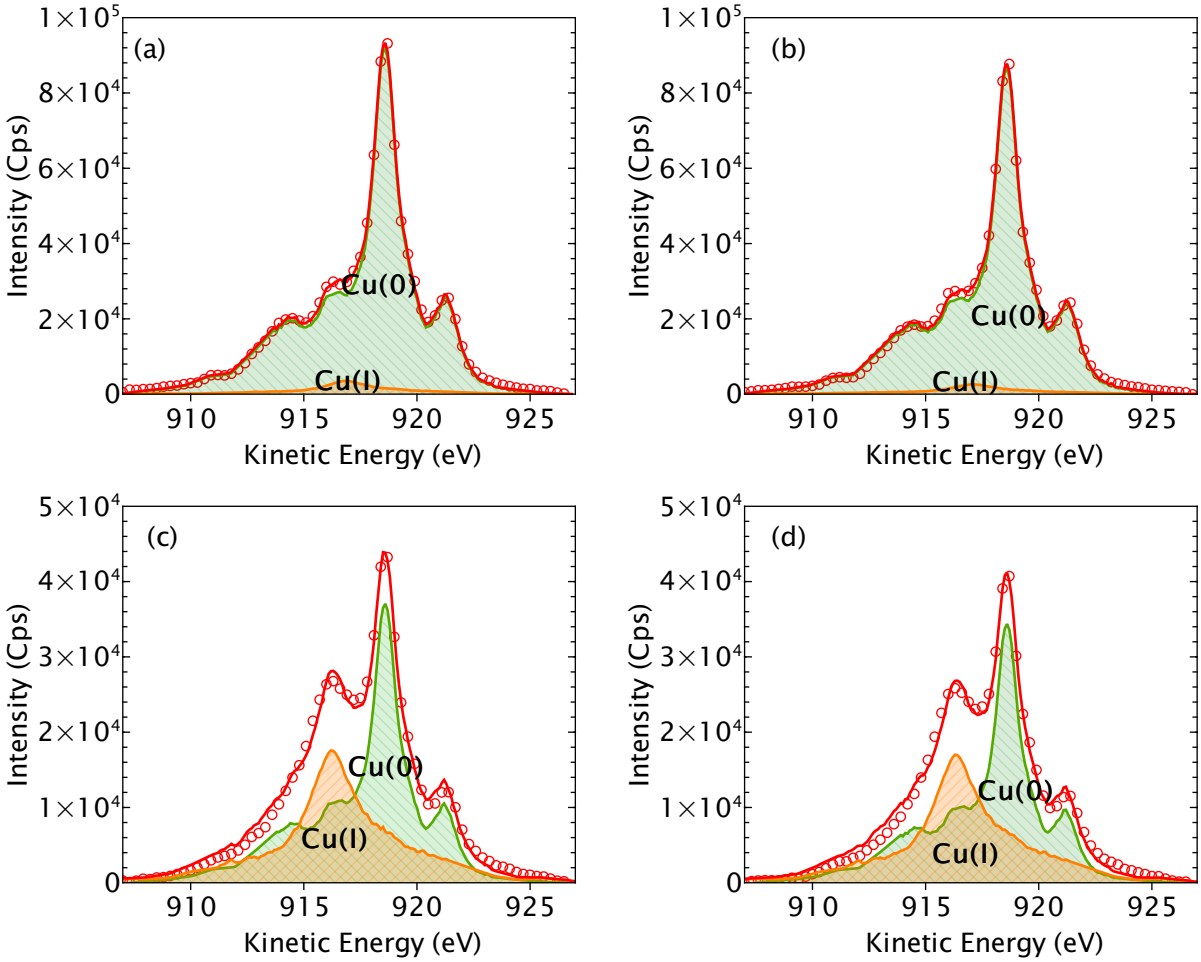

Figure 5.4: Cu LMM Auger spectra for copper exposed to 0.1 M NaOH + 1 mM 2-MBT solution at the (a) reduced state, (b) anodic state after cathodic pre-treatment in the absence of 2-MBT followed by 1 hour of exposure to 2-MBT, and at the (c) reduced state, (d) anodic state after cathodic pre-treatment in the presence of 2-MBT.

5.4d, after polarization of the surface, there is a minimal increase in the intensity of the Cu(I) component with the Cu(I)/Cu(0) intensity ratio increasing from 0.72 (±0.03) to 0.77 (±0.03). This agrees with the CV data in Figure 5.2d, where a slight increase in current density is seen upon anodic polarization. Although relatively thick, as shown by ToF-SIMS and confirmed below, the organic layer would not fully block anodic oxidation of the surface. This residual growth could occur in the more reactive local areas of the interface, i.e. those initially fully reduced after pre-treatment with no subsisting native oxide film. This view is supported by the quantitative analysis presented below.

It is important to note that a fraction of the Cu(I) intensity can arise from the contribution of the Cu-2-MBT complex, since the state of the copper ions in this complex is suggested to be Cu(I) [80]. This is most likely why we obtain such a high intensity for the Cu(I) component

in the reduced state obtained after pre-treatment in the presence of 2-MBT. However, we cannot distinguish the Cu(I) ions related to the complex from the Cu(I) ions related to the oxide matrix. Therefore, the O 1s spectrum is studied below to further resolve this issue.

Figure 5.5 shows the XPS S 2p, N 1s, C 1s, and O 1s core level spectra for the reduced states obtained after pre-treatment in the presence and absence of 2-MBT. The curves were decomposed using the peak components parameters defined in the previously (Chapter 4), with an uncertainty of ± 0.1 eV for the binding energy values.

In both cases, three components were observed for the S $2p_{3/2}$: S1 at 164.2 eV, S2 at 162.8 eV, and S3 at 161.9 eV. They correspond to endocyclic sulphur of 2-MBT, exocyclic sulphur of 2-MBT, and sulphur bonded directly to metallic Cu respectively, with sulphur from S1 and S2 components not bonded to metallic Cu. This is similar to that observed in the previous chapter (4) and in agreement with previous work of 2-MBT adsorption in aqueous and vapour phase on Cu [83, 84, 86, 88].

The N 1s spectra contain two components: N1 at 399.4 eV corresponding to nitrogen from the molecule not bonded to metallic Cu [83, 89], and N2 at 398.2 eV corresponding to a direct bonding between N and Cu [84]. This N2 component is a very small fraction compared to the N1 component (less than 5% of the overall nitrogen intensity), indicating that the quantity of nitrogen atoms of the molecule bonding to the metallic substrate is negligible for quantitative analysis. However, this does show that nitrogen, even though only a very small fraction, does bond directly to metallic Cu.

As for the C 1s spectra, they were decomposed into three peaks: C1 at 286.6 eV corresponding to C=S bonds, C2 at 285.6 eV for C–S and C–N bonds, and C3 at 284.8 eV corresponding to C–C and C–H bonds [70, 84]. The C1:C2:C3 intensity ratio was determined to be 1:2:4 indicating that the 7 carbon atoms fitted the 2-MBT molecule stoichiometry [84]. However, this was not the case for the experiment performed after pre-treatment in absence of 2-MBT followed by 1 hour exposure to the inhibitor solution, for which we observed an increased intensity at the binding energy of the C1 component (286.6 eV) attributed to an additional C4 component with an FWHM of 1.3 ± 0.1 (+0.2 eV compared to the C1 component). The presence of this C4 component is likely due to the formation of alcohols and/or ethers during the 1-hour exposure to the 0.1M NaOH + 1 mM 2-MBT electrolyte. Since their binding energies are very close to each other, 286.5 eV for alcohols and 286.4 eV for ethers [144, 155], it is difficult to distinguish which group is formed.

Three components were observed from the decomposition of the O 1s spectrum for both sets of experiments. The O1 component at 532.9 eV was assigned to oxygen adsorbed on the surface from water [83, 86, 143]. The O2 component at 531.4 eV corresponds to hydroxides

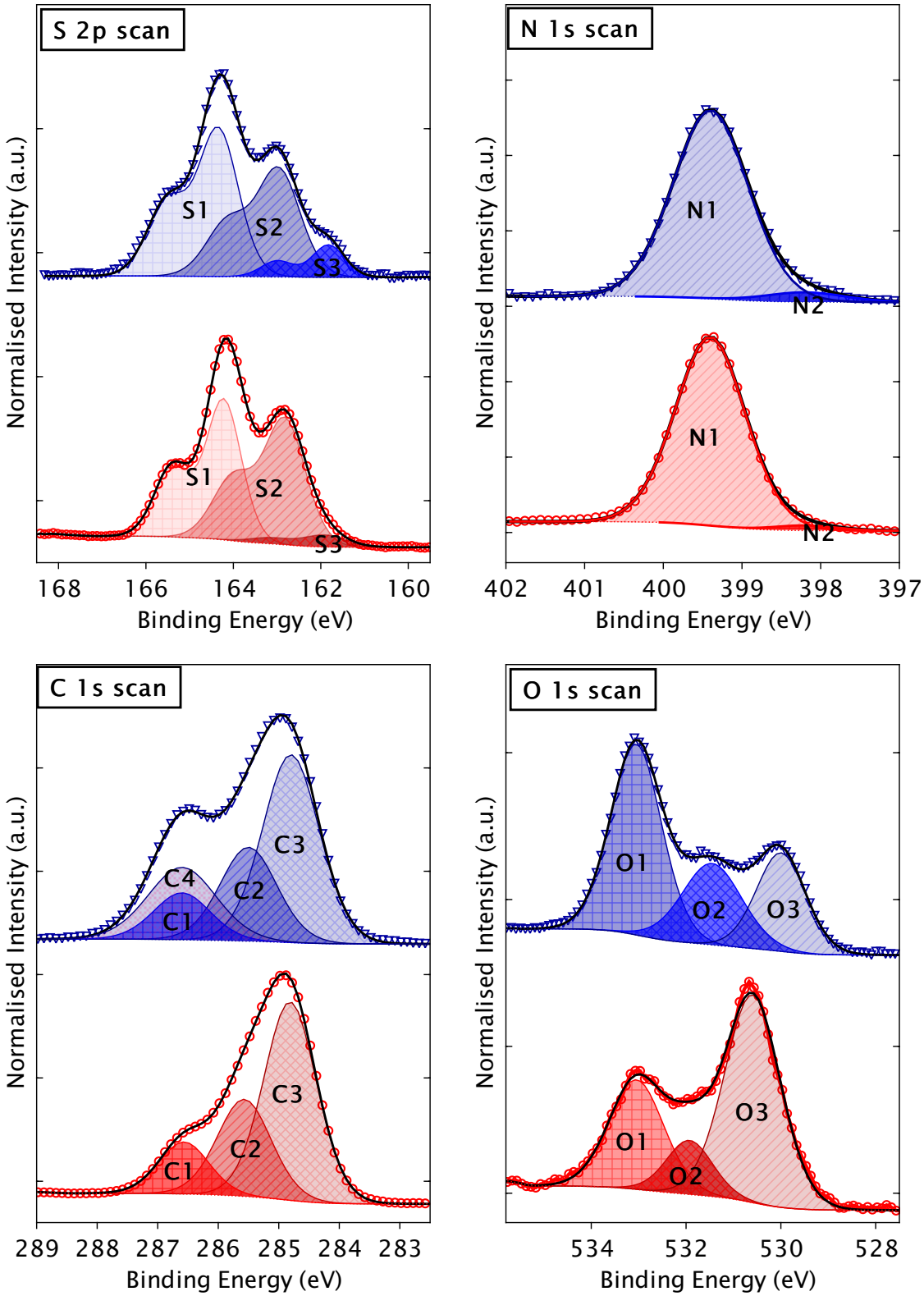

Figure 5.5: XPS S 2p, N 1s, C 1s, and O1s core level spectra of copper exposed to 0.1 M NaOH + 1 mM 2-MBT solution in reduced state after pre-treatment in presence of 2-MBT (red curves), and pre-treatment in absence of 2-MBT followed by 1 hour exposure to 2-MBT (blue curves).

formed on the surface [86, 146]. Lastly, the O3 component at 530 eV was assigned to the Cu(I) oxide present [83, 143, 146]. A positive shift in BE of 0.5 eV is observed for the O2 and O3 components after pre-treatment in presence of 2-MBT. Several authors have reported varying values of binding energies for the oxygen peaks in the O 1s spectrum relating to the oxide and hydroxide components, ranging from 529.6 to 530.6 eV for the oxide (O3) component and between 530.8 to 531.5 eV for the hydroxide (O2) component [30, 84, 86, 88, 89, 142, 143]. It is found that there is a correlation between the thickness of the oxide layer and the BE values reported, i.e. when the oxide is very thin ($\sim$ 0.2 nm) the BE is lower and increases with the oxide thickness (up to 1.5 nm). Additionally, previous work (Chapter 4) shows that when the oxide thickness was between 0.2 to 0.4 nm, the BE for the oxide component was 530.2 $\pm$ 0.1 eV. Hence, we can make the argument that the positive shift in BE for the O2 and O3 components here are most likely due to the presence of a thicker oxide layer/islands in this case (pre-treatment with 2-MBT), as evident from the differences in intensity between the O3 peaks of the O 1s spectra. While the shift can also be due to a change in the structure of the oxide layer and its composition, we do not have any evidence of the phenomenon, both experimentally and from literature.

Although observed for both experiments, the O1 component after pre-treatment in the absence of 2-MBT followed by 1 hour exposure to the 2-MBT + NaOH solution was much higher (blue curve). This phenomenon correlates to the C4 component of the C 1s spectrum of the same experiment, as mentioned above. However, in this case too, the binding energies of the two functional groups are too close to decompose, 532.9 $\pm$ 0.2 eV for alcohols and 532.7 $\pm$ 0.2 eV for ethers [144, 156]. Therefore, the atomic ratio of the C4 component from the C 1s spectrum and the O1 component of the O 1s spectrum was determined to give a more accurate representation of the species observed here. The atomic ratio for the C4/O1 intensities was found to be 2.54 $\pm$ 0.03, indicating that other than the adsorbed oxygen, this species also corresponds to one oxygen atom bonded to either two carbon atoms and/or three carbon atoms. Hence, the C4 component for the reduced state after pre-treatment in the absence of 2-MBT followed by 1 hour exposure to 2-MBT is assigned to the formation of ethers due to an interaction of the hydroxide ions with carbon from either the 2-MBT molecule or from contamination. Angle resolved measurements confirmed that this species is formed on the top-most surface above the 2-MBT layer. Nonetheless, we cannot completely exclude the possibility of formation of a low quantity of alcohols (oxygen bonded to one carbon atom) or a slightly increased oxygen adsorption on the surface.

Regarding the line shape of the N 1s and S 2p spectra shown in Figure 5.5, they are similar after either pre-treatment method which indicates resembling structures of the 2-MBT layers formed, despite the differences in thickness and in oxide quantities on the surface discussed

above. In both cases, it is mostly the sulphur atoms that bond to metallic copper, as evidenced from the S3 peak in the S 2p spectrum and the ToF-SIMS depth profiles, like observed in acidic environment (Chapter 4). Only a tiny fraction of the nitrogen atoms bonds directly to the metallic copper here, which is shown by the presence of a peak at 398.2 eV in both N 1s spectra [84].

5.4 Interface structure and composition.

In order to quantify the effect of the pre-treatment methods on the reduction of the native oxide film and formation of the 2-MBT barrier layers on the surface before and after anodic polarization, the photoelectron intensities of the elemental components obtained by spectral decomposition of the Cu 2p, N 1s, S 2p, and O 1s core levels were used as inputs in the model of photoelectron intensity attenuation, shown in Figure 2.16 in Chapter 2, in order to estimate the thickness and coverage of Cu_2O oxide remaining at the interface and the thickness of the covering 2-MBT organic layer. Despite the limitations of the model regarding the assumptions listed earlier in Chapter 2 and the high uncertainties on the coverage ($\pm$ 10%) and thickness ($\pm$ 0.2 nm) estimates, determined by the propagation of uncertainty, it remains an effective tool for comparison since enabling us to quantify differences between the differently prepared interfaces. The results for the present work are compiled in Table 5.2. The equivalent thickness of the oxide was calculated by weighing its thickness with its coverage, and the equivalent thickness of the 2-MBT layer was calculated by combining the products of thickness and coverage of the 2-MBT layer on the metallic surface and on the oxidized surface, for ease of comparison.

Table 5.2 shows that the pre-treatment in absence of 2-MBT followed by 1 hour exposure to the inhibitor results in low amounts of oxide remaining on the Cu surface. This is in agreement with the electrochemical CV data, ToF-SIMS depth profiles and Cu LMM Auger spectra. The coverage of the oxide islands is relatively high, 77% for the reduced state, and the thickness is estimated to be approximately 0.3 nm. The 2-MBT layer here is approximately 1.2 nm in equivalent thickness. In the anodic state of the surface, the coverage of oxide islands decreases marginally with their thickness remaining constant. It is proposed that during polarization, the ultra-thin Cu_2O oxide islands decompose, thus providing Cu atoms for the 2-MBT molecules to then bond with and thus increase the coverage of metallic Cu. The other hypothesis is that in the reduced state, there are regions of the surface not covered by the 2-MBT layer at all, which oxidize when in contact with air during sample transfer, thus giving a higher apparent coverage of oxide islands in this state. Upon anodic polarization, these uncovered regions would be oxidized to Cu(I) state, as suggested by the CV data, masking

Table 5.2: Coverage and thickness of the copper oxide islands and thickness of 2-MBT organic layer estimated from quantitative analysis of the XPS data. The uncertainty on the coverage was estimated to be ± 10% and the uncertainty on the thicknesses was estimated to be ± 0.2 nm.

	Conditions of interface formation	Coverage of Cu_2O islands (%)	Thickness of Cu_2O islands (nm)	Equivalent thickness of Cu_2O (nm)	Thickness of 2-MBT layer above oxides (nm)	Thickness of 2-MBT layer on metallic Cu (nm)	Equivalent thickness of 2-MBT layer (nm)
a	Pre-treatment w/o 2-MBT, 1 hr exposure to 2-MBT, reduced state.	77	0.31	0.24	1.11	1.42	1.18
b	Pre-treatment w/o 2-MBT, 1 hr exposure to 2-MBT, anodic state.	72	0.31	0.22	1.42	1.73	1.51
c	Pre-treatment with 2-MBT, reduced state	54	0.89	0.48	2.36	3.25	2.77
d	Pre-treatment with 2-MBT, anodic state	72	0.80	0.58	2.75	3.55	2.97

the artefact effects of air transfer. Regarding the 2-MBT layer, we observe a slight increase in the thickness after anodic polarization of the surface. This is discussed in detail later.

For the surface in reduced state after cathodic pre-treatment in the presence of 2-MBT, the initial coverage of the residual oxide islands is found lower, but their thickness approximately three times compared to the previous case due to either incomplete reduction of the native oxide film, as discussed earlier, or further oxidation of those regions during transfer of the samples through air. Although the coverage of the oxide islands in the reduced state is only around 54% of the surface, their thickness is estimated to be approximately 0.9 nm, indicating 3D oxide islands partially covering the Cu substrate. The 2-MBT organic layer is markedly thicker compared to the oxide islands, with an equivalent thickness of approximately 2.8 nm. This confirms our hypothesis of the formation of thicker organic multilayers as inferred from the ToF-SIMS data, and in agreement with previous work in acidic environment (Chapter 4).

Upon polarization, a moderate fraction of the surface is further oxidized, resulting in a higher coverage of the oxide islands while thickness is unchanged considering the experimental uncertainty. This supports residual anodic oxidation occurring mostly in the more reactive local areas of the interface initially with no subsisting native oxide film after pre-treatment. The trend for the thickness increase of the 2-MBT layer in the anodic state is observed in this case as well, from 2.77 to 2.97 nm (Table 5.2). It is proposed that during anodic polarization, the 2-MBT molecules interact with the Cu(I) ions released in the solution to form Cu-2-MBT

complexes that deposit on the surface and thus form a thicker organic layer, as evidenced in the ToF-SIMS depth profiles (Figure 5.3). An indication of this is the difference between the anodic and cathodic charge densities during the cyclic voltammetry tests. As evidenced from Table 5.1, there is a positive difference between the anodic and cathodic charge densities for all 4 experiments. Therefore, it is indisputable that there is some reacting Cu (from anodic charge) that is not involved in the growth of the oxide layer subsequently reduced (from cathodic charge). These excess Cu ions likely interact with the 2-MBT molecules to form the complexes and thus increase the thickness of the 2-MBT organic layer on the surface. In their work on corrosion inhibition of copper by 2-MBT, Ohsawa et al. concluded that it was indeed the Cu(I) ions that form complexes with the 2-MBT molecule [80]. This would also explain why we observe a thicker 2-MBT layer when there are more oxides on the copper surface in an alkaline environment (pre-treatment with 2-MBT) and why it increases upon polarization.

5.5 Effects of pH on the interface.

Several authors have hypothesized that the formation of the 2-MBT layer on copper differs based on the environment and the initial surface oxidation state [79, 80, 151]. Since we have studied the adsorption of the 2-MBT inhibitor on Cu in acidic conditions, we can now make a comparison with alkaline environment and discuss the differences in interface oxide layers and 2-MBT organic layers and try to understand why the changes in barrier layer formation occur.

It has been determined that in both environments, acidic and alkaline, the cathodic pre-treatment performed in absence of 2-MBT results in a nearly metallic state, whereas the pre-treatment performed in presence of 2-MBT results in a significant quantity of oxides unreduced. This indicates that in both environments there is an interaction between the 2-MBT molecules and copper oxide which then hampers the complete reduction of the native oxides present on the surface. Additionally, in both cases, the remaining oxides are trapped between the 2-MBT layer and the metallic substrate in the form of islands, instead of a fully covering layer.

Despite these similarities in the two environments, it was revealed that the thickness of the 2-MBT organic layer is larger on a relatively oxide free surface in the acidic environment, whereas it is the other way around in the alkaline environment, with a thicker 2-MBT layer observed in case of larger oxide quantities. Moreover, upon anodic polarization, a decrease in the thickness of the 2-MBT layer was observed in the acidic environment, whereas the present work shows that the 2-MBT layer increases in thickness in the alkaline environment.

This difference is likely due to the conformer of the 2-MBT molecule that is stable in each environment. In the alkaline environment, the molecule, of which pKa is 6.9 [81], would predominantly be in the thiolate form due to the excess OH^- ions present in the solution [78]. The deprotonation of the molecule offers an additional reactive site (N atom) in the molecule which increases the bonding possibilities with copper metal and copper oxides, as shown by DFT calculations [90, 91], and thus could promote the adsorption of 2-MBT molecules on the metallic substrate, increasing its coverage, and the formation of Cu-2-MBT complexes which then deposit on the surface, increasing the thickness of the organic layer. However, this is not the case in acidic environment where the molecule predominates in its protonated thione form [78] due to the excess H^+ ions in the solution, thus not offering an extra reactive site and limiting the possibilities of adsorbed configurations and bonding with copper metal and copper oxide. The presence of chloride ions in the acidic environment could also have effects that are not seen in the alkaline environment studied here. The adsorption of Cl^- ions would be rather competitive with the adsorption of 2-MBT on copper, thus limiting the adsorption of the 2-MBT molecules and the growth of the organic layer. However, in the alkaline environment the 2-MBT layer is allowed to grow more freely without the influence of the aggressive Cl^- ions, which could possibly be a reason for the thicker organic layer here.

Regardless of the growth mechanism of the 2-MBT layer on the surface, the bonding between the molecules and the surface remains largely similar. In both strongly acidic and strongly alkaline conditions, the 2-MBT molecules bond with metallic copper mostly via their sulphur atoms. In the strongly alkaline conditions, a small fraction of N bonds directly to the metallic copper which most likely occurs due to the additional reactive sites formed by deprotonation of the molecule in the NaOH solution, as mentioned above. However, we can neither confirm nor exclude the possibility that there is an interaction between the copper oxides and the sulphur and/or nitrogen atoms of the molecule, like shown by DFT calculations [91]. This remains as one of the major questions yet to be dealt with.

5.6 Conclusion

The adsorption of the 2-MBT organic corrosion inhibitor and its effects on the anodic oxidation of copper in an alkaline environment were investigated by electrochemical and surface analytical techniques. It was shown that the formation of the 2-MBT layer on the surface impedes the growth of anodic oxide in the Cu(I) potential range. However, the presence of native oxide on the surface plays a major role in the formation and subsequent effectiveness of the organic layer as a barrier against anodic activity. Reduction of the native oxide film by cathodic pre-treatment performed in the absence of 2-MBT in the solution resulted in a nearly metallic state of the surface, whereas an incomplete reduction of the native oxide film was observed in the presence of 2-MBT, owing to the adsorption of 2-MBT on copper oxide and therefore blocking electro-reduction. The resulting organic barrier layer was substantially thicker compared to a surface with negligible oxides and included metal-organic complexes. This thicker 2-MBT barrier layer was more effective in impeding the growth of oxides upon anodic polarisation. Longer exposure times to the inhibitor of a surface with negligible oxides increased the efficiency of the organic barrier layer in impeding the growth of anodic oxide.

The organic barrier layer is multi-layered with the inner layer bonded to the copper substrate principally via the sulphur atoms of the molecules, as determined from the XPS spectra and the ToF-SIMS depth profiles. Additionally, a limited fraction of the nitrogen molecule is also bonded directly to the metallic substrate. The interaction between the copper oxides and the sulphur and/or nitrogen atoms from the molecules could not be resolved. Upon anodic polarisation, the 2-MBT barrier layer grows in thickness, with inclusion of Cu-2-MBT complexes. It is proposed that the thiolate form of 2-MBT, which is the dominant conformer in an alkaline environment, allows for additional bonding possibilities to the Cu atoms and Cu(I) ions released from the surface oxide, forming Cu-2-MBT complexes that deposit on the surface and thus increase the thickness of the organic barrier layer.

CHAPTER 6

Inhibition of the initial stages of corrosion by 2-mercaptobenzothiazole adsorption and the effects of interfacial oxides on copper in neutral chloride conditions

This chapter is based on the work published in Corrosion Science by V. Garg, S. Zanna, A. Seyeux, F. Wiame, V. Maurice, and P. Marcus, entitled "Inhibition of the initial stages of corrosion by 2-mercaptobenzothiazole adsorption and the effects of interfacial oxides on copper in neutral chloride conditions." [157]

The objective of this chapter is to investigate 2-mercaptobenzothiazole (2-MBT) adsorption on a metallic state of the copper surface and evaluate the inhibiting effect of the molecule on the initiation of corrosion in a near neutral chloride solution (3.5% NaCl). We also explore the role of the remnant native oxide, that subsists at the interface between the 2-MBT layer and the metallic copper substrate, on the formation of the organic inhibitor layer, its role on the formation of the metal-organic Cu-2-MBT complexes, and finally its effect on the protection of the surface using advanced surface analysis techniques such as XPS and ToF-SIMS.

6.1 Experimental

The electrochemical experiments were performed using a classical three-electrode electrochemical cell with a saturated calomel electrode (+0.2415 V vs SHE) as the reference electrode. The electrolytes used for the experiment were a reference 0.5 M NaCl aqueous solution of pH 5.3 ± 0.1 without the inhibitor, and a 0.5 M NaCl + 0.1 mM 2-MBT aqueous solution of pH 5.2 ± 0.1 as the solution with inhibitor.

Cathodic pre-treatment was performed on the substrates to reduce the native oxide film initially present on the surface. After immersion at the open circuit potential, the potential was swept down to the onset of hydrogen gas evolution (-0.86 V vs SHE) and then back up to the potential at which the measured current was zero (-0.16 V vs SHE), with a scan rate of 20 mV/s. This was repeated 2 more times to ensure maximum reduction of the native oxide film. The anodic polarisation tests were performed by sweeping the potential from -0.16 V vs SHE up to the initiation of corrosion, followed by reverse sweeping to -0.56 V vs SHE, and then back to -0.16 V vs SHE. The electrochemical experiments were repeated in threefold to ensure reproducibility of the results.

Surface analysis was performed after cathodic pre-treatment followed by 2-MBT adsorption on the surfaces, and in the anodically polarized state (anodic state at 0.09 V vs SHE, before initiation of corrosion). Once the relevant electrochemical state was obtained, the cell was disconnected, the samples rinsed with ultra-pure water, dried using nitrogen, and transferred within 2 minutes for analysis by XPS and ToF-SIMS.

6.2 Formation of the 2-MBT organic barrier layer

Two methods of cathodic pre-treatment were used: (a) pre-treatment in a solution of 0.5 M NaCl + 0.1 mM 2-MBT (with inhibitor), and (b) pre-treatment in a solution of 0.5 M NaCl (without inhibitor). Figure 6.1 shows the three CV cycles of the cathodic pre-treatment in each electrolyte with the current density measured as the potential is swept from OCP to the onset of hydrogen gas evolution and back.

For the first cycle of the pre-treatment, a distinct cathodic peak of similar magnitude is observed at approximately -0.3 V vs SHE in both cases. This peak corresponds to the reduction of Cu(I) oxide (Cu_2O) natively formed on the Cu substrate, as seen in the previous chapter in alkaline environment (Chapter 5). Its similar amplitude in both solutions (with/without inhibitor) suggests no major effect of the inhibitor on the cathodic reduction of the oxide in this potential range, in contrast with the marked effect observed in chloride-free alkaline environment seen previously. A possible explanation is that chloride ions competitively

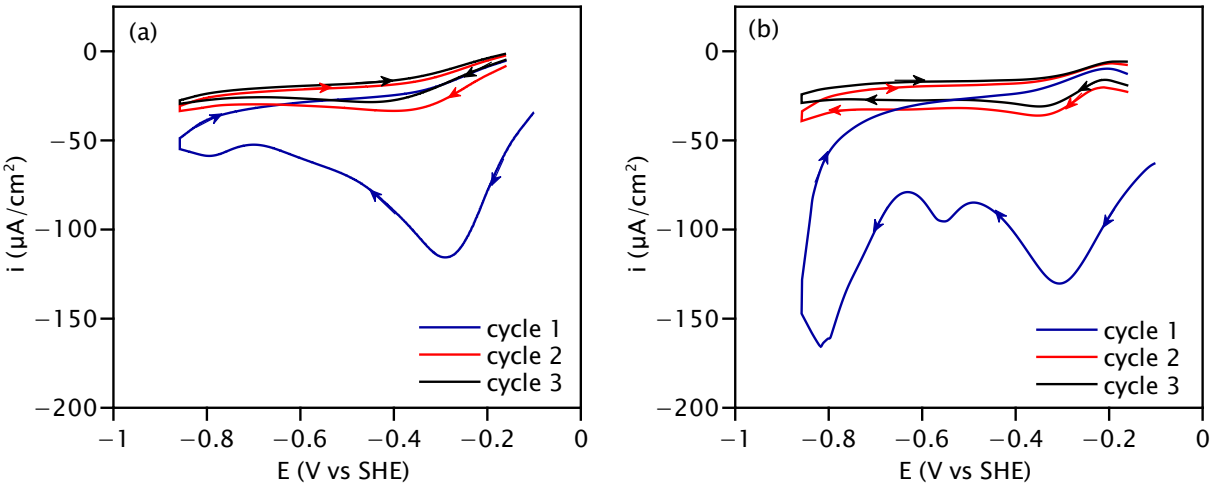

Figure 6.1: Cathodic pre-treatment curves obtained using cyclic voltammetry with a scan rate of 20 mV/s on copper in (a) 0.5 M NaCl + 0.1 mM 2-MBT solution (with inhibitor), and in (b) 0.5 M NaCl solution (without inhibitor). Arrowheads are added to each cycle to guide the reader's eye.

adsorb on the oxide film surface and poison the cathodic reduction reaction of the oxide in this potential range independently of the presence of the inhibitor. A second smaller peak is observed at -0.57 V vs SHE for the pre-treatment without inhibitor (Figure 6.1b) whereas only a shoulder is measured at this potential for the pre-treatment with inhibitor. The second peak for the pre-treatment with inhibitor is shifted to -0.78 V vs SHE (Figure 6.1a). The nature of the related cathodic reduction process remains unclear although it likely involves adsorbed chloride ions since it has not been observed in a chloride-free environment. The decrease in amplitude and the negative shift observed for the pre-treatment with the inhibitor suggest an influence of the 2-MBT molecules on this process. Finally, for the pre-treatment without inhibitor (Figure 6.1b), the hydrogen evolution initiates at around -0.65V vs SHE. However, this is not observed for the pre-treatment with 2-MBT even until a potential of approximately -0.9 V vs SHE (Figure 6.1a), indicating the influence of 2-MBT also on the cathodic reaction of water reduction occurring here.

The next two cycles for both pre-treatment methods result in much lower cathodic current densities compared to the first cycle. However, we do observe that the shape of the curves is slightly different for both methods. In the case of pre-treatment without inhibitor (Figure 6.1b), a small but distinct peak is observed at a potential of approximately -0.3V vs SHE for the second and third cycles, reminiscent of the peak from the first cycle. This suggests that there is still some reduction of the native oxide occurring here and decreasing in amplitude with repeated cycling. This distinct peak is not observed for the pre-treatment with inhibitor

(Figure 6.1a), where an increase in negative current density is observed and shifted negatively, however, not characteristic of a reduction peak. This suggests that the 2-MBT molecules have an inhibiting effect on the reduction of the remaining oxides, further observed in the third cycle of the pre-treatment. In the potential range negative to -0.65V vs SHE, the inhibiting effect of 2-MBT on the cathodic reaction of water reduction is confirmed in the second and third cycles with the absence of any discernible peak indicative of the reaction.

In order to characterize the reduction of the native oxides further and to study its effect on the formation of the 2-MBT inhibiting layer, surface analysis was carried out after the three cycles of pre-treatment in (a) 0.5M NaCl + 0.1 mM 2-MBT, (b) 0.5 M NaCl followed by 2 minutes exposure to the 2-MBT containing solution, and (c) 0.5 M NaCl followed by 1 hour exposure to the 2-MBT containing solution. In the latter two pre-treatment methods (without inhibitor), the 2-MBT containing solution was introduced after the three cycles to enable the adsorption of the molecule on the substrate.

The ToF-SIMS elemental depth profiles of the resulting interfaces are presented in Figure 6.2 (a-c). These profiles display the intensity of the selected secondary ions in logarithmic scale vs the sputtering time in seconds. The sputtering time relates to the depth of the substrate from the topmost surface. The Cu^- and Cu_2O^- ions were selected as characteristic of the metallic substrate and Cu oxide, respectively, as previously reported in Chapters 4 and 5. The $C_7H_4NS_2^-$ ion corresponds to the 2-MBT organic molecule as a whole, while the C_2N^- and C_2S^- ions are representative of the 2-MBT molecular fragments of nitrogen and sulphur in interaction with the substrate. The $^{34}S^-$ and $^{37}Cl^-$ ion profiles are characteristic of the overall sulphur and chloride species, respectively. Finally, the $CuC_7H_4NS_2^-$ ions were selected as characteristic of the Cu^-2-MBT interaction, both as bonding to the metallic/oxidized substrate and possible metal-organic complexes, as discussed in previouly. The positions of each layer were defined by the maximum intensity of the corresponding ions with an uncertainty of 5%.

For the depth profile obtained after cathodic pre-treatment in the presence of 2-MBT (Figure 6.2a), the Cu metallic substrate is reached at 22 seconds of sputtering as indicated by the maximum intensity of the Cu^- signal. Although cathodic pre-treatment was applied to the substrate, remnant oxides subsist at the interface between the metallic substrate and the 2-MBT organic layer, as indicated by the increase of the Cu_2O^- signal that reaches its maximum intensity at 14 seconds of sputtering. This is in agreement with the CV data suggesting the presence of oxide remnants after the cathodic pre-treatment in presence of the inhibitor. Considering the 2-MBT molecular fragment ion profiles, the C_2S^- ion profile peaks at a larger depth (12 s) compared to the C_2N^- ion profile (9 s), indicating that it is most likely the sulphur atoms which bond to the substrate and/or the remnant oxides.

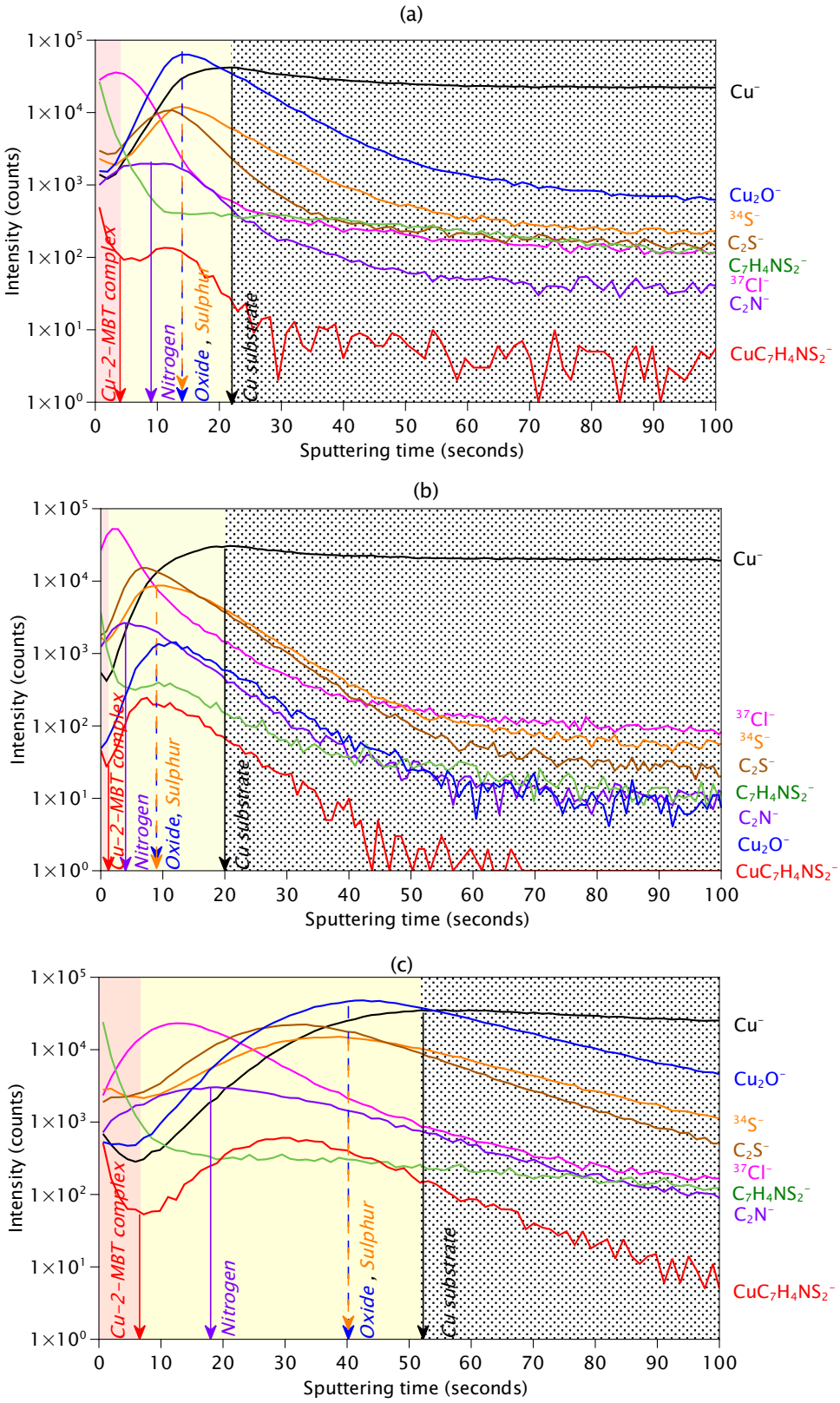

Figure 6.2: ToF-SIMS depth profiles for the 2-MBT/copper interfaces formed in 0.5 M NaCl solution after (a) cathodic pre-treatment in presence of 2-MBT, (b) cathodic pre-treatment in absence of 2-MBT followed by 2 minutes exposure to 2-MBT, and (c) cathodic pre-treatment in absence of 2-MBT followed by 1 hour exposure to 2-MBT.

Furthermore, the $^{34}S^-$ ion profile peaks at 14 seconds of sputtering, which endorses our claim of sulphur bonding. We also note that both the Cu_2O^- and $^{34}S^-$ ion profiles exhibit their maximum intensity at the same sputtering time of 14 seconds, suggesting that the oxides are not in the form of a homogeneous layer, but rather in the form of isolated and dispersed islands on the surface. These findings are consistent with our work of 2-MBT adsorption on copper surfaces in acidic and alkaline media. The ion profile of $C_7H_4NS_2^-$, characteristic of the 2-MBT molecule, shows a progressive intensity decrease from the surface up to 10 seconds of sputtering time where it reaches a minimum intensity plateau. This is associated with the formation of physisorbed multi-layers of 2-MBT on the surface, that are easily sputtered away within the initial few seconds of sputtering.

The $CuC_7H_4NS_2^-$ ion profile in Figure 6.2a exhibits a more complex behaviour. A decrease in intensity is observed up to 3 seconds of sputtering followed by a shoulder centered around 11 seconds of sputtering. The shoulder is assigned to the bonding of the molecule with the substrate, whereas the initial decrease is most likely due to the formation of metal-organic complexes which are deposited on the surface, as concluded in our work in alkaline media and suggested by other authors [80]. The formation of metal-organic complexes is also attested by the shape of the Cu^- ion profile for the first 3 seconds of sputtering time which correlates to that of the $CuC_7H_4NS_2^-$ ion profile, with a small decrease observed initially. Finally, the $^{37}Cl^-$ ion profile peaks at only 3 seconds of sputtering and decreases sharply with increased sputtering time. This indicates that the chloride ions are mostly adsorbed in the outer layer followed by a limited interaction with the oxides. The effect of the chloride ions on the metallic substrate is negligible, as attested by the shape of the ion profile.

The depth profile of the substrate pre-treated in absence of 2-MBT followed by 2 minutes of exposure to 2-MBT (Figure 6.2b) shows a similar structure to that of the substrate pre-treated in presence of 2-MBT (Figure 6.2a), regarding the presence of oxide islands, the sulphur bonding to the substrate, and the physisorbed 2-MBT molecules on the surface. Although the difference in sputtering time between the peaks of the Cu^- and Cu_2O^- ion profile is similar to the previous case, i.e., 8 - 10 seconds, the intensity of the Cu_2O^- ion is lower by almost 2 orders of magnitude here. This suggests that the overall oxide quantity (thickness and coverage) is lower in the substrate pre-treated in absence of 2-MBT (Figure 6.2b).

The major difference between the two depth profiles relates to the $CuC_7H_4NS_2^-$ ion profile, where the initial intensity is rather weak (Figure 6.2b) compared to the previous case (Figure 6.2a). This suggests very little formation of the metal-organic complexes in this case, also seen by the lower intensity of the Cu^- ion profile for the first 2 seconds of sputtering. The rationale for this phenomenon is discussed further on. However, the inner shoulder of the $CuC_7H_4NS_2^-$ ion profile remains consistent with the previous case, indicating bonding of

the molecule with the Cu substrate. The $^{37}Cl^-$ ion profile again peaks near the surface suggesting chloride ions adsorption on the surface and reduced interaction with the inner layers. Regarding the thicknesses of the interfacial oxide layer and the 2-MBT organic layer, it is difficult to conclude between the two pre-treatments since the structure of the layers and the surface roughness play an important role in the shape and the peak position of the ion depth profiles. Therefore, we leave the interpretation of the layer thicknesses by ToF-SIMS and rather estimate them using XPS analysis, as discussed further on.

For the depth profiles obtained after cathodic pre-treatment in absence of 2-MBT followed by 1 hour exposure to 2-MBT (Figure 6.2c), the range of sputtering time for each layer has significantly increased compared to the previous two methods of 2-MBT deposition on the substrate, by a factor of more than 2 times. This can be attributed to two main factors: the formation of a thicker 2-MBT layer and oxide islands (which we discuss further based on the XPS data), and the modification of the structure of the layers along with an increased surface roughness. Despite the changes observed regarding the range of sputtering time, the inhibitor layer and the interface oxide layer in Figure 6.2c are sequenced similarly to the previous two cases. The $C_7H_4NS_2^-$ ion profile shows a larger range of decrease, until 12 seconds of sputtering time, indicating a thicker outer physisorbed layer. The initial decrease of the $CuC_7H_4NS_2^-$ ion profile occurs for a longer sputtering time here, indicating increased formation of the Cu-2-MBT complexes upon a longer exposure time to the NaCl solution. This is confirmed by the Cu^- ion profile's initial decrease which coincides with that of the $CuC_7H_4NS_2^-$ ion profile.

Lastly, we observe that the $^{37}Cl^-$ ion profile exhibits its maximum intensity at approximately 12 seconds (Figure 6.2c), i.e. at the same sputtering time as the minimum intensity plateau of the $C_7H_4NS_2^-$ ion profile. This indicates that the chloride ions have penetrated the outer physisorbed 2-MBT layer in this substrate, unlike the previous two cases. Therefore, it is likely that the chloride ions also have an increased effect on the oxides here, caused by the prolonged exposure to the chloride containing solution. The intensity of the $^{37}Cl^-$ ion profile decreases steadily after 20 seconds of sputtering, indicating that the chloride effect is reduced at greater depths of the substrate, due to the inner 2-MBT layer impeding its pathways to the metal substrate and thus protecting it.

The Cu LMM Auger spectra obtained after cathodic pre-treatment for the three electrochemical conditions of interface formation are shown in Figure 6.3(a-c). They include the contributions of the Cu(0) and Cu(I) components corresponding to copper metal and copper oxide, respectively. The decomposition was done by least square fitting, using as components the 2 line-shapes measured, in same analytical conditions, on metallic copper and on a Cu_2O thick film, like previously done [86, 142, 146].

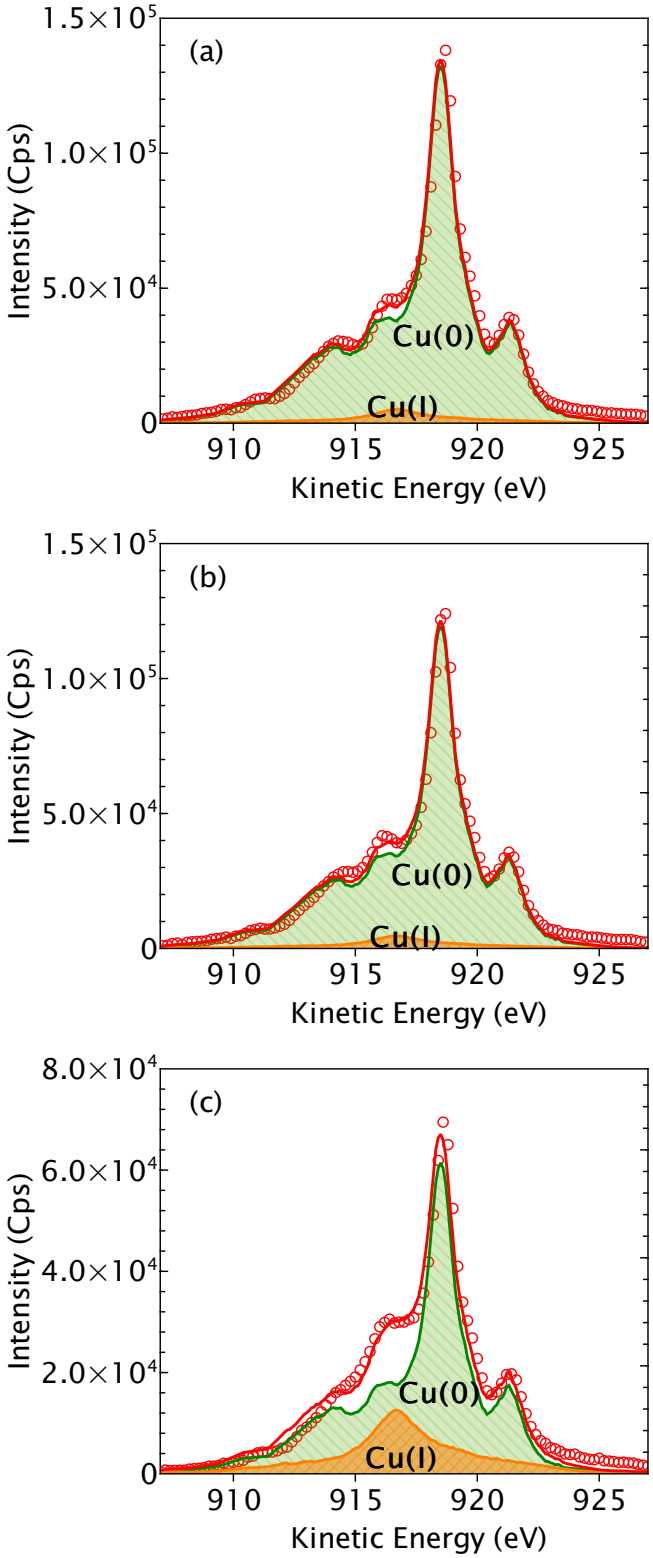

Figure 6.3: Cu LMM Auger spectra for the 2-MBT/copper interfaces formed in 0.5 M NaCl solution after (a) cathodic pre-treatment in the presence of 2-MBT, (b) cathodic pre-treatment in the absence of 2-MBT followed by 2 minutes exposure to 2-MBT, and (c) cathodic pre-treatment in the absence of 2-MBT followed by 1 hour exposure to 2-MBT.

It is observed that in the case of pre-treatment with 2-MBT (Figure 6.3a) and the pre-treatment without 2-MBT followed by 2 minutes exposure to 2-MBT (Figure 6.3b), the amount of oxides that subsist is very small. The Cu(I)/Cu(0) intensity ratio determined for the substrate pre-treated with 2-MBT was 0.06 ± 0.01, whereas the ratio of the substrate pre-treated without 2-MBT followed by 2 minutes exposure to 2-MBT was 0.05 ± 0.01. This indicates that both pre-treatment methods are quite effective in reducing the native oxides present initially on the surface. Although the changes are minimal between the two pre-treatment methods, the data are in agreement with the ToF-SIMS depth profiles presented earlier in Figure 6.2(a-b), where the interfacial oxide layer is quite similar for both cases based on the sputtering time, but slightly different in terms of overall oxide intensity. Despite the effectiveness of the pre-treatment methods, we observe that when the exposure time to 2-MBT is increased to 1 hour after pre-treatment in the absence of 2-MBT (Figure 6.3c), the quantity of the Cu(I) ions increases drastically compared to when the exposure time was only 2 minutes. The Cu(I)/Cu(0) intensity ratio determined here was 0.28 ± 0.01, which is a significant increase compared to the two cases observed earlier. This indicates that during the extended exposure time, some regions of the surface, which were most likely uncovered by the 2-MBT molecules, were further oxidized to form Cu(I) ions.

In the previous chapter, it was suggested that the metal-organic complexes formed by the Cu(I) ions and 2-MBT molecules could also contribute to the Cu(I) intensity. Given that we observe the presence of these complexes from the ToF-SIMS depth profiles (Figure 6.2c), it is likely that the increased Cu(I) intensity observed in Figure 6.3 (c) could contain some contribution from these metal-organic complexes.

The normalised XPS spectra for the C 1s, N 1s, and S 2p core levels obtained after cathodic pre-treatment in the three conditions are presented in Figure 6.4. Spectral decomposition was performed using the parameters of the peak components defined in the previous chapters. The uncertainty for the binding energy (BE) values and the full widths at half maximum (FWHM) are estimated to be ± 0.1 eV.

The C 1s spectra were decomposed into three chemical states. These components are C1 at 286.6 eV assigned to the C=S bonds, C2 at 285.6 eV for the C-S and C-N bonds, and finally C3 at 284.8 eV associated to the C-C and C-H bonds [84]. The ratio of 1:2:4 measured between these three components reflects the 7 carbon atoms from the 2-MBT molecule in their respective chemical states. This was also measured in previous work on 2-MBT adsorption on copper from vapour phase and liquid phase [83, 84, 88]. It is observed that for the substrate pre-treated in presence of 2-MBT, the shoulder corresponding to the C1 peak is less marked compared to the two substrates pre-treated in absence of 2-MBT. This is due to the slightly larger FWHM (+0.1 eV) of the three carbon components here, most

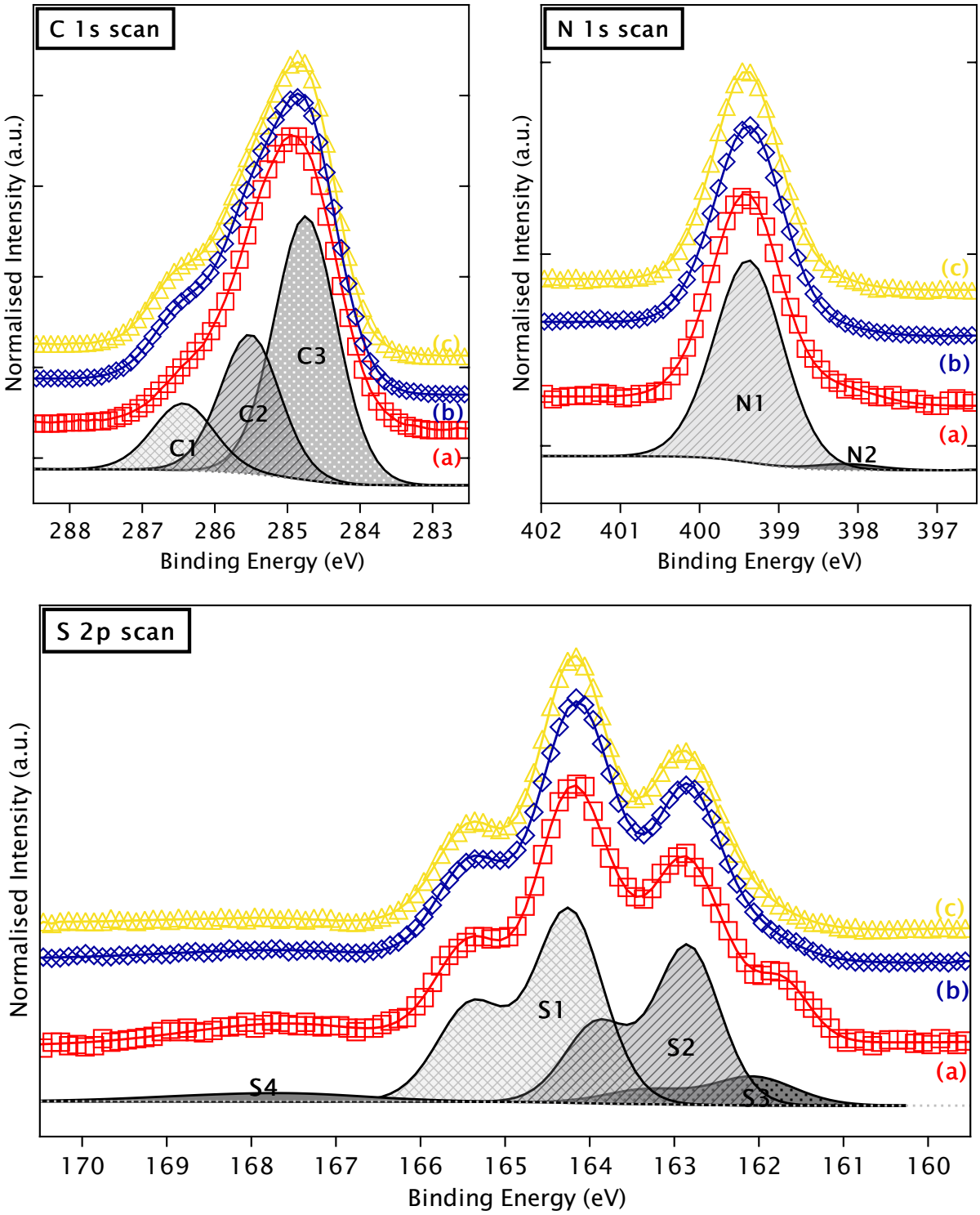

Figure 6.4: Normalised XPS C 1s, N 1s, and S 2p core level spectra for the 2-MBT/copper interfaces formed in 0.5 M NaCl solution after cathodic pre-treatment in (a) presence of 2-MBT, (b) absence of 2-MBT followed by 2 minutes exposure to 2-MBT, and (c) absence of 2-MBT followed by 1 hour exposure to 2-MBT. The symbols represent the experimental data and the corresponding coloured lines represent the fitted curves. The decompositions are shown for spectra (b).

likely caused by a change in the structure of the 2-MBT organic film formed on the substrate pre-treated in the 2-MBT-containing solution.

The N 1s spectra exhibits two components: N1 at 399.4 eV and N2 at 398.2 eV. These components correspond to N not bonded to Cu for N1 and N directly bonded to metallic Cu for the N2 component, as observed previously for adsorption from the vapour phase and in an aqueous alkaline environment [84]. Like in the previous chapter, the fraction of N2 is small, approximately 7% for the substrate pre-treated in presence of 2-MBT and less than 3% for the substrates pre-treated in the absence of 2-MBT, indicating that the bonding between the metallic substrate and nitrogen atoms of the molecule is limited and is not the major bonding mechanism between the metal and the 2-MBT molecule.

The S 2p spectra were decomposed using $2p_{3/2}$ - $2p_{1/2}$ spin-orbit doublets with a branching ratio of 0.5 and splitting of 1.18 eV. The S $2p_{3/2}$ chemical states at 164.2 eV (S1) and 162.8 eV (S2) correspond to the endocyclic and exocyclic sulphur atoms from the 2-MBT molecule, respectively [83, 84, 86]. Both these components are not directly bonded to metallic Cu, rather, they result from an interaction between the molecule and the copper oxides, and/or from the formation of 2-MBT multi-layers, and/or from the formation of Cu-2-MBT complexes. The S $2p_{3/2}$ component observed at 161.9 eV (S3) was associated to sulphur bonded directly to metallic Cu [83, 84, 143]. We have seen in the previous chapters that this component can arise from 2-MBT molecules in their entirety bonding via sulphur to the metallic substrate and from free dissociated sulphur bonding to the metallic substrate. The presence of the S3 component confirms our analysis from the ToF-SIMS depth profiles that the interfacial oxides are not in a homogeneous layer, but rather distributed as islands on the surface. From the atomic ratio between the sulphur and nitrogen intensities, it was established that there is indeed an excess of sulphur (approximately 15%) for all three substrates, compared to the theoretical value of 2:1 for the S:N ratio, confirming the presence of free dissociated sulphur atoms. Lastly, a fourth sulphur component (S4) at 167.6 $\pm$ 0.3 eV was observed for all three cases with a FWHM of 2.4 $\pm$ 0.2 eV. This component is representative of sulphate and/or sulphone groups that are likely formed by an interaction of sulphur from the 2-MBT molecules with oxygen, resulting in sulphur atoms doubly bonded to two oxygen atoms each [144]. However, this component represents a very small fraction of the overall sulphur intensity, less than 5% for all three S 2p spectra, and is considered inconsequential for quantitative analysis.

We observe that the line-shapes of the S 2p spectra for the interfaces prepared by pre-treatment in absence of 2-MBT are similar for 2 minutes and 1 hour exposure to 2-MBT, with negligible changes in relative intensities between the components. However, a distinct difference is observed for the line-shape of the S 2p spectrum for the interface prepared

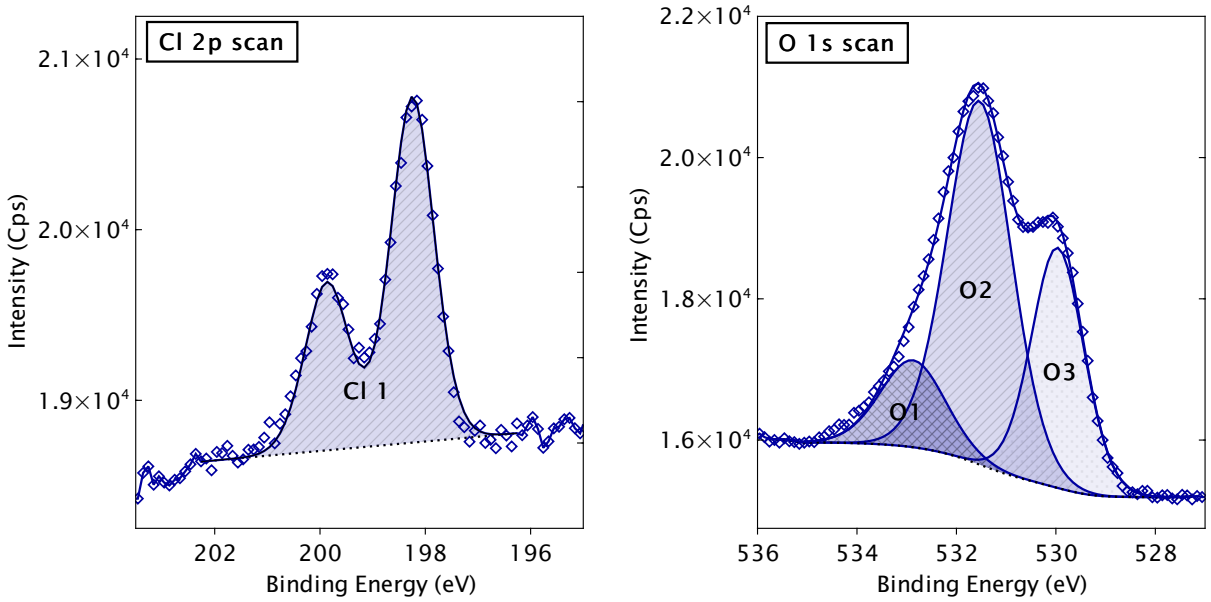

Figure 6.5: XPS Cl 2p and O 1s core level spectra for the 2-MBT/copper interface formed after cathodic pre-treatment in the absence of 2-MBT followed by 2 minutes of exposure to the 2-MBT containing 0.5 M NaCl solution. The symbols represent the experimental data and the corresponding coloured line represents the fitted curve.

by pre-treatment in presence of 2-MBT, with a marked shoulder at the position of the S3 component. This is due to the slightly increased relative intensity of the S3 component here. Further analysis of the sulphur components by determination of atomic ratios revealed that this relative increase in the S3 component originates from a slight decrease in the relative intensity of the S1 component (endocyclic sulphur). Therefore, for the substrate pre-treated in presence of 2-MBT (Figure 6.4, spectra a) the S3 originates both from the endocyclic and exocyclic sulphur, whereas for the substrates pre-treated in the absence of 2-MBT (Figure 6.4, spectra b and c), the S3 originates mainly from the exocyclic sulphur. As mentioned earlier, this is most likely due to the different bonding mechanisms and the structure of the organic film formed, possibly due to the presence and influence of the oxide remnants on the metallic substrate surface.

The Cl 2p spectra (Figure 6.5) exhibits only one component corresponding to adsorbed chloride on the surface at a BE of 198.3 eV (Cl $2p_{3/2}$), as seen previously (Chapter 4). However, due to the low signal to noise ratio for the Cl 2p spectra, we cannot completely exclude the possibility of the presence of CuCl at a BE of 199 eV. Nevertheless, the intensity of the Cl peaks is very low, indicating minimal interaction with the copper substrate, as indicated by the ToF-SIMS depth profiles presented above. Lastly, the O 1s spectra (Figure 6.5) are also consistent with that seen in the previous chapters, with three components

Table 6.1: Thickness and coverage of the interfacial copper oxide islands and the 2-MBT inhibitor layers formed on copper in 0.5 M NaCl solution depending on pre-treatment as listed. The equivalent thicknesses are tabulated by weighting the estimated thickness of each layer with its coverage. The uncertainty on the coverage is estimated to be ± 10% and the uncertainty on the thicknesses is estimated to be ± 0.2 nm.

	Conditions of interface formation	Coverage of Cu_2O islands (%)	Thickness of Cu_2O islands (nm)	Equivalent thickness of Cu_2O (nm)	Thickness of 2-MBT layer above oxides (nm)	Thickness of 2-MBT layer on metallic Cu (nm)	Equivalent thickness of 2-MBT layer (nm)
a	Pre-treatment with 2-MBT	83	0.3	0.3	0.7	1.0	0.7
b	Pre-treatment w/o 2-MBT, 2 mins exposure to 2-MBT	58	0.2	0.1	1.8	2.0	1.9
c	Pre-treatment w/o 2-MBT, 1 hr exposure to 2-MBT	46	0.9	0.4	1.7	2.6	2.2

observed, corresponding to metal oxides (Cu_2O) at a binding energy of 530 eV, hydroxides at 531.4 eV, and oxygen from water adsorbed on the surface at 532.9 eV.

To evaluate the differences in organic 2-MBT layers and interfacial oxide layers formed on the copper substrate by each pre-treatment method, the thickness and coverage of the films were estimated using the same bi-layer model as described earlier (Figure 2.16 in Chapter 2). The results are presented in Table 6.1. The uncertainty on the coverage of the oxide islands is estimated to be 10% and that on the thickness of the films to be ± 0.2 nm. The equivalent thicknesses are also estimated for the purpose of a straightforward comparison between the pre-treatment methods.

It is observed that for the pre-treatment in presence of 2-MBT, even though the thickness of the oxide islands is quite low, in the order of one monolayer of oxide, the coverage of the oxide islands on the surface is quite high. This is in agreement with the results from the ToF-SIMS depth profiles in Figure 6.2a. This indicates that although this pre-treatment does reduce most of the native oxides in terms of thickness, it is not effective enough to clear the surface of the oxides. Therefore, the bonding between the metallic substrate and sulphur from the 2-MBT molecule is limited to only 17% of the surface. Regarding the 2-MBT layer, it is only 0.7 nm in equivalent thickness. Assuming that the molecule is bonded in an upright position on the surface, this corresponds to only one monolayer of adsorbed molecules, since the height of the 2-MBT molecule is 0.8 nm [82]. However, we cannot discount the fact that the molecules may adsorb in different orientations on the surface, thus obtaining a second layer of the molecules (multi-layer film). Additionally, it is important to note that we have

considered a model which assumes homogeneity of the layers on the surface, which is not necessarily the condition of the substrate. Therefore, we could have regions of multi-layers and regions of monolayers on the substrate surface.

For the pre-treatment without 2-MBT followed by 2 minutes of exposure to 2-MBT, Table 6.1 shows that the coverage of the oxide islands is significantly less (58%), and their thickness is approximately one monolayer, demonstrating that pre-treatment in absence of 2-MBT results in a better reduction of the native oxides, as seen in acidic and alkaline media too. The lower oxide islands coverage also indicates a higher coverage of the 2-MBT molecules bonded to the metallic substrate, indicating that the adsorption of 2-MBT is favoured by direct bonding to the substrate, i.e., in the absence of oxides on the surface. In addition, the thickness of the 2-MBT layer is significantly higher in this case compared to when the pre-treatment was done in presence of 2-MBT. This suggests that the structure of the first 2-MBT adsorbed layer formed here is better suited for the adsorption of subsequent layers of the molecule even with a short exposure time. As the overall quantity of interfacial oxides is lower after pre-treatment without 2-MBT, we conclude that the formation of the metal-organic complexes on this substrate (pre-treated without 2-MBT, 2 minutes exposure to 2-MBT) is significantly less, as indicated by the depth profiles in Figure 6.2b. This implies that the Cu-2-MBT complexes are composed of Cu(I) ions which originate from the metal oxides (Cu_2O) present [80]. Cathodic reduction in the absence of 2-MBT would result in less capture of the released Cu(I) ions by the organic molecules and therefore in less complexes being formed.

When the exposure time to the 2-MBT solution with NaCl is increased to 1 hour, the coverage of the oxide islands decreases slightly, however, their thickness increases drastically (about four times compared to 2 minutes exposure with the same pre-treatment method, Table 6.1). This phenomenon is in line with the results of the Cu LMM Auger spectra in Figure 6.3c, where the increase in the Cu(I) ions was considerable after 1 hour exposure to the 2-MBT containing NaCl solution. This reveals that the oxide islands may not be well protected by the 2-MBT layer, which is likely defective in certain regions and not completely homogenous and covering as we assume it to be, thus enabling the growth of the oxide islands over time in a near neutral solution. The defects formed in the 2-MBT layer are most likely induced by the Cl^- ions present in the environment, which compete for adsorption with 2-MBT. It is important to note that we cannot rule out a slight oxidation of the surface in the defective regions of the 2-MBT barrier layer or in regions that may not be covered by the 2-MBT layer during transfer of the samples through air. Regardless, we do observe that the thickness of the 2-MBT layer has increased over time as reflected by an increase of approximately 0.3 nm of equivalent thickness compared to the shorter exposure time. However, this increase in 2-MBT layer thickness could also possibly be due to the increased

formation and subsequent deposition of the Cu-2-MBT complexes on the surface, as indicated by the depth profiles in Figure 6.2c. The increase in thickness of the oxide islands could promote the complex formation, owing to formation of Cu(I) ions which interact with the adsorbed 2-MBT molecules.

6.3 Inhibition of oxidation and corrosion initiation

Cyclic voltammetry was applied after preparation of the interface by the pre-treatment methods discussed above and in a reference 0.5 M NaCl solution in order to study the effect of 2-MBT on the inhibition of oxide growth and corrosion upon anodic polarisation. The CVs are presented in Figure 6.6, with the current density measured as the potential is swept up to the value where initiation of corrosion is observed, down to the point of hydrogen gas evolution, and back to the initial starting point. The corresponding anodic and cathodic charge densities, determined from each curve by integrating the current density over time, are presented in Table 6.2.

In the 0.5 M NaCl reference solution (black curve in Figure 6.6), oxidation of the sample (Cu(0) to Cu(I)) initiates immediately upon anodic polarisation, with a peak at -0.02 V vs SHE, followed by the initiation of corrosion at 0.05 V vs SHE, indicated by the sharp rise in current density. Additional experiments revealed that a continuous increase in current density was observed for increased anodic polarization, with the anodic current density reaching up to 25000 $\mu A/cm^2$ at 0.5 V vs SHE (from approximately 100 $\mu A/cm^2$ at 0.05 V vs SHE), thus corroding the surface severely. However, since we are investigating the initiation of corrosion and its inhibition in this work, we have limited the potential accordingly.

During the reverse scan, a single cathodic peak is observed at -0.27 V vs SHE, which corresponds to the reduction of Cu(I) to Cu(0). From Table 6.2, we observe that the difference, if any considering the error, between the anodic and cathodic charge densities for this experiment is very small, indicating that most, if not all, of the Cu(I) ions formed during the anodic branch of the cycle have been reduced during the cathodic sweep. Using Faraday's law [130], the equivalent thickness of copper metal reversibly consumed in this experiment is 0.86 ± 0.04 nm, using the anodic charge density where the molar volume of copper metal is 7.1 cm3/mol and the number of electrons exchanged per copper atom is 1. Assuming the formation of a homogeneous film of Cu(I) oxide, the equivalent thickness of grown Cu_2O is estimated to be 1.41 ± 0.06 nm, using the cathodic charge density where the molar volume of Cu_2O is 23.9 cm^3/mol and the number of electrons exchanged per Cu_2O molecule is 2, which is similar to that formed in Cl^- free alkaline solution in the potential range of Cu(I) oxidation (1.55 ± 0.01 nm from Chapter 5).

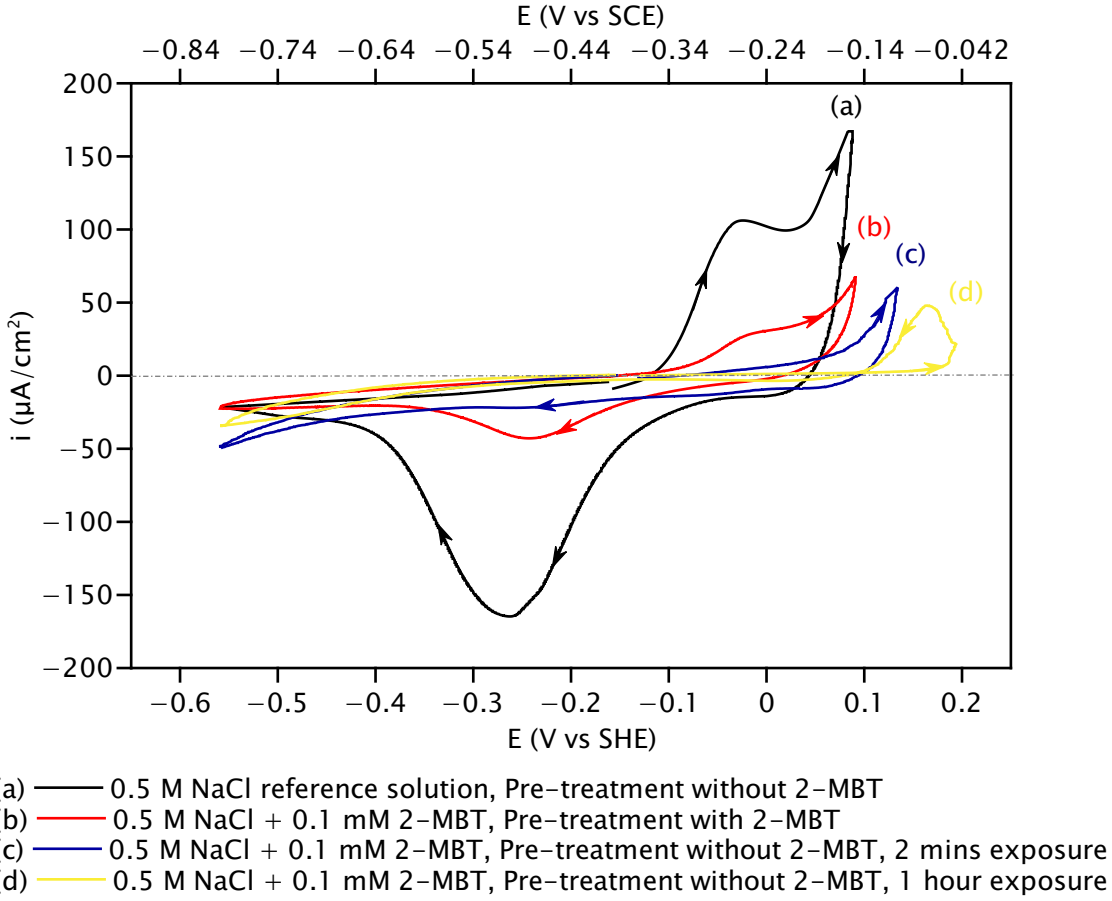

Figure 6.6: Cyclic voltammograms of copper showing anodic oxidation and subsequent initiation of corrosion in the absence or presence of 2-MBT in the 0.5 M NaCl electrolyte after cathodic pre-treatment as specified. Scan rate is 20 mV/s. Arrowheads are added to each cycle to guide the reader's eye.

When polarisation was carried out on the interface prepared by cathodic pre-treatment in presence of 2-MBT (red curve in Figure 6.6), a much lower anodic current density was observed, as evident from the significantly smaller anodic peak at -0.02 V vs SHE, resulting in an anodic charge density that is approximately 4 times less compared to that in the reference solution (Table 6.2). This suggests that the 2-MBT layer is effective in reducing the anodic oxidation of the substrate, as seen in the previous chapter in alkaline environment. However, this 2-MBT layer is likely defective in certain regions and not entirely effective in blocking the oxidation process, as indicated by the presence of the anodic peak. Assuming that the anodic and cathodic peaks relate to the formation and subsequent reduction of Cu(I) oxide, the equivalent thickness of grown Cu_2O estimated from the cathodic charge density is 0.31 ± 0.01 nm, which is significantly lower than the one obtained for the reference solution (4.5 times lower). Since we cannot confirm that the anodic charge corresponds only to Cu_2O formation

Table 6.2: Charge densities (anodic and cathodic) determined from the cyclic voltammetry tests by integrating the current densities with time.

	Electrolyte used for CV, Pre-treatment condition	Anodic charge ($\mu C/cm^2$)	Cathodic charge ($\mu C/cm^2$)
a	0.5 M NaCl ref. solution Pre-treatment without 2-MBT.	1175 ± 60	1141 ± 47
b	0.5 M NaCl + 0.1 mM 2-MBT Pre-treatment with 2-MBT.	282 ± 22	247 ± 11
c	0.5 M NaCl + 0.1 mM 2-MBT Pre-treatment without 2-MBT, 2 minutes exposure to 2-MBT.	55 ± 1	39 ± 1
d	0.5 M NaCl + 0.1 mM 2-MBT Pre-treatment without 2-MBT, 1 hour exposure to 2-MBT.	23 ± 1	14 ± 1

and the cathodic charge to its reduction at this point, it is analysed by XPS further on.

The initiation of corrosion, indicated by the sharp rise in anodic current density, occurs at 0.05 V vs SHE (red curve in Figure 6.6), like in the previous case where there was no 2-MBT. This confirms our hypothesis that the organic inhibitor layer is defective and not protective enough against corrosion initiation, despite its inhibition of the rate of oxidation. This is most likely due to the extensive coverage of native oxides on the surface (Table 6.1), which precludes a more protective direct bonding between the 2-MBT molecules and the metallic substrate. Additionally, the low thickness of the 2-MBT barrier layer could also play a role here in the attack of the copper substrate, since a thinner layer is more easily penetrated by the aggressive chloride ions.

For the CVs performed after pre-treatment in absence of 2-MBT followed by 2 minutes exposure to 2-MBT (blue curve in Figure 6.6), there is no oxidation peak observed indicating that the 2-MBT layer better protects the metallic surface from anodic oxidation. This is also attested by the fact that the anodic charge density is approximately 21 times lower than in the reference solution and 5 times lower than after pre-treatment in presence of 2-MBT (Table 6.2). Additionally, the initiation of corrosion is shifted to a more positive potential, 0.1 V vs SHE, indicating that the thicker 2-MBT layer formed in these conditions (Table 6.1)

Table 6.3: Thickness and coverage of the interfacial copper oxide islands and the 2-MBT inhibitor layers formed in 0.5 M NaCl solution after anodic polarization of the copper substrates pre-treated in (a) presence of 2-MBT, and (b) absence of 2-MBT followed by 1 hour of exposure to 2-MBT. Uncertainties on coverage and thickness are estimated to be ± 10% and ± 0.2 nm, respectively.

	Conditions of interface formation	Coverage of Cu_2O islands (%)	Thickness of Cu_2O islands (nm)	Equivalent thickness of Cu_2O (nm)	Thickness of 2-MBT layer above oxides (nm)	Thickness of 2-MBT layer on metallic Cu (nm)	Equivalent thickness of 2-MBT layer (nm)
a	Pre-treatment with 2-MBT	60	0.3	0.2	1.2	1.5	1.3
b	Pre-treatment w/o 2-MBT, 1 hr exposure to 2-MBT	58	0.7	0.4	1.7	2.4	2.0

does protect the surface from corrosion. In the reverse scan (cathodic sweep), no reduction peak is observed, which is consistent with the absence of an oxidation peak during the anodic branch of the cycle.

After longer exposure time (1 hour) to 2-MBT following pre-treatment in the absence of the inhibitor (yellow curve in Figure 6.6), there is a further decrease in anodic charge density by a factor of 2.4 compared to 2 minutes exposure (Table 6.2). This suggests that the increased coverage of metallic copper by 2-MBT and increase in overall 2-MBT layer thickness (Table 6.1) is more effective in hindering the oxidation reactions occurring during polarisation. We also observe a further shift in the initiation of corrosion potential to 0.17 V vs SHE. This shift demonstrates that longer exposure times to the inhibitor does aid in the formation of a better and more effective barrier layer against corrosion.

In order to evaluate the effects of anodic polarisation on the 2-MBT organic layers and interfacial oxide layers initially formed on the copper substrates pre-treated with 2-MBT or without 2-MBT followed by 1 hour exposure to 2-MBT, XPS analysis was carried out after polarisation up to the potential of 0.09V vs SHE (i.e., before initiation of corrosion). Since the differences in the elemental core level spectra, before and after polarisation, were not apparent in terms of line-shape and relative intensities, we discuss hereafter the thickness and coverage of the oxide islands and 2-MBT layers estimated using the bi-layer model used earlier (Table 6.3). These values are compared to the thickness and coverage values obtained after the various cathodic pre-treatment methods in reduced state, given in Table 6.1.

For the pre-treatment in presence of 2-MBT, the coverage of the oxide islands has reduced significantly, from 83 to 60%, when compared to before anodic polarisation (Table 6.1). However, the thickness of these oxide islands (0.3 nm) remains the same considering the

uncertainty. A possible explanation is that the coverage of the oxide islands reported in Table 6.1 from analysis prior to polarisation was overestimated, possibly due to oxidation of the sample in regions not covered by the defective 2-MBT layer during transfer of the samples through air. Upon anodic polarisation, the Cu atoms in these uncovered metallic substrate regions would oxidize and bond with 2-MBT molecules, which is why a lower coverage of the oxide islands is observed here. Since the equivalent thickness of the interfacial oxide has not increased upon polarisation, it is implied that the anodic peak observed for the CV performed after pre-treatment in presence of 2-MBT (blue curve in Figure 6.6) does not in-fact relate to the formation of Cu(I) oxide, since the growth of the oxide film was estimated to be a thickness of 0.31 ± 0.01 nm from the cyclic voltammetry tests. Therefore, the formation of the Cu(I) ions observed from the anodic peak would correspond to the formation of Cu(I)-2-MBT metal organic complexes, as seen in previous chapter in alkaline environment. This could also be the other possibility for the reduced coverage of oxide islands, where the most reactive Cu(I) ions from the oxide islands would preferably bind to 2-MBT molecules by a conversion reaction to form metal organic complexes induced by anodic polarization. The formation of metal organic complexes is also reflected by a significant increase in equivalent thickness of the 2-MBT layer after polarisation, from 0.7 to 1.3 nm as observed in Table 6.3. Regardless of their formation mechanism, it is important to note that the Cu-2-MBT complexes formed do not block the initiation of corrosion, as indicated by the similar potentials of corrosion initiation observed for the CV performed in the reference NaCl solution and for the substrate pre-treated in presence of 2-MBT (Figure 6.6).

In the case of pre-treatment without 2-MBT followed by 1 hour exposure to the inhibitor, the coverage of the oxide islands has increased (from 46 to 58%) compared to before polarisation and their thickness slightly decreased (from 0.9 to 0.7 nm), which results in an equivalent thickness that is unchanged (0.4 nm, Table 6.3). A first possibility to explain this phenomenon is that the reduction in oxide island thickness would be due to the chloride ions promoting the local thinning of the oxide islands, a mechanism proposed for the breakdown of passive oxide layers [5, 39]. In this case, the coverage increase of the oxide islands could be due to the oxidation of the substrate during transfer of the sample through air in the new regions exposed by the chloride-induced dissolution of the oxide islands. Another more likely explanation is that since the equivalent thickness remains the same before and after polarisation, the changes observed for the coverage and thickness of the oxide islands merely result from the uncertainty of the estimated values and the other limitations of the model, such as the assumption of homogeneity for the thickness and coverage of the layers. This is supported by the fact that during the anodic branch of the cyclic voltammetry test, negligible anodic current density is measured indicating little to no oxidation occurring on the substrate surface.

This is due to the better protection provided by the initially thicker deposited 2-MBT layer here than on the interface pre-treated in the presence of the inhibitor.

As for the 2-MBT layer, a decreasing trend in equivalent thickness (from 2.2 to 2.0 nm (Table 6.3)) is suggested after polarisation. Although the local thinning process is hypothesised for oxide films on metal surfaces [39], we assume that chloride ions would have a similar effect on the 2-MBT organic layer in order to initiate corrosion on the substrate (Figure 6.6, curve d), thus reducing the thickness of the 2-MBT layer. However, this cannot be ascertained with our analysis methods and remains a hypothesis.

6.4 Influence of environment on the adsorption of 2-MBT

In the previous chapters, the bonding mechanisms between the 2-MBT molecule and the copper substrate were shown to be influenced by the pH which dictates the dominant conformer of the 2-MBT molecule. Additionally, the presence and quantities of other species, such as surface oxides and chlorides, were also shown to play an important role in the bonding mechanisms and the protective properties of the organic barrier layer. Based on the adsorption mechanism of 2-MBT on copper in an acidic chloride environment and in an alkaline environment (chloride-free), we can evaluate how each individual parameter affects and changes 2-MBT adsorption on copper surfaces in a near neutral chloride environment.

The various conformers of the 2-MBT molecule - thione, thiol, and thiolate forms - are shown in Figure 6.7. It has been found that the thione form of the molecule is more stable over the thiol form in both solid and vapour phase [77]. In liquid environments, the dominant conformer depends on both the type of solvent and the pH of the environment. In acidic environments, the thione form is the dominant conformer of the molecule, whereas the thiolate form (ionized thiol conformer) is the dominant one in alkaline environments [78, 80]. In environments where the pH is between 4 and 9, the thione and thiolate forms both co-exist [80]. Therefore, the mechanisms of bonding between the 2-MBT molecules and the copper substrate can vary based on the pH of the environment.

In an acidic chloride environment of pH between 2 to 2.5 (2-MBT thione form, Figure 6.7a), the 2-MBT molecules bond to the metallic substrate only by the sulphur atoms, as seen in Chapter 4. The molecules also most likely interact with the residual native oxide-covered surface by the sulphur atoms, as suggested by ToF-SIMS depth profiling. The thickness of the residual islands of native oxide was relatively low (0.2 - 0.4 nm), even when the surfaces were pre-treated in presence of 2-MBT, mostly due to the instability of the oxide layer at pH

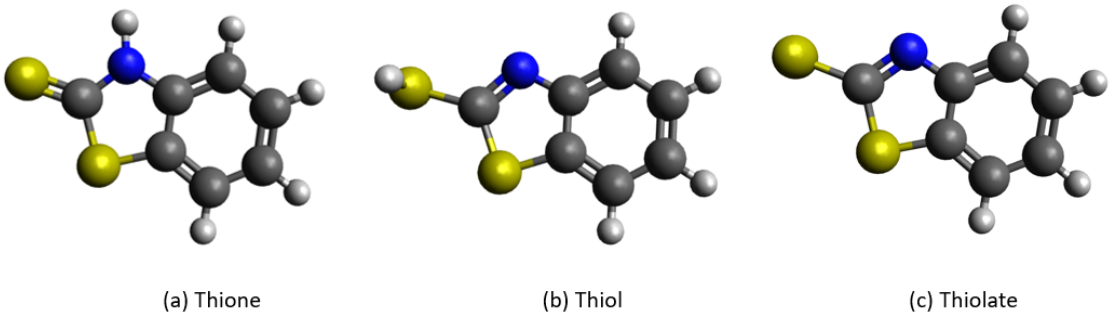

Figure 6.7: Models illustrating the various conformers of the 2-MBT molecule ($C_7H_5NS_2$) (a) thione form, (b) thiol form, and (c) thiolate form. The yellow atoms represent the sulphur, the blue atoms represent the nitrogen, the grey atoms represent the carbon, and the white atoms represent the hydrogen atoms in the molecule.

levels lower than 5. This relatively low amount of interfacial oxide enhanced the adsorption of the 2-MBT molecules on the surface, eventually leading to thicker organic layers ranging from 1 to 2.2 nm in equivalent thickness of 2-MBT for surfaces pre-treated with and without 2-MBT, respectively. Although the chloride ions are expected to strongly interact with the surface, this was not observed in the acidic environment. The first reason for this lack of chloride effect in the strongly acidic environment is that since most of the effects observed relate to the low pH of the electrolyte and the dominant thione conformer of the inhibitor, the effect of the chloride ions is relatively weaker and therefore masked by the strong pH effect. The second reason is that the bonding between the thione conformer of the 2-MBT molecules and the metallic substrate is rather strong and the 2-MBT layer densely covers the entire surface, including the residual oxidized regions as confirmed by DFT modelling [91, 92], thus hindering the penetration of the chloride ions.

On the other hand, in an alkaline environment of pH between 13 to 14, the thiolate form of the 2-MBT molecule (Figure 6.7c) is dominant [78, 80]. Here, bonding between the nitrogen atoms of the inhibitor molecules and the metallic copper substrate was observed in addition to bonding via the sulphur atoms (Chapter 5), like in the present work. Although the fraction of nitrogen bonding, in both alkaline and neutral chloride conditions, is rather low compared to that of sulphur bonding, it was a feature that was not observed in acidic environment. Additionally, the formation of Cu-2-MBT metal-organic complexes was observed from the ToF-SIMS depth profiles in the alkaline environment, especially when the surfaces were pre-treated with 2-MBT in the NaOH solution, also similar to the present conditions. This too was not seen in experiments performed in acidic media. It was proposed that the Cu(I) ions, released during the cathodic reduction (pre-treatment) process of the native oxide-covered

surface or subsequently formed upon anodic polarisation, interact with the 2-MBT molecules to form these complexes which deposited on the surface of the organic layer (Chapter 5).This was supported by the much thicker 2-MBT layer (2.7 - 3 nm) formed on surfaces pre-treated with 2-MBT, where the remaining interfacial oxide was relatively thicker (0.5 - 0.6 nm). Meanwhile, the surfaces pre-treated in absence of 2-MBT, where the interfacial oxide was comparatively thinner (0.2 nm), only formed 1.2 - 1.5 nm thick 2-MBT layers.

Despite the thickness variations, the 2-MBT layer in the alkaline environment covered the entire surface with minimal defects, similar to that observed in the acidic environment, resulting in no thickness increase of the oxide islands on longer exposure time to the inhibitor-containing alkaline solution. Since the experiments in alkaline media were conducted in the absence of corrosive chloride ions, we do not know what effect the chloride ions would have on surfaces where the oxide film is stable and what role would the metal-organic complexes play on corrosion protection.

The mechanisms of 2-MBT adsorption in neutral chloride solution exhibit middling characteristics from that observed in acidic chloride and alkaline media. This is in part due to the presence of both thione and thiolate forms of the 2-MBT molecules in environments where the pH is between 4 and 9 [80]. Given that the pH of the environment of the present work was towards the lower side, between 5.2 to 5.5, the estimated thicknesses of the 2-MBT layers formed by each pre-treatment method are similar to those observed in the acidic environment conditions, as the thione form would be more prevalent. Since the thiolate form is also present in this pH environment, like in the alkaline environment, the bonding of the molecules to metallic copper by nitrogen atoms is rather compelling. The other factor, which seems to be the more consequential one, is the behaviour of copper in the different environments and its interaction with chloride ions. Due to the possible oxidation of copper at this pH, we did observe oxidation of the surface regions uncovered by defective 2-MBT layer, especially during increased exposure time to the solution. The defects are most likely caused by the penetrating effect of chlorides in the organic barrier layer. The resulting oxidation of the surface leads to the growth of oxide islands which then enhances the formation of the metal-organic complexes, thus inducing an increase of the surface roughness revealed by ToF-SIMS depth profiling. Therefore, despite the similarities in bonding mechanisms of the 2-MBT molecules realized between the Cl-free alkaline and Cl-containing near neutral (NaCl) environments, there are features that are specific to the NaCl environment only and that we hope to have clarified in the present work.

6.5 Conclusion

The inhibition of corrosion initiation of copper by 2-MBT was investigated in a near neutral NaCl solution after the adsorption of the organic inhibitor. It is shown that 2-MBT adsorbs on the copper surface regardless of the surface state, altered using cathodic reduction pre-treatment methods of the native oxide layer. The 2-MBT molecules bond to the metallic substrate mostly by their sulphur atoms along with a very small fraction of nitrogen bonding with the metallic substrate. The interactions between the molecule and interfacial copper oxide occur most likely through the sulphur atoms of the molecule. However, the structure of the 2-MBT film and its protective properties highly depends on the surface state (interface) obtained after the pre-treatment methods used.

When the native oxide-covered surface is pre-treated with 2-MBT in the solution, a large coverage of the interfacial oxide still persists. The 2-MBT layer is relatively thin with Cu-2-MBT metal-organic complexes deposited on top, formed by an interaction between the Cu(I) ions (from Cu_2O) and the 2-MBT molecules. When pre-treated without 2-MBT in the solution, a wider coverage of the molecule adsorption is observed along with the formation of a thicker 2-MBT layer, even after just 2 minutes of exposure to 2-MBT, owing to lower amounts of interfacial oxide subsisting at the interface. A longer exposure time (1 hour) to 2-MBT after pre-treatment in its absence increases the thickness of the organic layer, but also results in a thickness increase of the interfacial oxide islands due to oxidation of the substrate at the defective regions of the 2-MBT layer. The formation of complexes is dependent on the quantity of interfacial oxides present, with a higher quantity of interfacial oxide resulting in an increased formation of the Cu-2-MBT metal-organic complexes.

Upon anodic polarization, the substrate pre-treated with 2-MBT shows reduced anodic activity compared to the substrate polarized in the reference NaCl solution. Surface analysis revealed an increase in the 2-MBT layer thickness after polarization and right before the initiation of corrosion, which is most likely due to the formation of further Cu-2-MBT complexes owing to the release of Cu(I) ions upon polarization. Despite this, no additional protection was offered to the substrate by the complexes. Pre-treatment in absence of 2-MBT followed by 2 minutes exposure to the inhibitor results in no anodic oxidation peak and a positive shift of the potential for corrosion initiation, indicative of better protective properties of the organic barrier layer formed. Longer exposure time to 2-MBT results in a higher positive shift of the potential for corrosion initiation. This further enhanced barrier properties of the inhibited interface results from both the higher coverage of the 2-MBT molecule on the surface and the thicker 2-MBT organic layer.

It is shown that the 2-MBT adsorption mechanisms on copper in a near neutral chloride

environment is between that of the acidic and alkaline environment. This is mainly due to the dominant conformer of the molecule which depends on the pH of the environment, and the presence of chloride ions which compete with 2-MBT to adsorb on the surface. These factors are established as the defining conditions for the adsorption of 2-MBT on copper and subsequently the protection against corrosion in the neutral chloride environment.

CHAPTER 7

Interfacial bonding and corrosion inhibition of 2-mercaptobenzimidazole organic films formed on copper surfaces under electrochemical control in acidic chloride solution

This chapter is based on the work published in Electrochimica Acta by V. Garg, S. Zanna, A. Seyeux, F. Wiame, V. Maurice, and P. Marcus entitled "Interfacial bonding and corrosion inhibition of 2-mercaptobenzimidazole organic films formed on copper surfaces under electrochemical control in acidic chloride solution." [158]

In this chapter, 2-MBI organic inhibitor was adsorbed on electrochemically controlled copper surfaces in an acidic chloride media (10 mM HCl solution). The conditions of formation of the 2-MBI organic film and the resulting bonding mechanisms between the inhibitor and copper were investigated using an approach which interlinked electrochemical methods (Cyclic Voltammetry) and surface analyses (X-ray photoelectron spectroscopy and time-of-flight secondary ion mass spectrometry). Furthermore, the corrosion inhibition offered to the substrate by the different organic layers formed on each surface, and the effect of anodic polarization on the stability of the 2-MBI organic layers were also evaluated.

7.1 Experimental

The samples used for experimental analysis were prepared as described earlier in Chapter 2. The electrochemical experiments were performed using Kel-F cells. The Pt pseudo-reference was calibrated before each experiment (+0.75 V vs SHE). The electrolytes were a 10 mM HCl aqueous acid solution of pH 2.4 as the reference solution without the inhibitor and a 10 mM HCl + 1 mM 2-MBI aqueous solution of pH 2.6 as the solution with inhibitor.

Reduction of the native oxides of copper were carried out by cathodic pre-treatment of the substrate surfaces. After immersion at the open circuit potential (OCP), the potential was swept cathodically to the onset of hydrogen evolution (down to -0.05 V vs SHE) and then swept back up to the value of +0.10 V vs SHE with a scan rate of 20 mV/s. This was repeated two times. The anodic dissolution tests were performed by sweeping the potential until the anodic apex of +0.37 V vs SHE or higher, followed by reverse sweeping to -0.05 V vs SHE, and then back to the start point at +0.10 V vs SHE with a scan rate of 20 mV/s. To ensure reproducibility, the electrochemical experiments were repeated three times.

Surface analysis was performed after cathodic pre-treatment, i.e., in the as-obtained cathodically reduced metallic state of the interface (reduced state), and after sweeping the potential to the anodic apex, i.e., in the anodically polarized state (anodic state). Once the electrochemical tests were performed and the desired state of the surface was achieved, the cell was disconnected and the samples were rinsed with ultra-pure water, dried using nitrogen, and immediately transferred to the UHV chambers for analysis with XPS and ToF-SIMS. The details of XPS and ToF-SIMS measurements have been described in the experimental chapter.

7.2 Reduction of native oxides by cathodic pre-treatment of the interface

The cathodic pre-treatment curves obtained for the reduction of the air formed native oxides in the absence and presence of 2-MBI in the HCl solution are shown in Figure 7.1. The cathodic charge density of the three cycles determined by integrating the cathodic current density with respect to time are presented in Table 7.1.

For the first cycle of cathodic pre-treatment in absence of 2-MBI (Figure 7.1a), the open circuit potential (OCP) measured at immersion was 0.21 V vs SHE. The reduction peak occurs at a potential of 0.18 V vs SHE with a significantly large cathodic charge density measured (1698 $\pm$ 38 $\mu C/cm^2$ from Table 7.1). The equivalent thickness of oxide reduced

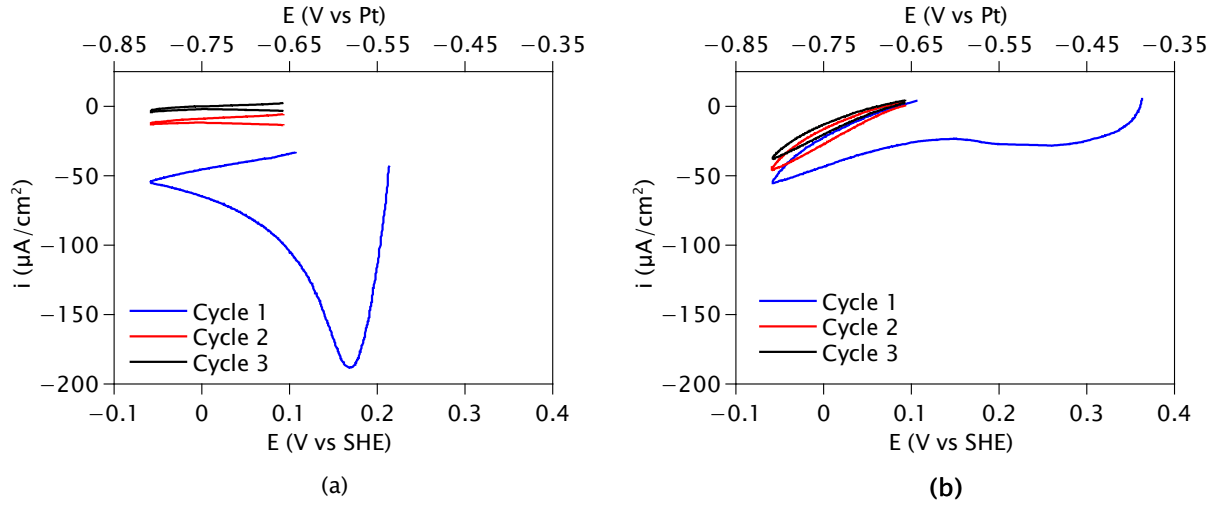

Figure 7.1: Cathodic pre-treatment CVs of copper obtained in (a) 10 mM HCl reference solution, and (b) 10 mM HCl solution with 1 mM 2-MBI (scan rate of 20 mV/s).

during this cycle, estimated using Faraday's Law [130], was 2.10 ± 0.01 nm, where the molar volume of Cu_2O was taken as 23.9 cm^3/mol and the number of electrons exchanged per Cu_2O molecule was 2. Additionally, in this case, the dissolution of oxides also occurs at OCP, prior to the first cycle of pre-treatment, due to the low pH of the electrolyte. However, the quantity of oxides dissolved by this cannot be quantified.

The first cycle of pre-treatment in presence of 2-MBI (Figure 7.1b) exhibits a stark difference with the previous case. The OCP measured at immersion was 0.34 V vs SHE, significantly higher than in absence of 2-MBI (increase of +0.13 V). This indicates that 2-MBI adsorbs on the surface immediately on immersion in the 2-MBI containing solution, even before the start of the cathodic pre-treatment cycles. We also observe the absence of a prominent reduction peak, and the measured charge density is lower by a factor of approximately 2.3 times (Table 7.1). This is most likely due to 2-MBI adsorbed on the substrate surface, either in the form of an organic layer or in the form of metal-organic complexes due to a conversion reaction, which prevents the reduction of native oxides. Since there is no reduction peak, we did not estimate the thickness of oxides reduced, if any oxides were reduced at all. We also cannot confirm the dissolution of oxides due to the low pH of the electrolyte here since the inhibitor is likely to restrict the access of the oxide layer from the electrolyte.

The next two cycles of pre-treatment in the absence of 2-MBI (Figure 7.1a) shows progressively lower cathodic charge densities measured (Table 7.1), indicating (nearly) complete reduction of the oxides on this substrate. The curves obtained for the second and third cycles of pre-treatment in the presence of 2-MBI (Figure 7.1b) also show very little charge densities

Table 7.1: Cathodic charge densities in $\mu C/cm^2$ determined from the three cycles of cathodic pre-treatment of copper in 10 mM HCl solution (without inhibitor), and in 1 mM 2-MBI + 10 mM HCl solution (with inhibitor), by integrating the current density measured with time.

Cycle	Cathodic charge densities ($\mu C/cm^2$)	
	Pre-treatment without 2-MBI	Pre-treatment with 2-MBI
1	1698 ± 38	751 ± 15
2	165 ± 9	284 ± 14
3	32 ± 5	211 ± 1

measured, although slightly higher than that of pre-treatment in absence of 2-MBI. However, no reduction peak was observed, similar to the first cycle, confirming that the reduction of native oxides is blocked, possibly due to an interaction between the organic molecules and the copper oxides present, as suggested by others [79, 112].

7.3 Surface analysis after adsorption of 2-MBI

To evaluate the surface state after cathodic pre-treatment, surface analysis was carried out on copper samples pre-treated in absence of 2-MBI followed by 1 hour exposure to 2-MBI, hereafter labelled (a), and on samples pre-treated in presence of 2-MBI, hereafter labelled (b). In the former pre-treatment method (without inhibitor), the inhibitor containing solution was introduced after the pre-treatment cycles as specified earlier in the experimental section.

The elemental ToF-SIMS depth profiles are presented in Figure 7.2, with the intensity in counts, plotted in logarithmic scale to enhance the low intensity signals, vs. sputtering time in seconds. The selected ions are Cu^-, CuO^-, O^-, and $^{37}Cl^-$, characteristic of the copper substrate, copper oxide, overall oxygen, and overall chlorine, respectively. The $C_7H_4N_2S^-$ ions were selected as characteristic of the 2-MBI molecule, and the $CuC_6H_4NS^-$, CuS^-, and CuN_2^- ions as representative of Cu interaction with the 2-MBI molecule in its entirety and its respective fragments. The difference in the number of carbon atoms between the ions selected as representative of the 2-MBI molecule and representative of Cu interaction with 2-MBI is due to the different ionization yields of the molecule resulting in varying signatures obtained for each species. The limits of each layer were defined by the maximum intensity of the corresponding ions with an uncertainty of 5%.

It is observed that for the sample pre-treated in absence of 2-MBI followed by 1 hour exposure

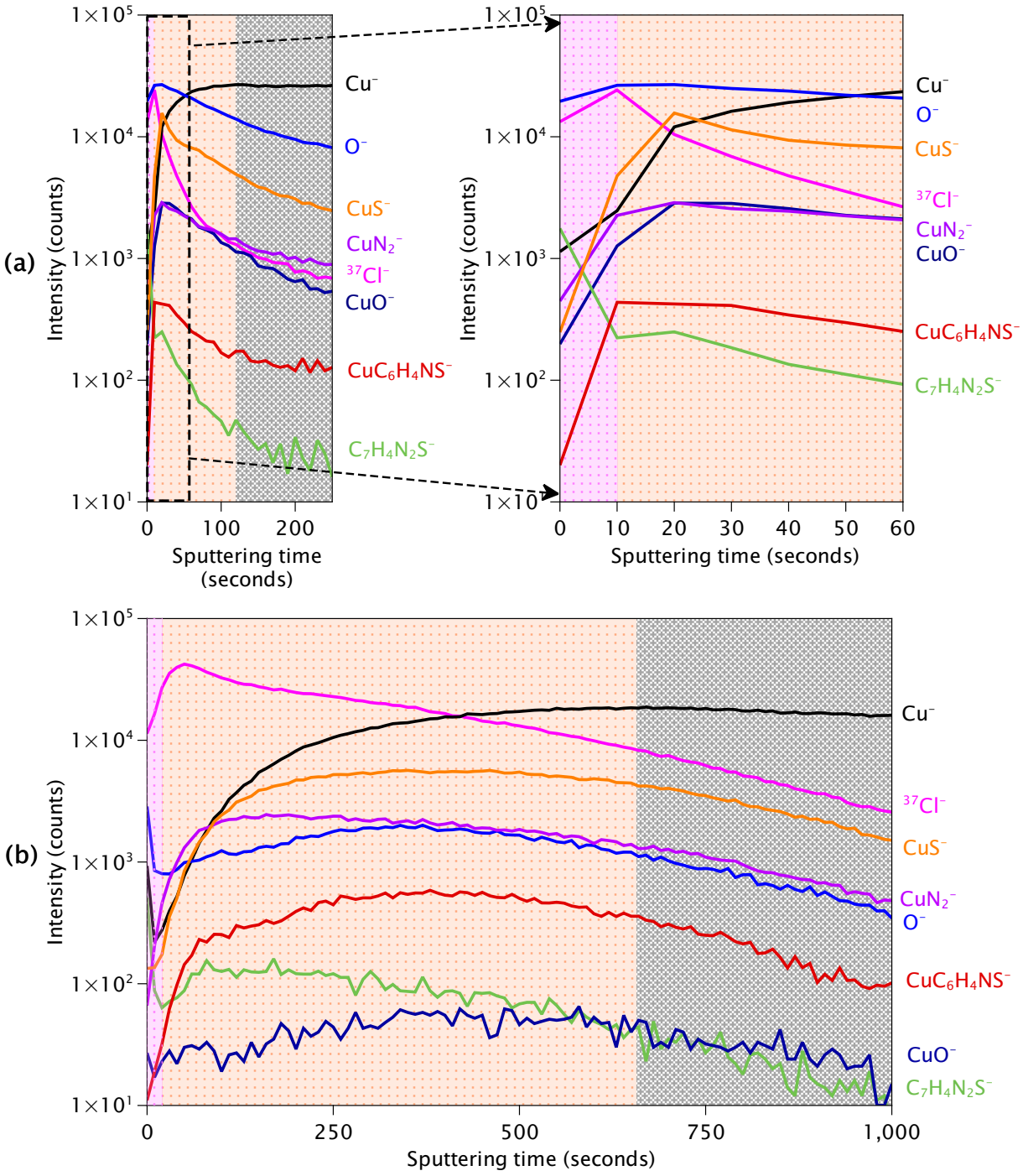

Figure 7.2: ToF-SIMS depth profiles obtained for 2-MBI films formed on copper surfaces at the reduced state in 10 mM HCl solution after cathodic pre-treatment (a) in the absence of 2-MBI followed by 1 hour exposure to 2-MBI, and (b) in the presence of 2-MBI.

to 2-MBI, Figure 7.2a, the maximum intensity of the Cu^- ion profile, which indicates the metal-oxide interface, corresponds to 120 seconds of sputtering. We also observe that the maximum intensity of the CuO^- ion profile is at 20 seconds of sputtering, indicating that the oxide interface is of approximately 100 seconds of sputtering time. Similarly, both the CuS^- ion profile and the CuN_2^- ion profile peak at 20 seconds of sputtering, indicating that the interaction between copper and the molecule occurs with both the nitrogen and sulphur atoms. This is in contrast to that observed for 2-MBT adsorption on copper in an acidic chloride environment (Chapter 4), where the sulphur was found at a greater sputtering time than the nitrogen of the molecule.

In the present case, the copper oxide profile peaks at the same sputtering time as the copper-sulphur and copper-nitrogen interaction and follows a similar decreasing profile until 120 seconds of sputtering. This indicates that the oxides subsist at the interface as islands along with the Cu-S and Cu-N interactions, as seen previously for 2-MBT adsorption on copper surfaces. This feature is corroborated with the peak of the O^- ion profile, also occurring at 20 seconds of sputtering.

The ion profile of $C_7H_4N_2S^-$, corresponding to the 2-MBI molecule, exhibits a sharp decrease in intensity from the initial top-most surface to 10 seconds of sputtering, followed by a slower decrease thereafter. This suggests multi-layers of the 2-MBI film physisorbed on the surface, also observed previously with 2-MBT organic inhibitor. The $CuC_6H_4NS^-$ ion profile, representative of Cu bonding with 2-MBI molecule, exhibits an increase in intensity up to 10 seconds, followed by a plateau until 30 seconds of sputtering. The initial low intensity is consistent with the absence of Cu-2-MBI bonding near the top-most surface. The following increase and the subsequent plateau are indicative of an inner chemisorbed layer, in which the 2-MBI molecules bond to the copper substrate. After 30 seconds there is a gradual decrease in intensity up to 120 seconds of sputtering, where the Cu substrate is reached.

The $^{37}Cl^-$ ion profile peaks near the surface and decreases sharply immediately after the peak. This suggests that the chloride ions are mostly present in the outer organic layer and their interaction is rather limited with the metal substrate due to the inner organic layer acting as a barrier between the substrate and the chloride ions, thus indicating effectiveness of the 2-MBI barrier layer formed by this pre-treatment method.

In Figure 7.2b, pre-treatment in presence of 2-MBI, it is observed that the metal oxide interface is at 657 seconds of sputtering time (maximum intensity of the Cu^- ion profile). The time taken to reach the interface for this sample is a drastic increase as compared to that for the pre-treatment shown in Figure 7.2a. This increase in sputtering time is indicative of the formation of much thicker organic layers on the sample. We also observe an increased

roughness of the inhibited interface, attested by the progressive increase of the Cu^- signal. The CuN_2^- ion profile peaks at 180 seconds of sputtering, while the CuS^- ion profile peaks at 360 seconds, suggesting mostly sulphur interaction with the substrate, unlike the previous case (Figure 7.2a) where both ion profiles peaked at the same sputtering time.

Next, the CuO^- ion profile does not exhibit a definite peak, rather a slightly curved profile centered around 400 seconds of sputtering. This is in contrast with the pre-treatment in absence of 2-MBI (Figure 7.2a), where a well-defined peak was observed for the CuO^- ion profile. Additionally, in this case (Figure 7.2b), the intensity of the CuO^- ion profile is extremely low throughout the 1000 seconds of sputtering. On the other hand, the O^- ion profile exhibits an intensity decrease for the first 10 seconds of sputtering, followed by a similar curve centered around 360 seconds. This suggests that, in this case, there are much smaller traces of copper oxides remaining at the interface that in the previous case (Figure 7.2a). The $C_7H_4N_2S^-$ ion profile (Figure 7.2b) exhibits a decrease in intensity for the first 20 seconds of sputtering, similar to the previous case (Figure 7.2a), suggesting the presence of an outer layer of the organic film. However, a similar decreasing trend is observed in this case for the Cu^- and O^- ion profiles for the first 20 seconds of sputtering. This could be possibly due to complexes formed by an interaction with copper oxides and the 2-MBI molecule, which would be deposited on the surface, as proposed by others [79, 112]. This phenomenon of the initial decrease in the intensity of the depth profiles corresponding to the molecule and copper has also been observed previously for 2-MBT adsorption on copper in neutral and alkaline media (Chapters 5 and 6) signifying the presence of complexes.

The $CuC_6H_4NS^-$ ion profile (Figure 7.2b) exhibits a sharp increase in intensity up to 60 seconds, followed by a slower and gradual increase in intensity up until 400 seconds of sputtering, confirming the presence of a thicker barrier layer on this sample. The ion profile shape is also in agreement with the interaction between copper and the molecule fragments seen with the CuN_2^- and CuS^- ion profiles. This would likely correspond to the Cu-2-MBI conversion layer formed by a reaction between the oxides and 2-MBI during cathodic pre-treatment. After 400 seconds, a gradual decrease in intensity is observed for the $CuC_6H_4NS^-$ ion profile till the Cu substrate is reached, similar to the sample pre-treated in absence of 2-MBI (Figure 7.2a) in terms of profile shape.

The $^{37}Cl^-$ ion profile exhibits its maximum intensity near the surface, like in the previous case. Here, the decrease is not as sharp as seen earlier for the sample pre-treated in absence of 2-MBI (Figure 7.2a). This could be due to two factors: the first is an increase in surface roughness, as attested by the other ion profiles in Figure 7.2b, the second is that the chloride ions interact with the inner layers too thus maintaining a higher intensity for the $^{37}Cl^-$ ion profile even until 400 seconds of sputtering time. This is investigated further by XPS analysis

of the surfaces.

The XPS core level spectra recorded for the two cathodically pre-treated copper surfaces, normalized to the background at the lower binding energy side, are shown in Figure 7.3. The intensities for the S 2p and Cl 2p spectra of curve (a), and the O 1s spectra of curve (b) are multiplied by a factor of 3 for better perceptibility of the decomposition of the peaks and the components observed.

The Cu 2p spectra exhibit spin-orbit doublets of $2p_{3/2}$ and $2p_{1/2}$ at the binding energies of 932.9 and 952.6 eV, respectively. Since the binding energies of the Cu metal, Cu_2O oxide, and CuS, are very close to each other, as discussed in Chapter 3 (Table 3.1), their contributions overlap and therefore we cannot decompose this peak. Nevertheless, the Cu $2p_{3/2}$ peak for curve (b), corresponding to the sample pre-treated in presence of 2-MBI, exhibits broadening with full width at half maximum (FWHM) of 1.4 eV, compared to 1.0 eV for the sample pre-treated in absence of 2-MBI (curve (a)). This broadening is most likely due to a change in the chemical state of copper that cannot be distinguished by the Cu 2p spectrum alone. We also observe a reduced intensity for curve (b), confirming that the surface layers are much thicker for this substrate, as indicated by the ToF-SIMS depth profiles in Figure 7.2, causing larger attenuation of the Cu signal from the substrate.

The C 1s spectrum for the sample pre-treated in presence of 2-MBI (curve (b)), was decomposed into three components - C1 at 286.8 eV corresponding to C=S bond, C2 at 285.6 eV corresponding to C-N bonds, and C3 at 284.6 eV corresponding to the C-C and C-H bonds, like in previous work on 2-MBI adsorption from the vapour on metallic copper under UHV conditions [99, 100]. A closer look at the intensities of these 3 components revealed that the ratio between the 3 peaks is approximately 1:2:4, indicative of the 7 carbon atoms of the 2-MBI molecule and their respective chemical states [99]. This phenomenon is similar to that observed for 2-MBT deposition on copper surfaces in varying conditions, as observed in the previous chapters and in other works [83, 84, 86].

For the sample pre-treated in absence of 2-MBI (curve (a)), we used the same fitting parameters for decomposition of the C 1s spectrum by maintaining the ratio between the components and the difference between the binding energies between each component. We observe that the binding energies of all the components are lower here by 0.7 ± 0.1 eV, with the C1 at 286 eV, C2 at 284.7 eV, and C3 at 284 eV. The lower binding energies obtained here have also been reported in previous work on adsorption of 2-MBI on pre-oxidized copper surfaces in vapour phase [99, 100]. Since the shift is observed for all the components while keeping the relative position of the components between each other within the uncertainty range of ± 0.1 eV, it is understood that this phenomenon is not due to a change of the

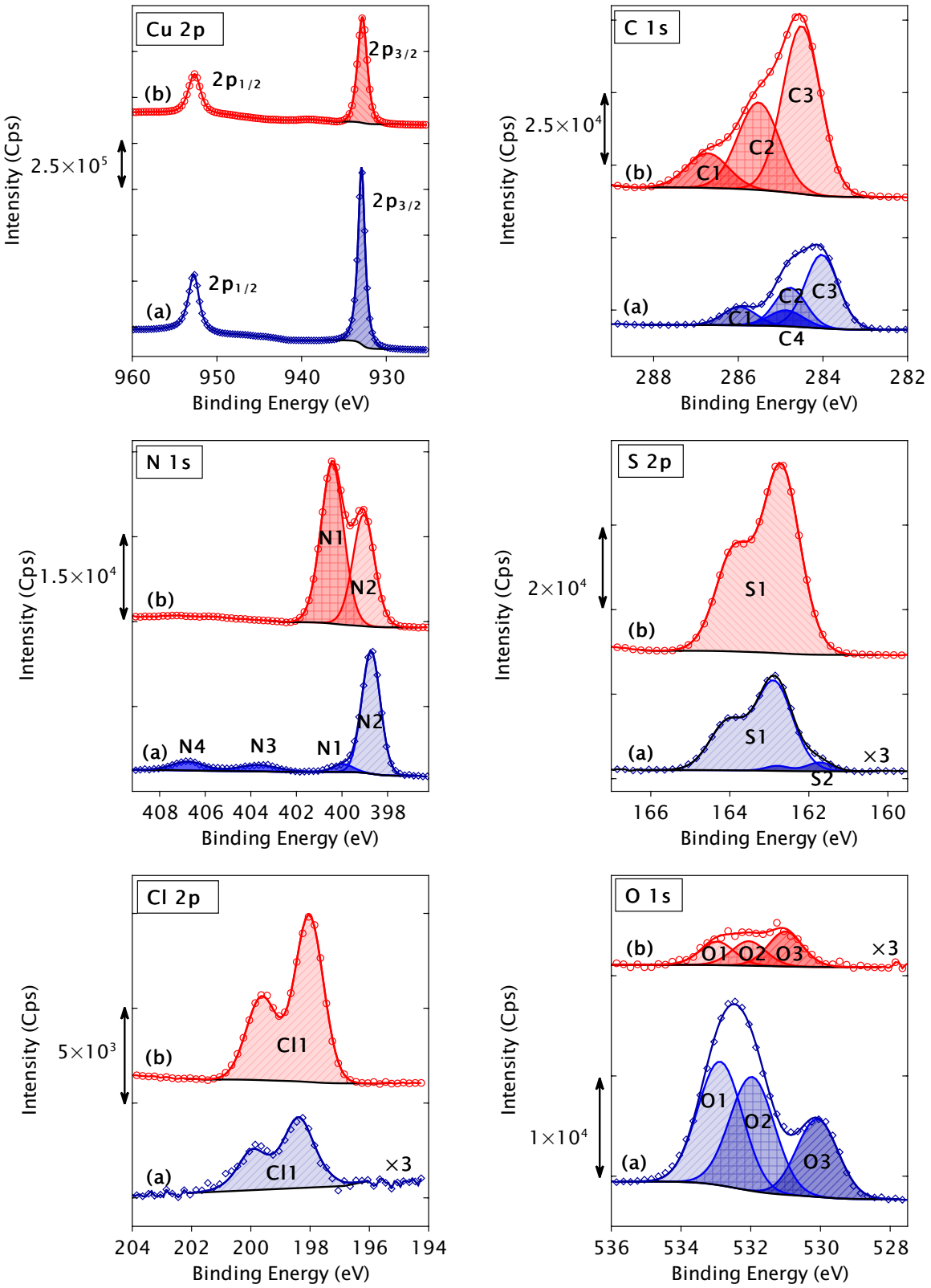

Figure 7.3: XPS Cu 2p, C 1s, N 1s, S 2p, Cl 2p, and O 1s core level spectra for 2-MBI films formed on copper surfaces at the reduced state in 10 mM HCl solution after cathodic pre-treatment (a) in the absence of 2-MBI followed by 1 hour exposure to 2-MBI (blue curves), and (b) in the presence of 2-MBI (red curves). The symbols represent the experimental data and the corresponding coloured lines represent the fit. Intensities are normalised to the background at the lower binding energy side.

chemical states. Rather, this shift is most likely due to a change in the Fermi level of the elements due to bad conductivity between regions of the surface layers and the XPS analyser for this sample. This causes an uneven charge compensation for each layer (organic and oxide layers, as discussed below) that is formed on the metallic substrate, thus resulting in shifted binding energies for the components. The binding energy values obtained for the carbon components are reproducible, thus confirming that it is not due to any experimental anomaly.

Additionally, a fourth component is realised at almost the same binding energy as that of the C-N bonds, at 284.6 eV, for the sample pre-treated in absence of 2-MBI (curve (a)). This component is either contamination on the surface (during ex-situ transfer of the sample in air), presumably due to easier access of the surface due to the thinner surface layers which may be defective, or an excess of C-N bonds present on the surface possibly due to partial dissociation/fragmentation of the 2-MBI molecule. Lastly, we observe that the intensity of the C 1s spectrum obtained for the sample pre-treated with 2-MBI (curve (b)) is more than twice the intensity for the sample pre-treated in absence of 2-MBI (curve (a)). This agrees with the ToF-SIMS analysis where we observed a thicker overall organic layer on the surface of the sample pre-treated with 2-MBI (Figure 7.2b).

The N 1s spectrum for curve (a) exhibited 4 chemical states. The N1 component at 400 eV corresponds to nitrogen from 2-MBI not bonded to metallic Cu [99, 100]. The N2 component at 398.7 eV is representative of an interaction between nitrogen and metallic copper, as seen in previous work where 2-MBI was adsorbed on a clean metallic surface of copper in vapour phase [99, 100]. The intensity of the N2 component is much higher than for the N1 component, suggesting that most of the nitrogen bonds with metallic copper. The formation of thicker multi-layers is restricted here despite exposing the surface to the 2-MBI containing solution for 1 hour. The atomic ratio of N1/Cu is 0.006 while that of N2/Cu is 0.080, given in Table 7.2, demonstrating that the intensity of N1 is approximately 13 times less than that of N2. The N3 component at 403.7 eV corresponds to the presence of azides [144], while the N4 component at 406.8 eV corresponds to the formation of nitrates [144]. Although it is unclear why these species are formed here, an explanation would be that due to the partial dissociation of the 2-MBI molecule during adsorption on the surface, the free nitrogen interacts with other species available such as oxygen or other free nitrogen-carbon chains to form these species.

For the sample pre-treated with 2-MBI, curve (b), we observe only two peaks - N1 and N2. A positive shift of 0.4 $\pm$ 0.1 eV for the binding energies is observed for this sample, but the relative positions of the 2 components with each other remain the same, as observed for the carbon spectra. These binding energies for nitrogen, N1 at 400.4 eV and N2 at 399.1 eV, are similar to those obtained for 2-MBI adsorption on pre-oxidized copper (3D oxide) under

Table 7.2: Atomic ratios obtained by quantitative analysis of the XPS measurements at the reduced state using the photoelectron intensities, normalised by the photoionization cross-sections, the inelastic mean free paths, and the transmission function of the analyser.

Component	Pre-treatment without 2-MBI, 1 hour exposure to 2-MBI	Pre-treatment with 2-MBI
N1/Cu	0.006 ± 0.001	0.44 ± 0.02
N2/Cu	0.080 ± 0.003	0.30 ± 0.01
N/Cu	0.086 ± 0.003	0.74 ± 0.03
S1/Cu	0.046 ± 0.001	0.44 ± 0.01
S2/Cu	0.003 ± 0.001	–
S/Cu	0.049 ± 0.001	0.44 ± 0.01
O3/Cu	0.038 ± 0.002	0.017 ± 0.001
O/Cu	0.164 ± 0.007	0.039 ± 0.002
Cl/Cu	0.011 ± 0.001	0.24 ± 0.01

UHV conditions [99]. Since the binding energies are not similar to the previous case, it is suggested that the chemical state of the nitrogen on this sample may be different. Therefore, we propose that the N2 component here corresponds to N bonded to Cu(I) ions dissociated by the conversion reaction of the oxide during cathodic pre-treatment, while the N1 component corresponds to N in the physisorbed multi-layers of the organic layer. It is also seen that the N1 component for curve (b) is significantly higher with the N1/Cu ratio of 0.44 versus the N2/Cu ratio of 0.30 (Table 7.2), supporting the presence of multi-layers of 2-MBI and also confirming the presence of a thicker organic layer than on the previous sample (curve (a)).

The S 2p spectra were decomposed by considering their spin orbit doublets of $2p_{3/2}$ and $2p_{1/2}$ with a branching ratio of 0.5 and splitting of 1.18 eV. For the sample pre-treated in absence of 2-MBI (curve (a)), two components were observed - S1 and S2. The S1 component at 162.9 eV, for the $2p_{3/2}$ spin orbit, corresponds to the exocyclic sulphur from the 2-MBI molecule that is not bonded with metallic copper [99]. The S2 component at 161.7 eV is representative of the interaction between metallic copper and sulphur, which was observed in previous work on adsorption of both 2-MBI and 2-MBT on metallic copper in UHV conditions [83, 84, 99, 100]. Moreover, this S2 component is at the same binding energy as that observed for copper exposed to H_2S gas, resulting in adsorbed atomic sulphur on the surface [142].

The sulphur of the S2 component can be from the entire molecule, its fragments, and/or even free sulphur dissociated from the molecule, as discussed in previous works of 2-MBT adsorption on copper [83, 84].

On the other hand, the sample pre-treated with 2-MBI, curve (b), exhibits only one component - S1 corresponding to sulphur not bonded to metallic copper. The intensity of the S1 peak for curve (b) is significantly greater than that of curve (a), even though curve (a) has been increased by a factor of 3 to show the spectrum properly. This is reflected in the S/Cu atomic ratio given in Table 7.2, where the S/Cu ratio for curve (a) is 0.049 and that for curve (b) is 0.44, which is a 9-fold increase in S intensity. Since the S2 component, S bonded to metallic Cu, generally exhibits very low intensity due to the restricted availability of the metallic Cu surface to bond with S, we cannot completely rule out the possibility of a very small S2 component for the sample pre-treated with 2-MBI (curve (b)). This also considers the fact that we do in fact have a nitrogen component, N2, which bonds directly to metallic Cu in this case, therefore sulphur bonding with the metallic substrate cannot be excluded here. Additionally, we did observe copper-sulphur interaction on this sample from the ToF-SIMS depth profile in Figure 7.2b at a greater sputtering time than copper-nitrogen interaction, which suggested sulphur bonding. Regardless, even if this S2 component is present for curve (b), its intensity is less than 1% of the total intensity of sulphur thus rendering it negligible for quantitative analysis.

From the C 1s spectra it is suggested that we may have some fragmentation of the 2-MBI molecule upon adsorption. In the previous chapters and in other works, it was also demonstrated that there is some free sulphur due to dissociation of the inhibitor molecule, for both 2-MBI and 2-MBT [83, 84, 99, 100]. To determine this, we calculate the atomic ratios between sulphur, nitrogen, and carbon using the intensities obtained from XPS and relate them to the stoichiometric ratio of atoms from the 2-MBI molecule. It is observed that for the sample pre-treated in the absence of 2-MBI, corresponding to spectra (a), we have 1.25 ± 0.06 sulphur atoms and 2.17 ± 0.02 nitrogen atoms, assuming the carbon intensity corresponds to the 7 carbon atoms of the molecule. This confirms that we have an excess of sulphur atoms present here along with some fragmented nitrogen from the 2-MBI molecule. For the ratios mentioned above, we have only considered the intensities corresponding to the molecule itself, i.e. we have ignored the contributions from the N3, N4, and the C4 components relating to the azides, nitrates, and the excess contamination, as discussed earlier.

Similarly, for the sample pre-treated in the presence of 2-MBI, corresponding to spectra (b) in Figure 7.3, we estimate that we have 1.21 ± 0.06 sulphur atoms and 2.05 ± 0.02 nitrogen atoms for the 7 carbon atoms. This indicates that again there is an excess of sulphur atoms here. Regarding the nitrogen atoms, the ratio determined is very close to the stoichiometric

ratio of the molecule. Therefore, using this pre-treatment method (with 2-MBI) of 2-MBI adsorption results in fragmentation of the molecule too, but mostly sulphur dissociation from the molecule and very little nitrogen dissociation, unlike for pre-treatment without 2-MBI followed by 1 hour exposure to 2-MBI. This would also explain why we have a strong intensity for the CuS^- ion profile for a longer sputtering time compared to the CuN_2^- ion profile, from the depth profiles in Figure 7.2b. The partial decomposition of the 2-MBI molecule was also observed in the work of Whelan et al. [159] on 2-MBI adsorption on a gold (Au(111)) surface. They concluded that when 2-MBI interacts directly with metallic Au, partial decomposition of the molecule occurs resulting in the formation of atomic sulphur. However, they did not note any excess nitrogen from partial decomposition, unlike our case, possibly due to differing experimental conditions.

The Cl 2p spectra, decomposed by their spin-orbit doublets $2p_{3/2}$ - $2p_{1/2}$ with a branching ratio of 0.5 and splitting of 1.6 eV, exhibit only one component (Cl1) at a binding energy of 198.2 eV. This Cl1 component has been assigned to adsorbed chloride [144], as seen and discussed in earlier chapters (Chapters 4 and 6). Although we cannot rule out $CuCl/CuCl_2$ formation due to decomposition limitations arising from the low intensity of the spectra, the absence of a distinct peak is rather interpretative in itself. It suggests that despite the aggressive nature of the electrolyte, strongly acidic with chloride ions, the 2-MBI organic inhibitor is always preferably bonded to the substrate over chloride ions, whatever the bonding mechanisms or structure of the film obtained. Nevertheless, the atomic ratio of adsorbed chloride is 0.011 for the sample pre-treated in absence of 2-MBI compared to 0.24 for the sample pre-treated in presence of 2-MBI, as seen in Table 7.2. This suggests that the former pre-treatment is more effective in protecting the surface from chloride ions, despite the lower thickness of the 2-MBI organic layer formed on the substrate as suggested by the N 1s and S 2p scans of spectra (a). This interpretation was also obtained from the ToF-SIMS depth profiles earlier, Figure 7.2, where we saw deeper penetration of chloride ions for sample (b) compared to sample (a) in terms of sputtering time.

The O 1s spectra of the two pre-treated surfaces are shown in Figure 7.3. For the sample pre-treated in absence of 2-MBI, curve (a), the spectrum was decomposed into 3 peak components. The O1 component at 532.9 eV corresponding to adsorbed water, O2 at 532 eV indicative of hydroxides, and O3 at 530.1 eV corresponding to metal oxide (Cu_2O) [142]. The O3/Cu atomic ratio obtained for this sample is 0.038, indicating a low quantity of oxides present here, due to the efficiency of the pre-treatment used, as seen earlier for 2-MBT adsorption of Cu in acidic conditions using a similar pre-treatment method (Chapter 4). This was also corroborated by the low intensity of the CuO^- ion in the ToF-SIMS depth profiles seen in Figure 7.2a. The overall O/Cu atomic ratio is 0.164, therefore demonstrating that the metal

oxide component is only 1/4th of the total oxygen present.

For the sample pre-treated in presence of 2-MBI, curve (b), the spectrum was decomposed using similar parameters as that for curve (a) and is increased threefold to make the decomposition and the components visible in the graph. We observe three components for this spectrum too. The O1 relates to water adsorbed while the O2 to hydroxides, as mentioned above. These components are found at the same binding energies as those for the previous case. However, we observe a shift of the O3 component to a higher binding energy by approximately 1 eV. This large shift suggests that there is a change in the chemical state of the O3 component here and it is not the same as the O3 component (Cu_2O metal oxide) found in the previous case. The O3/Cu atomic ratio is 0.017 for this sample (pre-treated with 2-MBI), which is half of that observed for the previous case. We also observe that the overall O/Cu atomic ratio is very low compared to the previous case, with a value of 0.039 compared to 0.164 for the previous sample.

Since we know that the pre-treatment method with 2-MBI is not as effective in reducing the native oxides, as indicated from the CVs in Figure 7.1, it is proposed that the initial copper oxides present on the surface undergo a conversion reaction during cathodic pre-treatment of the surface, resulting in the consumption/release of oxygen from the copper oxides. This reaction then leaves Cu(I) ions free from the oxides which allows them to interact with 2-MBI molecules to form metal-organic complexes here. Therefore, we obtain a much lower intensity for the O 1s spectrum for the sample pre-treated in presence of 2-MBI. The reduced intensity of oxygen for this sample was also observed in the ToF-SIMS depth profiles in Figure 7.2.

To understand the effect of oxides more clearly, we decomposed the Cu LMM Auger spectra obtained from the XPS analysis for the two experiments (Figure 7.4). The sample pre-treated in absence of 2-MBI followed by 1 hour exposure to 2-MBI (Figure 7.4a) exhibits a relatively low Cu(I) intensity, with a ratio of 0.26 $\pm$ 0.01 between Cu(I) and Cu(0) components. Although the Cu(I)/Cu(0) ratio obtained here is not as low as that observed for 2-MBT adsorption on Cu in a similar environment (Chapter 4) and using a similar pre-treatment method (0.05 $\pm$ 0.01), it still follows the trend where the ratio of Cu(I) ions is lower for the pre-treatment without inhibitor compared to that for the pre-treatment with inhibitor (Figure 7.4b).

For the sample pre-treated in presence of 2-MBI (Figure 7.4b), the Cu LMM Auger scan shows a drastically different profile. The Cu(I) component has a much higher relative intensity here, resulting in a Cu(I)/Cu(0) intensity ratio of 6.11 $\pm$ 0.22. Since we did not observe Cu_2O metal oxide in the O 1s spectrum for this sample, Figure 7.3, it is suggested that the Cu(I) component here is mostly due to the presence of complexes which are formed

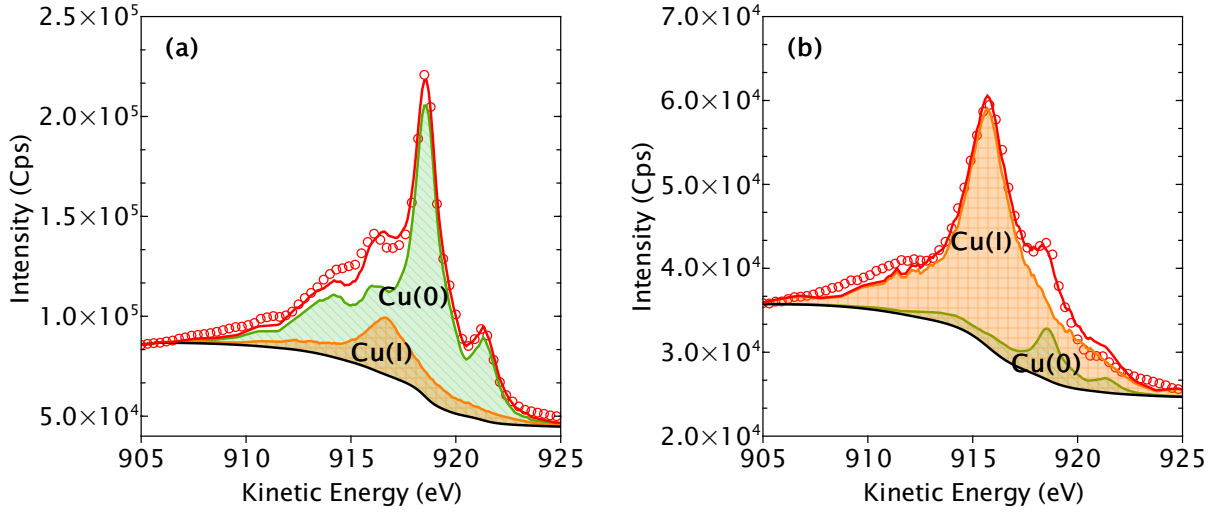

Figure 7.4: Cu LMM Auger spectra for 2-MBI films formed on copper surfaces at the reduced state in 10 mM HCl solution after cathodic pre-treatment (a) in the absence of 2-MBI followed by 1 hour exposure to 2-MBI, and (b) in the presence of 2-MBI.

by the conversion reaction of the copper native oxide during cathodic pre-treatment of the surface in presence of 2-MBI. The Cu(I) ions, released from the initial copper oxides present, interact with the 2-MBI molecules to form the complexes. This inference is in line with the observations from the ToF-SIMS depth profile of this sample seen in Figure 7.2b, where we observed an initial decrease in intensity of the Cu^-, O^-, and $C_7H_4N_2S^-$ ion profiles which was attributed to the presence of complexes on the surface.

The metal organic complexes formed by 2-MBI and copper are quite different than those formed by 2-MBT and copper. As seen earlier in Chapters 5 and 6, the Cu-2-MBT complexes are only formed in neutral and alkaline media, not in acidic media, despite both inhibitors utilizing Cu(I) ions for the formation of the complexes. This was attributed to the dominant conformer of the 2-MBT molecule in each environment. Only the thiolate form of the molecule enabled the formation of the complexes, most likely due to the absence of a hydrogen atom in the molecule thus leaving an extra reactive site for the interaction with the Cu(I) ions. However, in the present case, even though the dominant form of 2-MBI in acidic media is the thione conformer, significant quantities of the metal organic complexes are formed, as evidenced by the Cu LMM Auger spectrum. There can be two possibilities for this occurrence. The first is that the Cu(I) ions replace the hydrogen atoms attached to the nitrogen atoms of the molecule due to stronger affinity between them, thus forming the complexes. The second possibility is that due to some fragmentation of the molecule, there is a new reactive site for the Cu(I) ions to interact with, thus forming the complexes. However, we cannot confirm or rule out either hypothesis at this point.

7.4 Corrosion inhibition by 2-MBI organic films

To investigate the corrosion behaviour of copper in the acidic chloride environment and the inhibition offered by the 2-MBI molecule on various pre-treated surfaces, cyclic voltammetry tests were performed. The CVs are shown in Figure 7.5 and the corresponding anodic and cathodic charge densities along with equivalent thickness of copper reacting are given in Table 7.3. For the sample polarised in the reference 10 mM HCl solution, we observe a sharp increase in current density initiating at approximately 0.15 V vs SHE, corresponding to anodic dissolution of copper metal. The measured charge density for the anodic branch of the polarisation is 7032 ± 13 $\mu C/cm^2$ and the estimated equivalent thickness of reacting copper is 5.17 ± 0.02 nm, also given in Table 7.3. Subsequently, a cathodic peak corresponding to copper redeposition is observed during reverse sweeping at a potential of 0.08 V vs SHE. The measured cathodic charge density was 4503 ± 55 $\mu C/cm^2$. The large difference between the anodic and cathodic charge densities indicates a considerable quantity of copper metal being irreversibly dissolved during the cyclic voltammetry test, estimated to be approximately 1.86 ± 0.03 nm of equivalent thickness.

The copper surfaces with the 2-MBI inhibitor exhibited significantly lower rises in the current density during the anodic branch compared to the reference substrate. To examine the CVs clearly, they are enlarged in Figure 7.5b. The sample pre-treated in the absence of 2-MBI followed by 2 minutes of exposure to 2-MBI shows an increase in current density initiating at 0.23 V vs SHE, a positive shift of 0.07 V compared to the reference substrate. This indicates a delayed corrosion initiation on the 2-MBI covered surface along with a slower corrosion rate as expressed by the slower rise of current density. When the exposure time was increased to 1 hour for a similarly pre-treated sample, we observed a further positive shift of 0.05 V for corrosion initiation to 0.28 V vs SHE, indicating that the extended exposure time to the inhibitor results in a better protection of the substrate. The positive shifts observed for the two samples also result in progressively lower amounts of copper reacting, as seen in Table 7.3, due to the inhibitive effect of the 2-MBI molecule.

Lastly, the sample pre-treated in presence of 2-MBI also exhibits its rise in current density starting at 0.28 V vs SHE. However, the increase is much less here than for the previous two samples (pre-treatment without 2-MBI followed by exposure to 2-MBI) with an equivalent thickness of 0.40 ± 0.02 nm of reacting copper estimated from the anodic branch of the CV. This suggests that the sample pre-treated with 2-MBI results in the most protective barrier layer/interface of the three inhibited samples, which is likely due to the copper oxide-2-MBI interaction resulting in the formation of a conversion layer of protective complexes on the surface that better restrict the access of the electrolyte to the substrate. This is in contrast

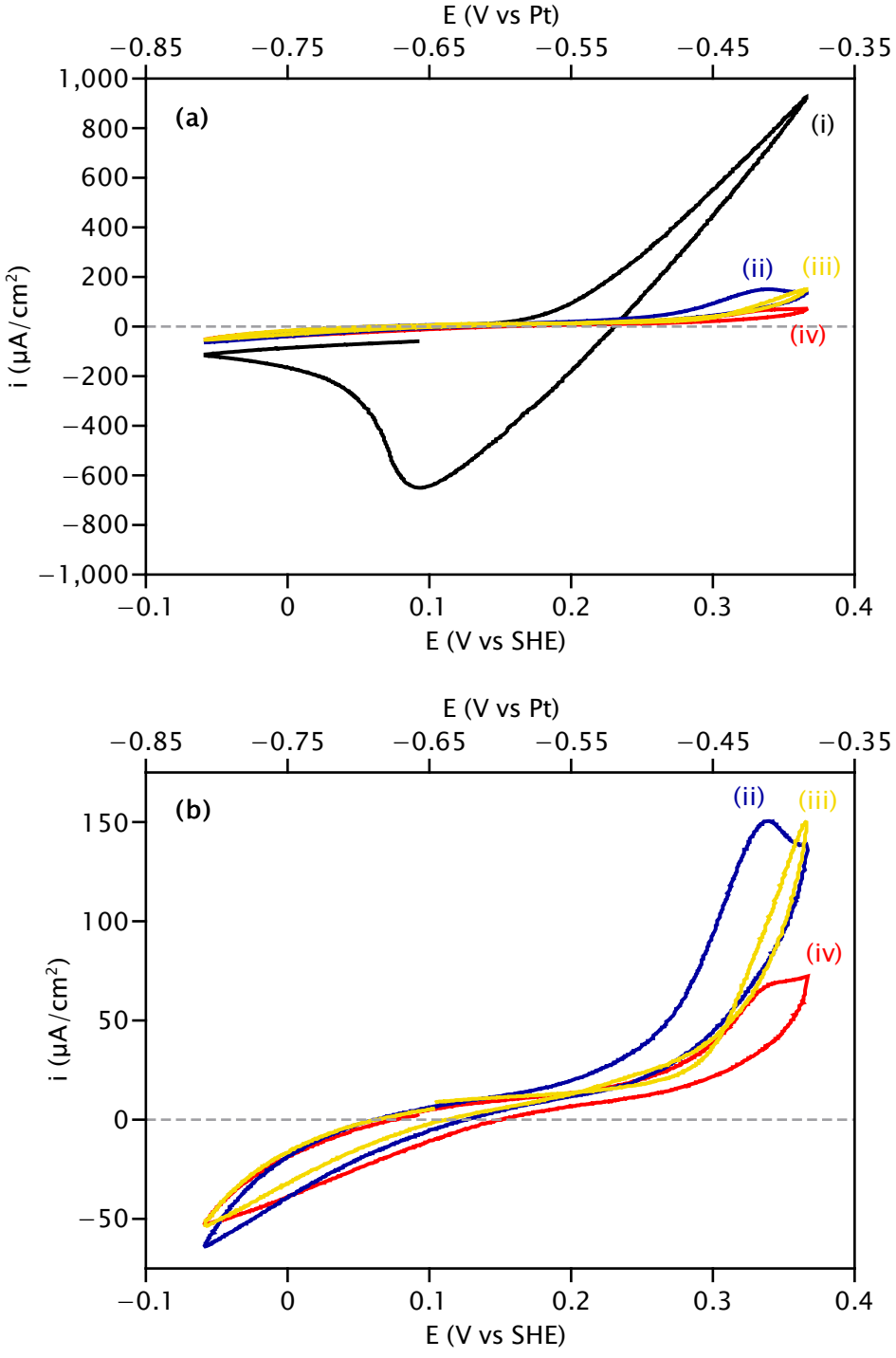

Figure 7.5: (a) CV tests of copper anodic dissolution in 10 mM HCl solution in (i) the absence of 2-MBI, and (ii-iv) the presence of 2-MBI, after the various cathodic pre-treatment methods of the interface. (b) Enlarged CVs of the copper surfaces polarised in the presence of 2-MBI.

Table 7.3: Anodic and cathodic charge densities ($\mu C/cm^2$) determined from the cyclic voltammetry anodic dissolution tests by integrating the current densities measured with time, and equivalent thickness (nm) of copper metal reacting estimated using Faraday's law.

	Electrolyte, Pre-treatment method	Anodic charge density ($\mu C/cm^2$)	Cathodic charge density ($\mu C/cm^2$)	Equivalent thickness of copper reacting (nm)
i	10 mM HCl reference solution, Pre-treatment without 2-MBI	7032 ± 13	4503 ± 55	5.17 ± 0.02
ii	1 mM 2-MBI + 10 mM HCl, Pre-treatment without 2-MBI, 2 minutes exposure to 2-MBI	1101 ± 4	282 ± 21	0.81 ± 0.01
iii	1 mM 2-MBI + 10 mM HCl, Pre-treatment without 2-MBI, 1 hour exposure to 2-MBI	839 ± 5	216 ± 6	0.62 ± 0.01
iv	1 mM 2-MBI + 10 mM HCl, Pre-treatment with 2-MBI	541 ± 7	296 ± 22	0.40 ± 0.02

with the work on 2-MBT adsorption on copper (Chapters 4 and 6), where the samples pre-treated in absence of the inhibitor followed by exposure to the inhibitor yielded far superior barrier layers in terms of protection against corrosion compared to the samples pre-treated in presence of the inhibitor.

To understand this effect further, cyclic voltammetry was carried out on the sample pre-treated without 2-MBI followed by 1 hour exposure to 2-MBI and on the sample pre-treated with 2-MBI, with an anodic branch extended up to 0.75 V vs SHE (Figure 7.6). We observe that for the sample pre-treated without 2-MBI followed by 1 hour exposure to 2-MBI, the anodic current density increase, seen earlier in Figure 7.5, corresponds to a peak at 0.38 V vs SHE with a subsequent decrease until 0.45 V vs SHE. This suggests that the rise in current density relates to a reaction preceding corrosion initiation. Since this peak is absent for the CV obtained for the sample pre-treated with 2-MBI, it is likely that the reaction responsible for this effect has already occurred on this latter sample during cathodic pre-treatment of the surface, i.e. by converting the Cu_2O native oxide to Cu-2-MBI complexes by consuming/releasing the oxygen atoms from the oxide and leaving the Cu(I) ions to interact with the 2-MBI molecules.

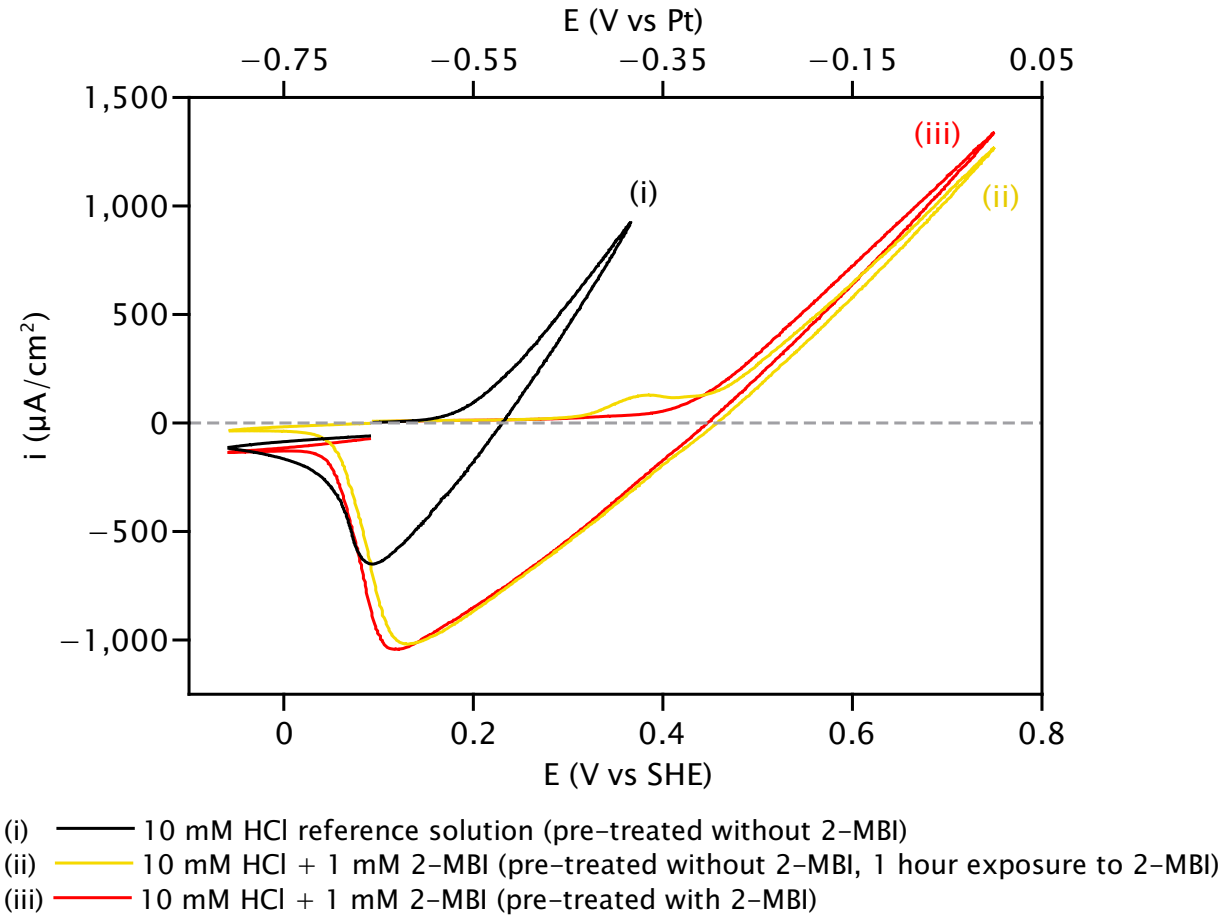

Figure 7.6: CV tests of copper anodic dissolution with extended anodic range in 10 mM HCl + 1 mM 2-MBI in (i) the absence of 2-MBI, and (ii-iii) the presence of 2-MBI, after the various cathodic pre-treatment methods of the interface.

Therefore, we propose that the peak observed for the sample pre-treated without 2-MBI followed by 1 hour exposure to 2-MBI at 0.38 V vs SHE is associated with the interaction between Cu(I) ions, formed during anodic polarisation in this case, and the 2-MBI organic inhibitor molecule, resulting in the formation of a metal-organic complex that prolongs the corrosion inhibition up until a slightly higher potential. The main distinction in the formation of the complexes for the two samples is that on the sample pre-treated with 2-MBI, the Cu(I) ions originate from the native oxide film and are released during the cathodic pre-treatment cycles while for the sample pre-treated without 2-MBI, the Cu(I) ions are formed by anodic oxidation of copper metal and thus the complexes are formed at a later stage.

The corrosion initiation, on the other hand, occurs later at a potential of 0.45 V vs SHE, indicated by a sharp rise in current density, similar to that of the sample pre-treated in 2-MBI where the corrosion initiation was observed at 0.28 V vs SHE. Therefore, the sample

pre-treated without 2-MBI followed by 1 hour exposure to 2-MBI does in fact protect the substrate for a greater potential range, indicating that the inner chemisorbed layer formed is more restrictive against the electrolyte for this sample.

In Chapter 4 where 2-MBT was used as an inhibitor for copper in acidic chloride media, it was established that the 2-MBT organic molecule is exceptionally effective for corrosion inhibition of copper. Since the present work was carried out in similar conditions, we can make comparisons between the corrosion inhibition effectiveness of the two different organic molecules on copper. In the present work, we observe that the sample pre-treated in presence of 2-MBI exhibits a reduction in anodic current density of approximately 92.25% at 0.37 V vs SHE (anodic peak), whereas the sample pre-treated in absence of 2-MBI followed by 1 hour exposure to 2-MBI exhibits a reduction of approximately 83.87%. Although we have seen and discussed the effects of the conversion peak in the latter sample, we are considering the anodic current density values at 0.37 V vs SHE for ease of comparison. On the other hand, for the 2-MBT molecule on copper in acidic chloride media, the sample pre-treated with 2-MBT obtains a 74.20% reduction while the sample pre-treated without 2-MBT followed by 1 hour exposure to 2-MBT obtains an astonishing 99.75% reduction in anodic current density at the same potential (0.37 V vs SHE).

This demonstrates that with a better control of the surface and/or interface of the copper sample, 2-MBT achieves a better result on the protection of copper metal from corrosive attack in an acidic chloride media. Additionally, the concentration of 2-MBT used was 0.1 mM due to its very low solubility in acidic media, whereas the concentration of 2-MBI used in the present work was 1 mM, an increase by a factor of 10. This in turn shows that even in lower concentrations, 2-MBT is more effective on copper than 2-MBI as an inhibitor.

7.5 Effects of anodic polarisation on the 2-MBI layer

The ToF-SIMS depth profiles obtained at the anodic state of the sample, i.e. anodically polarised to 0.37 V vs SHE, are shown in Figure 7.7. The plotted ion profiles and the defining position of each interface/layer is consistent with the depth profiles at the reduced state, presented above in Figure 7.2. Using the same criteria based of maximum peak intensity of the Cu^- ion profile, it is observed that the sputtering time taken to reach the Cu substrate for either sample has immensely increased compared to the reduced state. For the sample pre-treated in absence of 2-MBI (Figure 7.7a), the increase is approximately 6 times, reaching the metallic copper substrate at 716 seconds of sputtering time. For the sample pre-treated in presence of 2-MBI (Figure 7.7b), the increase is approximately 3.6 times, reaching the substrate at 2403 seconds of sputtering. The sequence of intensity maxima from the surface to

the copper substrate remains the same for either sample with copper-sulphur interaction found at a greater sputtering time than copper-nitrogen interaction. Additionally, the coincidence of the maxima of the copper oxides and copper-sulphur interaction peaks are also seen here.

An interesting feature observed for the sample pre-treated with 2-MBI is that for most ion profiles we observe an initial peak within the range of the first 500 seconds of sputtering (at 330 seconds for the Cu^- ion profile), followed by an inner wave of higher intensity in the range of 1800 – 2500 seconds of sputtering time. Although surface roughness could play a role here, the effect it has is generally on the shape of the ion profile, i.e. slow and creeping instead of sharp profiles. Here, we observe on both samples that the depth profiles exhibit a rather slow decrease in their ion intensities, indicating surface roughness is prevalent. From the extended anodic CVs in Figure 7.6, we have deduced that corrosion has initiated on the sample pre-treated with 2-MBI but not on the sample pre-treated in the absence of 2-MBI. Therefore, we propose that the outer peaks correspond to the non-homogeneously attacked depth of the sample, where the locally attacked and not yet attacked regions coexist, while the inner waves relate to a greater depth from the surface, beyond the depth of the non-homogeneous corrosive attack. Such an effect of an outer peak and an inner wave in the depth profiles has also been observed by Seyeux et al. [160] where they used ToF-SIMS to characterize the interface between the oxide film of stainless steel and non-homogeneously covering bacteria on the surface.

Another notable feature, this time for the sample pre-treated in absence of 2-MBI (Figure 7.7a), is the decrease in intensity for the CuO^- ion profile from the reduced state to the anodic state. This is consistent with the fact that the residual copper oxides trapped between the organic layer and the copper substrate are converted by reaction with the 2-MBI molecules and its fragments to form metal-organic complexes leaving only traces of copper oxides. However, we know that this is not the primary mechanism of complex formation for this pre-treatment method. Most of the complexes formed for the sample pre-treated in absence of 2-MBI result from anodic polarisation when the copper metal is oxidized to form Cu(I) ions which then interact with the 2-MBI molecules. Lastly, we observe that the chloride ions, represented by the $^{37}Cl^-$ ion profile, has penetrated considerably into the substrate for both experiments, although this effect is much larger for the sample pre-treated with 2-MBI (Figure 7.7b). The XPS spectra obtained for the two surfaces at the anodic state are shown in Figure 7.8. Like for Figure 7.3, curve (a) of the spectra relates to the sample pre-treated in absence of 2-MBI followed by 1-hour exposure to 2-MBI, whereas curve (b) corresponds to the sample pre-treated in presence of 2-MBI. The intensities of the Cl 2p spectrum of curve (a) and O 1s spectrum of curve (b) have been increased threefold for better visibility of the decomposition and the components. The decompositions of the spectra have also been

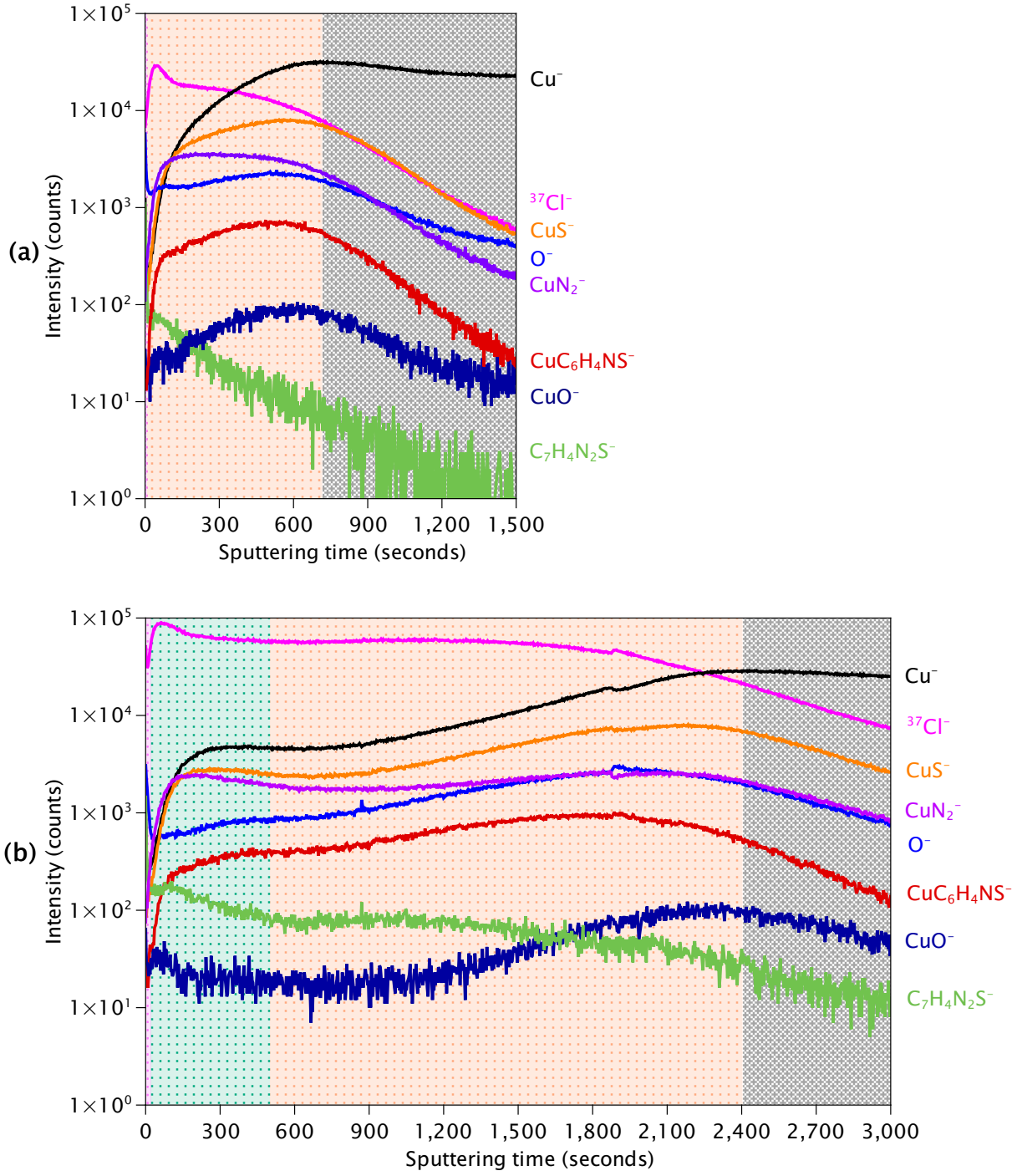

Figure 7.7: ToF-SIMS depth profiles obtained after anodic polarisation to 0.37 V vs SHE (anodic state) in 10 mM HCl + 1 mM 2-MBI solution for copper surfaces pre-treated (a) in the absence of 2-MBI followed by 1 hour exposure to 2-MBI, and (b) in the presence of 2-MBI. Intensity in counts (logarithmic scale) vs sputtering time in seconds.

detailed earlier.

The Cu 2p spectra exhibits their $2p_{3/2}$ peaks at 932.9 eV for both samples, like for the reduced state. However, the FWHM of the $2p_{3/2}$ peak for the sample pre-treated in absence of 2-MBI followed by 1 hour exposure to 2-MBI (curve (a)) has increased from 1 eV to 1.4 eV, which is similar to that of the sample pre-treated with 2-MBI at the reduced and anodic state, indicating that there is a change in the components upon polarisation. This was also attested by the change in ToF-SIMS depth profiles before and after polarisation, as seen in Figure 7.2a and Figure 7.7a. Additionally, a reduction in intensity of the Cu $2p_{3/2}$ peak is observed here, assigned to the increased thickness of organic surface layers, as confirmed by the depth profiles, resulting in a larger attenuation of the substrate signal. For the sample pre-treated in presence of 2-MBI (curve (b)), there is almost no difference observed in terms of BE or FWHM for the Cu 2p spectra before and after anodic polarisation, signifying that the induced changes are either insignificant or that they transpire at a depth greater than the probing depth of the XPS.

Regarding the C 1s spectra, we observe that there is a positive shift in the binding energies of all the components of 0.5 ± 0.2 eV compared to that at the reduced state for both the samples. Additionally, the ratio between the components has been slightly altered. The relative intensity of the C1 component corresponding to the C=S bond has decreased for both samples at the anodic state possibly due to cleavage of the C=S bond induced by anodic polarisation. Therefore, we see a slight relative gain in the intensities of the C2 and C3 components of the C 1s spectra. Although we do not know the exact reason for the shift in binding energies of the carbon components, it is likely that it occurs due to the increased thickness of the 2-MBI organic layer from the formation of complexes upon polarisation, thus causing a positive shift in the binding energies due to bad conductivity between the surface layers corresponding to carbon and the XPS analyser.

The N 1s spectra of the two samples exhibit 2 peak components here, N1 corresponding to nitrogen not bonded to metallic copper and N2 corresponding to nitrogen bonded to metallic copper. We do not observe the N3 and N4 components here for the sample pre-treated in absence of 2-MBI (curve (a)), unlike at the reduced state. This is in line with the absence of the C4 peak in the C 1s spectrum for the corresponding sample. An increase in the binding energies is noted for the two nitrogen components for both samples. For the sample pre-treated with 2-MBI, the increase in BE is a mere 0.1 eV, which is within the uncertainty range. However, for the sample pre-treated without 2-MBI, the increase in BE is 0.2 eV, suggesting a possible change in the chemical state. We also observe an increase in FWHM of 0.2 eV for the N1 and N2 components for this sample. This increase in BE and FWHM is most likely due to the formation of the metal-organic complexes which alters the chemical

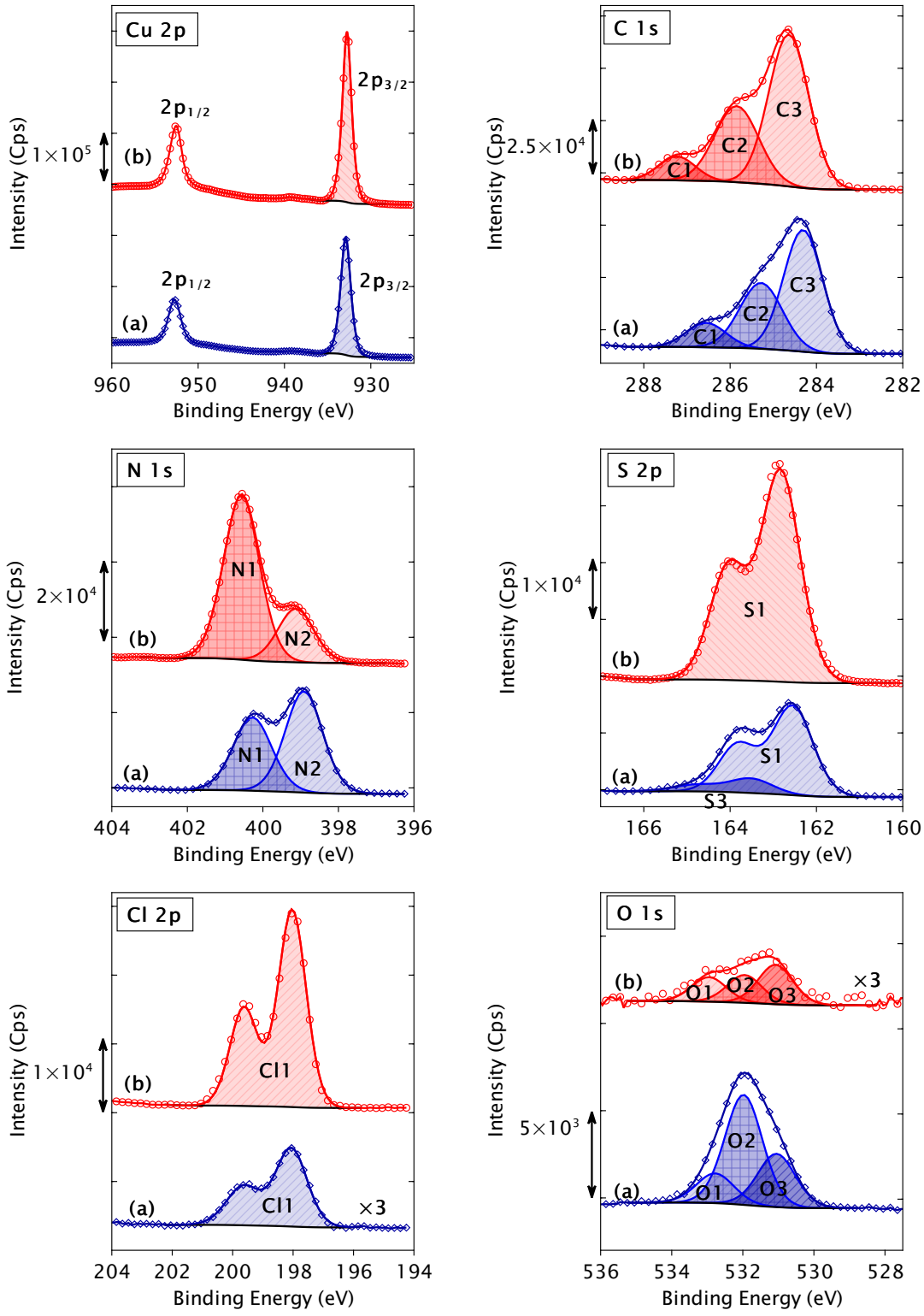

Figure 7.8: XPS Cu 2p, C 1s, N 1s, S 2p, Cl 2p, and O 1s core level spectra obtained after anodic polarisation to 0.37 V vs SHE (anodic state) in 10 mM HCl + 1 mM 2-MBI solution with for copper surfaces pre-treated (a) in the absence of 2-MBI followed by 1 hour exposure to 2-MBI (blue curves), and (b) in the presence of 2-MBI (red curves). The symbols represent the experimental data and the corresponding coloured lines represent the fit. Intensities are normalised to the background at the lower binding energy side.

state of the nitrogen, from the initial interaction with metallic Cu at the reduced state to the subsequent interaction with Cu(I) ions at the anodic state. For the sample pre-treated with 2-MBI, the interaction between copper and nitrogen at the reduced state was already due to the Cu(I) ions released from the oxides, thus the change is negligible. Lastly, an increase in the intensities of the N1 and N2 components relative to the Cu intensity is observed for both samples, as seen in Table 7.4. This indicates that we have increased bonding between nitrogen and metallic Cu and/or Cu(I) ions (N2 component) and also thicker multilayers of physisorbed 2-MBI not bonded to Cu (N1 component).

In the S 2p spectrum of the sample pre-treated in presence of 2-MBI (curve (b)), we observe only one component, S1 corresponding to sulphur not bonded to metallic copper. The ratio of this component relative to Cu has increased from 0.44 at the reduced state to 0.51 at the anodic state, confirming a thicker physisorbed layer. Meanwhile, for the sample pre-treated in absence of 2-MBI (curve (a)), we observe that the S2 component at 161.7 eV related to sulphur bonded to metallic copper is absent. Instead, another component, S3, is found at a binding energy of 163.5 eV ($2p_{3/2}$ peak). It is proposed that this S3 component is possibly due to a change in the oxidation state of sulphur from the S2 component seen at the reduced state, and thus results in a change of the binding energy of the species. However, the true nature of this species is not known to us. The S1 peak for curve (a) also exhibits an increased intensity with respect to the Cu intensity, from 0.046 at the reduced state (Table 7.2) to 0.34 at the anodic state (Table 7.4). A decrease of 0.3 eV in the BE is also seen for this sample. These observations are in line with that of the nitrogen spectra for the same sample suggesting a change in the chemical state of the molecule in the thicker chemisorbed inner layer after anodic polarisation.

Similar to the reduced state Cl 2p spectra (Figure 7.3), the anodic state Cl 2p spectra for the two samples (Figure 7.8) exhibit one component, Cl1 at 198.2 ± 0.2 eV, corresponding to adsorbed chloride. However, there is a substantial increase in the Cl intensity from the reduced state to the anodic state for both the samples with respect to the Cu intensity, from 0.011 to 0.11 for the sample pre-treated in absence of 2-MBI (curve (a)), and from 0.24 to 0.53 for the sample pre-treated in presence of 2-MBI (curve (b)). This is in agreement with the ToF-SIMS depth profiles (Figure 7.7) that show increased intensity of the $^{37}Cl^-$ ion profile for a larger sputtering time compared to that at the reduced state (Figure 7.2) for both samples. The increased intensity of chlorine insinuates that the 2-MBI organic layer, which consists of the chemisorbed layer including the metal-organic complexes and the physisorbed layer, is not entirely protective. Chloride ions do penetrate the organic layer to interact with the residual oxides and the metallic copper substrate, which can lead to attack. Although the acidic pH of the solution also plays a role in this attack, we have found that under the same

Table 7.4: Atomic ratios obtained by quantitative analysis of the XPS measurements at the anodic state using the photoelectron intensities, normalised by the photoionization cross-sections, the inelastic mean free paths, and the transmission function of the analyser.

Component	Pre-treatment without 2-MBI, 1 hour exposure to 2-MBI	Pre-treatment with 2-MBI
N1/Cu	0.30 ± 0.01	0.65 ±0.03
N2/Cu	0.41 ± 0.02	0.21 ± 0.01
N/Cu	0.71 ± 0.03	0.86 ± 0.03
S1/Cu	0.34 ± 0.01	0.51 ± 0.02
S3/Cu	0.057 ± 0.002	—
S/Cu	0.40 ± 0.01	0.51 ± 0.02
O3/Cu	0.045 ± 0.002	0.011 ± 0.001
O/Cu	0.164 ± 0.007	0.025 ± 0.001
Cl/Cu	0.11 ± 0.01	0.53 ± 0.02

conditions of organic layer formation in a similar media, 2-MBT is a more effective inhibitor against copper corrosive attack than 2-MBI.

Lastly, the O 1s spectrum for the sample pre-treated in absence of 2-MBI (curve (a)) exhibits a similar intensity for the overall oxygen content (Table 7.4) as that at the reduced state (Table 7.2) with respect to the copper intensity. However, there is a change in intensities among the three components of the O 1s spectrum, with a large increase in the O2 component (hydroxides) and a decrease in the O1 component (water adsorbed). The O3 peak has increased only slightly from 0.038 to 0.045, however, there is a large positive shift of 1 eV in the binding energy of this component from 530.1 eV to 531.1 eV. This component is at the same binding energy as the O3 component for the sample pre-treated in presence of 2-MBI at the reduced state, seen earlier in Figure 7.3, suggesting that the metal oxide initially present has undergone a change in its chemical state. Meanwhile, for the sample pre-treated in presence of 2-MBI (curve (b)), we observe that there is a slight reduction in the intensity of the oxygen peaks with respect to copper intensity at the anodic state, both individually and overall, compared to the reduced state. However, we did not observe any change in the binding energies of the three components from the reduced state. To deliberate on these observations further, we examine the Cu LMM Auger spectra for both samples (Figure 7.9).

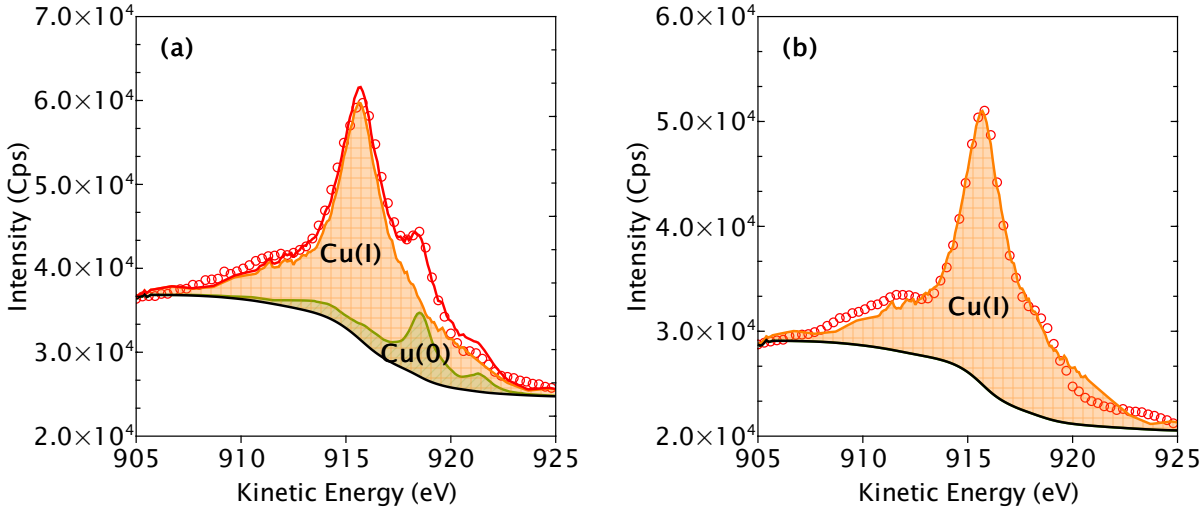

Figure 7.9: Cu LMM Auger spectra obtained for 2-MBI films formed on copper surfaces at the anodic state in 10 mM HCl solution after cathodic pre-treatment (a) in the absence of 2-MBI followed by 1 hour exposure to 2-MBI, and (b) in the presence of 2-MBI.

We observe that for the sample pre-treated in absence of 2-MBI followed by 1 hour exposure to 2-MBI (Figure 7.9a), the Cu(0) component intensity has profoundly decreased while the Cu(I) component is now the major component with a Cu(I)/Cu(0) ratio of 4.86 ± 0.18. However, we did not observe an increase in the oxygen intensity (O 1s) upon polarisation, as discussed above. This suggests that there is an increased formation of metal-organic complexes upon anodic polarisation of the sample, which is also most likely the reason for the shift in BE of the O3 component from the O 1s spectra for this sample. This Cu LMM Auger profile is quite similar to that of the sample pre-treated with 2-MBI at the reduced state (Figure 7.4b). Additionally, the shifts in BE, increased FWHMs, and the change in atomic ratios observed from the XPS core level spectra for this sample (pre-treated in absence of 2-MBI followed by 1 hour exposure to 2-MBI) suggest that the structure of the organic layer on the sample has changed drastically on anodic polarisation and is likely similar to that of the converted organic layer formed on the sample pre-treated in presence of 2-MBI at the reduced state. This is also consistent with the change of the ToF-SIMS depth profile from the reduced state to the anodic state.

The change in structure of the organic layer of the sample pre-treated in absence of 2-MBI followed by 1 hour exposure to 2-MBI is most likely due to the formation of the complexes on anodic polarisation. Since the sample was pre-treated in absence of 2-MBI, there was no interaction between the molecule and the released Cu(I) ions. Upon anodic polarisation, copper metal is oxidized to Cu(I), which then allows for interactions between the newly produced Cu(I) ions and the 2-MBI molecules. Thus, we obtain a structure similar to that of

the sample which was already pre-treated in presence of 2-MBI and formed the metal-organic complex-containing organic layer right at the first cycle of cathodic pre-treatment.

For the sample pre-treated with 2-MBI (Figure 7.9b), we observe only the Cu(I) component. The absence of Cu(0) from the profile shows that the metallic copper substrate on this sample is below the probing depth of the XPS, although the presence of Cu(0) cannot be completely excluded. This means that the organic layer on this sample, which mostly consists of the complexes, is of a thickness greater than 10 nm as estimated from the TPP-2M formula [139], far greater than the organic layer thickness of 2-MBT adsorbed on copper (Chapter 4). This inference also gives validation to our ToF-SIMS results in Figure 7.7b, where we proposed that the copper substrate is found at a larger sputtering time and the initial peak of the Cu^- ion profile corresponds to the initial top surface of the sample which was non-homogeneously attacked.

The proposed models of the layered structure of the 2-MBI inhibiting interfaces formed at the reduced state and their alteration at the anodic state on both pre-treated Cu substrates are shown in Figure 7.10. Additionally, the depth of the penetration of the chloride ions on each sample, based on the analysis of the depth profiles obtained by ToF-SIMS, is also shown in the figure. For the sample pre-treated without 2-MBI and subsequently exposed to the inhibitor at the reduced state, the 2-MBI film is bi-layered with inner chemisorbed and outer physisorbed layers and Cu_2O oxide islands trapped at the interface (Figure 7.10a). The chloride ions have penetrated the outer physisorbed layer, but not the inner chemisorbed layer in this case.

Upon anodic polarisation (Figure 7.10b), the Cu(I) oxide islands are converted into complexes, as evidenced by the shift in the O3 component binding energy in Figure 7.8 (curve (a) of O 1s spectrum). Further complexes are formed when Cu(I) ions are produced by anodic oxidation of the metallic Cu substrate, as indicated by the extended CVs in Figure 7.6 and confirmed by the large intensity of Cu(I) ions from the Cu LMM Auger spectra in Figure 7.9a. We have also seen from the ToF-SIMS depth profile in Figure 7.7a that the chloride ions are found even in the inner chemisorbed layer on this sample, signifying that the chloride ions have penetrated regions of this organic barrier layer.

For the sample pre-treated with 2-MBI and at the reduced state (Figure 7.10c), a conversion layer of 2-MBI complexes was already formed upon cathodic polarisation by the release of Cu(I) from the native oxide, thus also forming a bi-layered inhibiting interface but oxide-free and thicker than after pre-treatment without 2-MBI. The formation of complexes was verified by the low intensity of the O 1s spectrum of curve (b) in Figure 7.3 and the high intensity of the Cu(I) ions in the Cu LMM Auger spectra in Figure 7.4b. At the reduced state, we

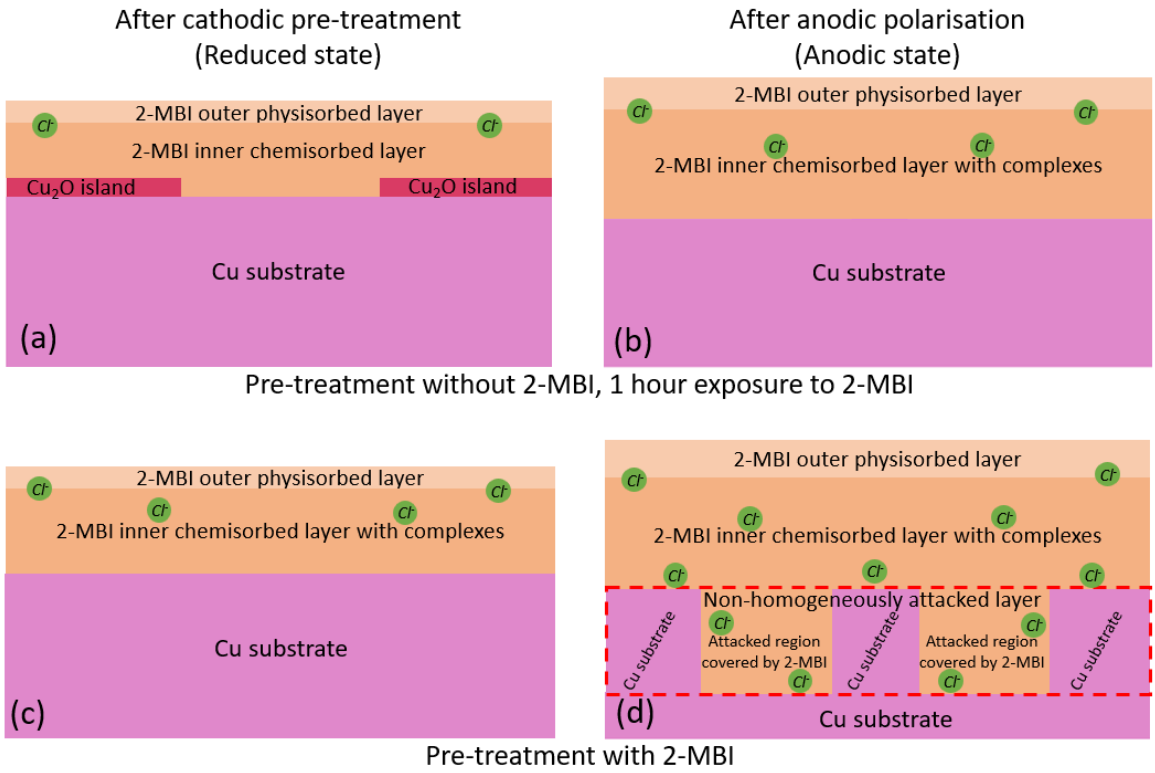

Figure 7.10: Bi-layered interfacial structure of the 2-MBI organic films formed on copper in (a,c) reduced and (b,d) anodic states in 10 mM HCl solution for pre-treatment (a,b) in the absence of 2-MBI followed by 1 hour exposure to 2-MBI, and (c,d) in the presence of 2-MBI. The green disks represent the chloride ions that have penetrated the organic film layers, as shown by ToF-SIMS.

already observed the presence of the chloride ions in the inner chemisorbed layer with the complexes suggesting that there are defects in the organic layer, thus rendering the organic layer not as protective as that on the sample pre-treated in absence of 2-MBI.

At the anodic state (Figure 7.10d), the interface is non-homogeneously attacked, with regions of the un-attacked Cu substrate and regions of the attacked substrate both covered by the organic bilayer, as seen from the ToF-SIMS depth profile in Figure 7.7b. The ion profile representing the chloride ions exhibits a very high intensity up until the inner copper substrate is reached, as shown in the model. The non-homogeneous attack of the substrate suggests an uneven protection offered by the 2-MBI organic bilayer, with the barrier properties of the inner chemisorbed layer possibly depending on the conversion reactions and local formation of Cu(I)-2-MBI complexes.

7.6 Conclusion

The 2-MBI inhibiting interfaces formed on copper surfaces in an acidic chloride media along with the corrosion protection capabilities of the organic layer were investigated. Pre-treatment of the copper surfaces by cathodic reduction in the absence of 2-MBI resulted in a near oxide free surface, while that in the presence of 2-MBI resulted in the formation of a conversion layer of Cu(I)-2-MBI metal organic complexes by the consumption of oxygen and release of Cu(I) ions from the native copper oxide film.

The bonding between copper and 2-MBI occurred primarily by the nitrogen atoms of the molecule. However, for the surface pre-treated in absence of 2-MBI, sulphur bonding to metallic Cu was also observed by XPS analysis. Depth profiling by ToF-SIMS revealed the formation of an inner chemisorbed layer and an outer physisorbed layer of the organic 2-MBI film. A rather low intensity of oxygen was observed from both XPS and ToF-SIMS for the sample pre-treated in presence of 2-MBI, while an unusually high intensity for Cu(I) ions was observed from the Cu LMM Auger spectrum, confirming the formation of Cu(I)-2-MBI complexes during pre-treatment by cathodic reduction in presence of 2-MBI.

CV corrosion tests confirmed that 2-MBI does protect the metal from corrosive attack, as seen by a positive shift in the potential for the onset of anodic dissolution and a slower increasing anodic current density. However, the protection offered to the metal varied depending on the pre-treatment used. For the sample pre-treated in absence of 2-MBI followed by 1 hour exposure to 2-MBI, which exhibited the highest resistance to corrosion initiation, a small anodic peak was observed prior to the initiation of anodic dissolution indicating a side protection reaction. It was established that this reaction corresponds to the formation of complexes resulting from the anodic oxidation of Cu metal to Cu(I) ions. Therefore, metal-organic complexes were formed on both pre-treated substrates, although by different mechanisms depending on the polarization of the interface.

Upon anodic polarisation, a thicker organic layer was formed on both substrates due to further formation of metal organic complexes. On the sample pre-treated with 2-MBI, the top-most substrate surface was non-homogeneously attacked by chloride ions, as evidenced by the shape of the ToF-SIMS depth profiles and the Cl intensity from XPS analysis. On the other hand, the sample pre-treated in absence of 2-MBI followed by 1 hour exposure to 2-MBI exhibited better protection at the same anodic potential and a much lower Cl intensity, demonstrating that electrochemical control of formation of the interface is instrumental for optimizing the inhibition properties.

Conclusions and perspectives

In the present work, the interaction between two sulphur based organic inhibitors, 2-mercaptobenzothiazole (2-MBT) and 2-mercaptobenzimidazole (2-MBI), and electrochemically controlled copper surfaces was investigated in various media. Additionally, the factors affecting the bonding mechanisms such as the presence of surface oxides, the role of pH, and the change in active sites of the molecule were also studied. Finally, the corrosion inhibition and anodic oxidation inhibition offered by these two different inhibitors were evaluated in each media. This was performed using an integrated approach of electrochemical methods such as cyclic voltammetry and surface analytical techniques such as XPS and ToF-SIMS.

2-MBT adsorption on copper surfaces

The adsorption of 2-MBT on copper surfaces was highly influenced by the pH of the electrolyte. This was due to the dominant conformer of the molecule — thiol, thione, or thiolate — in each electrolyte which resulted in either additional or fewer active sites in the molecule for bonding. Prior to adsorption of the inhibitor on the copper surfaces, the native oxides were reduced by cathodic pre-treatment of the surfaces either in the presence or absence of the inhibitor in the electrolyte. It was observed that in each electrolytic environment — acidic, neutral, and alkaline — the pre-treatment in absence of the inhibitor resulted in a nearly complete metallic state, with very little quantities of oxides trapped as thin islands at the interface. Although the pre-treatment in presence of the inhibitor also reduced the native oxides, XPS analysis revealed that there was still a larger coverage of unreduced oxides trapped at the interface between the organic layer and the metallic surface. Additionally, the trapped interfacial oxide islands were thicker in this case compared to that for the pre-treatment in absence of

the inhibitor. The quantity of these interfacial oxides resulted in differing structures of the organic films formed on the surface.

In acidic media, where the prevailing conformer of the molecule is its thione form, the bonding occurs by the sulphur atoms resulting in a strong chemisorbed organic layer on the surface. No evidence of nitrogen bonding was observed, most likely due to the hydrogen atom bonded to the nitrogen in the thione conformer. The presence of outer physisorbed layers of the molecule was also detected by both XPS and ToF-SIMS, although of varying thicknesses depending on the pre-treatment used and the exposure time to the inhibitor. Partial decomposition of the molecule was observed, resulting in free atomic sulphur bonded to metallic copper. On the sample pre-treated in absence of the inhibitor, the coverage of the molecule on the surface was wider due to lower quantities of interfacial oxides and the organic film was thicker due to a longer exposure time (1 hour) to the inhibitor. Upon anodic polarisation, further dissociation of the 2-MBT molecule was observed with an increase in the quantity of interfacial atomic sulphur, and defects were formed in the barrier layer thus compromising its protective properties.

In alkaline media, the bonding between the 2-MBT molecule and the copper surfaces also occurs by the sulphur atoms. However, a small fraction of nitrogen atoms are also involved in the bonding with the metallic surface, due to the additional reactive site of the molecule in its thiolate form, where the nitrogen atom does not have a hydrogen atom bonded to it. The ToF-SIMS results also indicated an interaction between sulphur and the residual oxide islands at the interface. Finally, the presence of Cu(I)-2-MBT complexes on the surface was evidenced by the ToF-SIMS depth profiles and the Cu LMM Auger spectra. These complexes, not observed in acidic media, were formed due to the interaction between the 2-MBT molecules and Cu(I) ions released from the native oxides upon cathodic polarisation. Since the sample pre-treated in presence of the inhibitor had a higher quantity of interfacial oxides, the formation of the metal-organic complexes was promoted on the sample resulting in thicker organic layers. Further complexes were formed upon anodic polarisation due to the oxidation of Cu metal ions to Cu(I) ions which then interact with the 2-MBT molecules, thus increasing the thickness of the organic layer on both samples.

In neutral environment, the bonding mechanisms were similar to that of the alkaline environment due to the equilibrium between the thione and thiolate forms of the molecule in neutral media. Sulphur along with a small fraction of nitrogen were bonded to metallic copper, and an interaction between sulphur and the oxide islands was suggested by ToF-SIMS. The formation of the metal-organic complexes was also observed. Although extended exposure time to the inhibitor resulted in a thicker organic film on the sample pre-treated in absence of 2-MBT, similar to the case in acidic environment, it also resulted in the increased thickness

of the interfacial oxide islands due to oxidation of the substrate at the defective regions of the 2-MBT layer. Anodic polarisation of the sample pre-treated in presence of 2-MBT increased the formation of metal-organic complexes due to the oxidation of Cu metal ions and the presence of trapped interfacial oxide islands acting as a source of Cu(I) ions, resulting in a thicker organic layer. However, this was not the case for the sample pre-treated in absence of 2-MBT followed by exposure to the inhibitor, indicating that the barrier layer was better formed and therefore more protective.

The cyclic voltammetry tests demonstrated that the 2-MBT films formed on copper did inhibit the corrosive attack of the substrate in acidic chloride and neutral chloride media, evidenced by a positive shift in the corrosion potential and a significant reduction in the anodic current density, and prevented the formation of copper chloride on the substrates. Furthermore, these 2-MBT films also inhibit the anodic oxidation of copper in the Cu(I) potential range in both alkaline media and in neutral chloride media. The pre-treatment used for the formation of the films had a major effect on the degree of corrosion inhibition and anodic oxidation inhibition. The presence of more interfacial oxide islands during pre-treatment with the inhibitor resulted in poorer protection of the substrate due to local defects in the barrier film. On the other hand, pre-treatment without the inhibitor followed by exposure to the inhibitor resulted in better barrier properties, due to lower quantities of interfacial oxides, with an enhanced protection of the surfaces obtained on longer exposure times to the inhibitor. Lastly, the presence of Cu(I)-2-MBT complexes did not offer any additional protection to the copper substrate.

2-MBI adsorption on copper surfaces

2-MBI adsorption in acidic media presents a stark contrast to that of 2-MBT in a similar environment. This has been attributed to the change of the active site element, i.e. from two sulphur and one nitrogen atoms in 2-MBT to one sulphur and two nitrogen atoms in 2-MBI. On a nearly metallic copper surface, achieved by pre-treatment in absence of the inhibitor, 2-MBI adsorbs by its nitrogen and sulphur atoms forming a chemisorbed layer. On the other hand, when pre-treatment of the surface was done in presence of the inhibitor, the bonding between 2-MBI and the substrate occurs only by its nitrogen atoms. Additionally, this pre-treatment method led to the formation of Cu(I)-2-MBI complexes in the chemisorbed layer, due to the release of Cu(I) ions from the native oxides followed by subsequent interaction with the inhibitor. The organic films formed by 2-MBI, with an inner chemisorbed layer and outer physisorbed layer, are much thicker than the 2-MBT organic films. These films inhibit copper dissolution in acidic chloride solution, with a reduction in current density and positive shift in potential. During anodic polarisation, the organic films grow in thickness due to

a build-up of metal organic complexes. However, the corrosion inhibition efficiency of the 2-MBI films is much lower than that of the 2-MBT films, despite the increased concentration of 2-MBI in the solution, the formation of thicker films, and the protection offered by the Cu(I)-2-MBI complexes. This effect is observed by the penetration of the chloride ions in the organic films leading to attack of the substrate on the sample pre-treated in presence of the inhibitor. On the sample pre-treated in absence of the inhibitor followed by its subsequent exposure to the 2-MBI molecule, the chloride ions do not reach the substrate indicating that electrochemical control of the surface during formation of the organic layer leads to a more protective barrier layer.

The results obtained from this work provide new insights on the functioning of organic inhibitors on copper. By understanding the mechanisms of inhibitor interaction with copper surfaces, methods were developed to enhance inhibitor action. The experimental conditions of this work represent real world conditions where an oxide-free and contaminant-free surface is unattainable. Although this leads to complications in data analysis, it is important to understand the effects they have on the adsorption of the inhibitor molecules and the susbsequent alteration of their performance. The optimization of the surface state prior to inhibitor adsorption resulted in a notable increase in inhibitor efficiency. This increase in effectiveness of the inhibitor was made possible by the electrochemical control of copper surfaces to obtain a relatively oxide-free surface, therby allowing the inhibitor to bond directly with the metallic surface and form a strong barrier layer. These vital findings can have far-reaching consequences on the way we use inhibitors for the protection of metals and alloys in crtical applications where failure is impermissible due to their potential aftermath.

Perspectives

Despite the advances of this project in understanding the bonding mechanisms of the two organic inhibitors on copper and the corrosion inhibition mechanisms, further work can be carried out to complement the work. The propositions are as follows:

- To study the effect of chloride ions on the 2-MBT films formed on copper in alkaline media.
- To investigate the effect of 2-MBT on the anodic oxidation of copper in Cu(II) potential range in alkaline media.
- To evaluate the adsorption mechanisms of 2-MBI on copper in neutral and alkaline media, with and without the presence of chloride ions.
- To investigate the effects of other aggressive ions, such as nitrates, sulphates, and

halides, on the protective capabilities of the organic films formed.

- To study the interaction of these inhibitors with copper alloys.
- Lastly, since this study is based on fundamental mechanisms of inhibitor interaction, it would be of particular interest to investigate their pertinence on pipelines, machinery, and other structures used in various fields of application.

APPENDIX A

Résumé étendu de thèse

Chapitre 1 : État de l'art

La corrosion est le processus de dégradation des matériaux qui résulte de leur exposition à l'environnement. C'est un phénomène qui touche la plupart des métaux, à l'exception des métaux nobles tels que l'or et le platine. Il entraîne une perte de résistance du matériau et peut même en altérer l'aspect, ce qui aboutit finalement à une lente défaillance/destruction du métal. Les dommages causés dans le monde entier par la corrosion sont considérables et sont estimés à environ 3,4 % du produit intérieur brut (PIB) mondial [1]. La corrosion d'un métal est un processus électrochimique impliquant des régions anodiques et cathodiques. La Figure A.1 présente le schéma d'un processus de corrosion où les réactions qui se produisent dans chaque région sont indiquées.

Le cuivre, 25ème élément le plus abondant sur terre, est un métal de transition avec un numéro atomique de 29 et un poids moléculaire de 63,546 g/mol [14]. Grâce à son point de fusion élevé de 1083°C [14], le cuivre est un excellent conducteur de chaleur et d'électricité. En outre, il s'agit d'un métal qui présente une ductilité et une malléabilité élevées. Ces propriétés du cuivre lui permettent d'être largement utilisé dans de nombreuses applications telles que les fils et les composants électriques, les tuyaux pour l'eau potable et les systèmes d'égouts, les machines industrielles, les pipelines pour le transport du pétrole et du gaz, ainsi que pour la bijouterie et les pièces de monnaie. Pour d'autres utilisations du cuivre, en

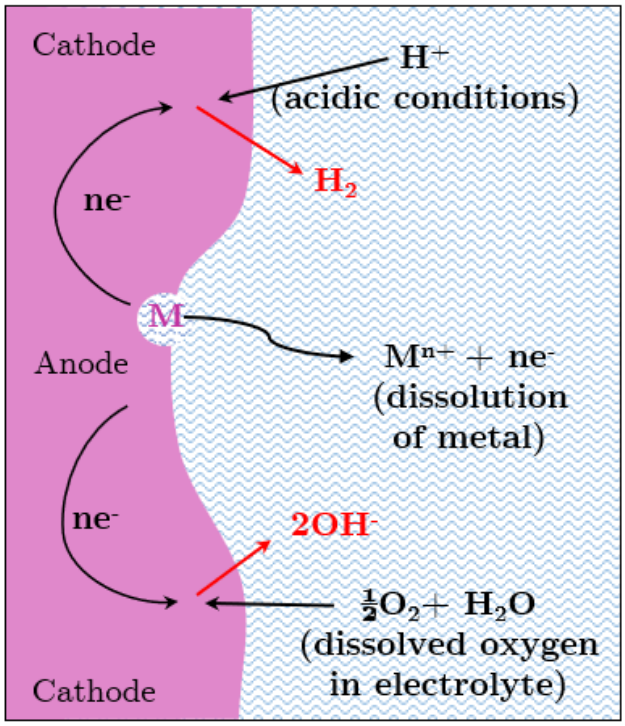

Figure A.1: Schéma montrant un processus de corrosion avec les réactions anodiques et cathodiques se produisant pour un métal M dans un électrolyte aqueux.

particulier dans les cas où une plus grande résistance est nécessaire, il est allié à d'autres métaux afin d'obtenir des propriétés supérieures.

En solution aqueuse, le cuivre se passive dans la plage de pH comprise entre 5 et 13, avec formation initiale d'une couche d'oxyde Cu_2O (Cu(I)). Le Cu_2O se forme aussi naturellement sur les surfaces de cuivre exposées à l'air. À des potentiels plus élevés, le cuivre s'oxyde à l'état Cu(II), ce qui entraîne la formation d'une couche d'oxyde CuO. Ces couches d'oxyde sont connues pour protéger la surface du métal cuivre contre la corrosion, car elles empêchent physiquement l'accès des ions corrosifs à la surface du métal [20, 21, 30, 32].

Bien que le cuivre soit quelque peu protégé dans les environnements neutres et alcalins, il est très vulnérable aux attaques dans les environnements acides où le film d'oxyde superficiel se dissout facilement, laissant le substrat métallique exposé aux agents corrosifs [15, 33–36]. Comme le montre le diagramme de Pourbaix de la Figure A.2, dans des conditions acides où le pH est inférieur à 5, le cuivre subit une corrosion. Ce phénomène a été attribué à l'instabilité des couches d'oxyde de cuivre dans cette plage de pH. En outre, dans des conditions neutres et alcalines, des espèces agressives telles que les chlorures et les nitrates en concentrations élevées peuvent déstabiliser les couches protectrices d'oxyde pour interagir avec le substrat métallique [33, 34, 38], provoquant une rupture de la passivité et l'apparition de corrosion

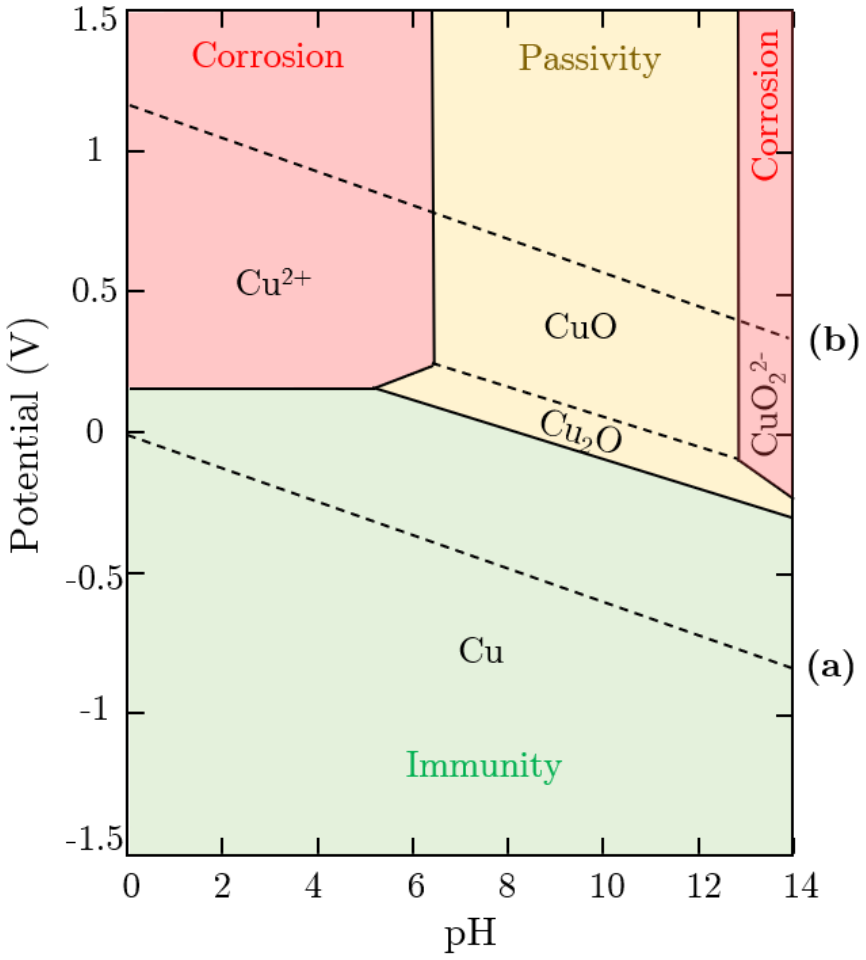

Figure A.2: Diagramme de Pourbaix du système cuivre-eau à 25°C. La figure est tirée de l'Atlas des équilibres électrochimiques en solutions aqueuses de Marcel Pourbaix [8].

localisée [39–42].

Les conséquences de la corrosion exigent que les métaux utilisés pour diverses applications soient protégés de la corrosion. L'une des techniques pour ralentir la corrosion est l'application d'inhibiteurs, des composés chimiques qui empêchent les réactions de se produire à la surface d'un métal en formant une barrière isolante sur la surface, ce qui inhibe la corrosion du métal [37, 53–55]. Ces composés sont ajoutés en très petites quantités soit dans l'environnement, par exemple dans l'électrolyte ou dans les revêtements, soit directement à la surface du métal, dans le but de réduire la vitesse de la corrosion ou la bloquer complètement. Dans ce travail, l'inhibition de la corrosion offerte par les molécules organiques à base de soufre, le 2-mercaptobenzothiazole et le 2-mercaptobenzimidazole, a été étudiée.

Le 2-Mercaptobenzothazole (2-MBT), $C_7H_5NS_2$, est un composé organique largement utilisé comme inhibiteur de corrosion pour de nombreux métaux et leurs alliages. Selon les conditions

environnementales, le 2-MBT existe sous sa forme thiol, thione ou thiolate [77–79]. Les différents conformères de la molécule de 2-MBT sont illustrés Figure A.3. Les hétéroatomes S et N à forte densité électronique sont des sites actifs qui peuvent se lier de manière coordonnée ou non à des atomes de surface, ce qui permet à la molécule de s'adsorber fortement et de former un film dense et protecteur à la surface du métal [83–85, 87–89, 95, 99].

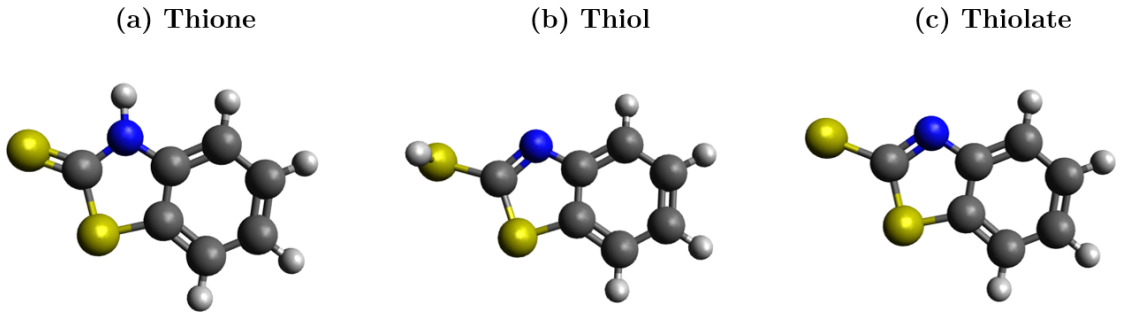

Figure A.3: Modèles illustrant les différents conformères de la molécule de 2-MBT ($C_7H_5NS_2$): (a) forme thione, (b) forme thiol, et (c) forme thiolate. Les atomes jaunes représentent le soufre, les atomes bleus représentent l'azote, les atomes gris représentent le carbone et les atomes blancs représentent les atomes d'hydrogène de la molécule..

Plusieurs travaux expérimentaux ont porté sur les mécanismes de liaison du 2-MBT avec les surfaces de cuivre. Certains auteurs ont conclu que la liaison se produit par l'intermédiaire des deux atomes de soufre de la molécule [84], tandis que d'autres ont indiqué qu'elle se faisait uniquement par l'intermédiaire de l'atome de soufre exocyclique [87]. En outre, l'implication de l'atome d'azote et du soufre exocyclique a également été proposée [83, 89]. La formation de complexes organométalliques due à une interaction entre les molécules de 2-MBT et le cuivre (métal/oxydes) a également été suggérée [79, 80, 87, 94].

Le 2-mercaptobenzimidazole (2-MBI), $C_7H_6N_2S$, est une autre molécule organique souvent utilisée comme inhibiteur de corrosion pour protéger les métaux tels que le cuivre et ses alliages, le zinc, les aciers inoxydables et les alliages d'aluminium [72, 75, 76, 99–105]. Les différents conformères de la molécule de 2-MBI sont représentés Figure A.4. Les changements dans le conformère dominant sont dus au pKa de la molécule, qui est de 10,4 [107, 108], déterminant ainsi la stabilité de la molécule en fonction du pH du milieu et des autres espèces présentes dans ce milieu.

Dans les travaux de Wu et al. [99, 100], Il a été constaté que le 2-MBI s'adsorbait sur les surfaces de cuivre métallique par son atome de soufre et ses deux atomes d'azote, la molécule étant posée à plat sur le cuivre. Sur les surfaces oxydées, la liaison se fait par l'atome de soufre et un seul atome d'azote avec une géométrie inclinée sur la surface. Ces mécanismes de

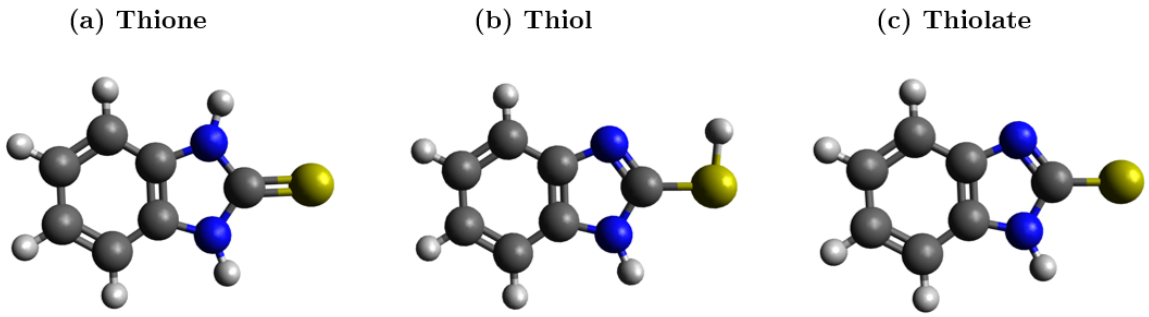

Figure A.4: Modèles illustrant les différents conformères de la molécule de 2-MBI ($C_7H_6N_2S$): (a) forme thione, (b) forme thiol et (c) forme thiolate. Les atomes jaunes représentent le soufre, les atomes bleus représentent l'azote, les atomes gris représentent le carbone et les atomes blancs représentent les atomes d'hydrogène de la molécule.

liaison ont également été suggérés par les calculs de théorie de la fonctionnelle de la densité (DFT) dans les travaux de Chiter et al. [110, 111]. La formation d'un film de complexes Cu(I)-MBI a été proposée par quelques auteurs [79, 108, 112]. Xue et al. [112] ont rapporté que les films de complexes formés entre le Cu et le 2-MBI différent en fonction de l'état d'oxydation du cuivre. Lorsque le 2-MBI réagit avec des oxydes de cuivre, il en résulte la formation d'un film complexe Cu(I)-2-MBI, alors que lorsque la molécule interagit avec du cuivre métallique, le film complexe formé est principalement $Cu^{+}MBI^{-}$ ou $Cu_2{}^{+}MBI^{2-}$.

Malgré de nombreux travaux, il subsiste des ambiguïtés sur la formation et les propriétés de protection des films organiques de 2-MBI et de 2-MBT formés sur les surfaces de cuivre métallique et de cuivre oxydé, en particulier en présence d'espèces agressives telles que les ions chlorure qui peuvent entrer en compétition avec les molécules d'inhibiteur pour interagir avec le métal. En outre, le rôle des oxydes natifs de surface du cuivre sur les mécanismes de liaison interfaciale et les propriétés d'inhibition a été négligé dans la plupart des cas. Le présent travail vise à clarifier ces questions et à déterminer le rôle du pH sur l'adsorption des molécules inhibitrices, l'effet du prétraitement électrochimique de la surface sur les mécanismes d'adsorption, l'influence des différents sites actifs dans les molécules et, enfin, la stabilité des films organiques sous polarisation anodique. Pour ce faire, nous avons utilisé une approche intégrée combinant méthodes électrochimiques et techniques analytiques de science des surfaces telles que la spectroscopie photoélectronique à rayons X (XPS) et la spectrométrie de masse d'ions secondaires à temps de vol (ToF-SIMS).

Chapitre 2: Techniques expérimentales et méthodologie

Les échantillons utilisés pour l'analyse expérimentale étaient des échantillons polycristallins de haute pureté (ETP-Cu). La préparation de la surface a été réalisée en deux étapes, par polissage mécanique puis polissage électrochimique. Les surfaces ont d'abord été poncées mécaniquement à l'aide de papiers abrasifs en carbure de silicium jusqu'à une granulométrie de 4000 afin d'obtenir une surface plane. Pour obtenir une surface miroir, les échantillons ont ensuite été polis mécaniquement à l'aide de pâtes diamantées de granulométrie 6 µm, 3 µm, 1 µm, et enfin 0.25 µm. Après la dernière étape de polissage mécanique, les échantillons ont été nettoyés aux ultrasons pendant 5 minutes dans des bains successifs d'acétone, d'éthanol et d'eau ultra-pure.

Le polissage électrochimique a été effectué afin d'éliminer la couche écrouie laissée par le polissage mécanique et de minimiser la contamination pouvant persister à la surface [126]. Il a été réalisé en utilisant une configuration à deux électrodes avec l'échantillon de cuivre comme électrode de travail et une plaque de cuivre comme contre-électrode dans un bain de solution d'acide orthophosphorique (H_3PO_4) à 60 % [125]. Une tension constante de 1,4 V a été appliquée à l'électrode de travail pendant 4 minutes pour dissoudre la couche supérieure et éliminer les contaminations contenues dans cette couche. Enfin, l'échantillon a été rincé avec une solution de H_3PO_4 à 10 %, puis avec de l'eau ultra-pure, avant d'être séché à l'azote.

Les électrolytes utilisés pour les expériences sont répertoriés dans le Table A.1, en fonction de l'environnement et avec le pH mesuré à température ambiante. Chaque environnement se compose d'un électrolyte sans inhibiteur, utilisé comme électrolyte de référence, et d'un électrolyte avec inhibiteur, 2-MBT ou 2-MBI, présent. Une concentration plus faible de 2-MBT a été utilisée pour les solutions acides et presque neutres en raison de la faible solubilité de cet inhibiteur dans les environnements à pH plus bas [127, 128].

Un prétraitement cathodique a été effectué avant les expériences afin de réduire le film d'oxyde natif couvrant la surface. Ce traitement a été effectué en présence ou en l'absence de l'inhibiteur dans la solution. Après immersion des échantillons au potentiel de circuit ouvert (OCP), le potentiel a été balayé cathodiquement, à une vitesse de 20 mV/s, jusqu'au début de l'évolution de l'hydrogène, puis balayé en retour jusqu'au potentiel où le courant mesuré était d'environ 0 ± 2 µA. Ce cycle de prétraitement cathodique a été répété deux fois de plus pour assurer une réduction maximale des oxydes natifs de surface.

Pour les substrats prétraités en présence de l'inhibiteur dans la solution, les tests de voltampérométrie cyclique ont été réalisés juste après le prétraitement cathodique du sub-

Table A.1: Concentrations des électrolytes avec et sans inhibiteur utilisés pour les expériences électrochimiques et valeurs de pH mesurées.

Environnement	Concentration de l'inhibiteur	pH mesuré (± 0.1)
0.1 M NaOH	-	13.5
	1 mM 2-MBT	13.6
	1 mM 2-MBI	13.6
10 mM HCl	-	2.3
	0.1 mM 2-MBT	2.6
	1 mM 2-MBI	2.4
0.5 M NaCl	-	5.3
	0.1 mM 2-MBT	5.2

strat. Pour les substrats prétraités en l'absence d'inhibiteur dans la solution, la solution de référence a été remplacée par une solution contenant un inhibiteur après le troisième cycle de prétraitement cathodique. Les substrats ont ensuite été exposés dans la solution pendant 2 minutes ou 1 heure à un potentiel fixe avant d'entamer les tests de voltampérométrie cyclique. Un schéma récapitulant le protocole expérimentale est présenté Figure A.5.

Des tests de voltampérométrie cyclique ont été effectués pour déterminer le comportement d'inhibition de la corrosion/oxydation des surfaces de cuivre. Ces tests ont été réalisés en balayant le potentiel depuis le point de courant nul jusqu'au pic anodique, correspondant à l'initiation de la corrosion pour les expériences en milieux HCl et NaCl ou à l'oxydation anodique dans la région Cu(I) pour les expériences en milieu NaOH, suivi d'un balayage inverse jusqu'au début de l'évolution de l'hydrogène, puis d'un retour au potentiel de départ. Les expériences ont été réalisées avec une vitesse de balayage de 20 mV/s. Chaque expérience a été répétée 3 fois pour assurer la reproductibilité des résultats.

La spectroscopie de photoélectrons X (XPS) est une technique spectroscopique très sensible à la surface qui permet d'obtenir des informations telles que l'environnement chimique des atomes, la composition élémentaire des couches superficielles d'un matériau et la stratification éventuelle de la surface. L'XPS repose sur le principe de l'effet photoélectrique, un phénomène découvert par Heinrich Hertz en 1883 [131]. L'effet photoélectrique est l'émission d'électrons lorsqu'un rayonnement électromagnétique (lumière, rayons X, rayons ultraviolets) frappe un

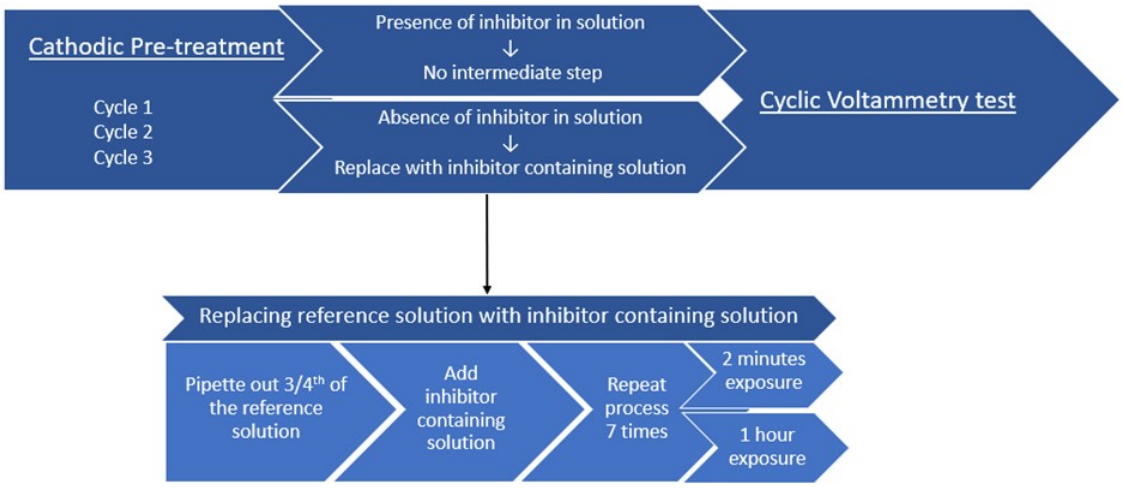

Figure A.5: Schéma montrant le protocole de prétraitement cathodique effectué à la fois dans la solution de référence sans inhibiteur et dans la solution contenant un inhibiteur. Pour le processus de prétraitement cathodique dans la solution de référence sans inhibiteur, la méthode de remplacement de la solution est également détaillée.

matériau (Figure A.6). Les électrons émis par le matériau sont appelés photoélectrons.

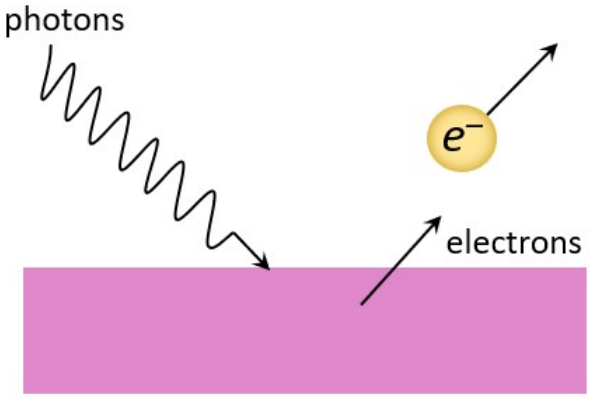

Figure A.6: Schéma montrant le principe de l'effet photoélectrique.

Pour l'XPS, une source de rayons X est utilisée pour produire des photons d'une certaine énergie, qui sont dirigés vers la surface de l'échantillon. Ces photons provoquent une excitation photoélectrique de l'échantillon qui entraîne l'émission de photoélectrons ayant une énergie cinétique de Ek (Figure A.7). Ces photoélectrons sont détectés et leur énergie cinétique est mesurée pour déterminer la nature et l'environnement chimique de l'atome émetteur. Cela est possible grâce à l'énergie de liaison de l'électron E_b, qui est caractéristique de l'atome émetteur. Si l'on connaît l'énergie cinétique E_k, l'énergie du photon hv, et le travail de sortie du spectromètre ϕ, l'énergie de liaison de l'électron émis peut être calculée à l'aide de l'équation ci-dessous.

$$E_b = hv - E_k - \phi \tag{A.1}$$

Dans ce travail, l'analyse XPS a été réalisée avec un spectromètre Thermo Electron Escalab 250 Xi. Une taille de spot de rayons X de 900 µm de diamètre a été utilisée. Les spectres XPS globaux ont été enregistrés entre -10 et 1350 eV avec une énergie de passage de 50 eV et un pas de 1 eV. Les spectres à haute résolution des niveaux de coeur C 1s, N 1s, O 1s, Na 1s, S 2p, Cl 2p, Cu 2p, de la transition Auger Cu LMM et du niveau de Fermi ont été enregistrés avec une énergie de passage de 20 eV et un pas de 0,1 eV. Les spectres ont été enregistrés avec un angle d'émission des photoélectrons collectés de 90°.

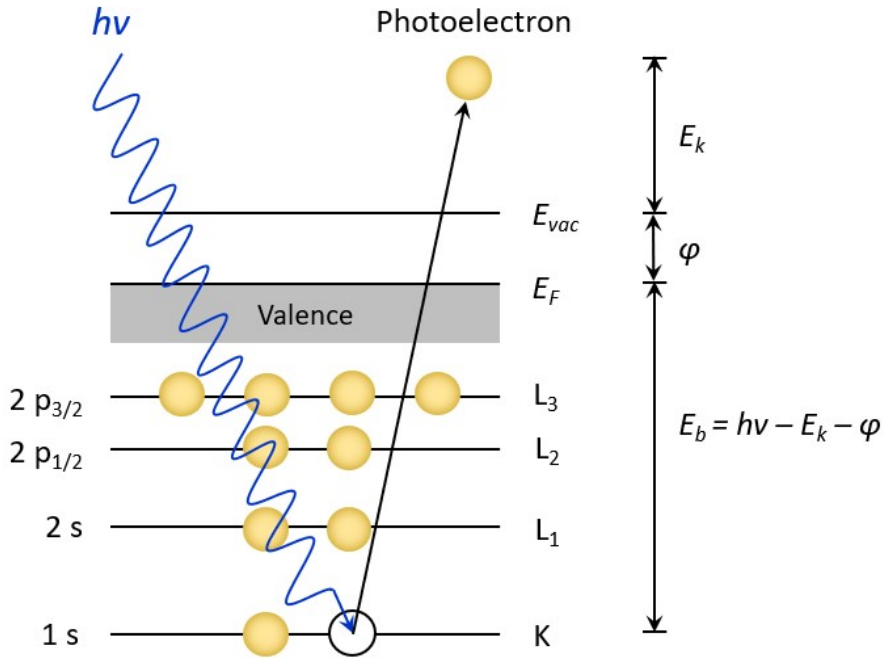

Figure A.7: Schéma montrant le processus de photoémission d'un électron de niveau cœur à partir d'un atome du matériau.

La spectrométrie de masse d'ions secondaires à temps de vol (ToF-SIMS) est une technique d'analyse de surface ultrasensible utilisée pour effectuer des analyses élémentaires, isotopiques et moléculaires des surfaces. La technique consiste à bombarder la surface avec des ions primaires qui provoquent une cascade de collisions sur une profondeur d'environ 1 nm et génère l'émission d'espèces (électrons, particules neutres et ions) (Figure A.8). Parmi toutes les espèces éjectées, seuls les atomes ou amas d'atomes de surface ionisés sont détectés par un analyseur de temps de vol. Cet analyseur trie les ions en fonction de leur rapport masse/charge, qui est déterminé par le temps qu'ils mettent à parcourir le trajet entre l'entrée de l'analyseur et le détecteur. Pour une charge donnée, les ions plus légers traversent plus

rapidement l'analyseur, puisque le temps de vol est directement proportionnel à la racine carrée du rapport masse/charge. Cela permet d'identifier les ions en mesurant le temps nécessaire aux ions secondaires pour arriver à l'analyseur.

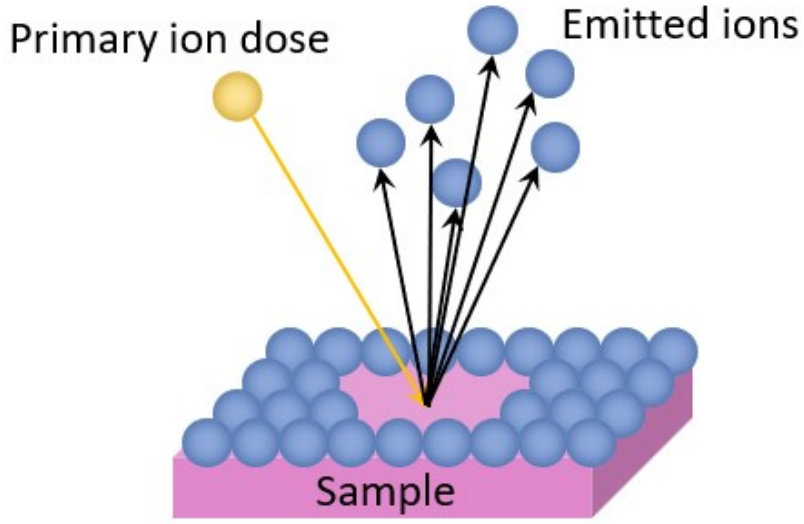

Figure A.8: Schéma de l'émission d'ions secondaires.

Pour effectuer une analyse de surface en profondeur, deux faisceaux d'ions fonctionnent alternativement. Un canon à ions de pulvérisation est utilisé pour pulvériser un cratère sur la surface, tandis qu'après chaque étape de pulvérisation, le fond du cratère est analysé par le faisceau d'ions primaires. Grâce à cette méthode, les spectres de masse sont enregistrés à chaque étape, ce qui permet d'obtenir un profil élémentaire sous-surfacique en traçant l'intensité d'un ion secondaire caractéristique en fonction du temps de pulvérisation.

Les profils élémentaires en profondeur ont été obtenus dans ce travail à l'aide d'un spectromètre ToF-SIMS 5 (IonTof - Münster Allemagne), fonctionnant à une pression de base de 5 x 10^{-9} mbar. L'analyse en mode SIMS statique a été effectuée en utilisant des ions primaires Bi^+ d'une énergie de 25 keV à un courant cible de 1,2 pA sur une surface de 100 x 100 μm^2. Les profils de profondeur ont été obtenus en entrelaçant analyse SIMS statique et pulvérisation au moyen d'un canon à ions Cs^+ de 0,5 keV délivrant un courant cible de 20 nA sur une zone de 500 x 500 μm^2. Les deux faisceaux d'ions étaient à une incidence de 45° par rapport à la surface de l'échantillon et bien alignés pour assurer l'analyse au centre du cratère pulvérisé. Les ions secondaires négatifs ont été enregistrés en raison de leur plus grande sensibilité aux fragments provenant de matrices oxydées. Trois mesures ont été enregistrées dans différentes régions de chaque échantillon afin de garantir la reproductibilité. Le logiciel SurfaceLab v6.5 a été utilisé pour l'acquisition des données et l'analyse post-traitement.

Chapitre 3: Etat de surface du cuivre

Les états chimiques d'une surface de cuivre sans oxyde préparée dans des conditions UHV, d'une surface polie mécaniquement et d'une surface polie électrochimiquement ont été caractérisés par XPS. La surface de cuivre préparée sous UHV a été étudiée pour obtenir les énergies de liaison (BE) de référence, les largeurs à mi-hauteur (FWHM) et la forme des spectres obtenus pour une surface métallique sans oxyde. L'échantillon de cuivre poli mécaniquement a été analysé pour étudier les effets du polissage et la présence d'éventuels contaminants. Enfin, la surface de cuivre polie électrochimiquement a été étudiée pour déterminer les changements survenant au cours du processus de polissage électrochimique, à savoir la nature et la quantité de contaminants qui persistent et la nature de la couche d'oxyde présente à la surface après polissage électrochimique. Il a été observé que l'échantillon de cuivre sans oxyde préparé sous UHV est exempt de contaminants tels que l'oxygène, le soufre et l'azote. Une petite fraction de contamination par le carbone (1 %) a été observée à la surface, probablement due à une contamination résiduelle par lors de la préparation par bombardement ionique puis recuit. Toutefois, la quantité de cette contamination au carbone était suffisamment faible pour ne pas interférer avec les valeurs de référence des BE et FWHM pour le cuivre métallique.

Sur le poli mécanique, une quantité importante de contaminants - carbone, soufre, azote et oxygène - a été trouvée sur la surface. Le film d'oxyde formé à la surface après le polissage mécanique est principalement constitué de Cu_2O, bien qu'une petite quantité de CuO ait également été observée dans le spectre Auger Cu LMM et attestée par le pic satellite trouvé à 947 eV dans le spectre Cu 2p. L'état de surface du cuivre après polissage mécanique n'est pas aussi propre qu'on pourrait le penser, malgré le nettoyage ultrasonique de l'échantillon de cuivre dans l'acétone, l'éthanol et l'eau ultra-pure après le processus de polissage.

L'échantillon de cuivre poli électrochimiquement présentait beaucoup moins de contaminants à la surface que l'échantillon poli mécaniquement. Nous avons observé des quantités négligeables de soufre et d'azote, et une quantité réduite de contamination par le carbone par rapport à l'échantillon poli mécaniquement. Cependant, la présence d'une espèce de phosphate de cuivre a été observée. Cette espèce se forme soit pendant le processus de polissage électrochimique, soit pendant le processus de rinçage après le polissage électrochimique. On a émis l'hypothèse que ce film de phosphate de cuivre était essentiel pour limiter la croissance du film d'oxyde sur la surface du cuivre après le polissage électrochimique. Cependant, il se dissout/ lave au cours des expériences électrochimiques menées après le polissage électrochimique, et ne reste donc pas comme une espèce interférente au cours des expériences. Le polissage électrochimique permet ainsi d'obtenir un état de surface plus propre de l'échantillon de cuivre et il est

préférable comme point de départ de nos expériences.

Chapitre 4: Amélioration de l'inhibition de la corrosion du cuivre en milieu acide par contrôle cathodique de la formation de l'interface avec le 2-mercaptobenzothiazole

Dans ce chapitre, la formation de l'interface inhibitrice 2-MBT/Cu sous contrôle électrochimique et la manière dont elle améliore la résistance à la corrosion du cuivre dans un environnement acide ont été étudiées. Avant adsorption de l'inhibiteur, les oxydes natifs ont été réduits par un prétraitement cathodique des surfaces en présence ou en l'absence de l'inhibiteur dans l'électrolyte. Le prétraitement en l'absence d'inhibiteur génère un état métallique presque pur, avec de très faibles quantités d'oxydes piégés sous forme d'îlots à l'interface. Bien que le prétraitement en présence de l'inhibiteur réduise également les oxydes natifs, l'analyse XPS a révélé qu'il subsistait une plus grande couverture d'îlots d'oxydes non réduits piégés à l'interface entre la couche organique et la surface métallique. En outre, les îlots d'oxydes interfaciaux piégés sont plus épais dans ce cas que pour le prétraitement en l'absence d'inhibiteur.

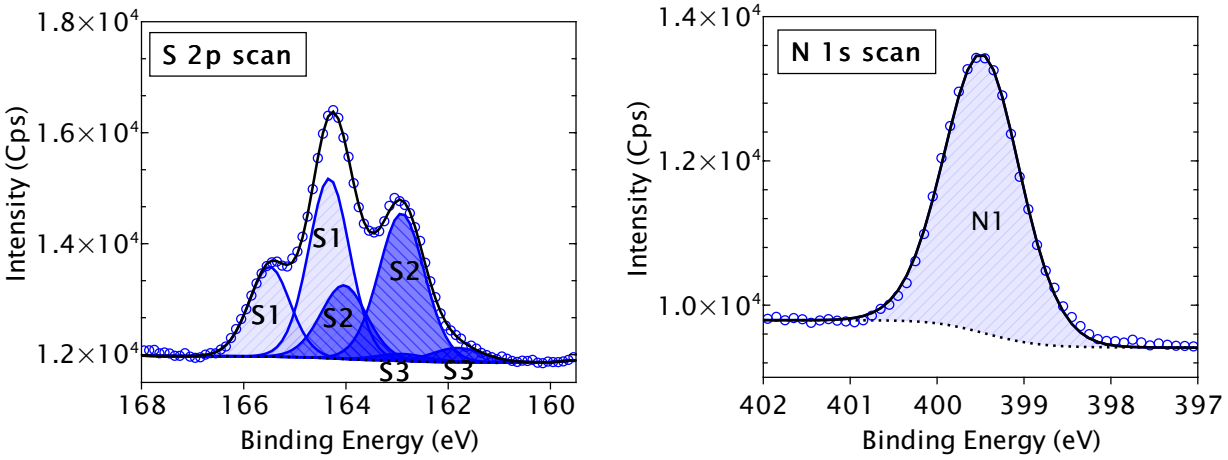

Figure A.9: Spectres XPS S 2p et N 1s après exposition du cuivre à la solution de 10 mM HCl + 0,1 mM 2-MBT à l'état réduit et prétraitement en présence de 2-MBT.

En milieu acide, où le conformère dominant de la molécule est sa forme thione, la liaison avec le cuivre se fait par les atomes de soufre, comme le montre la présence du composant S3 (Figure A.9). Cette liaison traduit la formation d'une couche organique chimisorbée à la surface. Aucun signe de liaison chimique du cuivre avec l'azote n'a été observé, probablement en raison de l'atome d'hydrogène lié à l'azote dans le conformère thionique. La présence de couches physisorbées externes de la molécule a également été détectée à la fois par XPS et

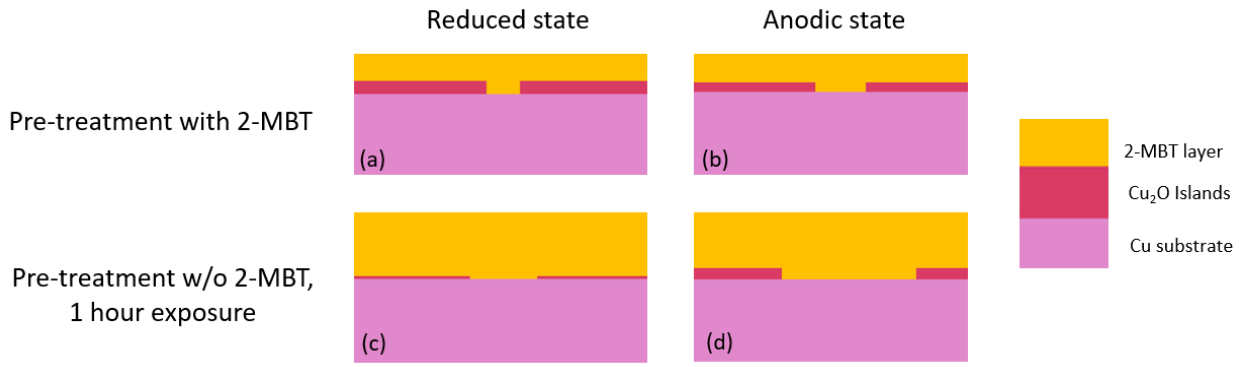

Figure A.10: Schéma montrant les différences de taux de couverture et d'épaisseur des îlots d'oxyde et d'épaisseur de la couche de 2-MBT déterminées par analyse XPS de la surface pour (a) l'état réduit, prétraitement avec MBT, (b) l'état anodique, prétraitement avec MBT, (c) l'état réduit, prétraitement sans MBT, 1 h d'exposition au MBT, (d) l'état anodique, prétraitement sans MBT, 1 h d'exposition au MBT.

ToF-SIMS, leur épaisseur variant en fonction du type de prétraitement utilisé et du temps d'exposition à l'inhibiteur. Une décomposition partielle de la molécule a également été observée, donnant lieu à un soufre atomique libre lié au cuivre métallique. Sur l'échantillon prétraité en l'absence d'inhibiteur, le taux de couverture de la molécule sur la surface est plus élevé en raison de quantités plus faibles d'oxydes interfaciaux résiduels et le film organique est plus épais en raison d'un temps d'exposition plus long (1 heure) à l'inhibiteur (Figure A.10). Lors de la polarisation anodique, une dissociation supplémentaire de la molécule de 2-MBT a été observée générant une augmentation de la quantité de soufre atomique interfacial. Des défauts sont formés dans la couche barrière, compromettant ainsi ses propriétés protectrices.

Les tests de voltampérométrie cyclique, présentés Figure A.11, démontrent que les films de 2-MBT formés sur le cuivre inhibent l'attaque corrosive du substrat en milieu acide chloruré, comme en témoignent un déplacement positif du potentiel de corrosion et une réduction significative de la densité du courant anodique. Ces films empêchent la formation de chlorure de cuivre sur les substrats. Le prétraitement utilisé pour la formation des films a un effet majeur sur le degré d'inhibition de la corrosion. La présence d'un plus grand nombre d'îlots d'oxyde interfaciaux pendant le prétraitement avec l'inhibiteur entraîne une moins bonne protection du substrat en raison de défauts locaux dans le film barrière. D'autre part, le prétraitement sans inhibiteur suivi d'une exposition à l'inhibiteur permet d'obtenir de meilleures propriétés barrière, en raison de quantités moindres d'oxydes interfaciaux, avec une protection accrue des surfaces obtenue pour des temps d'exposition plus longs à l'inhibiteur.

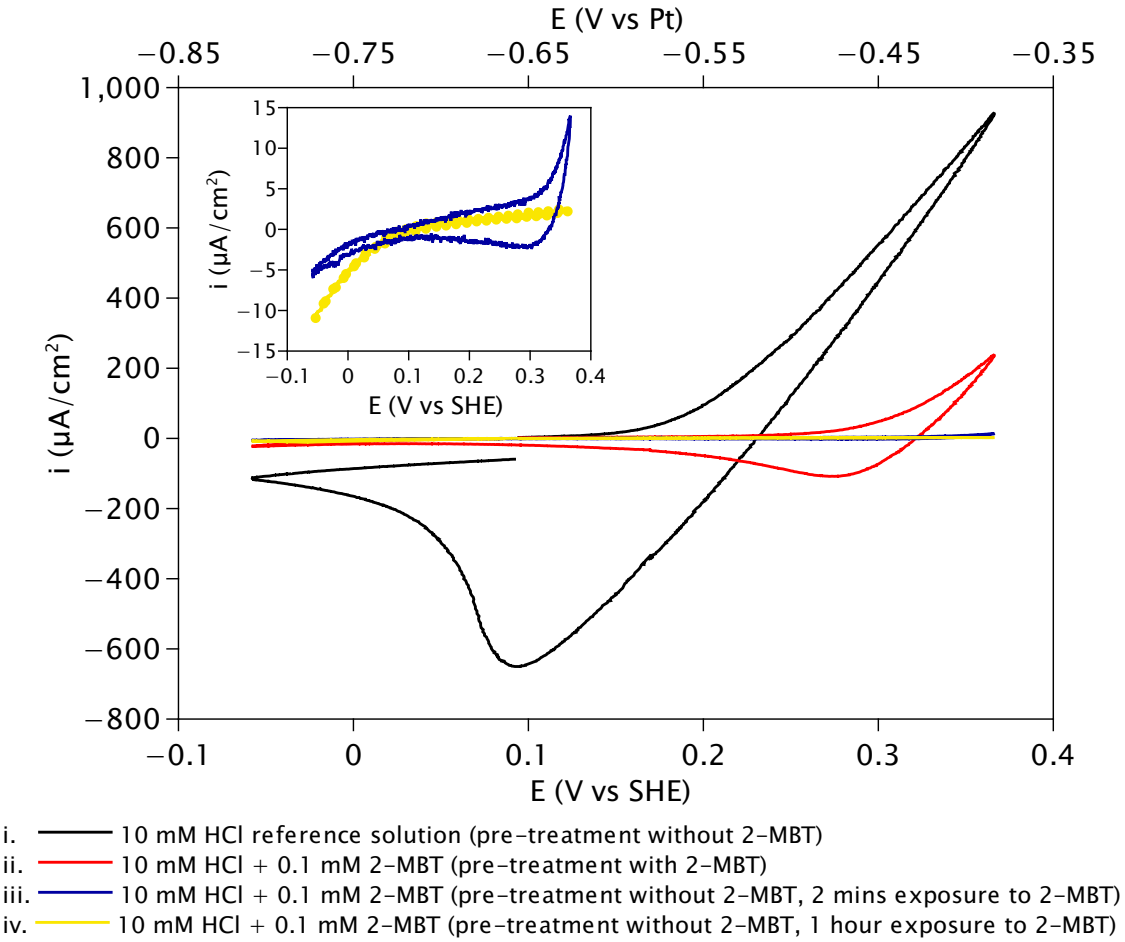

Figure A.11: Voltammogrammes du cuivre montrant la dissolution anodique en l'absence ou en présence de 2-MBT dans différentes conditions de prétraitement (vitesse de balayage de 20 mV/s). L'encadré montre les voltammogrammes agrandis pour les deux expériences réalisées après un prétraitement sans 2-MBT.

Chapitre 5: Adsorption de l'inhibiteur organique 2-mercaptobenzothiazole et effets sur l'oxydation anodique du cuivre en milieu alcalin

Dans ce chapitre, les effets du 2-MBT sur l'oxydation anodique du cuivre ont été étudiés après adsorption dans un environnement alcalin. Il a été établi que la présence d'oxyde natif sur la surface joue un rôle majeur dans la formation et l'efficacité ultérieure de la couche organique en tant que barrière contre l'activité anodique. La réduction du film d'oxyde natif par prétraitement cathodique effectué en l'absence de 2-MBT dans la solution génère un état presque métallique de la surface, alors qu'une réduction incomplète du film d'oxyde natif a été observée en présence de 2-MBT, en raison de l'adsorption du 2-MBT sur l'oxyde de cuivre et donc du blocage de l'électro-réduction.

La couche barrière organique formée est un système multicouche. La couche interne chimisorbée est liée au substrat de cuivre principalement par les atomes de soufre des molécules, comme le montrent les spectres XPS et les profils de profondeur ToF-SIMS. En outre, une fraction limitée des molécules est également liée directement au substrat métallique par l'atome d'azote, en raison du site réactif supplémentaire de la molécule sous sa forme thiolate. Les résultats ToF-SIMS, présentés Figure A.12, indiquent également une interaction entre le soufre et les îlots d'oxyde résiduels à l'interface. Enfin, la présence de complexes Cu(I)-2-MBT est indiquée par les profils de profondeur ToF-SIMS. En effet, l'intensité plus élevée du profil des ions $CuC_7H_4NS_2^-$ et du profil des ions Cu^- pendant les 4 premières secondes de pulvérisation indique que ces complexes sont adsorbés sur la surface la plus externe des échantillons. Ces complexes, non observés en milieu acide, sont formés par interaction entre les molécules de 2-MBT et les ions Cu(I) libérés des oxydes natifs lors de la polarisation cathodique, comme le confirment les spectres Auger de Cu LMM. L'échantillon prétraité en présence de l'inhibiteur présentant une plus grande quantité d'oxydes interfaciaux, la formation des complexes organométalliques est favorisée, produisant des couches organiques plus épaisses.

La formation de la couche de 2-MBT sur la surface du substrat de cuivre inhibe la croissance de l'oxyde anodique dans la région Cu(I) (Figure A.13). Des temps d'exposition plus longs à l'inhibiteur d'une surface avec des quantités d'oxydes négligeables augmentent le pouvoir bloquant de la couche barrière organique vis-à-vis de la croissance de l'oxyde anodique (Figure A.13c). L'échantillon prétraité en présence de 2-MBT, qui forme des couches organiques plus épaisses en raison de la formation accrue de complexes organométalliques, est le plus bloquant vis-à-vis de la croissance des oxydes anodiques (Figure A.13d). Lors de la polarisation anodique, il a été constaté que les couches barrières continuaient à s'épaissir. La forme thiolate du 2-MBT, le conformère dominant dans un environnement alcalin, offrirait des possibilités de liaison supplémentaires aux atomes de Cu et aux ions Cu(I) libérés par l'oxydation du substrat, formant d'autres complexes Cu-2-MBT et augmentant ainsi l'épaisseur de la couche organique barrière.

Chapitre 6: Inhibition des stades initiaux de corrosion du cuivre par adsorption du 2-mercaptobenzothiazole et effets des oxydes interfaciaux en milieu neutre chloruré

Dans cette partie, l'inhibition de la corrosion du cuivre par le 2-MBT a été étudiée dans une solution de NaCl de pH presque neutre après adsorption de l'inhibiteur organique. Le soufre ainsi qu'une petite fraction de l'azote sont liés au cuivre métallique, comme l'indiquent les

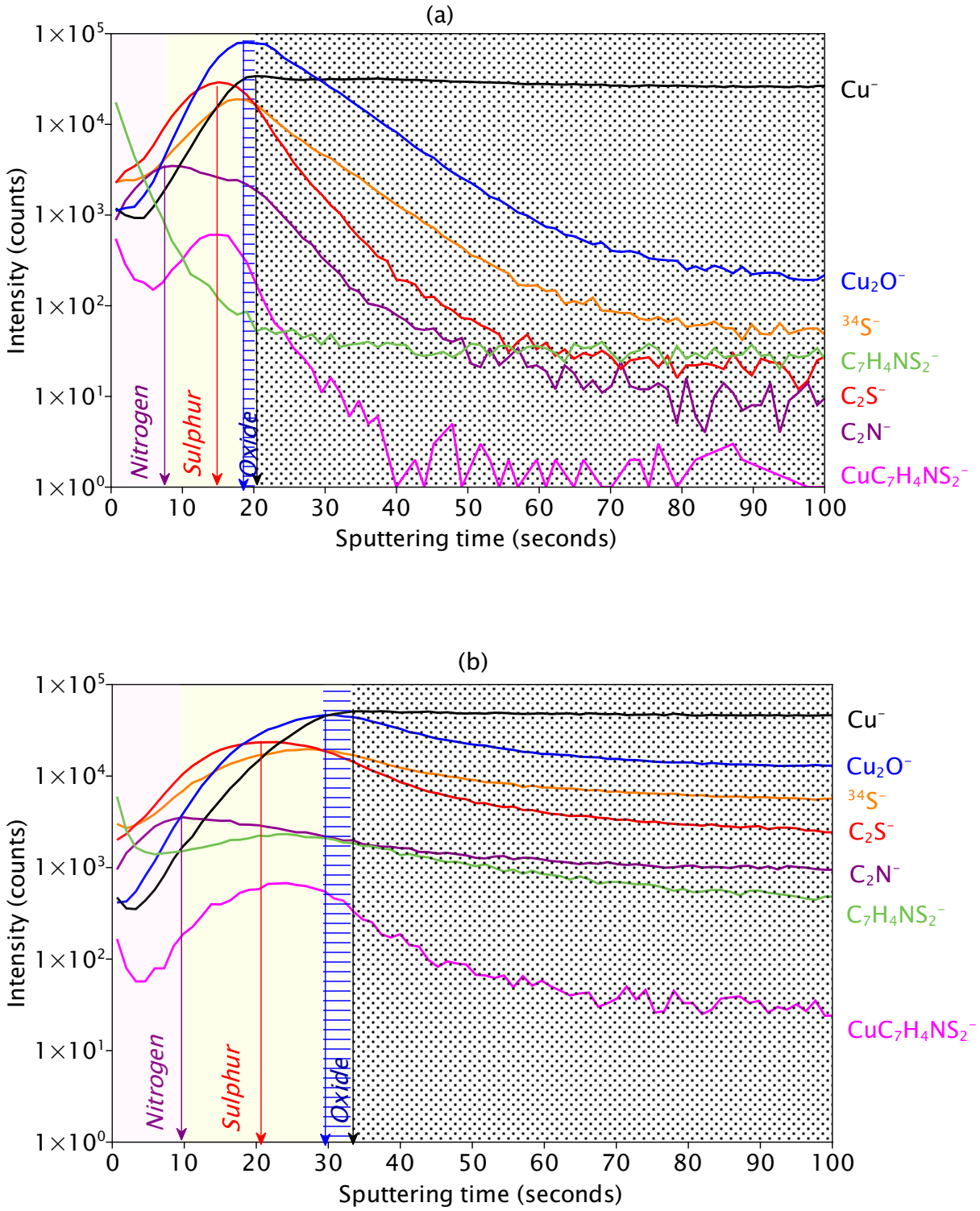

Figure A.12: Profils de profondeur ToF-SIMS des interfaces inhibitrices obtenues à l'état réduit après (a) un prétraitement cathodique en l'absence de 2-MBT suivi d'une heure d'exposition au 2-MBT et (b) un prétraitement cathodique en présence de 2-MBT.

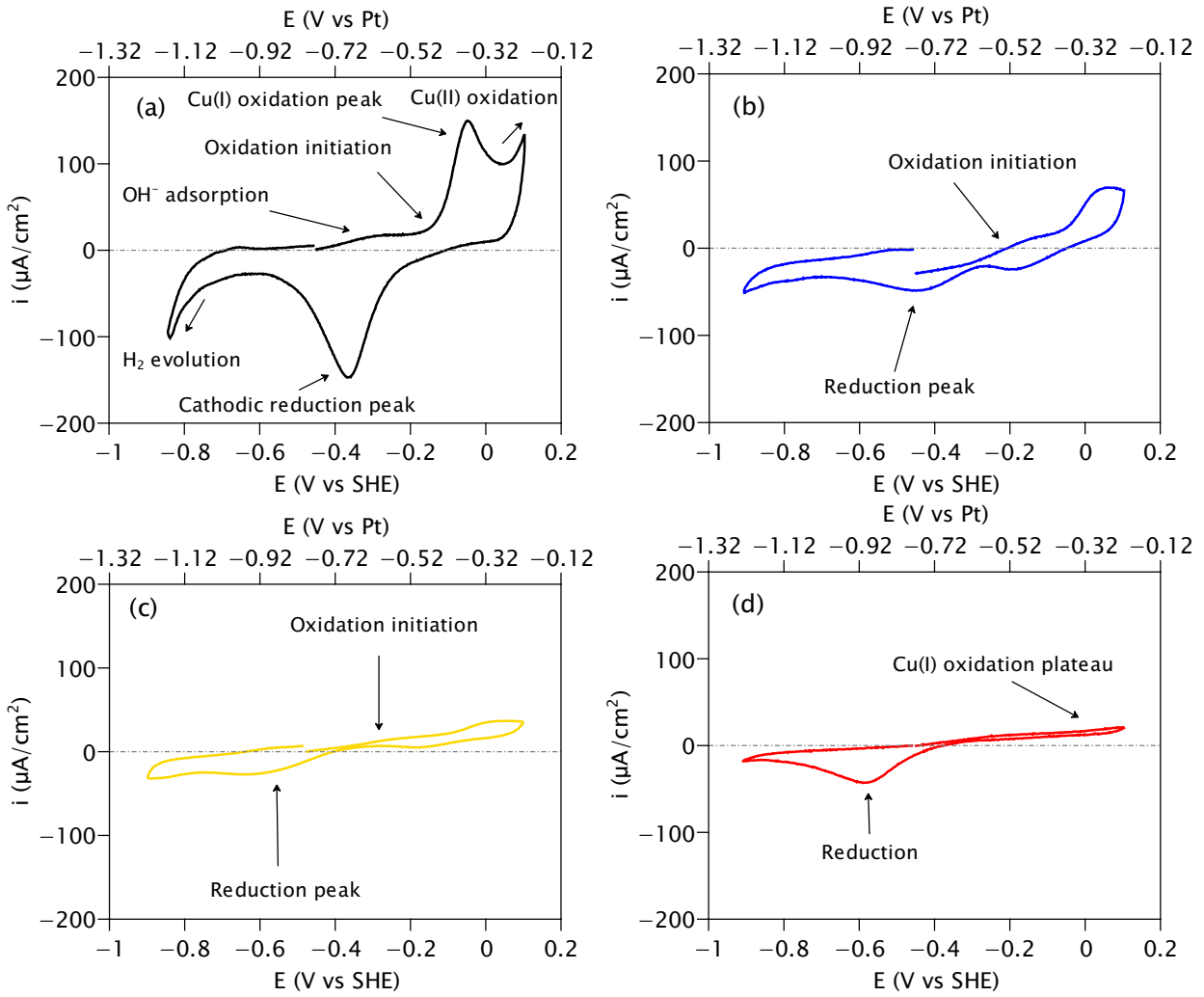

Figure A.13: Voltammogrammes d'oxydation anodique du cuivre dans (a) une solution de référence de NaOH 0,1 M après un prétraitement sans 2-MBT, et dans une solution de NaOH 0,1 M + 1 mM de 2-MBT après (b) un prétraitement sans 2-MBT suivi d'une exposition de 2 minutes au 2-MBT, (c) un prétraitement sans 2-MBT suivi d'une exposition d'une heure au 2-MBT, et (d) un prétraitement au 2-MBT. La vitesse de balayage est de 20 mV/s.

spectres XPS (Figure A.14). Une interaction entre le soufre et les îlots d'oxyde est suggérée par l'analyse ToF-SIMS. La formation de complexes organométalliques est également observée. Cependant, la structure du film de 2-MBT et ses propriétés protectrices dépendent fortement de l'état de l'interface obtenu après les méthodes de prétraitement utilisées.

Lorsque la surface couverte d'oxyde natif est prétraitée avec du 2-MBT dans la solution, une large couverture de l'oxyde natif persiste à l'interface. La couche de 2-MBT est relativement fine et des complexes organométalliques Cu-2-MBT sont adsorbés en extrême surface, résultant de l'interaction entre ions Cu(I) (provenat de la dissociation de Cu_2O) et molécules de 2-MBT. Le prétraitement sans 2-MBT dans la solution génère une couverture plus large des molécules

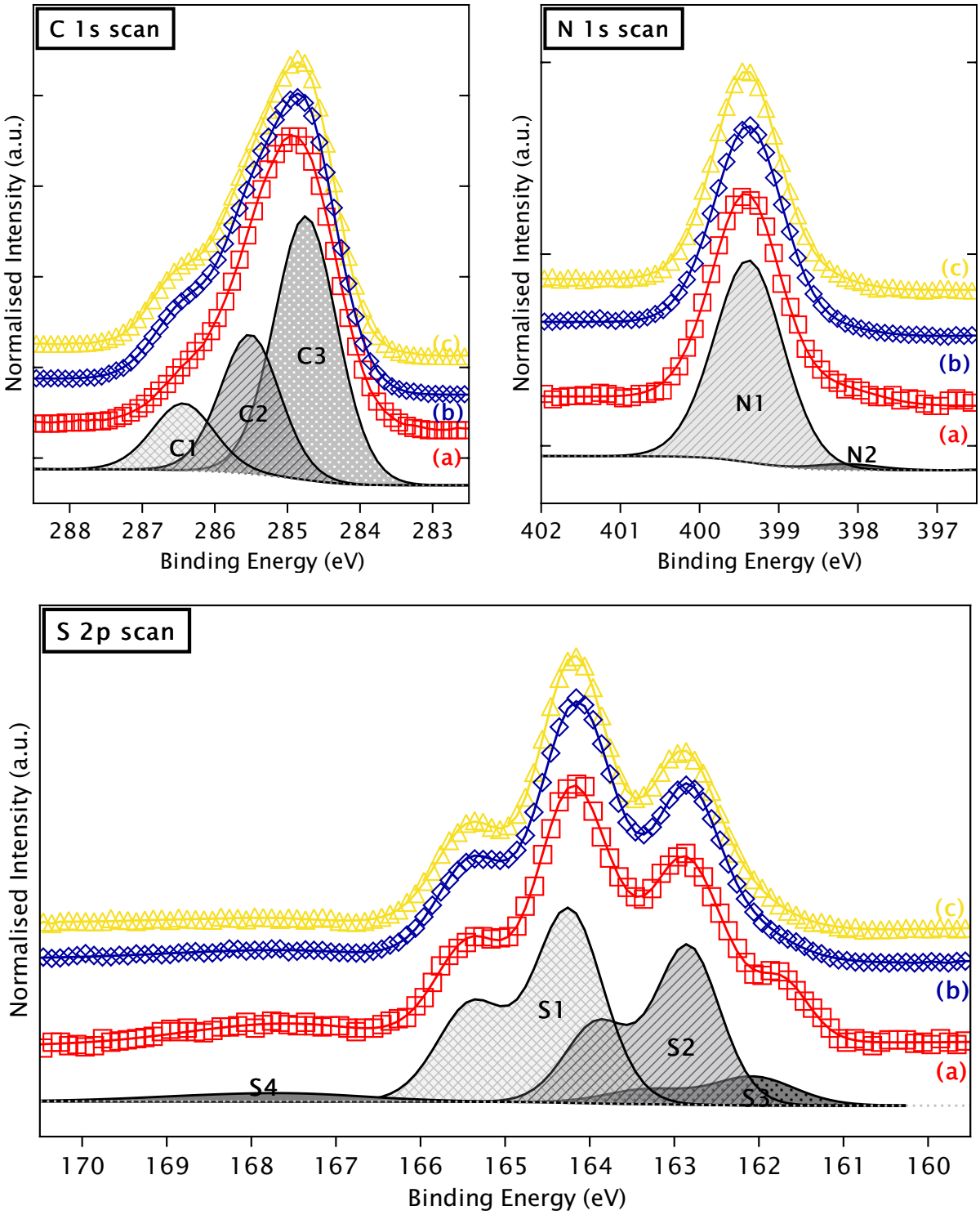

Figure A.14: Spectres XPS normalisés des niveaux de cœur C 1s, N 1s et S 2p pour les interfaces 2-MBT/cuivre formées dans une solution de NaCl 0,5 M après un prétraitement cathodique en (a) présence de 2-MBT, (b) absence de 2-MBT suivie d'une exposition de 2 minutes au 2-MBT, et (c) absence de 2-MBT suivie d'une exposition d'une heure au 2-MBT. Les symboles représentent les données expérimentales et les lignes colorées correspondantes représentent les courbes ajustées. La décomposition est présentée indiquées pour le spectre (b).

liées au métal ainsi que la formation d'une couche de 2-MBT plus épaisse, même après seulement 2 minutes d'exposition au 2-MBT, en raison de quantités plus faibles d'oxyde interfacial subsistant à l'interface. Une exposition plus longue (1 heure) au 2-MBT après un prétraitement en son absence augmente l'épaisseur de la couche organique, mais entraîne également une augmentation de l'épaisseur des îlots d'oxyde interfaciaux due à l'oxydation du substrat dans les zones défectueuses de la couche de 2-MBT. La formation de complexes dépend de la quantité d'oxydes interfaciaux présents, une plus grande quantité d'oxydes interfaciaux entraînant une formation accrue de complexes organométalliques.

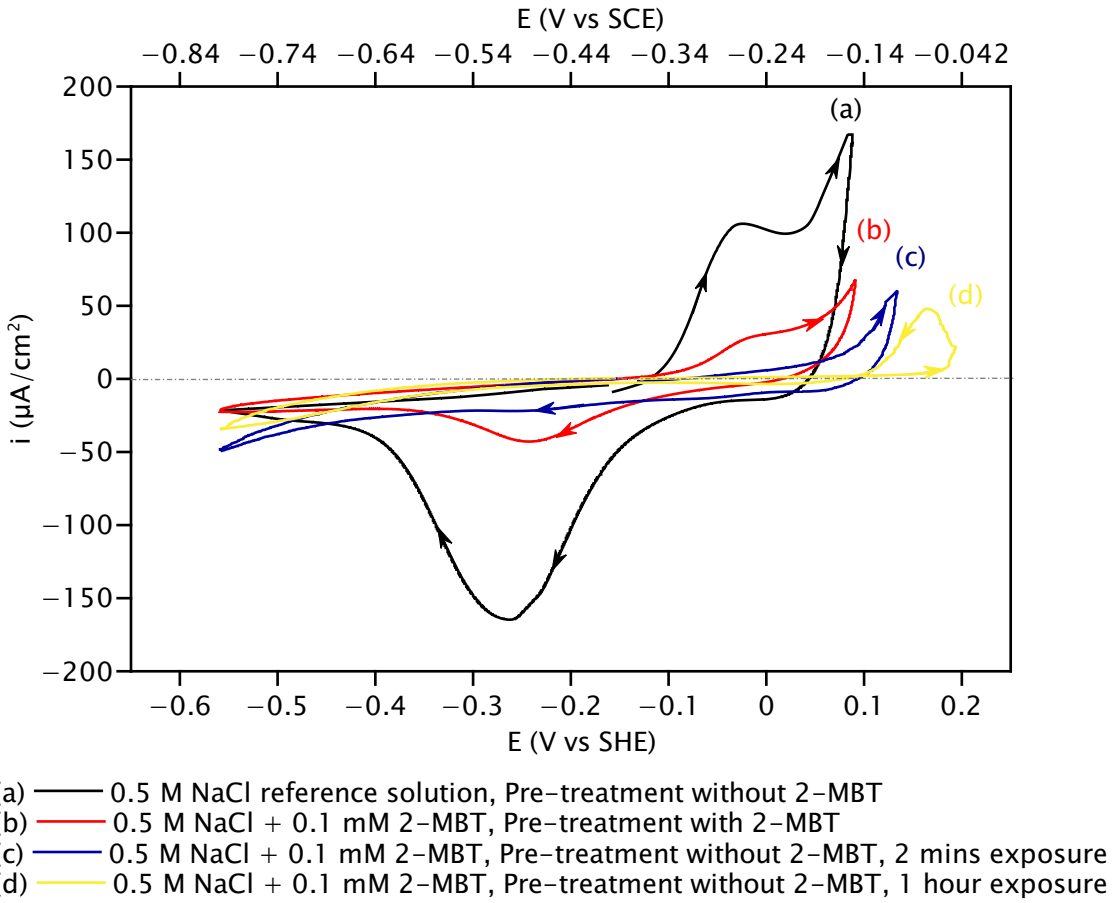

Figure A.15: Voltammogrammes du cuivre montrant l'oxydation anodique et l'initiation de la corrosion en l'absence ou en présence de 2-MBT dans l'électrolyte NaCl 0,5 M après le prétraitement cathodique spécifié. La vitesse de balayage est de 20 mV/s. Des flèches sont ajoutées à chaque cycle pour guider l'œil du lecteur.

Lors de la polarisation anodique, le substrat prétraité au 2-MBT présente une activité anodique réduite par rapport au substrat polarisé dans la solution de NaCl de référence (Figure A.15). L'analyse de la surface a révélé une augmentation de l'épaisseur de la couche de 2-MBT après la polarisation et juste avant l'initiation de la corrosion, ce qui est très probablement dû à la

formation de nouveaux complexes Cu-2-MBT en raison de la production d'ions Cu(I) lors de la polarisation. Malgré cela, aucune protection supplémentaire n'est offerte au substrat par les complexes. Le prétraitement en l'absence de 2-MBT suivi d'une exposition de 2 minutes à l'inhibiteur (Figure A.15, courbe c) génère l'absence de pic d'oxydation anodique et un décalage positif du potentiel d'initiation de la corrosion, ce qui indique de meilleures propriétés protectrices de la couche organique barrière formée. Un temps d'exposition plus long au 2-MBT entraîne un déplacement positif plus important du potentiel d'initiation de la corrosion (Figure A.15, courbe d). Cette amélioration des propriétés barrière de l'interface inhibitrice résulte à la fois de la couverture plus importante de la molécule de 2-MBT sur la surface et de la couche organique de 2-MBT plus épaisse.

Les mécanismes d'adsorption du 2-MBT sur le cuivre dans un environnement neutre chloruré se situent entre ceux observés en environnements acide et alcalin. Ceci est principalement dû au conformère dominant de la molécule - thiol, thione ou thiolate - qui module les sites actifs disponibles pour la liaison de la molécule avec le substrat en fonction du pH de l'environnement et de la présence d'ions chlorure qui entrent en compétition avec le 2-MBT pour s'adsorber sur la surface. Ces facteurs déterminent les conditions d'adsorption du 2-MBT sur le cuivre et la protection contre la corrosion conférée dans un environnement neutre chloruré.

Chapitre 7: Liaison interfaciale et inhibition de la corrosion de films organiques de 2-mercaptobenzimidazole formés sur des surfaces de cuivre sous contrôle électrochimique en solution acide chlorurée

Dans ce chapitre, les interfaces inhibitrices de 2-MBI formées sur les surfaces de cuivre dans un milieu acide chloruré ainsi que les capacités de protection contre la corrosion de la couche organique formée ont été étudiées. Le prétraitement des surfaces de cuivre par réduction cathodique en l'absence de 2-MBI produit une surface presque exempte d'oxyde, tandis que celui en présence de 2-MBI entraîne la formation d'une couche de conversion de complexes organiques métalliques Cu(I)-2-MBI par dissociation et libération d'ions Cu(I) de la couche native d'oxyde de cuivre. L'adsorption du 2-MBI en milieu acide présente un contraste frappant avec celle du 2-MBT dans un environnement similaire. Ceci a été attribué au changement de nature des sites actifs, de deux atomes de soufre et un atome d'azote dans le 2-MBT à un atome de soufre et deux atomes d'azote dans le 2-MBI. Sur une surface de cuivre presque métallique, obtenue par prétraitement en l'absence d'inhibiteur, le 2-MBI s'adsorbe par ses atomes d'azote et de soufre, formant une couche chimisorbée, comme le montre la Figure A.16 (courbe a). En revanche, lorsque le prétraitement de la surface est effectué en présence de l'inhibiteur, la liaison entre le 2-MBI et le substrat se fait uniquement

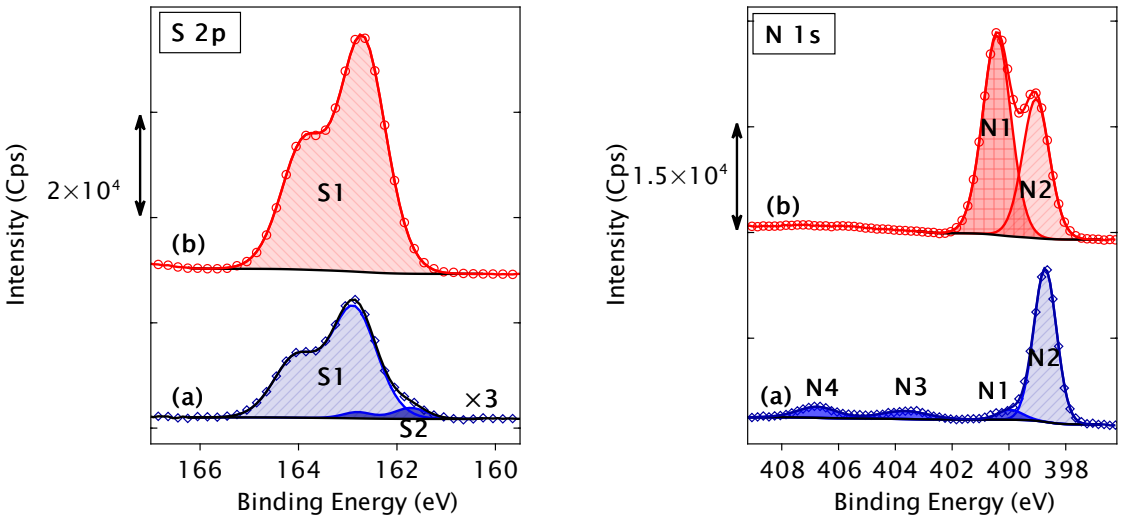

Figure A.16: Spectres XPS S 2p et N 1s pour des films de 2-MBI formés sur des surfaces de cuivre à l'état réduit dans une solution de HCl 10 mM après un prétraitement cathodique (a) en l'absence de 2-MBI suivi d'une exposition d'une heure au 2-MBI (courbes bleues), et (b) en présence de 2-MBI (courbes rouges). Les symboles représentent les données expérimentales et les lignes colorées correspondantes représentent l'ajustement. Les intensités sont normalisées par rapport au bruit de fond du côté de l'énergie de liaison la plus faible.

par ses atomes d'azote (Figure A.16 (courbe b)). Le profilage élémentaire en profondeur par ToF-SIMS a révélé la formation d'une couche chimisorbée interne et d'une couche physisorbée externe du film organique de 2-MBI, beaucoup plus épaisses que celles formée par le 2-MBT dans les mêmes conditions de préparation.

Ces films de 2-MBI inhibent la dissolution du cuivre en solution acide chlorurée, avec une réduction de la densité du courant et un déplacement positif du potentiel. Pour l'échantillon prétraité en l'absence de 2-MBI suivi d'une exposition d'une heure au 2-MBI, qui présente la plus grande résistance à l'initiation de la corrosion, un petit pic anodique a été observé avant l'initiation de la dissolution anodique, indiquant une réaction conjointe de protection. Il a été établi que cette réaction correspond à la formation de complexes résultant de l'oxydation anodique du métal Cu en ions Cu(I). Par conséquent, des complexes organométalliiques sont formés sur les deux substrats prétraités, bien que par des mécanismes différents en fonction de la polarisation de l'interface.

Pendant la polarisation anodique, les films organiques s'épaississent en raison de l'accumulation de complexes organométalliiques. Cependant, l'efficacité d'inhibition de la corrosion des films de 2-MBI est beaucoup plus faible que celle des films de 2-MBT, malgré une concentration de 2-MBI plus élevée dans la solution, la formation de films plus épais et la protection offerte par les complexes Cu(I)-2-MBI. Sur l'échantillon prétraité avec du 2-MBI, la surface du substrat

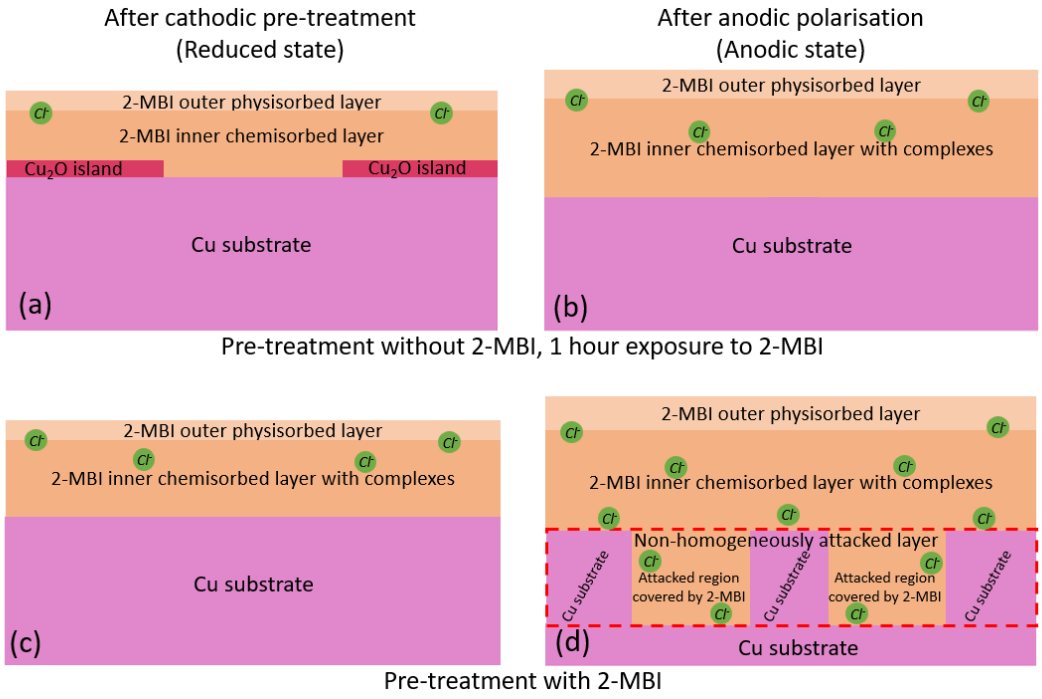

Figure A.17: Structure interfaciale bicouche des films organiques de 2-MBI formés sur le cuivre à l'état réduit (a,c) et anodique (b,d) dans une solution de HCl 10 mM par prétraitement (a,b) en l'absence de 2-MBI suivi d'une exposition d'une heure au 2-MBI, et (c,d) en présence de 2-MBI. Les disques verts représentent les ions chlorure qui ont pénétré les couches organiques.

est attaquée de manière non homogène par les ions chlorures, comme le montrent les profils élémentaires en profondeur ToF-SIMS et l'intensité du chlore mesurée par XPS. Ceci est illustré Figure A.17d. En revanche, sur l'échantillon prétraité en l'absence d'inhibiteur, puis exposé à la molécule de 2-MBI, les ions chlorure n'atteignent pas le substrat (Figure A.17b), ce qui indique que le contrôle électrochimique de la surface pendant la formation de la couche organique permet d'obtenir une couche organique barrière plus protectrice.

List of references

[1] Koch G (2017), "Cost of corrosion," *Trends in Oil and Gas Corrosion Research and Technologies: Production and Transmission*, pp. 3–30, doi:10.1016/B978-0-08-101105-8.00001-2.

[2] Hansson CM (2011), "The impact of corrosion on society," *Metallurgical and Materials Transactions A*, volume 42: pp. 2952–2962, doi:10.1007/s11661-011-0703-2.

[3] Warraky AE, Shayeb HAE, and Sherif EM (2004), "Pitting corrosion of copper in chloride solutions," *Anti-Corrosion Methods and Materials*, volume 51(1): pp. 52–61, doi:10.1108/00035590410512735.

[4] Allah AGG, Abou-Romia MM, Badawy WA, and Rehan HH (1991), "Effect of halide ions on passivation and pitting corrosion of copper in alkaline solutions," *Werkstoffe und Korrosion*, volume 42(11): pp. 584–591, doi:10.1002/maco.19910421105.

[5] Khalil W, Haupt S, and Strehblow HH (1985), "The thinning of the passive layer of iron by halides," *Materials and Corrosion*, volume 36(1): pp. 16–21, doi:10.1002/maco.19850360104.

[6] Amendola R and Acharjee A (2022), "Microbiologically Influenced Corrosion of Copper and Its Alloys in Anaerobic Aqueous Environments: A Review," *Frontiers in Microbiology*, volume 13: p. 806688, doi:10.3389/fmicb.2022.806688.

[7] Lou Y, Chang W, Cui T, Wang J, Qian H, Ma L, Hao X, and Zhang D (2021), "Microbiologically influenced corrosion inhibition mechanisms in corrosion protection: A

review," *Bioelectrochemistry*, volume 141: p. 107883, doi:10.1016/j.bioelechem.2021.107883.

[8] Pourbaix M (1966), "Atlas of Electrochemical Equilibria in Aqueous Solutions," *National Association of Corrosion Engineers (NACE)*.

[9] Kelly RG, Scully JR, Shoesmith DW, and Buchheit RG (2002), "Electrochemical techniques in corrosion science and engineering: Chapter 2 - Electrochemical thermodynamics and kinetics of relevance to corrosion." *Marcel Dekker Inc*, pp. 9–54.

[10] Pedeferri P (1996), "Cathodic protection and cathodic prevention," *Construction and Building Materials*, volume 10(5): pp. 391–402, doi:10.1016/0950-0618(95)00017-8.

[11] Szabo S and Bakos I (2006), "Cathodic Protection with Sacrificial Anodes," *Corrosion Reviews*, volume 24(3-4): pp. 231–280, doi:10.1515/CORRREV.2006.24.3-4.231.

[12] Wint N, Eaves D, Michailidou E, Bennett A, Searle JR, Williams G, and McMurray HN (2019), "The kinetics and mechanism of filiform corrosion occurring on zinc-aluminium-magnesium coated steel," *Corrosion Science*, volume 158: p. 108073, doi:10.1016/j.corsci.2019.06.028.

[13] Parthiban GT, Parthiban T, Ravi R, Saraswathy V, Palaniswamy N, and Sivan V (2008), "Cathodic protection of steel in concrete using magnesium alloy anode," *Corrosion Science*, volume 50(12): pp. 3329–3335, doi:10.1016/j.corsci.2008.08.040.

[14] National center for Biotechnology Information NCBI (2024), "PubChem Element Summary for Atomic Number 29, Copper." *https://pubchem.ncbi.nlm.nih.gov/element/Copper*.

[15] Feng Y, Siow KS, Teo WK, Tan KL, and Hsieh AK (1997), "Corrosion Mechanisms and Products of Copper in Aqueous Solutions at Various pH Values," *CORROSION*, volume 53(5), doi:10.5006/1.3280482.

[16] Hoar TP (1967), "The production and breakdown of the passivity of metals," *Corrosion Science*, volume 7: pp. 341–355, doi:10.1016/S0010-938X(67)80023-4.

[17] Takeno N (2005), "Atlas of Eh-pH diagrams Intercomparison of thermodynamic databases," *Geological survey of Japan open file report*, volume 419: pp. 85–87.

[18] King F (2010), "Critical review of the literature on the corrosion of copper by water," *Integrity Corrosion Consulting Ltd., Canada, & Swedish Nuclear Fuel and Waste Management Co., Sweden*.

[19] Hultquist G (1986), "Hydrogen evolution in corrosion of copper in pure water," *Corrosion Science*, volume 26(2): pp. 173–177, doi:10.1016/0010-938X(86)90044-2.

[20] Ambrose J, Barradas RG, and Shoesmith DW (1973), "Investigations of copper in aqueous alkaline solutions by cyclic voltammetry," *Journal of Electroanalytical Chemistry and Interfacial Electrochemistry*, volume 47(1): pp. 47–64, doi:10.1016/S0022-0728(73)80344-4.

[21] Miller B (1969), "Split-Ring Disk Study of the Anodic Processes at a Copper Electrode in Alkaline Solution," *Journal of the Electrochemical Society*, volume 116(2): pp. 1675–1680, doi:10.1149/1.2411657.

[22] Strehblow HH and Titze B (1980), "The investigation of the passive behaviour of copper in weakly acid and alkaline solutions and the examination of the passive film by ESCA and ISS," *Electrochimica Acta*, volume 25(6): pp. 839–850, doi:10.1016/0013-4686(80)90036-5.

[23] Maurice V, Strehblow HH, and Marcus P (2000), "In situ STM study of the initial stages of oxidation of Cu(111) in aqueous solution," *Surface Science*, volume 458: pp. 185–194, doi:10.1016/S0039-6028(00)00442-8.

[24] Kunze J, Maurice V, Klein LH, Strehblow HH, and Marcus P (2001), "In situ scanning tunneling microscopy study of the anodic oxidation of Cu(111) in 0.1 M NaOH," *Journal of Physical Chemistry B*, volume 105(19): pp. 4263–4269, doi:10.1021/jp004012i.

[25] Kunze J, Maurice V, Klein LH, Strehblow HH, and Marcus P (2004), "In situ STM study of the duplex passive films formed on Cu(111) and Cu(001) in 0.1 M NaOH," *Corrosion Science*, volume 46(1): pp. 245–264, doi:10.1016/S0010-938X(03)00140-9.

[26] Maurice V, Strehblow HH, and Marcus P (1999), "In Situ Scanning Tunneling Microscope Study of the Passivation of Cu (111)," *Journal of the Electrochemical Society*, volume 146(2): pp. 524–530, doi:10.1149/1.1391638.

[27] Wiame F, Maurice V, and Marcus P (2007), "Initial stages of oxidation of Cu(1 1 1)," *Surface Science*, volume 601(5): pp. 1193–1204, doi:10.1016/j.susc.2006.12.028.

[28] Pinnel MR, Tompkins HG, and Heath DE (1979), "Oxidation of copper in controlled clean air and standard laboratory air at 50C to 150C," *Applications of Surface Science*, volume 2: pp. 558–577, doi:10.1016/0378-5963(79)90047-3.

[29] Chialvo MRGD, Salvarezza RC, Moll DV, and Arvia AJ (1985), "Kinetics of passivation and pitting corrosion of polycrystalline copper in borate buffer solutions containing

sodium chloride," *Electrochimica Acta*, volume 30(11): pp. 1501–1511, doi:10.1016/0013-4686(85)80012-8.

[30] Kautek W and Gordon JG (1990), "XPS Studies of Anodic Surface Films on Copper Electrodes," *Journal of the Electrochemical Society*, volume 137(9): pp. 2672–2677, doi:10.1149/1.2087008.

[31] Subramanian R and Lakshminarayanan V (2002), "Effect of adsorption of some azoles on copper passivation in alkaline medium," *Corrosion Science*, volume 44(3): pp. 535–554, doi:10.1016/S0010-938X(01)00085-3.

[32] Touzé E and Cougnon C (2018), "Study of the air-formed oxide layer at the copper surface and its impact on the copper corrosion in an aggressive chloride medium," *Electrochimica Acta*, volume 262: pp. 206–213, doi:10.1016/j.electacta.2017.12.187.

[33] Crundwell FK (1992), "The Anodic dissolution of copper in hydrochloric acid solutions," *Electrochimica Acta*, volume 31(15): pp. 2701–2714, doi:10.1016/0013-4686(92)85197-S.

[34] Kear G, Barker BD, and Walsh FC (2004), "Electrochemical corrosion of unalloyed copper in chloride media–a critical review," *Corrosion Science*, volume 46(1): pp. 109–135, doi:10.1016/S0010-938X(02)00257-3.

[35] Diard JP, Canut JML, Gorrec BL, and Montella C (1998), "Copper electrodissolution in 1 M HCl at low current densities. I. General steady-state study," *Electrochimica acta*, volume 43(16-17): pp. 2469–2483, doi:10.1016/S0013-4686(97)10155-4.

[36] Diard JP, Canut JML, Gorrec BL, and Montella C (1998), "Copper electrodissolution in 1 M HCl at low current densities. II. Electrochemical impedance spectroscopy study," *Electrochimica acta*, volume 43(16-17): pp. 2485–2501, doi:10.1016/S0013-4686(97)10156-6.

[37] Fateh A, Aliofkhazraei M, and Rezvanian AR (2020), "Review of corrosive environments for copper and its corrosion inhibitors," *Arabian Journal of Chemistry*, volume 13(1): pp. 481–544, doi:10.1016/j.arabjc.2017.05.021.

[38] Turnbull J, Szukalo R, Zagidulin D, Biesinger M, and Shoesmith D (2021), "The kinetics of copper corrosion in nitric acid," *Materials and Corrosion*, volume 72(1-2): pp. 348–360, doi:10.1002/maco.202011707.

[39] Marcus P, Maurice V, and Strehblow HH (2008), "Localized corrosion (pitting): A model of passivity breakdown including the role of the oxide layer nanostructure," *Corrosion Science*, volume 50(9): pp. 2698–2704, doi:10.1016/j.corsci.2008.06.047.

[40] Parangusan H, Bhadra J, and Al-Thani N (2021), "A review of passivity breakdown on metal surfaces: influence of chloride- and sulfide-ion concentrations, temperature, and pH," *Emergent materials*, volume 4(5): pp. 1187–1203, doi:10.1007/s42247-021-00194-6.

[41] Figueroa MG, Salvarezza RC, and Arvia AJ (1986), "The Influence of temperature on the pitting corrosion of copper," *Electrochimica Acta*, volume 31(6): pp. 665–669, doi:10.1016/0013-4686(86)87033-5.

[42] Szklarska-Smialowska Z (2002), "Mechanism of pit nucleation by electrical breakdown of the passive film," *Corrosion Science*, volume 44(5): pp. 1143–1149, doi:10.1016/S0010-938X(01)00113-5.

[43] Srivastava A and Balasubramaniam R (2005), "Microstructural characterization of copper corrosion in aqueous and soil environments," *Materials Characterization*, volume 55(2): pp. 127–135, doi:10.1016/j.matchar.2005.04.004.

[44] Ingelgem YV, Hubin A, and Vereecken J (2007), "Investigation of the first stages of the localized corrosion of pure copper combining EIS, FE-SEM and FE-AES," *Electrochimica Acta*, volume 52(27): pp. 7642–7650, doi:10.1016/j.electacta.2006.12.039.

[45] Frankel GS (1998), "Pitting Corrosion of Metals: A Review of the Critical Factors," *Journal of The Electrochemical Society*, volume 145(6): pp. 2186–2198, doi:10.1149/1.1838615.

[46] Lin L, Chao C, and Macdonald D (1981), "A Point Defect Model for Anodic Passive Films: II. Chemical Breakdown and Pit Initiation," *Journal of the Electrochemical Society*, volume 128(6): pp. 1194–1198, doi:10.1149/1.2127592.

[47] Maurice V and Marcus P (2018), "Current developments of nanoscale insight into corrosion protection by passive oxide films," *Current Opinion in Solid State and Materials Science*, volume 22(4): pp. 156–167, doi:10.1016/j.cossms.2018.05.004.

[48] Bjorndahl WD and Nobe K (1984), "Copper Corrosion in Chloride Media. Effect of Oxygen," *CORROSION*, volume 40(2): pp. 82–87, doi:10.5006/1.3593920.

[49] Deslouis C, Tribollet B, Mengoli G, and Musiani MM (1988), "Electrochemical behaviour of copper in neutral aerated chloride solution. I. Steady-state investigation," *Journal of Applied Electrochemistry*, volume 18: pp. 374–383, doi:10.1007/BF01093751.

[50] King F, Quinn MJ, and Litke CD (1995), "Oxygen reduction on copper in neutral NaCl solution," *Journal of Electroanalytical Chemistry*, volume 385(1): pp. 45–55, doi:10.1016/0022-0728(94)03705-8.

[51] King F (2002), "Corrosion of copper in alkaline chloride environments," *Integrity Corrosion Consulting Ltd., Canada, & Swedish Nuclear Fuel and Waste Management Co., Sweden*.

[52] Sathiyanarayanan S, Sahre M, and Kautek W (1999), "In-situ grazing incidence X-ray diffractometry observation of pitting corrosion of copper in chloride solutions," *Corrosion Science*, volume 41(10): pp. 1899–1909, doi:10.1016/S0010-938X(99)00021-9.

[53] Brusic V, Frisch MA, Eldridge BN, Novak FP, Kaufman FB, Rush BM, and Frankel GS (1991), "Copper Corrosion With and Without Inhibitors," *Journal of the electrochemical society*, volume 138(8): pp. 2253–2259, doi:10.1149/1.2085957.

[54] Shaban A, Kálmán E, Telegdi J, Pálinkás G, and Dóra G (1998), "Corrosion and inhibition of copper in different electrolyte solutions," *Applied Physics A*, volume 66: pp. 545–549, doi:10.1007/s003390051199.

[55] Mihajlović MBP and Antonijević MM (2015), "Copper Corrosion Inhibitors. Period 2008-2014. A Review," *International Journal of Electrochemical Science*, volume 10(2): pp. 1027–1053, doi:10.1016/S1452-3981(23)05053-8.

[56] Dariva CG, Galio AF, Hart E, and (Ed) Aliofkhazraei M (2016), "Developments in Corrosion Protection: Chapter 16 - Corrosion inhibitors: Principles, mechanisms and applications," *IntechOpen*, pp. 365–379, doi:10.5772/57255.

[57] Strehblow HH and (Ed) Marcus P (2012), "Corrosion mechanisms in theory and practice: Chapter 1 - Fundamentals of Corrosion," *CRC Press*, pp. 1–104.

[58] Garcia SJ, Markley TA, Mol JM, and Hughes AE (2013), "Unravelling the corrosion inhibition mechanisms of bi-functional inhibitors by EIS and SEM-EDS," *Corrosion Science*, volume 69: pp. 346–358, doi:10.1016/j.corsci.2012.12.018.

[59] Michailidou E, Visser P, Mol JM, Kosari A, Terryn H, Baert K, and Gonzalez-Garcia Y (2023), "The effect of pH on the corrosion protection of aluminum alloys in lithium-carbonate-containing NaCl solutions," *Corrosion Science*, volume 210: p. 110851, doi:10.1016/j.corsci.2022.110851.

[60] Ma IA, Ammar S, Kumar SS, Ramesh K, and Ramesh S (2022), "A concise review on corrosion inhibitors: types, mechanisms and electrochemical evaluation studies," *Journal of Coatings Technology and Research*, volume 19(1): pp. 241–268, doi:10.1007/s11998-021-00547-0.

[61] Alvarez CC, Gómez MEB, and Zavala AH (2021), "Hexavalent chromium: Regulation

and health effects," *Journal of Trace Elements in Medicine and Biology*, volume 65: p. 126729, doi:10.1016/j.jtemb.2021.126729.

[62] Souza FSD, Giacomelli C, Gonçalves RS, and Spinelli A (2012), "Adsorption behavior of caffeine as a green corrosion inhibitor for copper," *Materials Science and Engineering C*, volume 32(8): pp. 2436–2444, doi:10.1016/j.msec.2012.07.019.

[63] Raja PB and Sethuraman MG (2008), "Natural products as corrosion inhibitor for metals in corrosive media - A review," *Materials Letters*, volume 62(1): pp. 113–116, doi:10.1016/j.matlet.2007.04.079.

[64] Gašparac R, Martin CR, Stupnišek-Lisac E, and Mandic Z (2000), "In Situ and Ex Situ Studies of Imidazole and Its Derivatives as Copper Corrosion Inhibitors II. AC Impedance, XPS, and SIMS Studies," *Journal of The Electrochemical Society*, volume 147(3): pp. 991–998, doi:10.1149/1.1393302.

[65] Mansikkamäki K, Haapanen U, Johans C, Kontturi K, and Valden M (2006), "Adsorption of Benzotriazole on the Surface of Copper Alloys Studied by SECM and XPS," *Journal of The Electrochemical Society*, volume 153(8): pp. B311–B318, doi:10.1149/1.2208912.

[66] Žerjav G and Milošev I (2015), "Corrosion protection of brasses and zinc in simulated urban rain: Part I: Individual inhibitors benzotriazole, 2-mercaptobenzimidazole and stearic acid," *Materials and Corrosion*, volume 66(12): pp. 1402–1413, doi:10.1002/maco.201508383.

[67] Balaskas AC, Curioni M, and Thompson GE (2015), "Effectiveness of 2-mercaptobenzothiazole, 8-hydroxyquinoline and benzotriazole as corrosion inhibitors on AA 2024-T3 assessed by electrochemical methods," *Surface and Interface Analysis*, volume 47(11): pp. 1029–1039, doi:10.1002/sia.5810.

[68] Antonijević MM, Milić SM, and Petrović MB (2009), "Films formed on copper surface in chloride media in the presence of azoles," *Corrosion Science*, volume 51(6): pp. 1228–1237, doi:10.1016/j.corsci.2009.03.026.

[69] Zhang DQ, Gao LX, and Zhou GD (2004), "Inhibition of copper corrosion in aerated hydrochloric acid solution by heterocyclic compounds containing a mercapto group," *Corrosion Science*, volume 46(12): pp. 3031–3040, doi:10.1016/j.corsci.2004.04.012.

[70] Tan YS, Srinivasan MP, Pehkonen SO, and Chooi SYM (2004), "Self-assembled organic thin films on electroplated copper for prevention of corrosion," *Journal of Vacuum*

Science & Technology A: Vacuum, Surfaces, and Films, volume 22(4): pp. 1917–1925, doi:10.1116/1.1763901.

[71] Finšgar M and Merl DK (2014), "2-Mercaptobenzoxazole as a copper corrosion inhibitor in chloride solution: Electrochemistry, 3D-profilometry, and XPS surface analysis," *Corrosion Science*, volume 80: pp. 82–95, doi:10.1016/j.corsci.2013.11.022.

[72] Mahdavian M and Ashhari S (2010), "Corrosion inhibition performance of 2-mercaptobenzimidazole and 2-mercaptobenzoxazole compounds for protection of mild steel in hydrochloric acid solution," *Electrochimica Acta*, volume 55(5): pp. 1720–1724, doi:10.1016/j.electacta.2009.10.055.

[73] Kokalj A, Gustinčič D, Poberžnik M, and Lozinšek M (2019), "New insights into adsorption bonding of imidazole: A viable C2-H bond cleavage on copper surfaces," *Applied Surface Science*, volume 479: pp. 463–468, doi:10.1016/j.apsusc.2018.12.246.

[74] Finšgar M (2013), "EQCM and XPS analysis of 1,2,4-triazole and 3-amino-1,2,4-triazole as copper corrosion inhibitors in chloride solution," *Corrosion Science*, volume 77: pp. 350–359, doi:10.1016/j.corsci.2013.08.026.

[75] Assouli B, Srhiri A, and Idrissi H (2004), "Effect of 2-Mercaptobenzimidazole and Its Polymeric Film on the Corrosion Inhibition of Brass (60/40) in Ammonia Solution," *CORROSION*, volume 60(4): pp. 399–407, doi:10.5006/1.3287749.

[76] Jakeria MR, Ward L, and Cole I (2021), "Long term durability studies on the corrosion inhibition effect of 2-mercaptobenzimidazole (C3H4N2S) on AA6022: Mechanism of film formation and influence of IMPs," *Surfaces and Interfaces*, volume 25: p. 101164, doi:10.1016/j.surfin.2021.101164.

[77] Rai AK, Singh R, Singh KN, and Singh VB (2006), "FTIR, Raman spectra and ab initio calculations of 2-mercaptobenzothiazole," *Spectrochimica Acta - Part A: Molecular and Biomolecular Spectroscopy*, volume 63(2): pp. 483–490, doi:10.1016/j.saa.2005.05.034.

[78] Ellis B and Griffiths PJF (1966), "The ultra-violet spectra of some heterocyclic thioamides and hydrogen bonding," *Spectrochimica acta*, volume 22(12): pp. 2005–2032, doi:10.1016/0371-1951(66)80051-6.

[79] Chadwick D and Hashemi T (1979), "Electron spectroscopy of corrosion inhibitors: Surface films formed by 2-mercaptobenzothiazole and 2-mercaptobenzimidazole on copper." *Surface Science*, volume 89(1-3): pp. 649–659, doi:10.1016/0039-6028(79)90646-0.

[80] Ohsawa M and Suetaka W (1979), "Spectro-electrochemical studies of the corrosion

inhibition of copper by mercaptobenzothiazole," *Corrosion Science*, volume 19(10): pp. 709–722, doi:10.1016/S0010-938X(79)80142-0.

[81] Danehy JP and Parameswaran KN (1968), "Acidic Dissociation Constants of Thiols," *Journal of Chemical & Engineering Data*, volume 13(3): pp. 386–389, doi:10.1021/je60038a025.

[82] Chesick JP and Donohue J (1971), "The molecular and crystal structure of 2-mercaptobenzothiazole," *Acta Crystallographica Section B Structural Crystallography and Crystal Chemistry*, volume 27(7): pp. 1441–1444, doi:10.1107/s0567740871004102.

[83] Wu X, Wiame F, Maurice V, and Marcus P (2021), "Effects of water vapour on 2-mercaptobenzothiazole corrosion inhibitor films deposited on copper," *Corrosion Science*, volume 189: p. 109565, doi:10.1016/j.corsci.2021.109565.

[84] Wu X, Wiame F, Maurice V, and Marcus P (2020), "2-Mercaptobenzothiazole corrosion inhibitor deposited at ultra-low pressure on model copper surfaces," *Corrosion Science*, volume 166: p. 108464, doi:10.1016/j.corsci.2020.108464.

[85] Wu X, Wiame F, Maurice V, and Marcus P (2020), "Adsorption and thermal stability of 2-mercaptobenzothiazole corrosion inhibitor on metallic and pre-oxidized Cu(1 1 1) model surfaces," *Applied Surface Science*, volume 508: p. 145132, doi:10.1016/j.apsusc.2019.145132.

[86] Wu X, Wiame F, Maurice V, and Marcus P (2020), "Moiré Structure of the 2-Mercaptobenzothiazole Corrosion Inhibitor Adsorbed on a (111)-Oriented Copper Surface," *Journal of Physical Chemistry C*, volume 124(29): pp. 15995–16001, doi:10.1021/acs.jpcc.0c04083.

[87] Woods R, Hope GA, and Watling K (2000), "A SERS spectroelectrochemical investigation of the interaction of 2-mercaptobenzothiazole with copper, silver and gold surfaces," *Journal of applied electrochemistry*, volume 30(11): pp. 1209–1222, doi:10.1023/A:1026561914338.

[88] Vernack E, Zanna S, Seyeux A, Costa D, Chiter F, Tingaut P, and Marcus P (2023), "ToF-SIMS, XPS and DFT study of the adsorption of 2-mercaptobenzothiazole on copper in neutral aqueous solution and corrosion protection in chloride solution," *Corrosion Science*, volume 210: p. 110854, doi:10.1016/j.corsci.2022.110854.

[89] Finšgar M and Merl DK (2014), "An electrochemical, long-term immersion, and XPS study of 2-mercaptobenzothiazole as a copper corrosion inhibitor in chloride solution," *Corrosion Science*, volume 83: pp. 164–175, doi:10.1016/j.corsci.2014.02.016.

[90] Chiter F, Costa D, Maurice V, and Marcus P (2022), "Chemical interaction, self-ordering and corrosion inhibition properties of 2-mercaptobenzothiazole monolayers: DFT atomistic modelling on metallic copper," *Corrosion Science*, p. 110658, doi: 10.1016/j.corsci.2022.110658.

[91] Chiter F, Costa D, Maurice V, and Marcus P (2021), "DFT investigation of 2-mercaptobenzothiazole adsorption on model oxidized copper surfaces and relationship with corrosion inhibition," *Applied Surface Science*, volume 537: p. 147802, doi:10.1016/j.apsusc.2020.147802.

[92] Chiter F, Costa D, Maurice V, and Marcus P (2023), "Corrosion inhibition at emergent grain boundaries studied by DFT for 2-mercaptobenzothiazole on bi-crystalline copper," *npj Materials Degradation*, volume 7(1): p. 5, doi:10.1038/s41529-022-00314-5.

[93] Chiter F, Costa D, Maurice V, and Marcus P (2021), "Corrosion inhibition of locally de-passivated surfaces by DFT study of 2-mercaptobenzothiazole on copper," *npj Materials Degradation*, volume 5(1): p. 52, doi:10.1038/s41529-021-00198-x.

[94] Arkhipushkin I, Pronin Y, Vesely S, and Kazansky L (2014), "Electrochemical and XPS study of 2-mercaptobenzothiazole nanolayers on zinc and copper surface," *International Journal of Corrosion and Scale Inhibition*, volume 3(2): pp. 078–088, doi:10.17675/2305-6894-2014-3-2-078-088.

[95] Sharma SB, Maurice V, Klein LH, and Marcus P (2020), "Local Inhibition by 2-mercaptobenzothiazole of Early Stage Intergranular Corrosion of Copper," *Journal of The Electrochemical Society*, volume 167(16): p. 161504, doi:10.1149/1945-7111/abcc36.

[96] Mohamed HA, Farag AA, and Badran BM (2010), "Friendly to environment heterocyclic adducts as corrosion inhibitors for steel in water-borne paints," *Journal of Applied Polymer Science*, volume 117(3): pp. 1270–1278, doi:10.1002/app.31838.

[97] Visser P, Terryn H, and Mol JM (2018), "On the importance of irreversibility of corrosion inhibitors for active coating protection of AA2024-T3," *Corrosion Science*, volume 140: pp. 272–285, doi:10.1016/j.corsci.2018.05.037.

[98] Sharma SB, Maurice V, Klein LH, and Marcus P (2021), "Local Effects of Organic Inhibitor Molecules on Passivation of Grain Boundaries Studied In Situ on Copper," *Journal of The Electrochemical Society*, volume 168(6): p. 061501, doi: 10.1149/1945-7111/ac0308.

[99] Wu X, Wiame F, Maurice V, and Marcus P (2021), "Molecular scale insights into

interaction mechanisms between organic inhibitor film and copper," *npj Materials Degradation*, volume 5(1): p. 22, doi:10.1038/s41529-021-00168-3.

[100] Wu X, Wiame F, Maurice V, and Marcus P (2020), "2-Mercaptobenzimidazole films formed at ultra-low pressure on copper: adsorption, thermal stability and corrosion inhibition performance," *Applied Surface Science*, volume 527: p. 146814, doi:10.1016/j.apsusc.2020.146814.

[101] Sharma SB, Maurice V, Klein LH, and Marcus P (2021), "In situ scanning tunneling microscopy study of 2-mercaptobenzimidazole local inhibition effects on copper corrosion at grain boundary surface terminations," *Electrochimica Acta*, volume 378: p. 138150, doi:10.1016/j.electacta.2021.138150.

[102] Finšgar M (2013), "2-Mercaptobenzimidazole as a copper corrosion inhibitor: Part I. Long-term immersion, 3D-profilometry, and electrochemistry," *Corrosion Science*, volume 72: pp. 82–89, doi:10.1016/j.corsci.2013.03.011.

[103] Kozlica DK, Izquierdo J, Souto RM, and Milošev I (2023), "Inhibition of the localised corrosion of AA2024 in chloride solution by 2-mercaptobenzimidazole and octylphosphonic acid," *npj Materials Degradation*, volume 7(1): p. 55, doi:10.1038/s41529-023-00368-z.

[104] Refaey SAM, Taha F, and El-Malak AMA (2006), "Corrosion and Inhibition of 316L stainless steel in neutral medium by 2-Mercaptobenzimidazole," *International Journal of Electrochemical Science*, volume 1(2): pp. 80–91, doi:10.1016/S1452-3981(23)17138-0.

[105] Wang L, Pu JX, and Luo HC (2003), "Corrosion inhibition of zinc in phosphoric acid solution by 2-mercaptobenzimidazole," *Corrosion Science*, volume 45(4): pp. 677–683, doi:doi.org/10.1016/S0010-938X(02)00145-2.

[106] Form GR, Raper ES, and Downie TC (1976), "The crystal and molecular structure of 2-mercaptobenzimidazole," *Acta Crystallographica Section B Structural Crystallography and Crystal Chemistry*, volume 32(2): pp. 345–348, doi:10.1107/s0567740876003026.

[107] Ansar SM, Haputhanthri R, Edmonds B, Liu D, Yu L, Sygula A, and Zhang D (2011), "Determination of the binding affinity, packing, and conformation of thiolate and thione ligands on gold nanoparticles," *Journal of Physical Chemistry C*, volume 115(3): pp. 653–660, doi:10.1021/jp110240y.

[108] Perrin FX and Pagetti J (1998), "Characterization and mechanism of direct film formation on a Cu electrode through electro-oxidation of 2-mercaptobenzimidazole," *Corrosion Science*, volume 40(10): pp. 1647–1662, doi:10.1016/S0010-938X(98)00060-2.

[109] Finšgar M (2013), "2-Mercaptobenzimidazole as a copper corrosion inhibitor: Part II.

Surface analysis using X-ray photoelectron spectroscopy," *Corrosion Science*, volume 72: pp. 90–98, doi:10.1016/j.corsci.2013.03.010.

[110] Chiter F, Costa D, Maurice V, and Marcus P (2020), "Adsorption of 2-mercaptobenzimidazole Corrosion Inhibitor on Copper: DFT Study on Model Oxidized Interfaces," *Journal of The Electrochemical Society*, volume 167(16): p. 161506, doi:10.1149/1945-7111/abcd4f.

[111] Chiter F, Costa D, Maurice V, and Marcus P (2021), "Atomic Scale Insight into Corrosion Inhibition: DFT Study of 2-Mercaptobenzimidazole on Locally De-Passivated Copper Surfaces," *Journal of The Electrochemical Society*, volume 168(12): p. 121507, doi:10.1149/1945-7111/ac405c.

[112] Xue G, Huang XY, Dong J, and Zhang J (1991), "The formation of an effective anti-corrosion film on copper surfaces from 2-mercaptobenzimidazole solution," *Journal of Electroanalytical Chemistry and Interfacial Electrochemistry*, volume 310(1-2): pp. 139–148, doi:10.1016/0022-0728(91)85257-P.

[113] Chen H, Bettayeb M, Maurice V, Klein LH, Lapeire L, Verbeken K, Terryn H, and Marcus P (2016), "Local passivation of metals at grain boundaries: In situ scanning tunneling microscopy study on copper," *Corrosion Science*, volume 111: pp. 659–666, doi:10.1016/j.corsci.2016.04.013.

[114] Bettayeb M, Maurice V, Klein LH, Lapeire L, Verbeken K, and Marcus P (2018), "Nanoscale Intergranular Corrosion and Relation with Grain Boundary Character as Studied In Situ on Copper," *Journal of The Electrochemical Society*, volume 165(11): pp. C835–C841, doi:10.1149/2.1341811jes.

[115] Bettayeb M, Maurice V, Klein LH, Lapeire L, Verbeken K, and Marcus P (2019), "Combined in situ microstructural study of the relationships between local grain boundary structure and passivation on microcrystalline copper," *Electrochimica Acta*, volume 305: pp. 240–246, doi:10.1016/j.electacta.2019.03.054.

[116] Martinez-Lombardia E, Maurice V, Lapeire L, Graeve ID, Verbeken K, Kestens L, Marcus P, and Terryn H (2014), "In situ scanning tunneling microscopy study of grain-dependent corrosion on microcrystalline copper," *Journal of Physical Chemistry C*, volume 118(44): pp. 25421–25428, doi:10.1021/jp507089f.

[117] Martinez-Lombardia E, Lapeire L, Maurice V, Graeve ID, Verbeken K, Klein LH, Kestens LA, Marcus P, and Terryn H (2014), "In situ scanning tunneling microscopy study of the intergranular corrosion of copper," *Electrochemistry Communications*, volume 41: pp. 1–4, doi:10.1016/j.elecom.2014.01.007.

[118] Jacquet PA (1936), "On the anodic behavior of copper in aqueous solutions of orthophosphoric acid," *Transactions of the Electrochemical Society*, volume 69(1): pp. 629–655, doi:10.1149/1.3498234.

[119] Hoar TP and Farthing TW (1952), "Solid Films on Electropolishing Anodes," *Nature*, volume 169: pp. 324–325, doi:10.1038/169324b0.

[120] Hoar TP and Rothwell GP (1964), "The influence of solution flow on anodic polishing. Copper in aqueous o-phosphoric acid," *Electrochimica Acta*, volume 9: pp. 135–150, doi:10.1016/0013-4686(64)85001-5.

[121] Vidal R and West AC (1995), "Copper Electropolishing in Concentrated Phosphoric Acid I. Experimental Findings," *Journal of the Electrochemical Society*, volume 142(8): pp. 2682–2689, doi:10.1149/1.2050074.

[122] Vidal R and West AC (1995), "Copper Electropolishing in Concentrated Phosphoric Acid. II. Theoretical Interpretation," *Journal of the Electrochemical Society*, volume 142(8): pp. 2689–2694, doi:10.1149/1.2050075.

[123] Aksu S (2009), "Electrochemical Equilibria of Copper in Aqueous Phosphoric Acid Solutions," *Journal of The Electrochemical Society*, volume 156(11): pp. C387–C394, doi:10.1149/1.3215996.

[124] Fang JL and Jun NW (1990), "XPS and AES studies of the composition of the viscous liquid film in the electropolishing of copper," *Journal Of Applied Electrochemistry*, volume 20: pp. 231–234, doi:10.1007/BF01033599.

[125] Gabe DR (1972), "Electropolishing of copper and copper-based alloys in orthophosphoric acid," *Corrosion Science*, volume 12: pp. 113–120, doi:10.1016/S0010-938X(72)90826-8.

[126] Mirhashemihaghighi S, Światowska J, Maurice V, Seyeux A, Klein LH, Härkönen E, Ritala M, and Marcus P (2015), "Electrochemical and Surface Analysis of the Corrosion Protection of Copper by Nanometer-Thick Alumina Coatings Prepared by Atomic Layer Deposition," *Journal of The Electrochemical Society*, volume 162(8): pp. C377–C384, doi:10.1149/2.0081508jes.

[127] National center for Biotechnology Information NCBI (2023), "PubChem Compound Summary for CID 707035, 2-Mercaptobenzimidazole," *https://pubchem.ncbi.nlm.nih.gov/compound/2-Mercaptobenzimidazole.*

[128] National center for Biotechnology Information NCBI (2023), "Pub-

Chem Compound Summary for CID 697993, 2-Mercaptobenzothiazole," *https://pubchem.ncbi.nlm.nih.gov/compound/2-Mercaptobenzothiazole.*

[129] Kunze J, Maurice V, Klein LH, Strehblow HH, and Marcus P (2003), "In situ STM study of the anodic oxidation of Cu(0 0 1) in 0.1 M NaOH," *Journal of Electroanalytical Chemistry*, volume 554(1): pp. 113–125, doi:10.1016/S0022-0728(03)00115-3.

[130] Diggle JW, Downie TC, and Goulding CW (1969), "Anodic Oxide Films On Aluminum," *Chemical Reviews*, volume 69(3): pp. 365–405, doi:10.1021/cr60259a005.

[131] Hertz H (1887), "Ueber einen Einfluss des ultravioletten Lichtes auf die electrische Entladung," *Annalen der Physik*, volume 267(8): pp. 983–1000, doi:10.1002/andp.18872670827.

[132] Einstein A (1905), "Über einen die Erzeugung und Verwandlung des Lichtes betreffenden heuristischen Gesichtspunkt," *Annalen der Physik*, volume 332(132): pp. 132–148, doi:10.1002/andp.19053220607.

[133] Siegbahn K (1967), "Atomic, molecular and solid state structure studied by means of electron spectroscopy," *In ESCA*.

[134] Hofmann S (2012), "Auger-and X-Ray Photoelectron Spectroscopy in Materials Science: A User-Oriented Guide," *Springer Science and Business Media*, volume 49.

[135] Greczynski G and Hultman L (2020), "X-ray photoelectron spectroscopy: Towards reliable binding energy referencing," *Progress in Materials Science*, volume 107: p. 100591, doi:10.1016/j.pmatsci.2019.100591.

[136] Major GH, Fairley N, Sherwood PMA, Linford MR, Terry J, Fernandez V, and Artyushkova K (2020), "Practical guide for curve fitting in x-ray photoelectron spectroscopy," *Journal of Vacuum Science & Technology A*, volume 38(6): p. 061203, doi:10.1116/6.0000377.

[137] Tougaard S (2021), "Practical guide to the use of backgrounds in quantitative XPS," *Journal of Vacuum Science & Technology A*, volume 39(1): p. 011201, doi:10.1116/6.0000661.

[138] Scofield JH (1976), "Hartree-Slater Subshell Photoionization cross-sections at 1254 and 1487 eV," *Journal of Electron Spectroscopy and Related Phenomena*, volume 8(2): pp. 129–137, doi:10.1016/0368-2048(76)80015-1.

[139] Shinotsuka H, Tanuma S, and Powell CJ (2022), "Calculations of electron inelastic mean free paths. XIII. Data for 14 organic compounds and water over the 50 eV to 200

keV range with the relativistic full Penn algorithm," *Surface and Interface Analysis*, volume 54(5): pp. 534–560, doi:10.1002/sia.7064.

[140] Thomson JJ (1913), "Rays of positive electricity," *Proceedings of the Royal Society of London. Series A, Containing Papers of a Mathematical and Physical Character, 89*, pp. 1–20, doi:10.1098/rspa.1913.0057.

[141] Benninghoven A (1969), "Analysis of submonolayers on silver by Negative Secondary Ion Emission," *Physica Status Solidi B Basic Research*, volume 34(2): pp. K169–K171, doi:10.1002/pssb.19690340267.

[142] Galtayries A and Bonnelle JP (1995), "XPS and ISS studies on the interaction of H2S with polycrystalline Cu, Cu2O and CuO surfaces," *Surface and Interface Analysis*, volume 23(3): pp. 171–179, doi:10.1002/sia.740230308.

[143] Deroubaix G and Marcus P (1992), "X-ray photoelectron spectroscopy analysis of copper and zinc oxides and sulphides," *Surface and Interface Analysis*, volume 18(1): pp. 39–46, doi:10.1002/sia.740180107.

[144] Moulder JF, Stickle WF, Sobol PE, Bomben KD, and (Ed) Chastain J (1992), "Handbook of X-ray Photoelectron Spectroscopy: A Reference Book of Standard Spectra for Identification and Interpretation of XPS Data," *Eden Prairie, Minnesota: Physical Electronics Division, Perkin-Elmer Corporation*, volume 221.

[145] Biesinger MC, Lau LW, Gerson AR, and Smart RSC (2010), "Resolving surface chemical states in XPS analysis of first row transition metals, oxides and hydroxides: Sc, Ti, V, Cu and Zn," *Applied Surface Science*, volume 257(3): pp. 887–898, doi:10.1016/j.apsusc.2010.07.086.

[146] Wiame F, Jasnot FR, Świątowska J, Seyeux A, Bertran F, Fèvre PL, Taleb-Ibrahimi A, Maurice V, and Marcus P (2015), "Oxidation of α-brass: A photoelectron spectroscopy study," *Surface Science*, volume 641: pp. 51–59, doi:10.1016/j.susc.2015.05.013.

[147] Biesinger MC (2017), "Advanced analysis of copper X-ray photoelectron spectra," *Surface and Interface Analysis*, volume 49(13): pp. 1325–1334, doi:10.1002/sia.6239.

[148] Siow KS, Britcher L, Kumar S, and Griesser HJ (2018), "XPS study of sulfur and phosphorus compounds with different oxidation states," *Sains Malaysiana*, volume 47(8): pp. 1913–1922, doi:10.17576/jsm-2018-4708-33.

[149] Rokosz K, Hryniewicz T, Matỳsek D, Raaen S, Valíček J, Łukasz Dudek, and Harničárová M (2016), "SEM, EDS and XPS analysis of the coatings obtained on titanium after

plasma electrolytic oxidation in electrolytes containing copper nitrate," *Materials*, volume 9(5): p. 318, doi:10.3390/ma9050318.

[150] Garg V, Sharma SB, Zanna S, Seyeux A, Wiame F, Maurice V, and Marcus P (2023), "Enhanced corrosion inhibition of copper in acidic environment by cathodic control of interface formation with 2-mercaptobenzothiazole," *Electrochimica Acta*, volume 447: p. 142162, doi:10.1016/j.electacta.2023.142162.

[151] Kazansky LP, Selyaninov IA, and Kuznetsov YI (2012), "Adsorption of 2-mercaptobenzothiazole on copper surface from phosphate solutions," *Applied Surface Science*, volume 258(18): pp. 6807–6813, doi:10.1016/j.apsusc.2012.03.097.

[152] Garg V, Zanna S, Seyeux A, Wiame F, Maurice V, and Marcus P (2023), "Adsorption of 2-Mercaptobenzothiazole Organic Inhibitor and its Effects on Copper Anodic Oxidation in Alkaline Environment," *Journal of The Electrochemical Society*, volume 170: p. 071502, doi:10.1149/1945-7111/ace33b.

[153] Strehblow HH, Maurice V, and Marcus P (2001), "Initial and later stages of anodic oxide formation on Cu, chemical aspects, structure and electronic properties," *Electrochimica Acta*, volume 46: pp. 3755–3766, doi:10.1016/S0013-4686(01)00657-0.

[154] Chen H, Maurice V, Klein LH, Lapeire L, Verbeken K, Terryn H, and Marcus P (2015), "Grain boundary passivation studied by in situ scanning tunneling microscopy on microcrystalline copper," *Journal of Solid State Electrochemistry*, volume 19(12): pp. 3501–3509, doi:10.1007/s10008-015-2787-x.

[155] Briggs D and Beamson G (1992), "Primary and Secondary Oxygen-Induced C1s Binding Energy Shifts in X-ray Photoelectron Spectroscopy of Polymers," *Analytical Chemistry*, volume 64(15): pp. 1729–1736, doi:10.1021/ac00039a018.

[156] Briggs D and Beamson G (1993), "XPS Studies of the Oxygen 1s and 2s Levels in a Wide Range of Functional Polymers," *Analytical Chemistry*, volume 65(11): pp. 1517–1523, doi:10.1021/ac00059a006.

[157] Garg V, Zanna S, Seyeux A, Wiame F, Maurice V, and Marcus P (2023), "Inhibition of the initial stages of corrosion by 2-mercaptobenzothiazole adsorption and the effects of interfacial oxides on copper in neutral chloride conditions," *Corrosion Science*, volume 225: p. 111596, doi:10.1016/j.corsci.2023.111596.

[158] Garg V, Zanna S, Seyeux A, Wiame F, Maurice V, and Marcus P (2024), "Interfacial bonding and corrosion inhibition of 2-mercaptobenzimidazole organic films formed on

copper surfaces under electrochemical control in acidic chloride solution," *Electrochimica Acta*, volume 484: p. 144114, doi:10.1016/j.electacta.2024.144114.

[159] Whelan CM, Smyth MR, Barnes CJ, Brown NMD, and Anderson CA (1998), "An XPS study of heterocyclic thiol self-assembly on Au 111," *Applied Surface Science*, volume 134: pp. 144–158, doi:10.1016/S0169-4332(98)00204-9.

[160] Seyeux A, Zanna S, Allion A, and Marcus P (2015), "The fate of the protective oxide film on stainless steel upon early stage growth of a biofilm," *Corrosion Science*, volume 91: pp. 352–356, doi:10.1016/j.corsci.2014.10.051.

RÉSUMÉ

Les mécanismes de liaison interfaciale de deux inhibiteurs organiques contenant du soufre, le 2-mercaptobenzothiazole (2-MBT) et le 2-mercaptobenzimidazole (2-MBI), adsorbés sur le cuivre ainsi que l'inhibition de la corrosion qu'ils offrent dans diverses solutions aqueuses ont été étudiés à l'aide de méthodes électrochimiques et de techniques analytiques de surface avancées telles que la spectroscopie de photoélectrons (XPS) et la spectrométrie de masse d'ions secondaires à temps de vol (ToF-SIMS). En milieu acide, le 2-MBT se lie au cuivre métallique par l'intermédiaire de ses atomes de soufre, formant une couche chimisorbée. La formation de couches physisorbées de la molécule organique a également été détectée par ToF-SIMS. Dans les milieux alcalins et neutres, une fraction des atomes d'azote de la molécule est également impliquée dans la liaison avec le cuivre métallique. La présence d'oxydes natifs à l'interface entraîne des défauts dans la couche barrière, et favorise la formation de complexes organométalliques dans les milieux alcalins et neutres. La modification des mécanismes de liaison est attribuée au conformère dominant de la molécule dans chaque milieu, qui change en fonction du pH de la solution, ce qui entraîne un changement des sites actifs au sein de la molécule. Le film organique formé inhibe la corrosion du cuivre dans les milieux chlorés acides et neutres, tandis que dans les milieux alcalins, il inhibe l'oxydation anodique de la surface. En milieu acide, le 2-MBI se lie au cuivre ses atomes d'azote pour former une couche interne chimisorbée sous-jacente à la couche externe physisorbée. La liaison avec le soufre se produit également lorsque la surface métallique est directement accessible aux molécules de 2-MBI. La présence d'oxydes natifs entraîne la formation de complexes organométalliques par relâchement des ions Cu(I) des oxydes dissociés. Il en résulte des couches organiques plus épaisses pour le 2-MBI que pour le 2-MBT. Les films organiques formés par le 2-MBI inhibent la dissolution anodique du cuivre dans des milieux chlorurés acides. Cependant, l'efficacité inhibitrice du 2-MBI sur le cuivre est inférieure à celle du 2-MBT malgré la formation de films plus épais et les propriétés protectrices des complexes formés par le 2-MBI. Cet effet est attribué au changement des sites actifs entre les deux molécules, d'un atome d'azote et deux atomes de soufre dans le 2-MBT à un atome de soufre et deux atomes d'azote dans le 2-MBI, ce qui modifie les mécanismes de liaison interfaciale et, par conséquent, l'efficacité d'inhibition de la corrosion du cuivre.

MOTS CLÉS

Cuivre, Inhibition de la corrosion, Inhibiteurs organiques, 2-mercaptobenzothiazole, 2-mercaptobenzimidazole, Voltampérométrie cyclique, Analyse de surface, XPS, ToF-SIMS.

ABSTRACT

The interfacial bonding mechanisms of two sulphur containing organic inhibitors, 2-mercaptobenzothiazole (2-MBT) and 2-mercaptobenzimidazole (2-MBI), adsorbed on copper along with the corrosion inhibition offered by them in various aqueous solutions were investigated using electrochemical methods and advanced surface analytical techniques such as X-ray photoelectron spectroscopy (XPS) and time-of-flight secondary ion mass spectrometry (ToF-SIMS). In acidic media, 2-MBT bonds to metallic copper via its sulphur atoms forming a chemisorbed layer. The formation of physisorbed layers of the organic molecule was also detected by ToF-SIMS. In alkaline and neutral media, a fraction of the nitrogen atoms from the molecule is also involved in the bonding with metallic copper. The presence of native oxides at the interface results in defects within the barrier layer but also promotes the formation of metal-organic complexes in both the alkaline and neutral media. The change in bonding mechanisms was attributed to the dominant conformer of the molecule in each media, which changes based on the pH of the solution, thus resulting in the change of active sites within the molecule. The adsorbed organic film formed inhibits the corrosion of copper in acidic chloride and neutral chloride media, while in alkaline media it inhibits anodic oxidation of the surface. The 2-MBI bonding with copper, in acidic media, occurs by its nitrogen atoms forming an inner chemisorbed underneath the outer physisorbed layer. Sulphur bonding also occurs when the metallic surface is directly accessible to the 2-MBI molecules. The presence of native oxides results in the formation of metal-organic complexes owing to the release of Cu(I) ions from the dissociated oxides. This results in thicker organic layers for 2-MBI as compared to 2-MBT. The organic films formed by 2-MBI also inhibit the anodic dissolution of copper in acidic chloride media. However, the inhibitor efficiency of 2-MBI on copper is lower than that of 2-MBT despite forming thicker films and the protective properties of the metal-organic complexes formed by 2-MBI. This effect has been attributed to the change in active sites between the two molecules, from one nitrogen and two sulphur atoms in 2-MBT to one sulphur and two nitrogen atoms in 2-MBI, which alters the bonding mechanisms and subsequently the corrosion inhibition efficiency on copper.

KEYWORDS

Copper, Corrosion Inhibition, Organic Inhibitors, 2-mercaptobenzothiazole, 2-mercaptobenzimidazole, Cyclic Voltammetry, Surface analysis, XPS, ToF-SIMS.